Synthesis and Characterization of Bionanocomposites of Natural Rubber

Thesis submitted to

The Maharaja Sayajirao University of Baroda

For the degree of

DOCTOR OF PHILOSOPHY

In

CHEMISTRY

Submitted by

Mr. Mayur Valodkar

Department of Chemistry

Faculty of Science

The Maharaja Sayajirao University of Baroda

Vadodara- 390 002

Gujarat (INDIA)

June-2012

DEDICATED TO MY PARENTS,

GRANDFATHER, LATE GRANDMOTHER

AND MY WIFE

CERTIFICATE

This is to certify that the thesis entitled "***Synthesis and Characterization of Bionanocomposites of Natural rubber***" submitted for Ph.D. Degree in Chemistry by ***Mr. Mayur Valodkar*** incorporates the original research work carried out by him under my supervision.

(Dr. Sonal Thakore)
Research Guide

Head
Chemistry Department

Dean,
Faculty of Science,
The M. S. University of Baroda,
Vadodara

DECLARATION

I hereby declare that the matter embodied in the thesis entitled "**Synthesis and Characterization of Bionanocomposites of Natural Rubber**" is a result of investigation carried out by me at Department of Chemistry, Faculty of Science, The Maharaja Sayajirao University of Baroda, Vadodara, Gujarat, India, under the supervision of Dr. Sonal Thakore and that it has not been submitted elsewhere for the award of degree.

Date:

Place:

(Mayur Valodkar)

ACKNOWLEDGMENT

First and foremost I would like to thank GOD, who gave me the power to believe in my passion and pursue my dreams. I could never have done this without the faith I have in you, the Almighty.

I take immense pleasure to express my sincere and deep sense of gratitude to my supervising guide and mentor, ***Dr. Sonal I. Thakore****, Assistant Professor, Department of Chemistry, The M.S.University of Baroda, for her sustained enthusiasm, creative suggestions, motivation and exemplary guidance throughout the course of my doctoral research. Apart from the subject of my research, I learnt a lot from her, which I am sure, will be useful in different stages of my life. I solemnly submit my honest and humble thanks to her for bringing my dreams into reality.*

I thank ***Head, Department of Chemistry****, for providing me with the laboratory facilities. I also thank the authorities of* ***The Maharaja Sayajirao University*** *for sanctioning the University Scholarship which supported me while carrying out initial work of this study. I thank* ***Prof. B.V. Kamath*** *and all the teachers and the non teaching staff for their valuable support.*

I can barely find words to express all the wisdom, love and support given me for that I am eternally grateful to my beloved parents, ***My Father and Mother*** *for their unconditional love, fidelity, endurance and encouragement. They have been selfless in giving me the best of everything and I express my deep gratitude for their love without which this work would not have been completed.*

My Grandfather and my Late Grandmother *has always been my well wishers. I take this moment to express my never ending love and respect towards them for their blessings.*

*I would also like to thank my wife **Chandni Valodkar**. Her support, encouragement, quiet patience and unwavering love were undeniably the bedrock upon which the past few years of my life have been built. She was always there cheering me up and stood by me through the good times and bad.*

*It is with gratitude I express my thankfulness to my uncle **Dr. Vaibhav Valodkar** for his concern and enthusiastic support during the course of my work. Without his constant support and guidance the work would not have been possible.*

*I offer my profound gratitude to **Dr. Ishit Thakore and his staff member**, Mouldtech Rubber Industries, Dabhoi road, Vadodara for providing the necessary raw materials and all other facilities for my work.*

I would also like to thank the following members who helped me during my work.

*I sincerely would like to acknowledge my colleagues **Puran Singh Rathore, Shardul Bhatt, Jigar Y. Soni, Ashok, Vishwanath, Amit, Arun, Harnish, Shilpi, Ketan, Dr. Angshuman Pal, Dr. Sunil Shah, Mahendrasinh Zala, Hemant Mande, Ageetha, Sanjay, Harsha, Priyanka, Namrata** and all other research students of the Department of Chemistry for their support and encouragement in my research work.*

*Also, I am deeply indebted to my **in-laws** and family for their concern, prayers and constant enthusiasm revealed throughout my work.*

I am also thankful to the authorities of IIT, Chennai for helping me in carrying out my DMA analysis.

I would also like to thank the following persons/Institutes who helped me during my work:

Name	***Industry/Institute***	***Work***
Dr. Mehul Patel	*Department of Chemistry, Sardar Patel University, Vidyanagar*	*Mechanical properties of composites of natural rubber.*
Dr. John Varguease & Dr. Vikram Patel	*Electrical Research Development Agency (ERDA), Vadodara*	*Mechanical properties of composites of natural rubber.*
Dr. Vandana Rao,	*Department of Metallurgy, Faculty of Technology, The M.S. University of Baroda, Vadodara*	*SEM analysis*
Dr. Prasanna Ghalsasi	*Department of Chemistry, Faculty of Science, The Maharaja Sayajirao University of Baroda, Vadodara*	*DSC analysis*
Prof. Ganpati and Mr. Mukesh	*Department of Geology, Faculty of Science, The Maharaja Sayajirao University of Baroda, Vadodara*	*TGA analysis*
Dr. Mehta	*Department of Physics, Faculty of Science, The Maharaja Sayajirao University of Baroda, Vadodara and Sterling Gelatin ltd.*	*XRD analysis*
Mr. Rawal	*Department of Chemistry, Faculty of Science, The Maharaja Sayajirao University of Baroda, Vadodara*	*IR study*
SICART and SAIF	*Vidyanagar*	*TEM analysis*

I would also like to thank Dr. R.N. Jadeja & Miss Komal Vyas Department of Chemistry, The M. S. University of Baroda for carrying out DNA studies & Dr. R.V. Devkar, Dr. Ravirajsinh Jadeja & Dr. Menaka Thounaojam Department of Zoology, The M. S. University of Baroda, for carrying out Cytotoxicity studies. I would also like to mention ***Nirjara Gandhi*** *and* ***Dipak Patel*** *for their support and help during my research.*

I cherish the friendship I had and take this opportunity to thank each one of them. My friends have been an encouragement every time and their motivation my confidence that had helped me reach here. To my friends ***Sunny Prakashkar, Dr. Sonal Deshkar, Dr. Jagruti Rathod, Dr. Niraj Joshi and Anupama Sharma*** *for the support and motivation in all my efforts during the course of my work.*

There are so many others whom I may have inadvertently left out and I sincerely thank all of them for their help.

Mayur Valodkar

INDEX

List of some frequently used abbreviations

Sr. No.	Name	Abbreviations
1	Parts per hundred parts of rubber	Phr
2	Carbon black	C-black
3	Natural rubber	NR
4	Transmission electron microscopy	TEM
5	Scanning electron microscopy	SEM
6	Thermal gravimetric analysis	TGA
7	Differential scanning calorimetry	DSC
8	Tensile strength	T.S
9	Fourier transform infrared spectroscopy	FT-IR
10	Nuclear magnetic resonance	NMR
11	Dynamic mechanical analysis	DMA
12	X-ray diffraction	XRD
13	Degree of substitution	DS
14	Cellulose	Cel
15	Starch acetate	StAc
16	Starch cinnamate	Stcin
17	Starch phthalate	Stph
18	Cellulose acetate	CelAc
19	Nanoparticles	NPs

20	Cellulose nanoparticles	CelNPs
21	Starch nanoparticles	StNPs
22	Isocyanate modified starch nanoparticles	StINPs
23	Starch acetate nanoparticles	StAcNPs
24	Starch cinnamate nanoparticles	StcinNPs
25	Starch benzoate nanoparticles	StbenNPs
26	Starch palmiate nanoparticles	StpalNPs
27	Starch phthalate nanoparticles	StphNPs
28	Cellulose acetate nanoparticles	CelAcNPs
29	Polyurethanes	PUs
30	Copper nanoparticles	CuNPs
31	Silver nanoparticles	AgNPs
32	Silver nanoparticles immobilized polyurethane membrane	PU-Ag
33	Copper nanoparticles immobilized polyurethane membrane	PU-Cu

Chapter 1 Introduction

Outline

Progresses in the field of materials science and technology have given birth to fascinating and wonderful materials known as 'composites'. The aim of composites is to develop products with unique properties that cannot be attained from individual constituents. They are developed because no single, homogeneous structured material can be found that has all of the desired properties for a given application [1]. A composite material can provide superior and unique mechanical and physical properties because it combines the most desirable properties of its constituents while suppressing their least desirable properties.

1.1 Composites and fillers

Composites consist of two (or more) distinct constituents or phases, which when combined result in a material with entirely different properties from those of the individual components. Typically, a manmade composite would consist of a reinforcement phase of stiff, strong material, frequently fibrous in nature, embedded in a continuous matrix phase (Figure. 1.1). Two of the main functions of the matrix are to transmit externally applied loads, via shear stresses at the interface, to the reinforcement and to protect the latter from environmental and mechanical damage [2]. The advantage of such a coupling is that the high strength and stiffness of fibers may be exploited.

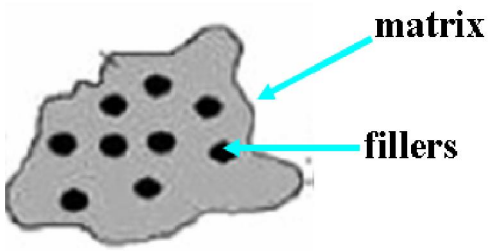

Figure.1.1 Formation of composite

Traditionally, fillers were considered as additives, which due to their unfavorable geometrical features, surface area or surface chemical composition, increases the strength of polymer. Their major contribution was in lowering the cost of materials by replacing the more expensive polymer. The term reinforcing filler has been coined to describe discontinuous additives, the form, shape, and/or surface chemistry of which have been

suitably modified with the objective of improving the mechanical properties of the polymer, particularly strength. Fillers exist in a variety of systems such as organic, inorganic, biological, biomimetic, and polymeric materials [3]. On the one hand the replacement aims at reducing costs, on the other, a synergistic effect of different fillers might be obtained due to the complicated cooperative interactions.

Inorganic reinforcing fillers are stiffer than the matrix and deform less. This causes an overall reduction in the matrix strain, especially in the vicinity of the particle and hence particle matrix adhesion is poor. As shown in Figure.1.2, the fiber "pinches" the polymer in its vicinity, reducing strain and increasing stiffness [4]. Reinforcing fillers are characterized by relatively high aspect ratio, α, defined as the ratio of length to diameter for a fiber, or the ratio of diameter to thickness for platelets and flakes. For spheres, which have minimal reinforcing capacity, the aspect ratio is unity. A useful parameter for characterizing the effectiveness of a filler is the ratio of its surface area, A, to its volume, V, which needs to be as high as possible for effective reinforcement. In developing reinforcing fillers, the aims of process or material modifications are to improve their compatibility and interfacial adhesion with the chemically dissimilar polymer matrix. Such modifications may enhance and optimize not only the primary function of the filler but may also introduce or enhance additional functions. The main problem of using inorganic fillers is that they are very expensive.

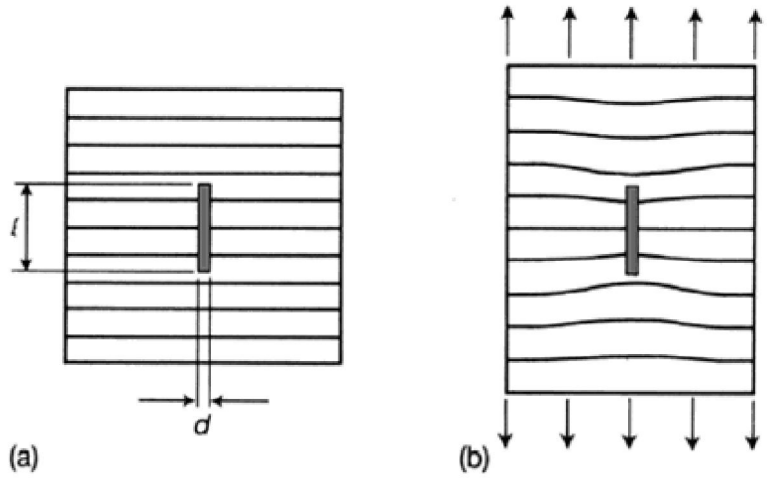

Figure. 1.2 A cylindrical reinforcing fiber embedded in polymer matrix (a) under undeformed state and (b) under tensile load

1.1.1 Classification of Composites

According to the nature of the reinforcement used, composites are classified into particulate, fibrous, laminate and hybrid composites.

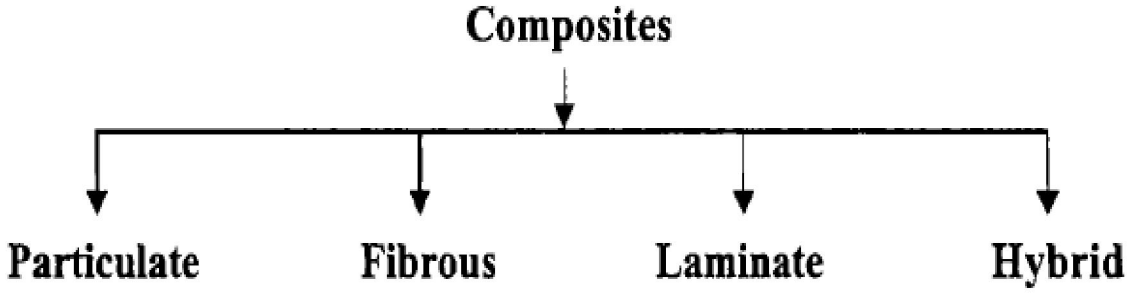

Particulate reinforcement

Particulate fillers are employed to improve high temperature performance, reduce friction, increase wear resistance and to reduce shrinkage [5]. In many cases particulate fillers are used to reduce the cost, under these conditions the additive is filler, whereas when a considerable change in the properties of the composite occurs, the additive is reinforcement. The particles will also share the load with the matrix, but to a lesser extent than a fibre. A particulate reinforcement will therefore improve stiffness but will not generally strengthen. Hard particles in a brittle matrix will cause localized stress concentrations in the matrix, which will reduce the overall impact strength.

Fibrous reinforcement

Fibrous reinforcement represents physical rather than a chemical means of changing a material to suit various engineering applications [6]. The measured strength of most materials is much less than that predicted by theory because flaws in the fonn of cracks perpendicular to the applied load are present in bulk materials. Fibres of non polymeric materials have much higher longitudinal strengths in this fonn because the larger flaws are not generally present in such small cross sectional areas. In the case of fibres from polymeric materials such as Kevlar, the orientation of the polymeric molecules along the long dimension produces strength in that direction. The fibres dispersed in the matrix may be continuous or discontinuous. In continuous fibre reinforcement, the transference of the load from matrix to the fibres will be easy and very effective whereas in

discontinuous (or short) fibre reinforcement, the fibres must beof sufficient length to have load transference effectively (Figure. 1.3 (a)). In short fibre composites, the properties of the composite vary with fibre length. Most continuous (long) fibre composites in fact contain fibres that are comparable in length to the overall dimensions ofthe composite part.

Laminates

A laminate is fabricated by stacking a number of laminas in the thickness direction (Figure. 1.3 (b)). Generally three layers are arranged alternatively for better bonding between reinforcement and the polymer matrix, for example plywood and paper. These laminates can have unidirectional or bi-directional orientation of the fibre reinforcement according to the end use of the composite. A hybrid laminate can also be fabricated by the use of different constituent materials or of the same material with different reinforcing pattern. In most of the applications of hminate composite, man made fibres are used due to their good combination of physical, mechanical and thermal behaviour.

Hybrid composites

Composite materials incorporated with two or more different types of fillers especially fibres in a single matrix are commonly known as hybrid composites (Figure. 1.3 (c)). Hybridisation is commonly used for improving the properties and for lowering the cost of conventional composites. There are different types of hybrid composites classified according to the way in which the component materials are incorporated. Hybrids are designated as i) sandwich type ii) interply iii) intraply and iv) intimately mixed [7]. In sandwich hybrids, one material is sandwiched between layers of another, whereas in interply, alternate layers of two or more materials are stacked in regular manner. Rows of two or more constituents are arranged in a regular or random manner in intraply hybrids while in intimately mixed type, these constituents are mixed as much as possible so that no concentration of either type is present in the composite material.

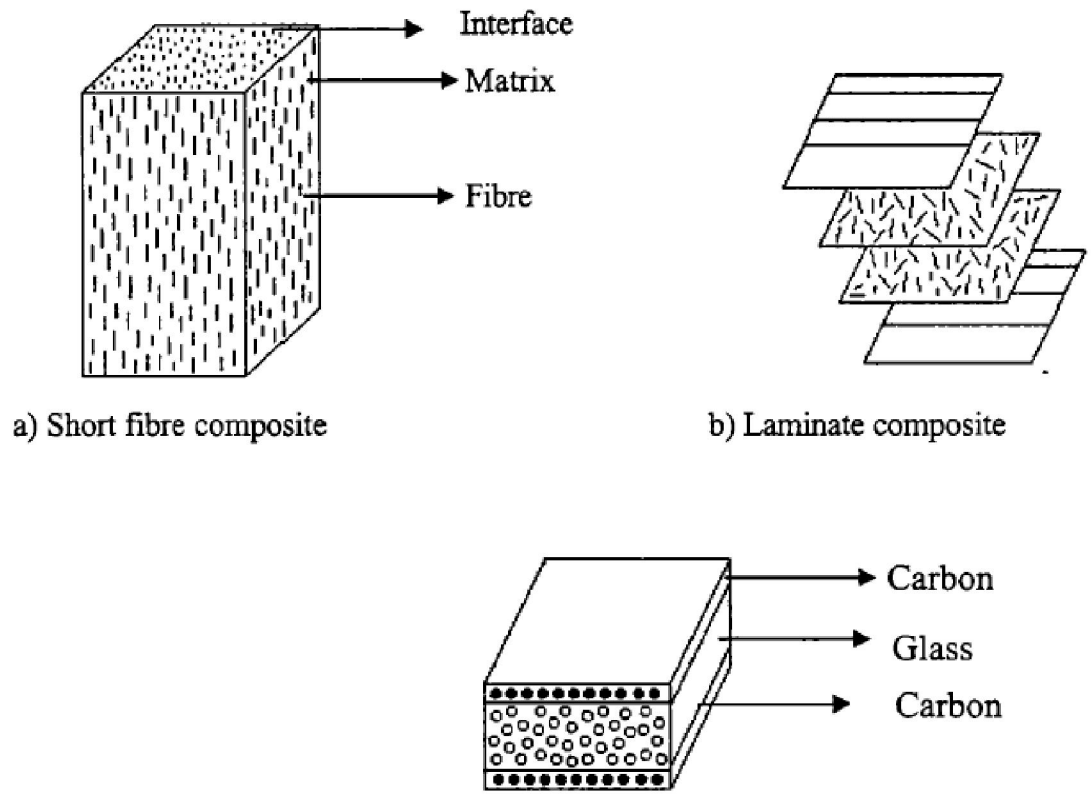

Figure-I.3 Schematic model of different composites

1.1.2 Factors affecting the performance of composites

Many factors combine to affect the properties of a composite material. However, the properties of composites are dictated by the intrinsic properties of the constituents. The two most important factors that affect the performance of composites are (i) The architecture of fillers and (ii) filler–matrix interface

(i) Filler architecture

Filler geometry to some extent is influenced by the way in which the fillers are extracted and processed. The aspect ratio (the ratio of filler length to diameter) is an important characteristic for any materials to be used as fillers. Thus fillers with high aspect ratio are long and thin, while that with low aspect ratio are shorter in length and broader in the

transverse direction. These high aspect ratio fillers tend to impart more strength to the matrix as compared to the low aspect ratio fillers.

(ii) The filler–matrix interface

The interface between filler and matrix is also crucial in terms of composite performance. The interface serves to transfer externally applied loads to the reinforcement via shear stresses over the interface. Controlling the 'strength' of the interface is very important. Clearly, good bonding is essential if stresses are to be adequately transferred to the reinforcement and hence provide a true reinforcing function. Owing to the general incompatibility between natural fillers and most matrix polymers, methods of promoting adhesion are frequently needed. Several approaches have been explored, including chemical modification of the filler prior to composite manufacture and introducing compatibilizing agents to the polymer/filler during processing

1.2 Natural rubber (NR),

Natural rubber is chemically cis 1, 4 polyisoprene; its structure is given in figure 1.4. It is an elastomer (an elastic hydrocarbon polymer) that was originally derived from latex, a milky colloid produced by some plants. The commercial major source of natural rubber latex is the para rubber tree (*Hevea brasiliensis*). Apart from this other plants containing latex include gutta-percha (*Palaquium gutta*),[8] rubber fig (*Ficus elastica*), Panama rubber tree (*Castilla elastica*), spurges (*Euphorbia* spp.), lettuce, common dandelion (*Taraxacum officinale*), Russian dandelion (*Taraxacum kok-saghyz*), *Scorzonera (tau-saghyz)*, and guayule (*Parthenium argentatum).* Although, these are not the major sources of natural rubber. To obtain latex the plants are tapped, that is, an incision made into the bark of the tree and the sticky, milk colored latex sap is collected and refined into a usable rubber. Further it is vulcanized, a process by which the rubber is heated in the presence of sulfur, to improve its resilience, elasticity and durability. The purified form of natural rubber is known as polyisoprene, which can also be produced synthetically. NR is normally very stretchy and flexible and extremely waterproof and hence is used extensively in many applications and products, as is synthetic rubber. The use of rubber is widespread, ranging from household to industrial products. Tires and tubes are the largest

consumers of rubber. The unique mechanical properties of NR result from both its highly stereoregular microstructure and the rotational freedom of the α-methylene C-C bonds. While the entanglements resulting from the high molecular weight which contributes to its high elasticity. The properties of NR can be tailored by the addition of fillers of varying surface chemistry and aggregate size/aspect ratio to suit the application concerned [9]. The performance of a polymer is determined by various factors, including the nature of the individual components, type of vulcanizing agent, processing parameters, and, to a certain extent, the application for which it is intended [10,11].

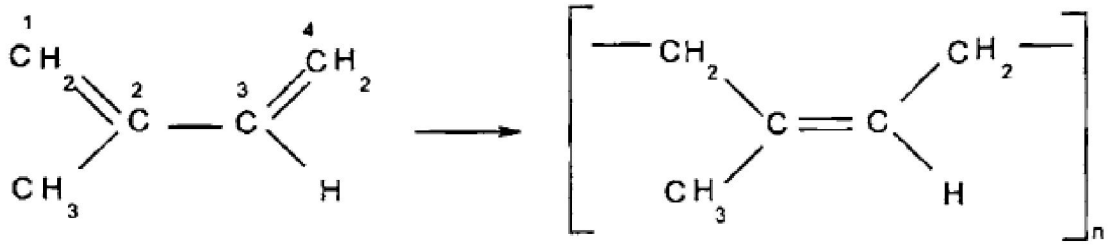

isoprene *cis* -1,4 - polyisoprene

Figure.1.4 Structure of natural rubber

1.2.1 Fillers used in natural rubber

Carbon black (C-black) and silica are the main fillers used in the compounding of NR [5]. For C-black filled rubbers, reinforcement is generally attributed to the nanoscale particle size, large specific surface area, high structure degree of C-black and, the formation of extensive rubber-C-black interactions [12,13]. Generally, on addition of fillers the increase in modulus is achieved at the expense of strength and elongation at break. There are some exceptions, particularly C-black, which induces an increase in both strength and modulus. We already know that C-black is produced by the incomplete combustion of heavy petroleum products such as FCC tar, coal tar, ethylene cracking tar, and a small amount from vegetable oil. Due to its origin from petroleum, it causes pollution and gives black color to the rubber. Recently, International Agency for Research on Cancer (IARC) evaluated that, it is possibly carcinogenic to humans. Hence research was focused on the development of other reinforcing agents to replace C-black in rubber compounds. Silica

and other types of fillers have a weaker polymer-filler interaction and are extensively used where a high degree of reinforcement is not essential [14,15].

Sombatsompop et al., [16] introduced untreated fly ash particles into NR vulcanizates, and found that the mechanical properties of fly ash-filled NR vulcanizates appeared to be very similar to those of commercial silica-filled vulcanizates at silica content of 0-30 phr. Above these concentrations, the properties of the fly ash-filled compounds remained unchanged, the fly ash particles being used as an extender. David et al., [17] studied the mechanical properties of twaron/natural rubber composites.

Carbon black (C-black)

Carbon black is a colloidal form of elemental carbon. It owes its reinforcing character to its colloidal morphology, the size and shape of the ultimate units, and to its surface properties. The particles of carbon black are not discrete but are fused clusters of individual particles. Carbon black is prepared by incomplete combustion or by thermal cracking of hydrocarbons. They are classified into furnace blacks, channel blacks, thermal blacks, lamp black and acetylene black depending on their method of manufacture. The major types of rubber reinforcing carbon blacks are manufactured by the furnace process. The predominant purpose of furnace type carbon blacks in elastomers is the reinforcement they impart to the vulcanisates [18,19]. Carbon black has reactive organic groups on the surface that cause affinity to rubber. Incorporation of carbon black into rubber gives enhanced modulus, improved fatigue, abrasion resistance and better overall technological properties. Details of a range of furnace blacks generally used for rubber reinforcement are given in table 1.1 [20].

Kaolin

Kaolin or china clay consists chiefly of the mineral kaolinite and has been selected based on its abundant availability and low cost to favor synthesis of a product having industrial utility.

Kaolinite [$Al_4Si_4O_{10}(OH)_8$] is a dioctahedral aluminosilicate, which is built with a tetrahedral SiO_4 sheet and an octahedral $AlO_4(OH)_2$ sheet linked together by oxygen atoms. The crystal consists of several of these layers extending in a two-dimensional

array, which are stacked along the c-axis and held together essentially by (i) hydrogen bonds between the external hydroxyls of the octahedral sheet and the basal oxygens of the adjacent layer tetrahedral sheet, (ii) van der Waal's attractive forces, and (iii) electrostatic interactions due to net fractional charges of opposite sign on each basal surface (Figure. 1.5). Although the surface silicate sheet of kaolinite is not particularly amenable to covalent attachment, the relatively reactive aluminol surface is similar to that in the case of montmorillonopkites and has the potential to be functionalized via Al-O-R bonds. In fact, a number of polar organic molecules such as urea, dimethyl sulfoxide, formamide, hydrazine, fatty acid salt, potassium acetate, and so on, are reportedly able to disrupt the interlayer bonding between the adjacent siloxane and hydroxy aluminium surfaces and to penetrate the interlayer space to form a complex by hydrogen bonding to both surfaces [21]. Such a process is known as intercalation. Successful intercalation agents decrease the electrostatic attraction between the lamellae by causing an increase in the dielectric constant when the compounds penetrate between the layers [22].

Table. 1.1 Various types of C-black

Name	**Abbrevation**	**ASTM Desig.**	**Particle size (nm)**
Super abrasion furnace	SAF	N110	20-25
Intermediate SAF	ISAF	N220	24-33
High abrassion furnace	HAF	N330	28-36
Easy processing channel	EPC	N300	30-35
Fast extruding furnace	FEF	N550	39-55
High modulus furnace	HMF	N683	49-73
Semi-reinforcing furnace	SRF	N770	70-96
Fine thermal	FT	N880	180-200
Medium thermal	MT	N990	250-350

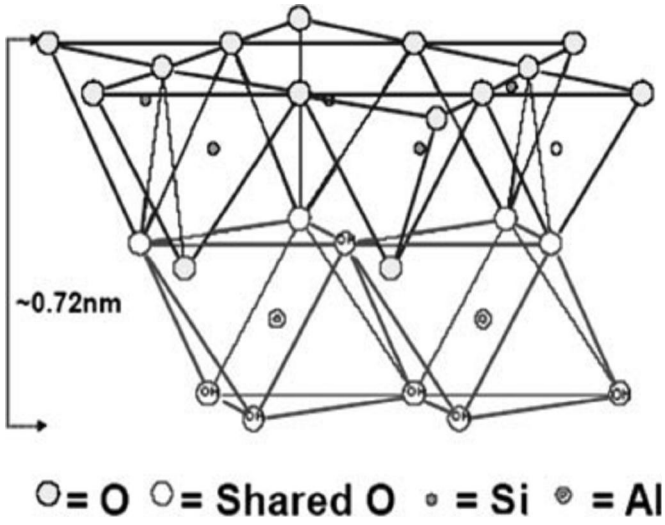

Figure. 1.5 Schematic representation of the structure of kaolinite

1.2.2 Blends and composites of natural rubber

The blending of rubbers produces new materials with a wide range of applications because they have the potential to combine the attractive properties of both the constituents in the blends. Usually, the outdoor properties of high diene rubbers such as polybutadiene (BR), nitrile rubber (NBR), styrene-butadiene rubber (SBR) or NR can be very significantly improved by the incorporation of low-unsaturated rubbers such as ethylene propylene diene monomer (EPDM) rubber [23,24,25,26,27]. Arayapranee and Rempel [28] studied the properties of NR/EPDM blends with or without Methyl Methacrylate-Butadiene-Styrene (MBS) as a compatibilizer. They found out that the incorporation of the EPDM in NR exhibits better stable mechanical properties as compared to the NR rich blend due to good thermal and weathering resistance of EPDM. The addition of graft copolymer into the 50/50 NR/EPDM blend increased the Mooney viscosity with an increase in graft copolymer concentration. The curing time became shorter with increasing graft copolymer content due to an increased compatibilizer interaction between NR and EPDM. Consequently, the tensile strength and elongation at break show improvement by the addition of the graft copolymer. Sombatsompop and Kumnuantip [29,30] introduced tire- tread reclaimed rubber into two natural rubber

grades and investigated various properties of the blends. They found that the Mooney number, shear viscosity and cure rate increased with reclaimed content, while the cure time was independent of the reclaimed content. Sreeja & Kutty [31] studied the cure characteristics and mechanical properties of NR/RR blends using EV system. They observed that the scorch time and tensile properties of the blends reduced with the reclaimed loadings. Hanafi et al., [32] checked the tensile properties of natural rubber filled with halloysite tubes and found out that the optimum tensile strength was obtained at 20 phr.

1.2.3 Methods of preparation of composites

Various commercial methods such as extrusion, injection molding and casting or compression molding are used to prepare composites. Generally two methods are used to prepare composites of natural rubber.

(i) Solution casting and (ii) Dry blending process

(i) Solution casting process

In this process polymer solution along with filler is stirred for long time to obtain homogenous suspension. The solvent is then evaporated at elevated temperature. This method has some disadvantages such as high consumption of solvent and time and it is not used commercially.

(ii) Dry blending process

This process is carried out on a two roll mixing mill where polymer along with filler is mixed until homogenous mixing occurs. It is then followed by vulcanization to obtain composites. However, this method is superior because (i) it is environmentally safe due to absence of organic solvents and (ii) it is compatible with the current industrial processes, such as extrusion and injection molding. Also, like other methods this method yields composites with structures ranging from intercalated to exfoliate, depending on the degree of penetration of the polymer chains [33].

1.3 Biocomposites of natural rubber

Biocomposites are composite materials comprising one or more phase(s) derived from a biological origin. In terms of the reinforcement, this could include plant fibres such as cotton, flax, hemp and the like, or fibres from recycled wood or waste paper, or even by-products from food crops. Fowler et al., [34] studied the technology, environmental credentials and market forces of biocomposites. They observed that there is a huge range of potential reinforcing fibers/fillers and an extensive range of processing options to ensure the right fiber at the right price. In parallel, significant developments have been seen in the realm of biopolymers in recent years due to more environmentally aware consumers, increased price of crude oil and global warming. They are used in variety of applications, like therapeutic aids, medicines, coatings, food products and packing materials.

The manufacture of true biocomposites demands that the matrix be made predominantly from renewable resources, although the current state of biopolymer technology dictates that synthetic thermoplastics and thermosets dominate commercial biocomposite production.

1.3.1 Polysaccharide as fillers

Natural fibers are pervasive throughout the world in plants such as grasses, reeds, stalks, and woody vegetation. They are also referred to as cellulosic fibers, related to the main chemical component cellulose, or as lignocellulosic fibers, since the fibers usually often also contain a natural polyphenolic polymer, lignin, in their structure. Results suggest that these agro-based fibers are a viable alternative to inorganic/ mineral based reinforcing fibers The use of lignocellulosic fibers derived from annually renewable resources as a reinforcing phase in polymeric matrix composites provides positive environmental benefits with respect to ultimate disposability and raw material use [35]. Compared to inorganic fillers, the main advantages of natural materials are listed below:

- wide variety of fillers available throughout the world
- nonfood agricultural based economy

- low energy consumption
- high specific strength and modulus
- comparatively easy processability due to their nonabrasive nature, which allows high filling levels, resulting in
- significant cost savings
- relativαely reactive surface, which can be used for grafting specific groups.

In addition, the recycling by combustion of natural materials filled composites is easier in comparison with inorganic fillers systems. Therefore, the possibility of using natural fillers in the plastic industry has received considerable interest. Automotive applications display strong promise for natural fiber reinforcements [36,37]. Potential applications of agrofiber based composites in railways, aircraft, irrigation systems, furniture industries, and sports and leisure items are currently being researched [38]. Various researchers have tried to use biofillers in place of commercially used fillers. A variety of fibers like sisal [39], bamboo [40], short coir fibres [41] etc. have been used to prepare biocomposites of NR. However, the use of polysaccharide as fillers or reinforcing agents in NR has not been extensively reported in the literature [42,43]. Carvalho et al., [44] prepared starch/NR composite by blending NR latex and starch paste. Jobish et al., [45] studied the mechanical and thermal properties of chitosan/natural rubber composites and concluded that the thermal stability of chitosan increases on formation of blend with natural rubber. Fernandes et al., [46] synthesized natural rubber/expoxidized natural rubber/cellulose II blend and found out that vulcanization increases in the presence of cellulose. Zaman et al., [47] synthesized jute/natural rubber composite and concluded that this composite showed excellent biodegradable properties. There have been many attempts investigating effects of the addition of rice husk ash into rubber [48,49].

Use of polysaccharide such as starch, cellulose and chitin have received significant importance due to their

- Abundance availability
- Low cost
- Renewability
- Biodegradability and
- Non-toxic nature

1.3.2 Starch

Starch is a natural, renewable, and biodegradable polymer produced by many plants as a source of stored energy. It is the second most abundant biomass material in nature and is found in plant roots, stalks, crop seeds, and staple crops such as rice, corn, wheat, tapioca, and potato [50,51]. Worldwide, the main sources of starch are maize (82%), wheat (8%), potatoes (5%), and cassava (5%) [52]. The starch powder consists of microscopic granules with diameters ranging from 2 to 100 μm, depending on the botanic origin, and with a density of 1.5. The basic formula of this polymer is $(C_6H_{10}O_5)n$, and the glucose monomer is called α-D-glycopyranose (or α-D-glycose) when in cycle. Depending on their botanic origin, starch raw materials have different conversion factors, size, shape, and chemical content. It consists of mainly two glucosidic macromolecules: amylose and amylopectin (Figure.1.6). In most common types of starch the weight percentages of amylose range between 72 and 82%, and the amylopectins range from 18 to 28%. However, some mutant types of starch have very high amylose content (up to 70% and more for amylomaize) and some very low amylose content (1% for waxy maize).

Amylose is defined as a linear molecule of glucose units linked by (1-4) α-D-glycoside bonds, slightly branched by (1-6) α-linkages. Amylopectin is a highly branched polymer consisting of relatively short branches of α-D-(1-4) glycopy-ranose that are interlinked by α-D-(1-6)-glycosidic linkages approximately every 22 glucose units [53].

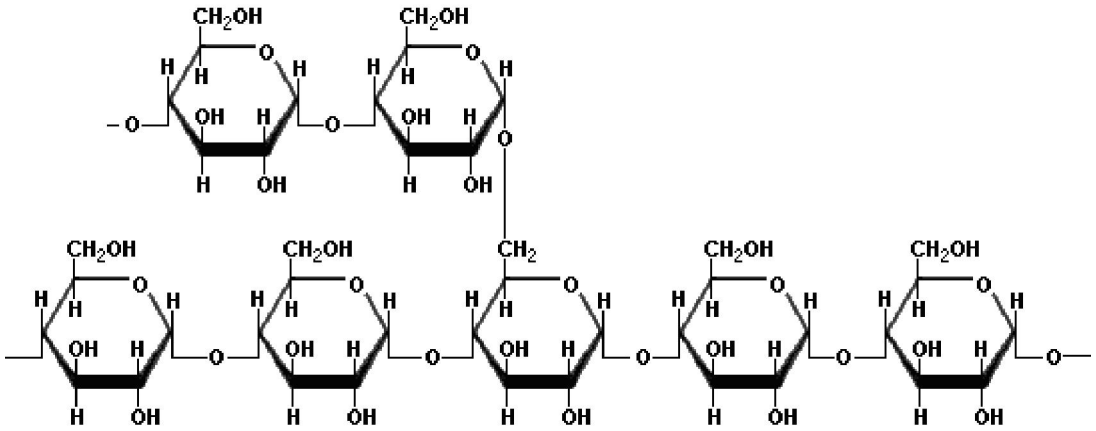

Figure. 1.6 Sturcture of starch

1.3.3 Cellulose

Cellulose is the most abundant renewable organic material produced in the biosphere, having an annual production over 7.5×10^{10} tons [54]. Cellulose is widely distributed in higher plants, in several marine animals (for example, tunicates), and to a lesser degree in algae, fungi, bacteria, invertebrates, and even amoeba (protozoa), for example, *Dictyostelium discoideum*. In general, cellulose is a fibrous, tough, water-insoluble substance that plays an essential role in maintaining the structure of plant cell walls. It was first discovered and isolated by Anselme Payen in 1838, [55] and since then, multiple physical and chemical aspects of cellulose have been extensively studied. Several reviews have already been published reporting the state of knowledge of this fascinating polymer [56,57]. Regardless of its source, cellulose can be characterized as a high molecular weight homopolymer of -1,4-linked anhydro-D-glucose units in which every unit is corkscrewed 180° with respect to its neighbors, and the repeat segment is frequently taken to be a dimer of glucose, known as cellobiose (Figure.1.7). Each cellulose chain possesses a directional chemical asymmetry with respect to the termini of its molecular axis: one end is a chemically reducing functionality (i.e., a hemiacetal unit) and the other has a pendant hydroxyl group, the nominal nonreducing end.

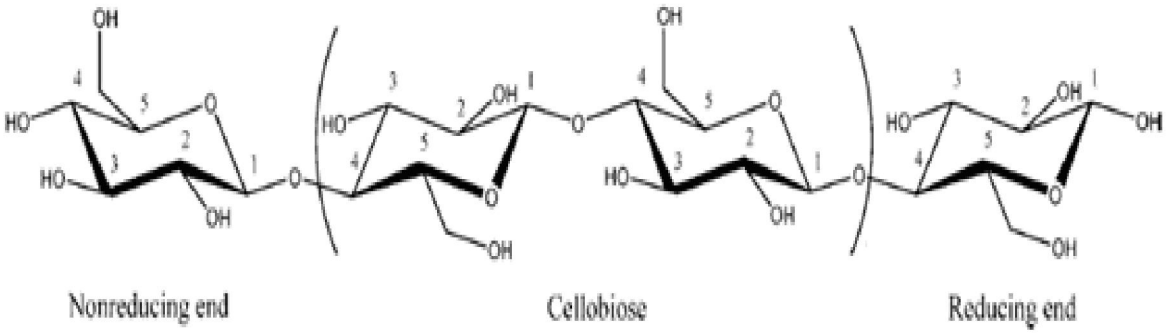

Figure. 1.7 Structure of cellulose

1.3.4 Chitin

Chitin is the other polysaccharide used extensively. It constitutes the structure of the external skeleton in shellfish and insects and is one of the major components of the fibrous material of cellular walls in mushrooms and algae [58,59]. In terms of structure, chitin may be compared to the polysaccharide cellulose and, in terms of function, to the protein keratin. It has also proven useful for several medical and industrial purposes. It is a modified polysaccharide that contains nitrogen; it is synthesized from units of *N*-acetylglucosamine (to be precise, 2-(acetylamino)-2-deoxy-D-glucose). These units form covalent β-1,4 linkages (similar to the linkages between glucose units forming cellulose). Therefore, it may be described as cellulose with one hydroxyl group on each monomer substituted with an acetyl amine group (Figure.1.8). This allows for increased hydrogen bonding between adjacent polymers, giving the chitin-polymer matrix increased strength. In its pure form, chitin is leathery, but in most invertebrates it occurs largely as a component of composite materials. It is used in industry in many processes. It is used as an additive to thicken and stabilize foods and pharmaceuticals. It also acts as a binder in dyes, fabrics, and adhesives. Industrial separation membranes and ion-exchange resins can be made from chitin. It has some unusual characteristics that accelerate healing of wounds in humans. This combined with, its flexibility and strength makes it favorable for use as surgical thread. Its biodegradibility is such that it wears away with time as the wound heals.

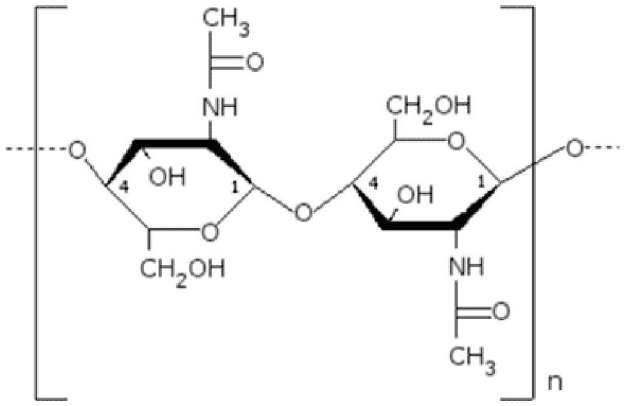

Figure. 1.8 Structure of chitin

1.3.5 Disadvantages of polysaccharide as fillers

- Despite these attractive properties, natural fillers are used only to a limited extent in industrial practice due to difficulties associated with surface interactions. The inherent polar and hydrophilic nature of polysaccharide and the nonpolar characteristics of most of the thermoplastics result in difficulties in compounding the filler and the matrix and, therefore, in achieving acceptable dispersion levels, which results in inefficient composites.
- Moreover, the processing temperature of composites is very low because these biofillers start to degrade at high temperature (around 230 °C). This limits the type of thermoplastics that can be used in association with polysaccharide fillers to commodity plastics such as polyethylene, polypropylene, poly(vinyl chloride), and polystyrene.
- Another drawback of biofillers is their high moisture absorption and the resulting swelling and decrease in mechanical properties. Moisture absorbance and corresponding dimensional changes can be largely prevented if the hydrophilic filler is thoroughly encapsulated in a hydrophobic polymer matrix and there is good adhesion between both components. However, if the adhesion level between the filler and the matrix is not good enough, a diffusion pathway can preexist or can be created under mechanical solicitation. The existence of such a pathway is also related to the filler connection and therefore to its percolation threshold.

Hence, several researchers have modified these biopolymers into nanosize for better encapsulation in hydrophobic polymers.

1.4 Nanocomposites of natural rubber

Recently there is considerable interest in polymer composites having rigid particles, with at least one dimension in the nanometer range, as fillers. This class of materials which has attracted the attention of academicians as well as industrialists is known as 'Nanocomposites'.

1.4.1 Advantages of nanofillers

Nanofillers have strong reinforcing effects, and studies have also shown their positive impact in barrier packaging. The pioneer work on nanocomposites that was initiated by researchers at Toyota in the early 1990′s created nanoclay reinforced polymers, opening a new research path on composites. Due to their nanometric size effect, these composites have some unique properties Nanoparticles (fillers) not only enhance mechanical properties, but also physical properties. Their properties depend on the nature and effectiveness of interactions at the interfacial region, that is, on both the surface area and the dispersion of the particles. The surface area depends on the dimensions of the dispersed particles from 0.5 to 250 g/m2 for natural fibers and up to 1000 g/m^2 for cellulose nanofibrils, exfoliated clays, and carbon nanotubes [60].

1.4.2 Classification of nanoparticles

One of the most wide sprayed classifications of nanoparticles is based on particle shape:

(i) Particulate nanoparticles, such as metallic nanoparticles or carbon black are generally iso-dimensional and show moderate reinforcement due to their low aspect ratio. They are used to enhance resistance to flammability and decrease permeability or costs.

(ii) Elongated particles that show better mechanical properties due to their high aspect ratio. Such particles include cellulose nanofibrils (also called whiskers or nanocrystals) and carbon nanotubes.

(iii) Layered particles, like nanoclays, also referred to as layered polymer nanocomposites. This latter family is the most used industrially and can show different degrees of dispersion, as shown in Figure. 1.9, namely, intercalated nanocomposites (intercalated polymer chains between layered nanocomposites), exfoliated nanocomposites (separation of individual layers), and flocculated or phase-separated nanocomposites, which are also called microcomposites and consequently show the poorer physical properties. Exfoliation is sought by nanocomposite

producers as it gives, by far, the best results. In light of reviewed classifications for fillers, biopolymer nanocrystals fit the last category, "layered particles".

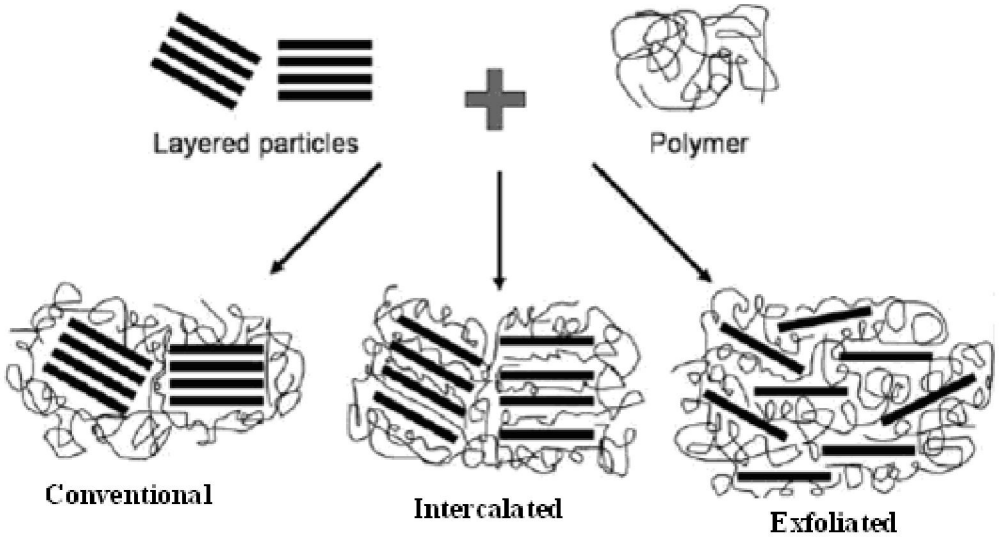

Figure. 1.9 Schematic representation of three types of polymer composites

1.4.3 Natural rubber/clay nanocomposites

Polymer matrix/clay-based nanocomposites have largely dominated the polymer literature [61,62,63,64,65], since their first applications as reinforcement in the automotive industry. The packaging industry has focused its attention mainly on layered inorganic solids like clays and silicates due to their availability, significant enhancement, and relatively simple processability [66]. Several studies have reported the effectiveness of nanoclay to decrease water vapor [67,68,69] and oxygen permeabilities [70,71,72] and improve mechanical properties. Attention has been more recently directed toward organic and renewable fillers. The use of clay minerals such as montmorillonite (MMT) [73,74] and organoclays [75,76,77] has also been extended to NR, and they seem to be a potential substitute to carbon black. Hrachova et.al., [78] studied the effect of MMT modification on mechanical properties of vulcanized natural rubber composites and found out that the mechanical properties improved by addition of MMT to natural rubber. Usuki et al.,. [79,80] first reported the superior nylon 6 MMT nanocomposites, polymer-layered silicate nanocomposites have attracted great interest from researchers due to their academic and industrial importance [81,82]. The special structure of MMT play

important roles in improving mechanical, thermal and diffuse barrier properties of polymer-layered silicate nanocomposites [83,84,85]. Many polymer matrices have been used to prepare polymer-MMT nanocomposites (such as polyimide, polyurethane, polypropylene, polyanilene) [86,87,88,89,90]. Due to poor compatibility of MMT with organic monomers and polymer matrices, it is necessary to modify MMT. At, present, alkylammonium and alkylphosphonium are used widely to treat MMT [91,92]. To further improve the properties of polymer-clay nanocomposites, alternate functional modifiers are being used to prepare polymer-clay nanocomposites [93,94,95,96].

Single-walled carbon nanotubes (SWNTs) have been widely used with different kinds of polymers. Some work has been done on incorporating the SWNTs in rubber. The concept of nano-sized filler-reinforced elastomer was demonstrated by the incorporation of nanoparticles in a rubbery polymer matrix such as SWNTs into silicone rubber [97]. Although rubbers are known to be a thermal and electrical insulator, incorporation of conductive fillers into these materials could produce composite materials with some electrical conductivity. The interest in ceramic particle reinforced composites has begun a decade ago. SiC nanoparticles have become popular recently as the reinforcement phase for polymer or ceramic matrices [98,99,100,101]. In the last few years, SiC has attracted more interest due to its desirable properties for potential applications as semiconductor devices [102]. Niihara [103] has reported that nano-sized (20-300 nm) ceramic composites provided considerably higher fracture toughness and strength than conventional ceramic composite. K.Kueseng and K.I.Jacob [104] studied the natural rubber nanocomposites with SiC nanoparticles and carbon nanotubes.

1.5 Bionanocomposites of natural rubber

Bionanocomposites are novel materials born out of the growing interest in nanomaterials and in the development of materials derived from renewable sources [105]. Polysaccharide such as starch, cellulose and chitin are potential renewable sources of nanosized reinforcements. The use of starch is receiving significant attention because of the abundant availability of starch, low cost, renewability, biocompatibility, biodegradation and non-toxicity [106].

1.5.1 Polysaccharide nanoparticles

Among the biopolymers cellulose NPs were used first as reinforcing phase by Favier et al., in 1995 [107], new nanocomposites materials with original properties were obtained using cellulose whiskers and micro fibrillated cellulose and led to the development of studies on chitin whiskers [108, 109, 110] and starch nanocrystals [111, 112, 113, 114, 115] by analogy. In comparison to nanoclay, studies on these bionanofillers are scarce.

1.5.2 Preparation of starch nanocrystal

Structure of starch

Starch occurs as a flour-like white powder insoluble in cold water. This powder consists of microscopic granules with diameters ranging from 2 to 100 μm, depending on the botanic origin, and with a density of 1.5 [116]. Starch structure has been under research for years, and because of its complexity, a universally accepted model is still lacking. However, in this past decade a model seems predominant. It is a multiscale structure, shown in Figure 1.10.

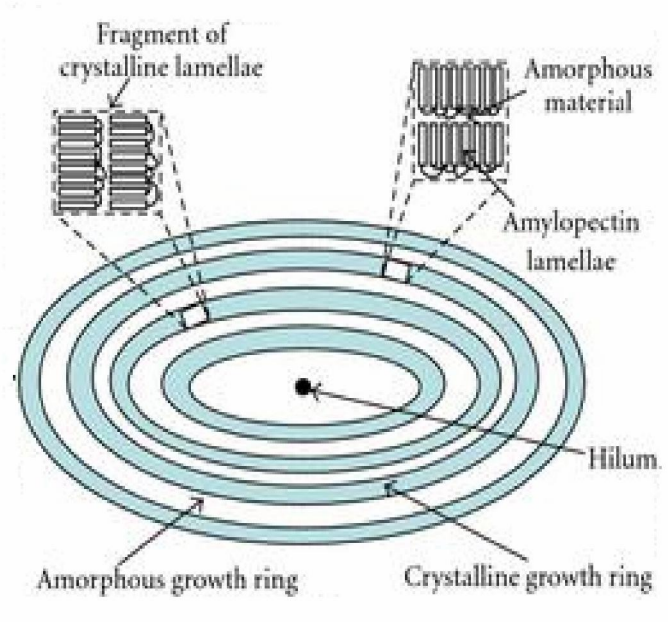

Figure. 1.10 Multiscale structure of starch

Many interesting reviews and articles on structure of starch have been published. Starch's composition was first determined by studying the residue of its total acid hydrolysis. As discussed earlier it consists of mainly two glycosidic macromolecules amylopectin and amylose. Minor components associated with starch granules are of three types:

(i) cell-wall fragments,

(ii) surface components, and

(iii) internal components.

The main constituents of surface components are proteins, enzymes, amino acids, and nucleic acids, whereas internal components are composed mainly of lipids. The proportion of these components depends on the botanical origin.

An X-ray diffraction study showed that starch is a semicrystalline polymer [117]. Starch granules consist of concentric alternating amorphous and semicrystalline growth rings. They grow by apposition from the hilum of the granule. The number and thickness of these layers depends on the botanical origin of starch. They are thought to be 120-400 nm thick. Details on the structure of the amorphous growth ring are not found in literature.

More recently SEM observations have enabled the observation of blocklets structure [118,119,120]. Although the blocklet concept is not commonly mentioned in the literature, it was heavily supported and brought back to discussion by Gallant et al.,. [121]. They suggested that both semicrystalline and amorphous growth rings are subdivided into respectively large (diameter 20-500 nm for wheat) and small (25 nm) spherical blocklets. More recently, Tang et al., [122] supposed the blocklets of the amorphous region and the surface pores (as mentioned earlier) to be defective blocklets, with lower branching molecules. On average, two endto- end blocklets would constitute a single semicrystalline growth ring. These blocklets have an average size of 100 nm in diameter and are proposed to contain 280 amylopectin side chain clusters [123]. Schematically, the semicrystalline growth rings consist of a stack of repeated crystalline and amorphous lamellae. The thickness of the combined layers is 9 nm regardless the botanic origin [124]. In reality, it is believed that the crystalline region is created by the interwining of chains with a linear length above 10 glucose units to form double helixes [125] that are packed and form the crystallites, and the amorphous region corresponds to branching points.

Tang et al., [107] illustrated this model, making amylopectin the backbone of the blocklet structure. Amylose molecules are thought to occur in the granule as individual molecules, randomly interspersed among amylopectin molecules and in close proximity with one another, in both the crystalline and amorphous regions [92]. Depending on the botanic origin of starch, amylose is preferably found in the amorphous region (e.g., wheat starch), interspersed among amylopectin clusters in both the amorphous and the crystalline regions (e.g., normal maize starch), in bundles between amylopectin clusters, or cocrystallized with amylopectin (e.g., potato starch) [126].

Native starches contain between 15 and 45% of crystalline material. Depending on their X-ray diffraction pattern, starches are categorized in three crystalline types called A, B, and C. Hizukuri et al., [127,128] postulated that amylopectin chain length was a determining factor for crystalline polymorphism. Imberty et al., [129,130] proposed a model for the double helices packing configuration to explain difference between A and B types starches. A-type structures are closely packed with water molecules between each double helical structure, whereas B-types are more open and water molecules are located in the central cavity formed by six double helices, as shown in Figure.1.11. It was later envisaged that branching patterns of the different types of starch may also differ [131]. It was suggested that the B-type amylopectin branching points are clustered, forming a smaller amorphous lamella, whereas A-type amylopectin branching points are scattered in both the amorphous and the crystalline regions, giving more flexibility to double helixes to pack closely. Gerard et al., [132] recently confirmed that the distance between two α-(1-6) linkages and the branching density inside each cluster are determining factors for the development of crystallinity in starch granules. Clusters with numerous short chains and short linkage distance produce densely packed structures which crystallizes into the A allomorphic type. Longer chains and distances lead to a B-type. The C-type starch pattern has been considered to be a mixture of both A- and B-types because its X-ray diffraction pattern can be resolved as a combination of the previous two. It has been suggested by Bogracheva et al., [133] that C-type starch granules contain both types of polymorph: the B-type at the center of the granule and the A-type at the surrounding.

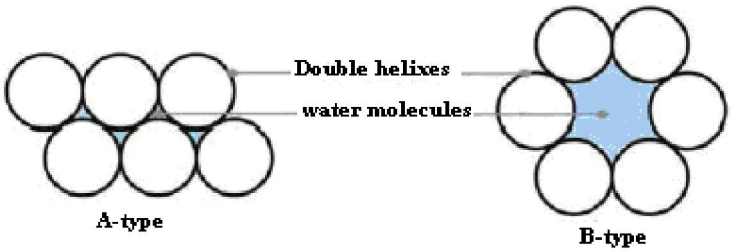

Figure. 1.11 Double helixes packing configuration of starch according to crystalline type.

Several attempts of structural characterization of C-type starch were conducted using acid hydrolysis by Wang et al., [134,135]. They revealed that the core part of C-type starch was preferably hydrolyzed and that hydrolyzed starch showed an A-type diffraction pattern, suggesting that B-type polymorphs consists of mainly the amorphous regions and are more readily hydrolyzed than A-types constituting mainly the crystalline region. This is in agreement with the previous conclusions of Jane et al., [98] that B-type starches are more acid-resistant than A-types. These conclusions are of importance for starch nanocrystal production. Another V-type was also identified as the result of amylase being complexed with other substances such as iodine, fatty acid, emulsifiers, or butanol. This crystalline form is characterized by a simple left helix with six glucose units per turn [136]. Jenkins and Donalds [137] concluded that an increase in amylose content has the effect of increasing the size of the crystalline lamella and acts to disrupt their packing. Two mechanisms to explain this disrupting have been introduced: first, cocrystallization between amylose and amylopectin chains and, second, the penetration of amylose into amorphous regions.

Synthesis of polysaccharide nanoparticles such as starch and cellulose is carried out using acid hydrolysis. Various strong acids such as sulfuric acid, hydrochloric acid, phosphoric acid were employed to polysaccharide for acid hydrolysis.

First interest in starch nanocrystals has been studied by analogy with cellulose whiskers to be used as reinforcing fillers in a matrix. In 1996, Dufresne et al., [138] reported a method for producing “microcrystalline starch” and which they reported to be agglomerated particles of a few tens of nanometers in diameter. The procedure consisted of hydrolyzing starch (5 wt %) in a 2.2 N HCl suspension for 15 days. Because it was

shown that classical models for polymers containing spherical particles could not explain the reinforcing effect of microcrystals, further studies on the morphology of these microcrystals were conducted by Dufresne and Cavaille in light of aggregate formation and percolation concept [139]. In 2003, Putaux et al., [140] revealed the morphology of "nanocrystals resulting from the disruption of the waxy maize starch granules by acid hydrolysis". After 6 weeks of hydrolysis, TEM observations (Figure. 1.12) showed (a) a longitudinal view of lamellar fragments consisting of a stack of elongated elements with a width of 5-7 nm and (b) a planar view of an individualized platelet after hydrolysis. Shapes and lateral dimensions were derived from the observation of individual platelets in planar view: a marked 60-65 °C acute angles for parallelepipedal blocks with a length of 20-40 nm and a width of 15-30 nm. However, more recent publications report bigger starch nanocrystals (40-70 nm for potato starch nanocrystals; [141,142] and 60-150 nm [143,144] for pea starch nanocrystals; and 50 [145] and 70-100 nm [146] for waxy starch nanocrystals), with round edges [147] and found as grape-like aggregates of 1-5 μm. The heterogeneity in particle size could be explained by the differences in starch types and also by the difficulty to obtain well-defined pictures of non-aggregated nanocrystals.

Acid hydrolysis has been used for a long time to modify starch and its properties. Nageli [148] reported low molecular weight acid-resistant fraction after the hydrolysis of potato starch at room temperature in a 15% H_2SO_4 suspension for 30 days. The fraction would be known as Nageli amylodextrin. Lintner [149] also gave his name to a hydrolysis process consisting of a 7.5% (w/v) HCl suspension of potato starch at 30-40 °C to produce a high molecular weight starch suspension called "lintnerized starch".

Only a few studies have reported the use of acid hydrolysis to produce microcrystalline starch [150] and starch nanocrystals [151]. For all starches, a two-stage hydrolysis profile can be evidenced, namely, an initial fast hydrolysis step, presumably due to the hydrolysis of the amorphous regions of starch granules, and a second slower step, presumably due to the hydrolysis of the crystalline regions [152,153]. Some authors distinguish three steps of hydrolysis: a rapid one, a slow one, and a very slow one, [154] presumably corresponding to the hydrolysis of amorphous layers, semicrystalline layers and crystalline ones, respectively. There are two common hypotheses to account for the slower hydrolysis rate of the crystalline domain. The first one is that the dense packing of

starch in the crystalline regions does not readily allow the penetration of H_3O^+ [117]. The second one is that the hydrolysis of the glucosidic bonds requires a change in conformation from chair to halfchair [155].

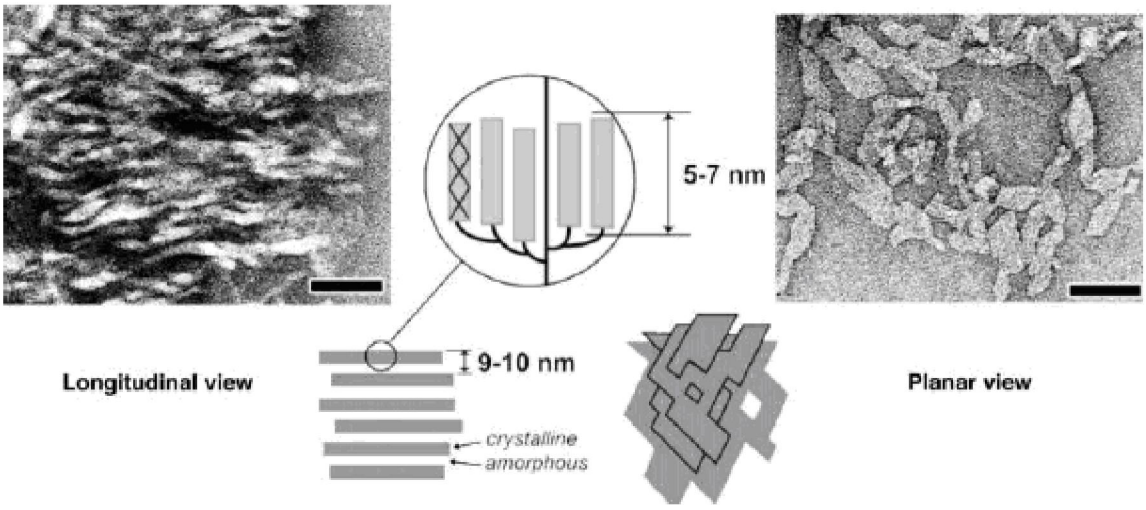

Figure.1.12 TEM of starch nanocrystals: longitudinal view and planar view.

The obvious factors influencing hydrolysis kinetics are time, acid type, acid concentration, and temperature. The influence of acid and starch type has been studied extensively by various researchers [156,157,158,159]. They showed, through different characterization techniques (alkali fluidity number, number average molecular weight, intrinsic viscosity) that, for the same equal normalities, HCl and HNO_3 gave the highest thinning effect followed respectively by H_2SO_4 and H_3PO_4. Angellier et al., [160] also obtained a lower yield of hydrolysis with H_2SO_4 compared to HCl for the production of nanocrystals but showed that final suspensions were more stable with H_2SO_4 due to the presence of sulfate groups at the surface. The difference in the rate and yield of hydrolysis among starch types was attributed to the difference in granule sizes and number of pores on the granule surface [146]. Jayakody and Hoover studied further the susceptibility of different cereal starches to hydrolysis [161]. Roughly, the extent of hydrolysis was more pronounced in waxy maize than in oat, rice, normal maize, amylomaize V (50-60% amylose), and amylomaize VII (70% amylose) starches. They concluded that (i) the first stage of hydrolysis (amorphous regions) is influenced by the

granule size, pores on the surface, amylase content, and the amount of lipid-complexed amylose chains and (ii) the second step of hydrolysis (crystalline region) is influenced by the amylopectin content, mode of distribution of R(1-6) branches between the amorphous and the crystalline regions, and degree of packing of the double helices within the crystallites (i.e., the parameters also influencing crystallinity). Wang et al., [162] observed as expected that the rate of hydrolysis increased when increasing the concentration of acid while the temperature was kept constant at 50 °C. Angellier et al., [146] in the intent of producing starch nanocrystals studied the influence of these parameters using a surface response methodology. They concluded that both the acid concentration and the temperature should not be too high: acid concentration was kept at 3.16 M and the temperature was kept at 40 °C. However, techniques for following the extent of hydrolysis are numerous.

The use of acid hydrolysis and even though a variety of starch sources has been used, they all refer to the same two processes: (1) Dufresne et al., process using HCl as previously discussed [163] and (2) Angellier et al., optimized the process using H_2SO_4, [128].

In most recent studies, new processes have been tried out to produce starch nanoparticles by (i) precipitation of amorphous starch by Ma et al., [164] and Tan et al., [165] (ii) combining complex formation and enzymatic hydrolysis by Kim and Lim, [166] yielding nanocrystals (ie. complexed with lipids), and (iii) microfluidization by Liu et al., [167]. It is worth noting that such starch nanoparticles are following totally different strategies than starch nanocrystals as described in Figure. 1.13. Consequently, ensuing nanoparticles have different properties, crystallinity, and shape.

Ma et al., [132] prepared starch nanoparticles by precipitating a starch solution within ethanol as the precipitant. However, this process for producing starch nanoparticles does not allow producing nanocrystals. Kim and Lim studied alternative ways to obtain starch nanoparticles [134]. They proposed a process for preparing nanoscale starch particles by complex formation with other components. Experiments were conducted with *n*-butanol. However, the complex contained a large portion of amorphous matrix so that its selective removal by enzymatic hydrolysis was needed. The disadvantage of this method is that most of the starch was hydrolyzed (85-90%) and the resulting yield of the nanoparticles

was extremely low. Starch nanoparticles obtained by this method display a spherical or oval shape, with diameters in the range of 10-20 nm.

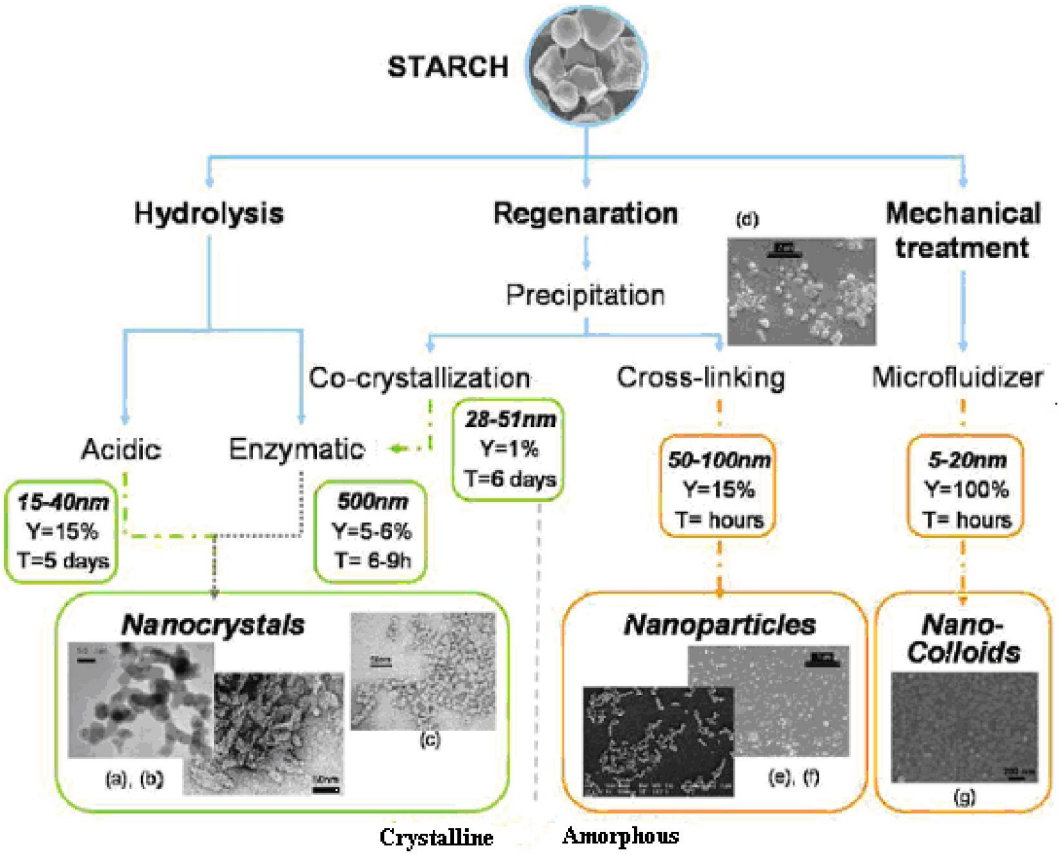

Figure. 1.13 Different approaches of producing crystalline and amorphous starch nanoparticles

Liu et al., carried out a method in which 5% slurry of high amylose corn starch was run through a Microfluidizer for several passes (up to 30) [135]. The particle size of the samples obtained from more than 10 passes was below 100 nm and the gel-like suspension remained stable for more than a month. The thermal stability was not affected, and because no chemical or thermal degradation occurred during the treatment, the reported yield was almost 100%. However, in this method the resultant starch colloids were obtained from breaking down both amorphous and crystalline domains, rendering an amorphous diffraction pattern after 10 passes.

1.5.3 Preparation of cellulose nanocrystals

Structure of cellulose

Cellulose constitutes the most abundant renewable polymer resource available today. As a chemical raw material, it is generally well-known that it has been used in the form of fibers or derivatives for nearly 150 years for a wide spectrum of products and materials in daily life. What has not been known until relatively recently is that when cellulose fibers are subjected to acid hydrolysis, the fibers yield defect-free, rod-like crystalline residues. Cellulose nanocrystals have garnered in the materials community a tremendous level of attention that does not appear to be relenting. These biopolymeric assemblies warrant such attention not only because of their unsurpassed quintessential physical and chemical properties (as will become evident in the review) but also because of their inherent renewability and sustainability in addition to their abundance. They have been the subject of a wide array of research efforts as reinforcing agents in nanocomposites due to their low cost, light weight, nanoscale dimension, and unique morphology. Surprisingly, a focus on nanoscale phenomena involving these materials has not been realized until the past few years in which a virtual collection of information has become available.

In nature, cellulose does not occur as an isolated individual molecule, but it is found as assemblies of individual cellulose chain-forming fibers. This is because cellulose is synthesized as individual molecules, which undergo spinning in a hierarchical order at the site of biosynthesis. Typically, approximately 36 individual cellulose molecules assemble into larger units known as elementary fibrils (protofibrils), which pack into larger units called microfibrils, and these are in turn assembled into the familiar cellulose fibers. However, celluloses from different sources may occur in different packing as dictated by the biosynthesis conditions.

In the 1950s, Ranby reported for the first time that colloidal suspensions of cellulose can be obtained by controlled sulfuric acid-catalyzed degradation of cellulose fibers [168, 169,170]. This work was inspired by the studies of Nickerson and Habrle [171 61] who observed that the degradation induced by boiling cellulose fibers in acidic solution reached a limit after a certain time of treatment. Transmission electron microscopy

(TEM) images of dried suspensions revealed for the first time the presence of aggregates of needle-shaped particles, while further analyses of these rods with electron diffraction demonstrated that they had the same crystalline structure as the original fibers [172,173]. Simultaneously, the development by Battista [174,175] [of the hydrochloric acid-assisted degradation of cellulose fibers derived from high-quality wood pulps, followed by sonification treatment, led to the commercialization of microcrystalline cellulose (microcrystalline cellulose). Stable, chemically inactive, and physiologically inert with attractive binding properties, microcrystalline cellulose offered a significant opportunity for multiple uses in pharmaceutical industry as a tablet binder, in food applications as a texturizing agent and fat replacer, and also, as an additive in paper and composites applications. After the acid hydrolysis conditions were optimized, Marchessault et al., [176] demonstrated that colloidal suspensions of cellulose nanocrystals exhibited nematic liquid crystalline alignment. Since the discovery of spectacular improvements in the mechanical properties of nanocomposites with cellulose nanocrystals, [177,178] substantial research has been directed to cellulose nanocrystal composites because of the growing interest in fabricating materials from renewable resources.

The main process for the isolation of cellulose nanocrystals from cellulose fibers is based on acid hydrolysis. Disordered or paracrystalline regions of cellulose are preferentially hydrolyzed, whereas crystalline regions that have a higher resistance to acid attack remain intact [179,180]. Thus, following an acid treatment that hydrolyzes the cellulose rod-like nanocrystals are produced. The obtained cellulose nanocrystals have a morphology and crystallinity similar to the original cellulose fibers; examples of such elements are given in Figure. 1.14. The actual occurrence of the acid cleavage event is attributed to differences in the kinetics of hydrolysis between amorphous and crystalline domains. In general, acid hydrolysis of native cellulose induces a rapid decrease in its degree of polymerization (DP), to the so-called level-off DP (LODP). The DP subsequently decreases much more slowly, even during prolonged hydrolysis [146,181]. LODP has been thought to correlate with crystal sizes along the longitudinal direction of cellulose chains present in the original cellulose before the acid hydrolysis. This hypothesis was based on the reasonable assumption that disordered or para-crystalline domains are regularly distributed along the microfibers and therefore they are more

susceptible to acid attack (in contrast to crystalline regions that are more impervious to attack). Also, homogeneous crystallites were supposed to be generated after acid hydrolysis. These assumptions were actually confirmed by X-ray crystal diffraction [182] electron microscopy with iodine-staining, small-angle X-ray diffraction, and neutron diffraction analyses [183]. Contrary to cellulose nanocrystals, starch nanocrystals are not almost 100% crystalline, but rather 45% crystalline, with variations depending on the botanic origin, as recently presented by Le Corre et al., [184]. Typical procedures currently employed for the production of cellulose nanocrystals consist of subjecting pure cellulosic material to strong acid hydrolysis under strictly controlled conditions of temperature, agitation, and time. The nature of the acid and the acid-to-cellulosic fibers ratio are also important parameters that affect the preparation of cellulose nanocrystals. A resulting suspension is subsequently diluted with water and washed with successive centrifugations.

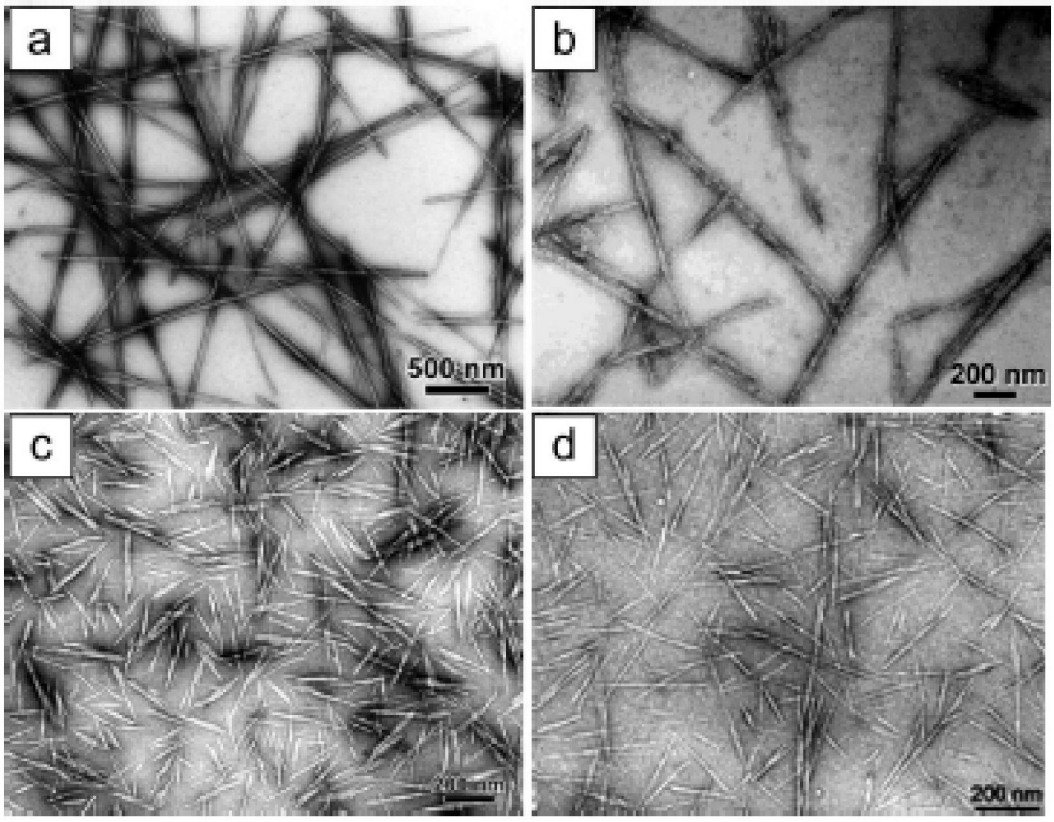

Figure. 1.14 TEM images of dried dispersion of cellulose nanocrystals derived from (a) tunicate (b) bacterial (c) ramie and (d) sisal.

Specific hydrolysis and separation protocols have been developed that depend on the origin of the cellulosic fibers. Most common sources include among others, cellulose fibers from cotton [185,186] ramie [187,188,189] hemp [190], flax [191,192], sisal [193,194], wheat straw [195], palm [196], bleached softwood [197] and hardwood [198] pulps, cotton linters pulp [199,200], microcrystalline cellulose [201], sugar beet pulp [202], bacterial cellulose [203], jute and Tunicates [204]. Similar to preparation of starch nanocrystals here also sulfuric and hydrochloric acids have been extensively used for cellulose nanocrystals preparation. Other acids such as phosphoric [205] and hydrobromic [206] have also been reported for such purposes. If the cellulose nanocrystals are prepared by hydrolysis in hydrochloric acid, their ability to disperse is limited and their aqueous suspensions tend to flocculate [207]. On the other hand, when sulfuric acid is used as a hydrolyzing agent, it reacts with the surface hydroxyl groups of cellulose to yield charged surface sulfate esters that promote dispersion of the cellulose nanocrystals in water [208]. However, the introduction of charged sulfate groups compromises the thermostability of the nanocrystals [209]. Also, differences in the rheological behavior have been shown between suspensions obtained from sulfuric acid hydrolysis and those obtained from hydrochloric acid. In fact, the sulfuric acid treated suspension has shown no time-dependent viscosity, whereas the hydrochloric acid-treated suspension showed a thixotropic behavior at concentrations above 0.5% (w/v) and antithixotropic behavior at concentrations below 0.3% [178]. Post-treatment of cellulose nanocrystals generated by hydrochloric acid hydrolysis with sulfuric acid has been studied to introduce, in a controlled fashion, sulfate moieties on their surfaces. Cellulose nanocrystals generated from hydrochloric acid hydrolysis and then treated with sulfuric acid solution had the same particle size as those directly obtained from sulfuric acid hydrolysis; however, the surface charge density could be tuned to given values by sulfuric acid hydrolysis. With respect to the morphology of the particles, a combination of both sulfuric and hydrochloric acids during hydrolysis steps appears to generate spherical Cellulose nanocrystals instead of rod-like nanocrystals when carried out under ultrasonic treatment [210]. These spherical Cellulose nanocrystals demonstrated better thermal stability mainly because they possess fewer sulfate groups on their surfaces [211].

The concentration of sulfuric acid in hydrolysis reactions to obtain Cellulose nanocrystals does not vary much from a typical value of ca. 65% (wt); however, the temperature can range from room temperature up to 70 °C and the corresponding hydrolysis time can be varied depending upon the source of cellulose. In the case of hydrochloric acid-catalyzed hydrolysis, the reaction is usually carried out at reflux temperature and an acid concentration between 2.5 and 4 N with variable time of reaction depending on the source of the cellulosic material. Bondenson et al., [212] investigated optimizing the hydrolysis conditions by an experimental factorial design matrix (response surface methodology) using microcrystalline cellulose that was derived from Norway spruce (*Picea abies*) as the cellulosic starting material. The factors that were varied during the process were the concentrations of microcrystalline cellulose and sulfuric acid, the hydrolysis time and temperature, and the ultrasonic treatment time. The responses that were measured were the median size of the cellulose particles and the yield of the reaction. Prolongation of the hydrolysis time induced a decrease in nanocrystal length and an increase in surface charge [156]. Reaction time and acid-to-pulp ratio on nanocrystals obtained by sulfuric acid hydrolysis of bleached softwood (black spruce, *Picea mariana*) sulfite pulp was investigated by Beck-Candanedo et al., [169]. They reported that shorter nanoparticles with narrow size polydispersity were produced at longer hydrolysis times. Recently, Elazzouzi-Hafraoui et al., [213] studied the size distribution of Cellulose nanocrystals resulting from sulfuric acid hydrolysis of cotton treated with 65% sulfuric acid over 30 min at different temperatures, ranging from 45 to 72 °C. By increasing the temperature, they demonstrated that shorter crystals were obtained; however, no clear influence on the width of the crystal was revealed.

To the best of our knowledge, there are no commercial starch and cellulose nanocrystals available in the market. In fact, only two patents, in Chinese and from the same authors, dealing with starch nanocrystals have been found [214,215].

The aim of producing such polysaccharide nanocrystals or nanoparticles is to use them as fillers in polymeric matrices to improve their mechanical and barrier properties.

1.5.4 Polysaccharide nanocrystal reinforced polymers and their properties

After 2006, most work has been oriented towards the use of new environment-friendly polymers such as waterborne polyurethane [216] (WPU also called organic solvent free polyurethane), starch (waxy maize [217], cassava [218], pullulan [219] (obtained by starch fermentation), PLA [220] [65] polyvinyl alcohol (PVA), [221] and, most recently, soy protein isolate (SPI)[222] [66].

Processing.

There are various methods reported for the preparation of composites. Dufresne and Cavaille, [223] Angelier at al., [185] reported preparation of composite by hot pressing. Casting-evaporation was found out to be another approach for preparation of composites. From 2006 to present, authors have opted for a simpler casting-evaporation method at 40 °C for 24 h. Ma et al., [224] and Garcia et al., [225] prepared the composites of starch nanoparticles by casting-evaporation at 50 °C. Dufresne et al., [100] also prepared composites of natural rubber containing starch and cellulose nanocrystals by casting-evaporation method. Most recently, compression molding was used to prepare glycerol-plasticized starch nanocrystal composites at 120 °C from a freeze-dried powder [193].

Mechanical Properties

Using starch nanocrystals as a reinforcing phase in a polymeric matrix has been evaluated from a mechanical point of view both in the nonlinear (tensile test) and linear range (DMA). Dufresne and Cavaille [226] found that starch nanocrystals brought great reinforcing effect especially in the rubbery plateau region, that is, at temperatures higher than *T*g of the matrix. Later, this observation was confirmed by most authors.

The reinforcing effect of starch nanocrystals was evidence from tensile tests results. In most of the cases the introduction of nanofillers resulted in an increase in both the elastic modulus and the tensile strength of the composite together [227,228,229,230]. The reinforcement increased with the amount of nanofillers in most of the cases [202]. Whereas, increasing relative humidity was shown to have a strong negative impact on the reinforcing effect. Zheng et al., [231] reported an increase in strength and Young's modulus, together with a decrease in the elongation at break, at low pea starch

nanocrystal loading level (lower than 2 wt %) in a soy protein isolate (SPI) matrix. They attributed this result to a uniform dispersion. For higher content, the authors believe that nanocrystals gets self-aggregate which decreases the surface for interactions with the soy protein isolate matrix and destroys the ordered structure. This leads to a decrease of strength and modulus at 40 wt % filler content to values close to those obtained for the unfilled matrix. Another interesting reported phenomenon is the observation, for some composite, of a constant elongation at break with increasing filler content. Indeed, Wang and Zhang [232] reported the preparation of a high strength WPU-based elastomer reinforced with 1-5% waxy maize starch nanocrystals. Low filler content allowed better dispersion of the starch nanocrystals in the WPU matrix, allowing stronger interactions. The same observations have been made on NR/starch nanocrystals composites, by different authors, and for 5 and 30% starch nanocrystals from different botanic origins [233].

The reinforcing effect of starch nanocrystals is more significant in thermoplastic starch than in natural rubber. The higher reinforcing effect observed with the former matrix is assumed to result from strong interactions between the filler and amylopectin chains and a possible crystallization at the filler/ matrix interface [200]. Also, the reinforcing effect of starch nanocrystals within a thermoplastic starch matrix was higher than with tunicin or sugar cane bagasse cellulose whiskers [234]. An interesting and innovative approach to use polysaccharide nanocrystals as fillers is the investigation of a synergistic reinforcement of waterborne polyurethane by both starch nanocrystals and cellulose whiskers [235]. The authors attributed results to the formation of a new type of network allowed by strong hydrogen bondings interactions both between the nanofillers and between the nanofillers and the WPU matrix.

Reinforcing Effect

The literature is significantly lacking in a comprehensive explanation of the reinforcing mechanism of starch nanocrystals, contrary to cellulose nanocrystals, for instance. Similar to cellulose nanocrystals, the reinforcing effect of starch nanocrystals is generally ascribed to the formation of hydrogen bonded percolating filler network above a given starch content corresponding to the percolation threshold. However, this assumption is

difficult to prove because the connecting particles should be starch clusters or aggregates with ill-defined size and geometry [236]. This phenomenon should most probably affect the mechanical properties of the composites in the linear range. This percolation mechanism should depend on among other parameters the dimensions of the primary starch nanoparticles, the isolation process, processing method of nanocomposite films, and interactions with the polymeric matrix.

Water Uptake

Biopolymers change their dimensions with varying moisture content because the cell wall of polymers contain hydroxyl and other oxygen containing groups, which attract moisture through hydrogen bonding [237]. Their porous nature accounts for the large initial uptake at the capillary region. The hydroxyl group (-OH) in biopolymers build a large amount of hydrogen bonds between the macromolecules in the plant fibre cell wall. Subjecting the plant fibres to humidity causes the bonds to break. The hydroxyl group then forms new hydrogen bond with water molecules, which induce swelling [238]. The schematic representation of swelling process in cellulose is given in figure. 1.15.

The hydrophilic nature of these polysaccharide nanocrystals generally limits the formation of nanocomposites to water-soluble polymers only. In hydrophobic matrices repulsive forces lead to aggregation and poor interfacial contact. Though the approach leads to good filler dispersion, composites cannot be obtained by simply melt blending the filler with the polymer as desired in industrial processes.

Several authors have accessed water uptake of the composites containing polysaccharide nanocrystals. Dufresne and Cavaille reported that as the amount of starch nanocrystals increases the water uptake increases [118]. The unfilled natural rubber matrix displayed the lowest water uptake value, and the addition of starch nanocrystals induced an increase in water diffusivity [100]. The critical volume fraction of starch nanocrystals at the percolation is difficult to determine due to their heterogeneity and ill-defined geometry. Other authors preferred a conditioning technique, at different relative humidity, to assess the water sensitivity of films.

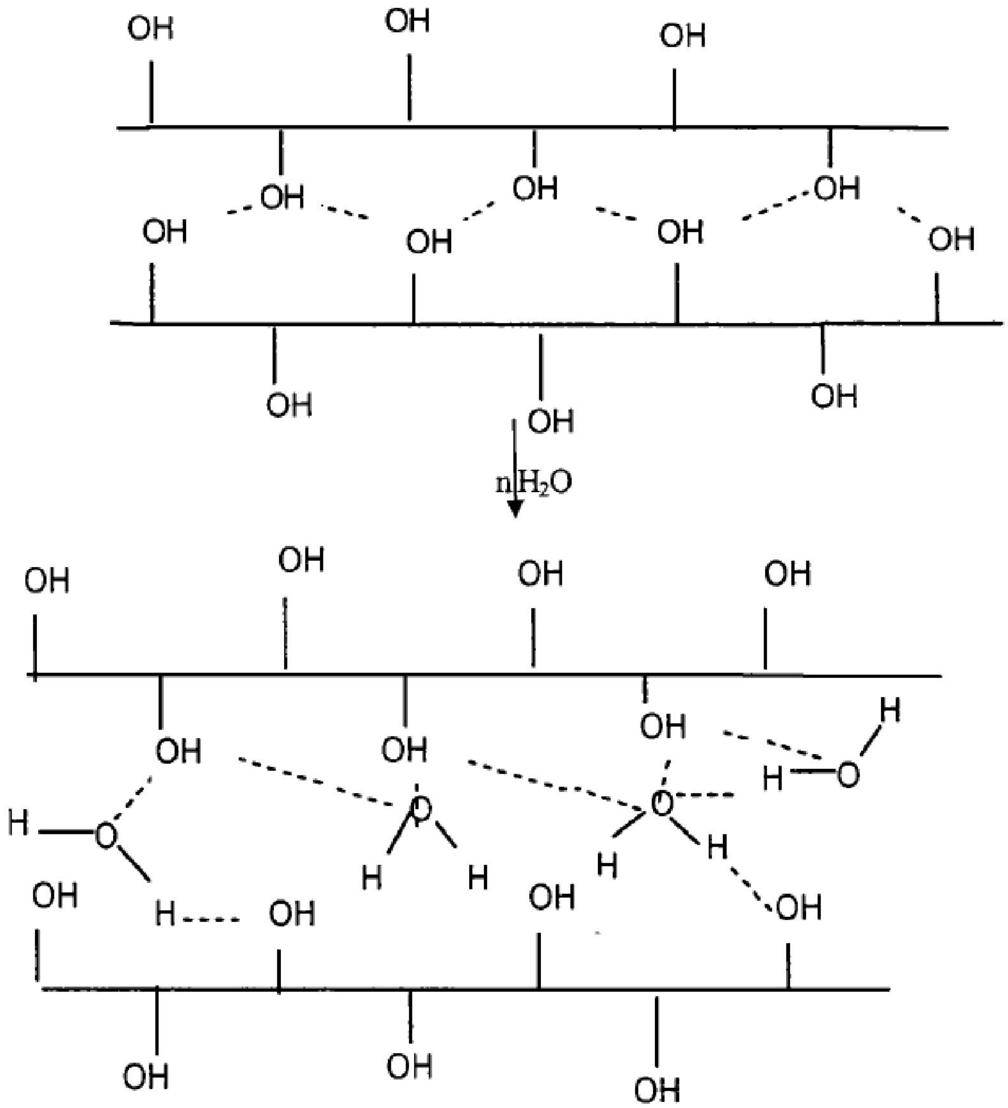

Figure.1.15 Schematic representation of the water absorption of cellulosic fibres

1.6 Modification of polysaccharide nanoparticles

For the processing of composite materials, starch and cellulose nanocrystals are used in the form of aqueous suspensions and the matrices are latexes. To disperse starch nanocrystals in nonpolar solvent surfactant was used [239,240]. However, a large amount of the surfactant is needed to maintain the stability of the suspension. Such a drawback hinders the use of this technique for composites processing in organic solvents [241]. Therefore, physical or chemical modifications on polysaccharide nanocrystals have been extensively studied, among which the surface chemical modification is a sound approach and a lot of relevant research work has been done [242]. In the past years, it has been

reported that some polymers such as poly(tetrahydrofuran), poly(propylene glycol) momobutyl ether, poly(carprolactone) and poly(styrene) [243] were used to chemically modify the properties of starch nanocrystals. However, the polymer modified starch nanocrystals aggregation still exists and the solubility with organic solutions is not satisfactory. Starch nanocrystals with short grafting agents was also reported [244], but the grafting extent is not sufficient to induce a partial solubilization of starch molecules located at the surface of the nanocrystals. Heterogeneous esterification of polysaccharide nanofibres with organic acids usually resulted in significant bulk modification, characterised by loss of crystallinity and high degree of substitutions [245]. Cellulose has also been esterified homogeneously in ionic liquids to produce cellulose acetate but the crystal structure of modified cellulose once regenerated is destroyed [246]. By restricting the modification only to the surface of cellulose nanofibres, the highly crystalline bulk structure of cellulose can be retained, while the surface is rendered hydrophobic.

The mechanical properties of natural rubber filled with polysaccharide are dominated by many factors, such as the dispersing ability, the interfacial combination. As polysaccharide contain many hydroxyl groups with strong polarity, its compatibility with NR is poor. Hence, the mechanical properties (elasticity and tear) of composite filled by direct loading of polysaccharide NPs will deteriorate. A large amount of work has been contributed to improve the mechanical properties of polysaccharide/NR composites. In the 1970s, Buchanan et al., prepared crosslinked starch xanthide–styrene butadiene rubber (SBR) master batches. It was demonstrated that crosslinked starch xanthide could improve the fatigue life and abrasion resistance, when used to partially replace carbon black in a premium tread [247,248]. Goodyear Company employed modified cornstarch which was called filler of biological polymer to partly replace traditional fillers like black carbon or white carbon to improve the properties of tyres. Those tyres reinforced with cornstarch possess many advantages, such as light quality, low rolling resistance, low noise and low emission of carbon dioxide [249]. Rouilly et al., [250] prepared the composite by blending dimethylaminoethyl methacrylate grafted latex and starch. Nakason et al., [251] synthesized grafted copolymer by grafting NR with methyl methacrylate, and then blending the copolymer with NR and cassava starch. The results

showed that the induction period of cure of the composite decreased with the increase of cassava starch loading.

There is no doubt that, polysaccharide nanocrystals are promising fillers. This field is at the moment much less reported in the literature. It is worth noting that the main interest of starch in addition to a low cost is that the raw material is relatively pure. This point is important to broaden their further application, and there are significant scientific and technological challenges to take up.

Based on the above discussions our broad objectives were:

- To investigate the performance of polysaccharides as green reinforcing agents and substitutes for carbon black in natural rubber.
- To improve the reinforcing ability of polysaccharides through chemical modification and hence to synthesise hydrophobic nanofillers.
- Synthesis and characterization of bionanocomposites of natural rubber reinforced with nanosized polysaccharide derivatives and compare their performance with conventional composites.
- To develop bionanocomposites of natural rubber with high filler loading.
- To explore other possible applications of nanosized polysaccharide derivatives.

1.7 References

1. Encyclopedia of Polymer Science Engineering, H.F. Mark Edition, John Wiley and Sons, New York. **1985,** 145.
2. F. L. Matthews, R. D. Rawlings. Composite Materials: Engineering and Science, Chapman & Hall, London, **1994,** 278.
3. Y. Zhang, S. Ge, B. Tang, T. Koga, M. H. Rafailovich, J. C. Sokolov, D. G. Peiffer, Z. Li, A. J. Dias, K. O. McElrath, M. Y. Lin, S. K. Satija, S. G. Urquhart, H. D. Ade, *Macromolecules*, **2001**, 43, 7056.
4. N. G. McCrum, C. P. Buckley, C. B.Bucknall. Principles of Polymer Engineering, 2nd Ed., Oxford University Press, New York, **1997**, 242.
5. T. Richardson. *Composites-a design guide,* Industrial Press Inc., 200 Madison Avenue, Newyork, **1987**.
6. S.B. Warner. Fibre Science., Prentice Hall, Engle wood Cliffs, New Jersey, **1995**.
7. P.K. Mallick. *Fibre reinforced composite materials, manufacturing and design.,* Marcel Dekker, Inc., Newyork **1988,** p.I8
8. Burns, Bill. "The Gutta Percha Company". History of the Atlantic Cable & Undersea Communications, **2009.**
9. M. Valodkar, S. Thakore, *J. Appl. Polym. Sci.* **2012**, 124, 3815.
10. M. T. Rameshan, T. K. Manoj Kumar, R. Alex, B. Kuriakose, *J. Mater. Sci.* **2002,** 37, 109.
11. H. Ohishi, *J. Appl. Polym. Sci.,* **2004,** 93, 1567.
12. A. K. Ghosh, S. Maiti, B. Adhikari, G. S. Ray, S. K. Mustafi, *J. Appl. Polym. Sci.*, **1997**, 66, 683.
13. X. Liu, S. Zhao, Y. Yang, X. Zhang, Y. Wu, *Polym. Adv. Technol.*, **2009**, 20, 818.
14. Y. Liu, L. Li, Q. Wang, *J. Appl. Polym. Sci.* **2010**, 118, 1111.
15. N. Rattanasom, T. Saowapark, C. Deeprasertkul, *Polym. Test.*, **2007**, 26, 369.
16. N. Sambatsompop, S. Thongsang, T. Markpin, E. Wimolmala, *J. Appl. Polym. Sci.*, **2004**, 93, 2119.
17. N. V. David, X.-L. Gao, J. Q. Zheng, *Mech. Adv. Mater. Struct.* **2010**, 17, 246.

18. A. I. Medalia, G. Kraus, In: Science and Technology of Rubber, Eds., Mark J. E., Erman, B. and Eirich R. F., Academic Press, New York, **1994,** 387.
19. Kraus, G., In: Reinforcement of Elastomers, Editor, Kraus, G., Interscience Publishers, John Wiley & Sons, New York 1965, 329.
20. Werner Hofmann, In: Rubber Technology Handbook, Editor, Werner HofmarU1, Hanser Publishers, Munich, 1989, 284,.
21. M. J. Wilson, A Handbook of Determinative Methods in Clay Mineralogy; Blackie & Son Ltd: London, **1987**.
22. P. G. Rouxhet, N. Samudacheata, H. Jacobs, O. Anton, *Clay Miner,* **1977**, 12, 171.
23. A. L. G. Saad, S. El-Sabbagh, *J. Appl. Polym. Sci.*, **2001**, 79, 60.
24. N. Suma, R. Joseph, K. E. George, *J. Appl. Polym, Sci.*, **1993**, 49, 549.
25. N. Sombatsompop, *J. Appl. Polym. Sci,*, **1999**, 74, 1129.
26. S. H. Botros, A. M. Sayed, *J. Appl. Polym. Sci.*, **2001**, 82, 3052.
27. S. H. Botros, *Polm. Plast. Technol. Eng.*, **2002**, 41, 341.
28.W. Arayapranee, G. L. Rempel., *Int. J. Mater.Struct. Relia.*, **2007**, 5, 1.
29. N. Sombatsompop, C. Kumnuantip, Rheology, *J. Appl. Polym. Sci.*, **2003**, 87, 1723.
30. C. Kumnuantip, N. Sombatsompop, *Mater. Lett.*, **2003**, 57, 3167.
31. T. D. Sreeja, S. K. N. Kutty, *Polym. Plast. Technol. Eng.*, **2000**, 39, 501.
32. H. Ismail, S. Z. Salleh, Z. Ahmad, *Polym. Plast. Technol. Eng.*, **2011**, 50, 681.
33. S. J. Ahmadi, C. G'Sell, Y. Huang, N. Ren, A. Mohaddespour, J. M. Hiver, *Compos.* Sci. Technol., **2009**, 69, 2566.
34. P. A. Fowler, J. M. Hughes, R. M. Elias, *J. Sci, Food Agric.*, **2006**, 86, 1781.
35. S. J. Eichhorn, C. A. Baillie, N. Zafeiropoulos, L. Y.Mwaikambo, M. P. Ansell, A. Dufresne, K. M. Entwistle, P. J.Herrera-Franco, G. C. Escamilla, L. Groom, M. Hugues, C. Hill, T. G. Rials, P. M. Wild, *J. Mater. Sci.*, **2001**, 36, 2107.
36. S. Hill, Cars that grow on trees. New Scientist. **1997**, 36.
37. B. Dahlke, H. Larbig, H. D. Scherzer, R. Poltrock*, J. Cellular. Plast.*, **1998**, 34, 361.
38. A. S. Herrmann, J. Nickel, U. Riedel, *Polym. Degrad. Stab.*, **1998**, 59, 251.
39. M. Jacob, S. Thomas, K. T. Varughese, *Compos. Sci. Technol.*, **2004**, 64, 955.
40. H. Ismail, M. R. Edyham, B. Wirjosentono, *Polym. Test*, **2002**, 21, 139.

41 V. G. Geethamma, M. K. Thomas, R. Laxminarayan, S. Thomas, *Polymer*, **1998**, 39, 1483.

42. R. Tantatherdtam, K. Sriroth, J. Kasetsart, *Nat Sci.*, **2007**, 41, 279.

43. J. Johns, V. Rao, *Int. J. Polym. Anal. Charact.*, **2009**, 14, 508.

44. A. J. F. Carvalho, A. E. Job, N. Alves, A. A. S. Curvelo, A. Gandini, *Carbohyd.. Polym.*, **2003**, 53, 95.

45. J. Johns, V. Rao, *Int. J. Polym. Anal. Charact.*, **2008**, 13, 280.

46. R. M. B. Fernandes, L. L. Y. Visconte, R. C. R. Nunes, *Int. J. Polymer. Mater.*, **2011**, 60, 351.

47. H. U. Zaman, M. A. Khan, R. A. Khan, Md. D. H. Beg, *Int. J. Polymer. Mater.*, **2011**, 60, 303.

48. H. M. Da Dosta, L. L.Y. Visconte, R. C. R. Nunes, C. R. G. Furtado, *J. Appl. Polym. Sci.*, **2002**, 83, 2331.

49. P. Sae-oui, C. Rakdee, P. Tanmathorn, *J. Appl. Polym. Sci.*, **2002**, 83, 2485.

50. A. Bule´on, P. Colonna, V. Planchot, S. Ball, *Int. J. Biol. Macromol.*. **1998**, 23, 85.

51. R. L. Whistler, E. F. Paschall, Starch: Chemistry and Technology; Academic Press: New York, **1965**.

52. H. Angellier, L. Choisnard, S. Molina-Boisseau, P. Ozil,; A. Dufresne, *Biomacromolecules*, **2004**, 5, 1545.

53. A. Dufresne, Polymer nanocomposites from biological sources. Biopolymers Technology; Bertolini, A. C., Ed.; Cultura Acadeˆmica: Sao Paulo, **2007,** 59.

54. A. D. French, N. R. Bertoniere, R. M.Brown, H. Chanzy, D. Gray, K. Hattori, W. Glasser, In Kirk-Othmer Encyclopedia of Chemical Technology 5th ed.; Seidel, A., Ed.; John Wiley & Sons, Inc.: New York, **2004**.

55. Y. Habibi, L. A. Lucia, O. J. Rojas, *Chem. Rev. A.C.S.*, **2010**, 110, 3479.

56. D. Klemm, B. Heublein, H. P. Fink, A.Bohn, Angew. *Chem.* **2005**, 44, 3358.

57. R. H. Atalla, J. W. Brady, J. F. Matthews, S. Y. Ding, M. E. Himmel, *Biomass Recalcitrance*, **2008**, 188.

58. D. K. Singh, A. R. Ray, *J. Macromol Sci Rev Macromol. Chem. Phys.*, **2000**, 40, 69.

59 J. B. Zeng, Y. S. He, S. L. Li, Y. Z. Wang, Biomacromolecules, **2012**, 13, 1.

60. A. Dufresne, E. S. Meideiros, W. Orts, Starch-based nanocomposites. Starch: Characterization, Properties and Applications; Bertolini, A., Ed.; CRC Press: Rio de Janeiro, **2009,** 205.
61. R. Sengupta, S. Chakraborty, S. Bandyopadhyay, S. Dasgupta, R. Mukhopadhyay, K. Auddy, A. S. Deuri, *Polym. Eng. Sci*, **2007**, 47, 1956.
62. G. Choudalakis, A. D. Gotsis, *Eur. Polym. J.*, **2009**, 45, 967.
63. C. Lu, Y.-W. Mai, *Phys. Rev. Lett.*, **2005**, 95, 088303.
64. L. Peiyao, W. Li, S. Guojun, Y. Lanlan, Q. Feng, S. Liangdong, *J. Appl. Polym. Sci.*, **2008**, 109, 3831.
65. H. M. Wilhelm, M. R. Sierakowski, G. P. Souza, F. Wypych, *Carbohydr. Polym.*, **2003**, 52, 101.
66. H. M. C. Azeredo, d. *Food Res. Int.*, **2009**, 42, 1240.
67. J.-W. Rhim, P. K. W Ng, *Crit. Rev. Food Sci. Nutr.*, **2007**, 47, 411.
68. J.-W. Rhim, S.-I . Hong, C.-S. Ha, *Food Sci. Technol.*, **2009**, 42, 612.
69. A. Saxena, A. J. Ragauskas, *Carbohydr. Polym.*, **2009**, 78, 357.
70. G. Choudalakis, A. D. Gotsis*, Eur. Polym. J.*, **2009**, 45, 967.
71. C. Lu, Y.-W. Mai, *Phys. Rev. Lett.*, **2005**, 95, 088303.
72. C. Lu, Y.-W.Mai, *Compos. Sci. Technol.*, **2007**, 67, 2895.
73. Y. T. Vu, J. E. Mark, L. H. Pharm, M. Englebardt, *J. Appl. Polym. Sci.* **2001**, 82, 1391.
74. L. F. Valadares, C.A.P. Leite, F. Galembeck, *Polymer*, **2004**, 53, 406.
75. A.Okada, A. Usuki, T. Karauchi , O. Kamigaito , J. Mark , C. Lee , P. Bianconi, P. Eds, *ACS Symp. Ser.*, **1995**, 55.
76. J. T. Kim, T. S. Oh, D. H.Lee, *Polym. int.*, **2004**, 53, 406.
77 P. Bala, B. K. Samantaray, S. K. Srivastava, G. B. Nando, *J. Appl. Polym. Sci.* **2004**, 92, 3583.
78. J. Hrachova, P. Komadal, I. Chodak, *Journal of Material Science.*, **2007**, 43, 6.
79. A. Usuki, M. Kawasumi, Y. Kojima, A. Okada, T. Kurauchi, O. Kamigaito, *J. Matter. Res.*, **1993**, 8, 1174.

80. A. Usuki, Y. Kojima, M. Kawasumi, A. Okada, Y. Fukushima, T. Kurauchi, *J. Matter. Res.*, **1993**, 84, 1179.

81. M. Bohning, H. Goering, A. Fritz, K-W. Brzezinka, G. Turky, A. Schonhals, *Macromolecules,* **2005**, 38, 2764.

82. Y. S. Choi, H. T. Ham, I. J. Chung, *Chem. Mater*., **2004**, 16, 2522.

83. F. M. Uhi, S. P. Davuluri, S-C. Wong, D. C. Webster, *Chem. Mater*., **2004**, 16, 1135.

84. V. Krikorian, D. J. Pochan, *Macromolecules*, **2004**, 37, 6480.

85. D. J. Chaiko, A. A. Leyva, *Chem. Mater.*, **2005**, 17, 13.

86. M. O. Abdalla, D. Dean, S. Campbell, *Polymer*, **2002**, 43, 5887.

87. F. Gardebien, A. Gaudel-Siri, J-L. Bredas, R. Lazzaroni, *J. Phys. Chem. B*, **2004**, 108, 10678.

88. A. Somwangthanaroj, E. C. Lee, M. J. Solomon, *Macromolecules*, **2003**, 36, 2333.

89. W. J. Bao ,K. H. Kim, W. H. Jo, Y. H. Park, *Macromolecules*, **2004**, 37, 9850.

90. M. A. Osman, V. Mittal, M. Morbidelli, U. W. Suter, *Macromolecules*, **2003**, 36, 9851.

91. T.D. Fornes , D. L. Hunter, D. R. Paul, **2003**, 37, 1793.

92. J-M. Yeh, S-J Liou, C-Y. Lin, C-Y. Cheng, Y-W. Chang, *Chem. Mater.*, **2002**, 14, 154.

93. P. Vivile, R. Lazzaroni, E. Pollet, M. Alexandre, P. Dubois, *J. Am. Chem. Soc.* **2004**, 126, 9007.

94. X. Fan, C. Xia, R. C. Advincula, *Langmuir*, **2005**, 21, 2537.

95. N. N. Herrera, J-M. Letoffe, J-L. Putaux, L. David, E. Bourgeat-Lami, *Langmuir*, **2004**, 20, 1564.

96. T. K. Chen,Y. I. Tien, K. H. Wei, *Polymer*, **2000**, 41,1345.

97. M. D. Frogley, D. Ravich, H. D. Wagner, *Comps. Sci. Technol*.**,2003**, 63,1647.

98. Y. Xu, A. Zangvil, A. Kerberb, *J. Eur. Ceram. Soc.* **1999**, 77, 21.

99. N.Chisholm, H. Mahfuz, V. Rangari, R. Rodgers, S. Jeelani, In: CD-Rom proceedings of nanotech, Boston. **2004**.

100. E. Bertran, G. Viera, E. Martnez, J. E. Esteve, Y. Maniette, J. Farjas, *Thin Solid Films*, **2000**, 377, 495.

101. H. Mahfuz, V. K. Rangari, M. S. Islam, S. Jeelani, *Compos. Part A*, **2004**, 35, 453.

102. E. Martensson, A. U. Gafvert, C. Onneby, *J. Appl. Phys.*, **2001**, 90, 2870.

103. K. Niihara, *J. Ceram. Soc. Jpn.*, **1991**, 99, 945.

104. K. Kueseng, K. I. Jacob, *Eur. Polym. Journl.*, **2006**, 42, 220.

105. W. Thielemans, M. Nacur, A. Dufresne. Starch nanocrystals with large chain surface modifications. *Langmuir***, 2006**, 22, 4804.

106. S. Chakraborty, B. Sahoo, I. Teraoka, L. M. Miller, R. A. Gross. *Macromolecules* **2005**, 205, 38.

107. V. Favier, G. R. Canova, J. Y. Cavaille, H. Chanzy,A. Dufresne, C. Gauthier, *Polym. Adv. Technol.* **1995**, 6, 351.

108. M. Paillet, A. Dufresne, *Macromolecules* **2001**, 34, 6527.

109. K. Gopalan Nair, A. Dufresne, *Biomacromolecules* **2003**, 4, 666.

110. A. Morin, A. Dufresne, *Macromolecules* **2002**, 35, 2190.

111. H. Angellier, S. Molina-Boisseau,L. Lebrun, A. Dufresne, *Macromolecules* **2005**, 38, 3783.

112. H. Angellier, S. Molina-Boisseau, A. Dufresne, *Macromolecules,* **2005**, 38, 9161.

113. H. Angellier, S. Molina-Boisseau, A. Dufresne, P. Dole, *Biomacromolecules,* **2006**, 7, 531.

114. H. Angellier, S. Molina-Boisseau, A. Dufresne, M. N. Belgacem, A. *Langmuir*, **2005**, 21, 2425.

115. J. L. Putaux, S. Molina-Boisseau, T. Momaur, A. Dufresne, *Biomacromolecules,* **2003**, 4, 1198.

116. A. Bule´on, P. Colonna, V. Planchot, S. Ball, *Int. J. Biol. Macromol.* **1998**, 23, 85.

117. J. R. Z. Katz, *Phys. Chem.*, **1930**, 150, 37.

118. D. J. Gallant, Contribution a` l'e´tude de la structure et de l'ultrastructure du grain d'amidon. Ph.D. Thesis, University of Paris VI, Paris, France, **1974**.

119. D. J. Gallant, B. Bouchet, A. Buleon, S. Perez, Eur. *J. Clin. Nutr.*, **1992**, 46, S3–S16.

120. F. Duprat, D. J. Gallant, A. Guilbot, C. Mercier, J. P. Robin, L'amidon. Les Polyme`res Ve´ge´taux. Polyme`res parie´taux et al.,imentaires non azote´s; Monties, B., Ed.; Gauthier Villars: Paris, **1980,** 176.

121. D. J. Gallant, B. Bouchet, P. M. Baldwin, *Carbohydr. Polym.*, **1997**, 32, 177.

122. H. Tang, T. Mitsunaga, Y. Kawamura, *Carbohydr. Polym.*, **2006**, 63, 555.

123. G. E. Vandeputte, J. A. Delcour, *Carbohydr. Polym.*, **2004**, 58, 245.

124. D. J. Gallant, B. Bouchet, P. M. Baldwin, *Carbohydr. Polym.*, **1997**, 32, 177.

125. C. G. Oates, Trends Food Sci. Technol. **1997**, 8, 375.

126. J. M. V. Blanshard, Starch granule structure and function: a physicochemical approach. Starch: Properties and Potentials; Galliard, T., Ed.; Society of Chemical Industry: London, **1987**, 16.

127. S. Hizukuri, *Carbohydr. Res.*, **1986**, 147, 342.

128. S. Hizukuri, T. Kaneko, Y. Takeda, *Biochem. Biophys. Acta*. *Gen Subj.,* **1983**, 760, 188.

129. A. Imberty, H. Chanzy, S. Perez, A. Buleon, V. Tran, *Macromolecules,* **1987**, 20, 2634.

130. A. Imberty, S. Perez, *Biopolymers*, **1988**, 27, 1205.

131. J.-L . Jane, K.-S. Wong, A. E. McPherson, *Carbohydr. Res.*, **1997**, 300, 219.

132. C. Ge´rard, V. Planchot,P. Colonna, E. Bertoft, *Carbohydr. Res.,* **2000**, 326, 130.

133. T. Y. Bogracheva, V. J. Morris,S. G. Ring, C. L. Hedley, *Biopolymers*, **1998**, 45, 323.

134. S. Wang, J. Yu, F. Jin, J. Yu, *Int. J. Biol. Macromol.,* **2008**, 43, 216.

135. S. Wang, J. Yu, J. Yu, *Carbohydr. Polym.*, **2008**, 74, 731.

136. A. Luc, J. H. Peter, *Biofuels, Bioprod. Biorefin.*, **2009**, 3, 329.

137. P. J. Jenkins, A. M. Donald, *Int. J. Biol. Macromol.*, **1995**, 17, 315.

138. A. Dufresne, J. Y. Cavaille, W. Helbert, *Macromolecules* **1996**, 29, 7624.

139. A. Dufresne, J.-Y. Cavaille´, *J. Polym. Sci., Part B: Polym. Phys.*, **1998**, 36, 2211.

140. J. L. Putaux, S. Molina-Boisseau, T. Momaur, A. Dufresne, *Biomacromolecules,* **2003**, 4, 1198.

141. G. Chen, M. Wei, J. Chen, J. Huang, A. Dufresne, P. R. Chang, *Polymer*, **2008**, 49, 1860.

142. Y. Chen, X. Cao, P. R. Chang, M. A. Huneault, *Carbohydr. Polym.*, **2008**, 73, 8.

143. J. Yu, F. Ai, A. Dufresne, S. Gao, J. Huang, P. R. Chang, *Macromol. Mater. Eng.,* **2008**, 293, 763.

144. H. Zheng, F. Ai, P. R. Chang, J. Huang, A. Dufresne, *Polym.Compos.*, **2009**, 30, 474.

145. N. L. Garcı´a, L. Ribba, A. Dufresne, M. I. Aranguren, S. Goyanes, *Macromol. Mater. Eng.*, **2009**, 294, 169.

146. H. Namazi, A. Dadkhah, *J. Appl. Polym. Sci.,* **2008**, 110, 2405.

147. Y. Wang, L. Zhang, *J. Nanosci. Nanotechnol.*, **2008**, 8, 5831.

148. W. Na¨geli, Justus Liebigs, *Ann. Chem.*, **1874**, 173, 218.

149. C. J. Lintner, J. Prakt. *Chem.*, **1886**, 34, 378.

150. W. Li, H. Corke, T. Beta, *Carbohydr. Polym.,* **2007**, 69, 398.

151. H. Angellier, L. Choisnard, S. Molina-Boisseau, P. Ozil, A. Dufresne, *Biomacromolecules,* **2004**, 5, 1545.

152. C. G. Biliaderis, D. R. Grant, J. R. Vose, *Cereal Chem.*, **1981**, 496.

153. L. Jayakody, R. Hoover, *Food Res. Int.*, **2002**, 35, 665.

154. H. Angellier, Nanorenforts d'amidon de maı¨s cireux pour applications nanocomposites. Ph.D. Thesis, University Joseph Fourier, Grenoble, France, **2005**.

155. D. French, Organization of starch granules. Starch: Chemistry and Technology; R. L. Whistler, J. N. BeMiller, E. F. Paschall, Eds.; Academic Press: New York, **1984,** 183.

156. V. Singh, S. Z. Ali, *Starch/Staerke*, **1987**, 39, 402.

157. V. Singh, S. Z. Ali, *Starch/Staerke*, **1993**, 45, 59.

158. V. Singh, S. Z. Ali, *Carbohydr. Polym.,* **2000**, 41, 191.

159. V. Singh, S. Z. Ali, *Int. J. Food Prop.*, **2008**, 11, 495.

160. H. Angellier, L. Choisnard, S. Molina-Boisseau, P. Ozil, A. Dufresne, *Biomacromolecules,* **2004**, 5, 1545.

161. L. Jayakody, R. Hoover, Food Res. Int. **2002**, 35, 665.

162. Y.-J.Wang, V.-D. Truong, L. Wang, *Carbohydr. Polym.* **2003**, 52, 327.

163. A. Dufresne, J. Y. Cavaille, W. Helbert, *Macromolecules* **1996**, 29, 7624.

164. X. Ma, R. Jian, P. R. Chang, J. Yu, *Biomacromolecules* **2008**, 9, 3314.

165. Y. Tan, K. Xu, L. Li,C. Liu, C. Song, P. Wang, *ACS Appl. Mater. Interfaces*, **2009**, 1, 956.

166. J.-Y. Kim, S.-T. Lim, *Carbohydr. Polym.,* **2009**, 76, 110.

167. D. Liu, Q. Wu, H. Chen, P. R. Chang, *J. Colloid Interface Sci.*, **2009**, 339, 117.

168. H. Chanzy, K. Imada, A. Mollard, R. Vuong, F. Barnoud, *Protoplasma*, **1979**, 100, 303.

169. W. Helbert, J. Sugiyama, M. Ishihara, S. J. Yamanaka, *Biotechnol*., **1997**, 57, 29.

170. B. G. Rånby, *Acta Chem*. *Scand*., **1949**, 3, 649.

171. B. G. Rånby, Discuss. *Faraday Soc*., **1951**, 11, 158.

172. Y. Habibi, H. Chanzy, M. R. Vignon, *Cellulose,* **2006**, 13, 679.

173. S. M. Mukherjee,H. J. Woods, *Biochem*. *Biophys*. *Acta,* **1953**, 10, 499.

174. O. A. Battista, *Ind*. *Eng*. *Chem*., **1950**, 42, 502

175. O. A.Battista, S. Coppick, J. A. Howsmon, F. F. Morehead, W. A. Sisson, *Ind*. *Eng*. *Chem*., **1956**, 48, 333.

176. R. H. Marchessault, F. F. Morehead, N. M. Walter, *Nature,* **1959**, 184, 632.

177. V. Favier, G. R. Canova, J. Y. Cavaille, H. Chanzy, A. Dufresne, C. Gauthier, *Polym. Adv. Technol.*, **1995**, 6, 351.

178. V. Favier, H. Chanzy, J. Y. Cavaille, *Macromolecules,* **1995**, 28, 6365.

179. M. N. Angles, A. Dufresne, *Macromolecules,* **2001**, 34, 2921.

180 P. Lu, Y. L. Hsieh, Carbohydr.Polym. **2012**, 87, 2546.

181. H. Håkansson, P. Ahlgren, *Cellulose,* **2005**, 12, 177.

182. J. Schurz, K. John, *Cellul*. *Chem*. *Technol*., **1975**, 9, 493.

183. Y. Nishiyama, U. J. Kim, D. Y. Kim, K. S. Katsumata, R. P. May, P. Langan, *Biomacromolecules,* **2003**, 4, 1013.

184. D. Le Corre, J. Bras, A. Dufresne, 2nd International Conference on Biodegradable Polymers and Sustainable Composites (BIOPOL **2009**), Alicante, Spain, 2009.

185. X. M. Dong, J.-F. Revol,D. G. Gray, *Cellulose*, **1998**, 5, 19.

186. J. Araki, M. Wada, S. Kuga, T. Okano, *Langmuir*, **2000**, 16, 2413.

187. Y. Habibi, A.-L. Goffin, N. Schiltz, E. Duquesne, P. Dubois, A. Dufresne, *J. Mater. Chem.*, **2008**, 18, 5002.

188. Y. Habibi, A. Dufresne, *Biomacromolecules,* **2008**, 9, 1974.

189 Y. Habibi, L. Foulon, V. Aguie´-Be´ghin, M. Molinari, R. J. Douillard, *Colloid Interface Sci.*, **2007**, 316, 388.

190. X. Cao, Y. Chen, P. R. Chang, M. Stumborg, M. A. Huneault, *J. Appl. Polym. Sci.,* **2008**, 109, 3804.

191 A. Kahil, H. P. S. Bhat, A. H. Ireana, A. F. Yusra, Carbohydr. Polym., **2011**, 87, 963.

192. X. Cao, H. Dong, C. M. Li, *Biomacromolecules,* **2007**, 8, 899.

193. N. L. Garcia de Rodriguez, W. Thielemans, A. Dufresne, *Cellulose*, **2006**, 13, 261.

194. G. Siqueira, J. Bras, A. Dufresne, *Biomacromolecules,* **2009**, 10, 425.

195. W. Helbert, J. Y. Cavaille, A. Dufresne, *Polym. Compos.*, **1996**, 17, 604.

196. A. Bendahou, Y. Habibi, H. Kaddami, A. Dufresne, *J. Biobased Mater. Bioenergy* , **2009**, 3, 81.

197. J. Araki, M. Wada, S. Kuga, T. J. Okano, *Wood Sci.*, **1999**, 45, 258.

198. S. Beck-Candanedo, M. Roman, D. G. Gray, *Biomacromolecules,* **2005**, 6, 1048.

199. M. Roohani, Y. Habibi, N. M. Belgacem, G. Ebrahim, A. N. Karimi, A. Dufresne, *Eur. Polym. J.*, **2008**, 44, 2489.

200. X. Cao, Y. Habibi, L. A. Lucia, *J. Mater. Chem.,* **2009**, 19, 7137.

201. J. R. Capadona, K. Shanmuganathan, S. Trittschuh, S. Seidel, S. J. Rowan, C. Weder,. *Biomacromolecules,* **2009**, 10, 712.

202. M. A. S. Azizi Samir, F. Alloin, M. Paillet, A.Dufresne, *Macromolecules*,**2004**, 37, 4313.

203. A. Hirai, O. Inui, F. Horii, M. Tsuji, *Langmuir,* **2009**, 25, 497.

204 N. Kasyapi, V. Chaudhary, A. K. Bhowmick, Carbohydr. Polym., **2012**, 92, 1116.

205. T. Koshizawa, Kami Pa Gikyoshi **1960**, 14, 455.

206. I. Filpponen, Ph.D. Thesis, North Carolina State University, Raleigh NC, **2009**.

207. J. Araki, M. Wada, S. Kuga, T. Okano, *Colloids Surf. A,* **1998**, 142, 75.

208. J. F. Revol, H. Bradford, J. Giasson, R. H. Marchessault, D. G. Gray, *Int. J. Biol. Macromol*, **1992**, 14, 170.

209. M. Roman, W. T. Winter, *Biomacromolecules,* **2004**, 5, 1671.

210. N. Wang, E. Ding, R. Cheng, *Langmuir,* **2008**, 24, 5.

211. N. Wang, E. Ding, R. Cheng, *Polymer,* **2007**, 48, 3486.

212. D. Bondeson, A. Mathew, K. Oksman, *Cellulose* **,2006**, 13, 171.

213. S. Elazzouzi-Hafraoui, Y. Nishiyama, J.- L. Putaux, L. Heux, F. Dubreuil, C. Rochas, *Biomacromolecules,* **2008**, 9, 57.

214. J. Huang, G. Chen, A. Dufresne, M. Wei, G. Cui, CN 101020739 A, 20070822, **2007**.

215. J. Huang, F. Yi, R. Zhang, W. Xia, M. Wei, CN 101230189 A, 20080730, 2008.

216. G. Chen, M. Wei, J. Chen, J. Huang, A. Dufresne, P. R. Chang, *Polymer* **,2008**, 49, 1860.

217. H. Angellier, S. Molina-Boisseau, P. DoleA. Dufresne, *Biomacromolecules,* **2006**, 7, 531.

218. N. L. Garcı´a, L. Ribba, A. Dufresne, M. I. Aranguren, S. Goyanes, *Macromol. Mater. Eng.*, **2009**, 294, 169.

219. E. Kristo, C. G. Biliaderis, *Carbohydr. Polym.,* **2007**, 68, 146.

220. J. Yu, F. Ai, A. Dufresne, S. Gao, J. Huang, P. R. Chang, *Macromol. Mater. Eng.,* **2008**, 293, 763.

221. Y. Chen, X. Cao, P. R. Chang, M. A. Huneault, *Carbohydr. Polym.,* **2008**, 73, 8.

222. H. Zheng, F. Ai, P. R. Chang, J. Huang, A. Dufresne, *Polym. Compos*., **2009**, 30, 474.

223. A. Dufresne, J. –Y. Cavaille´, *J. Polym. Sci*., *Part B: Polym. Phys*., **1998**, 36, 2211.

224. X. Ma, R. Jian, P. R. Chang, J. Yu, *Biomacromolecules,* **2008**, 9, 3314.

225. N. L Garcı´a, L. Ribba, A. Dufresne, M. I Aranguren, S. Goyanes, Macromol. Mater. Eng. **2009**, 294, 169.

226. A. Dufresne, J. Y. Cavaille, W. Helbert, *Macromolecules,* **1996**, 29, 7624.

227. H. Angellier, S. Molina-Boisseau, A. Dufresne, *Macromolecules,* **2005**, 38, 9161.

228. H. Angellier, S. Molina-Boisseau, A. Dufresne, P. Dole, *Biomacromolecules,* **2006**, 7, 531.

229. G. Chen, M. Wei, J. Chen, J. Huang, A. Dufresne, P. R. Chang, Polymer **2008**, 49, 1860.

230. E. Kristo, C. G. Biliaderis, Carbohydr. Polym*.,* **2007**, 68, 146.

231. H. Zheng, F. Ai, P. R. Chang, J. Huang, A. Dufresne, *Polym.Compos*., **2009**, 30, 474.

232. Y. Wang, L. Zhang, *J. Nanosci. Nanotechnol*., **2008**, 8, 5831.

233. D. Le Corre, J. Bras, A. Dufresne, 2nd International Conference on Biodegradable Polymers and Sustainable Composites (BIOPOL 2009), Alicante, Spain, 2009.

234. M. N. Angles, A. Dufresne, *Macromolecules,* **2000**, 33, 8344.

235. Y. Wang, H. Tian, L. Zhang, *Carbohydr. Polym.* 2009, 10.1016/ j.carbpol. 2009.10.043.

236. H. Angellier, S. Molina-Boisseau, A. Dufresne, *Macromolecules,* **2005**, 38, 9161.

237. Rowel R.M., Banks W.B., Gen. Teeh.Rep.FPL-GTR-50; USDA Forest service, Forest Products Laboratory, Madison, WI, **1985,** 24.

238. Joly C., Gauthier R., Coubles E.S., J Appl Polym Sci, **1996,** 61, 57.

239. C. Bonini, L. Heux, J.- Y. Cavaille, P. Lindner, C. Dewhurst, P. Terech, *Langmuir*, 2002, 18, 3311

240. L. Heux, G. Chauve, C. Bonini, *Langmuir*, **2000**, 16, 8210.

241. M. A. S. Azizi Samir, F. Alloin, J. Y. Sanchez, N. ElKissi, N, A. Dufresne, A. *Macromolecules*, **2004**, 37, 1386.

242. M. Labet, W. Thielemans, A. Dufresne, *Biomacromolecules*, **2007**, 8, 2916.

243. R. Peter, F. A. Y. C. A. D. J. H. Chang, *Journal of Applied Polymer Science*, 2009, 111, 619.

244. S. Tsuji, H. Kawaguchi, H. *Langmuir*, **2005**, 21, 2434.

245. S. Berlioz , S. Molina-Boisseau , Y. Nishiyama ,L. Heux *Biomacromolecules*, **2009**, 10:2144.

246. K. Schlufter, H. P. Schmauder, S. Dorn, T. Heinze, *Macromol Rapid Commun*, **2006**, 27, 1670.

247. R. A. Buchanan, W. F. Kwolek, H. C. Katz, C. R. Russell, *Starch/Stärke***, 1971**, 23, 350.

248. R. A. Buchanan, Starch xanthide styrene–butadiene rubbers. *Starch/Stärke***, 1974**, 26, 165.

249. The Goodyear Tire & Rubber company. Preparation of starch reinforced rubber and use thereof in tires. US Pat 7156137; **2007**.

250. A. Rouilly, L. Rigal, R. G. *Polymer***,2004**, 45, 7813.

251. C. Nakason, A. Kaesaman, K. Eardrod. *Mater Lett,* **2005**, 59, 4020.

Chapter-2 Polysaccharides as reinforcing fillers in natural rubber

Outline

Introduction

The use of fillers in rubber is almost as old as the use of rubber itself. As soon as the rubber-mixing machinery was developed, fillers were added to natural rubber with the aim of improving certain properties and to reduce the price of the rubber compound [1]. Carbon black is the most important reinforcing agent used in the rubber industry, but because of its origin from petroleum, this filler causes pollution and gives black color to rubber. As a result, in the last two decades research was focused on the development of other reinforcing agents derived from inorganic [2,3] and natural organic [4,5] materials to replace carbon black in rubber compounds. Natural rubber has excellent mechanical properties and heat resistance but poor solvent resistance [6].

Organoclays were already introduced in various polymer systems including for example polypropylene [7,8], polyamide [9,10,11], polystyrene [12], polycarbonate [13] and rubbers [14]. Research has also been done on natural rubber (NR) by Ismail and Ramli [15], which showed that the faster curing rate and enhanced mechanical properties were obtained in the presence of organoclay. Studies on clay rubber composites have been made using various elastomers such as natural rubber [16,17], styrene butadiene rubber [18,19] ethylene propylene diene rubber [20,21] nitrile rubber [22], fluoro elastomers [23], polyurethane rubber [24], etc. A review of the literature on clay/natural rubber composites as mentioned earlier shows that montmorillonite clays (bentonites) have been studied extensively as the ideal filler in natural rubber. As the natural deposits of montmorillonite minerals are rather limited, and as the demand for bentonites goes ever increasing, there has been considerable investigation for finding substituted for this type of products. While a few reports show the use of other layered silicates such as hectorite clay/smectite clay. In this context, only scanty data is available with the relatively less expensive and abundantly available mineral kaolin [25].

Hence the composites of natural rubber containing C-black and kaolin were prepared and their results were compared.

2.1 Synthesis of composites with commercial fillers

2.1.1 Experimental

2.1.1.1 Materials

NR and C-black (N330) were kindly supplied to us by Mouldtech Rubber Industries, Vadodara, India. Kaolin was supplied by Qualigens chemicals, Mumbai, India.

2.1.1.2 Preparation of composite

The composites of NR containing kaolin and C-black are prepared on two roll mixing mill and the mastication has to be continued for a long time so as to obtain homogenous composites. During this process the temperature was controlled at ~ 40 ^{o}C. A conventional vulcanization system was used for compounding. Table.2.1.1 shows the composition of other additives used in the rubber compound prepared throughout the work. Upto 30 phr of fillers were added along with the accelerators listed in table. 2.1.1 This was followed by vulcanization carried out at 150 ºC for 7-8 min using a hot press. The pressure of the hot press was adjusted (~300 k Pa) to obtain rubber composite sheets with 2 mm thickness.

Table.2.1.1 List of accelerators used in compounding of natural rubber

Accelerators used	**Amount (phr)**
Sulphur	1.8
Tetramethylene thiuram disulphide	0.5
Mercaptobenzo thiazyl disulphide	1.0
Zinc oxide	5
Stearic acid	1.0

2.1.1.3 Characterization techniques

Hardness

Shore hardness was measured on Frank hardness tester with shore A durometer at several points on the surface of the specimen. An average of 6 measurements was taken as the result.

Mechanical properties

Stress/strain properties of all the NR composites were measured on a Universal Testing Machine (UTM, Lloyd Instrument) using test specimen in the form of dumbbells according to ASTM standard and procedure (D638). The gauge length was 50.0 mm. The crosshead speed was 10 mm/min at 25°C and 50% humidity. The data given are the average of five measurements.

Scanning electron microscopy (SEM)

The surface morphology of the tensile fractured surfaces was examined by means of Jeol Scanning Electron Microscope (JEOL JSM–5610LV). An accelerating potential of 15 kV was used for the analysis of the sample.

Thermal analysis

Thermal gravimetric analysis (TGA)

TGA was recorded on TG-DTA 6300 INCARP EXSTAR 6000 in nitrogen atmosphere in temperature range of 30 ºto 450 ºC at heating rate of 10 ºC/min.

Differential scanning calorimetry (DSC)

DSC was performed on DSC 60 Shimadzu in nitrogen atmosphere in temperature range of -80 º to 0 ºC at heating rate of 10 ºC/min.

2.1.2 Results and discussion

2.1.2.1 Mechanical properties

Hardness

The results of hardness are expressed in Figure.2.1.1. It is observed that in all the composites the hardness increases with increase in concentration of fillers as expected. Thus the kaolin did not have any negative effect on hardness at increased concentration although the increase was more rapid in case of carbon black.

Tensile strength (T. S.)

The tensile strength imparted by kaolin is higher than that imparted by C-black upto 20 phr (Figure.2.1.1). After this the T.S decreases which is due to poor compatibility between NR and kaolin clay. Addition of 5 phr of kaolin imparted higher T.S than that imparted by 15 phr of C-black.

% Elongation at break

Addition of kaolin increases the % elongation upto 20 phr (Figure.2.1.1). This shows that kaolin does not have any effect on elasticity of natural rubber. Increase in % elongation in case of C-black was steep as compared to that of kaolin.

2.1.2.2 Scanning electron microscopy

The kaolin composite did not show presence of hole or particles but tearing off of the surface which explains the consistency observed in mechanical strength. The composite of C-black shows the presence of holes formed during fracture as evident from Figure. 2.1.2

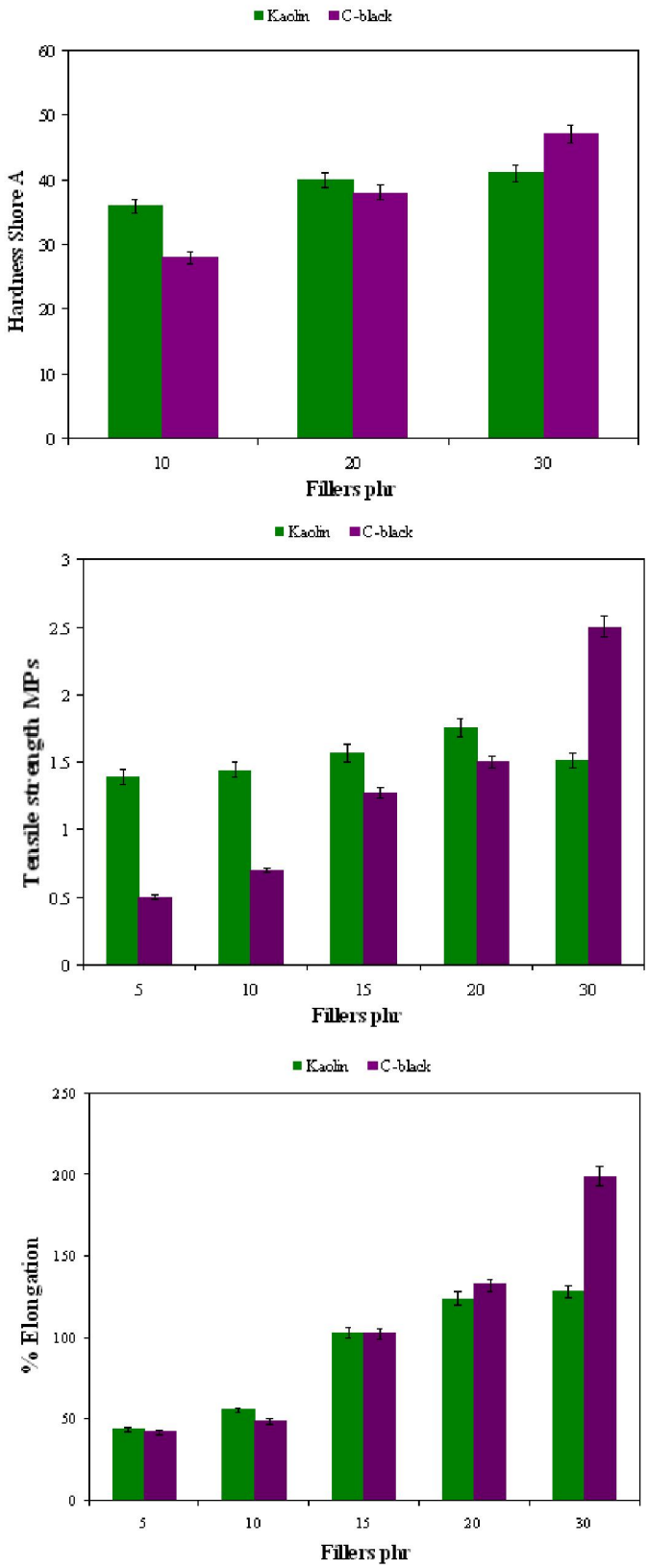

Figure2.1.1. Mechanical properties of NR composites

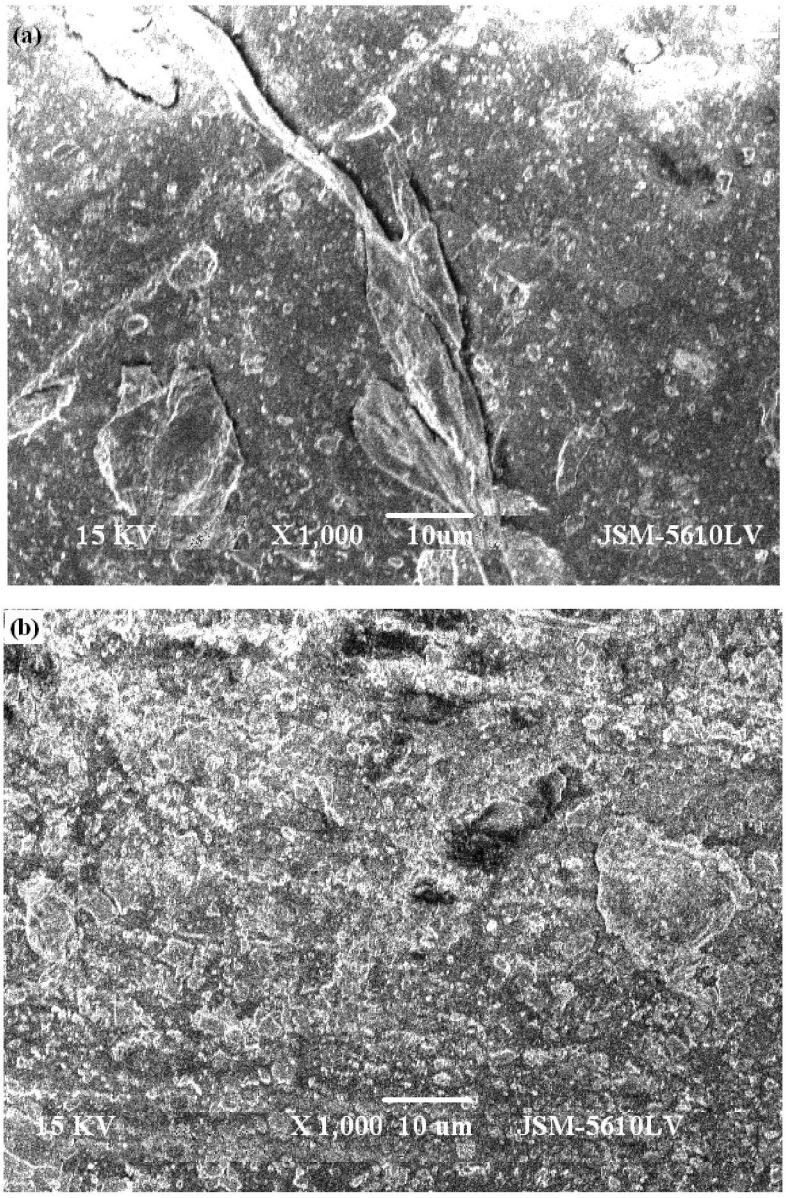

Figure. 2.1.2 SEM micrographs of NRs composites containing (a) kaolin and (b) C-black at 20 phr.

2.1.2.3 Thermal Properties

Thermo gravimetric analysis (TGA)

Kaolin itself has a good thermal stability [26]. To check its thermal stability on formation of composites thermal analysis was carried out. It was found out that its thermal stability

was comparable with that of NR composite containing C-black (Figure.2.1.3 (a)). This may be due to the high vulcanization temperatures which may have resulted in crosslinking of composites.

Differential scanning calorimetry (DSC)

The Tg of NR composites at 20 phr filler loading shows that the two composites have a comparable Tg (Figure. 2.1.3 (b)). The Tg of unfilled NR is around -66ºC [27], while that of C-black/NR composite and kaolin/NR composite are -62.24 ºC and -62.28 ºC. The results suggested that fillers impart rigidity and strength to the network which leads to increase in Tg.

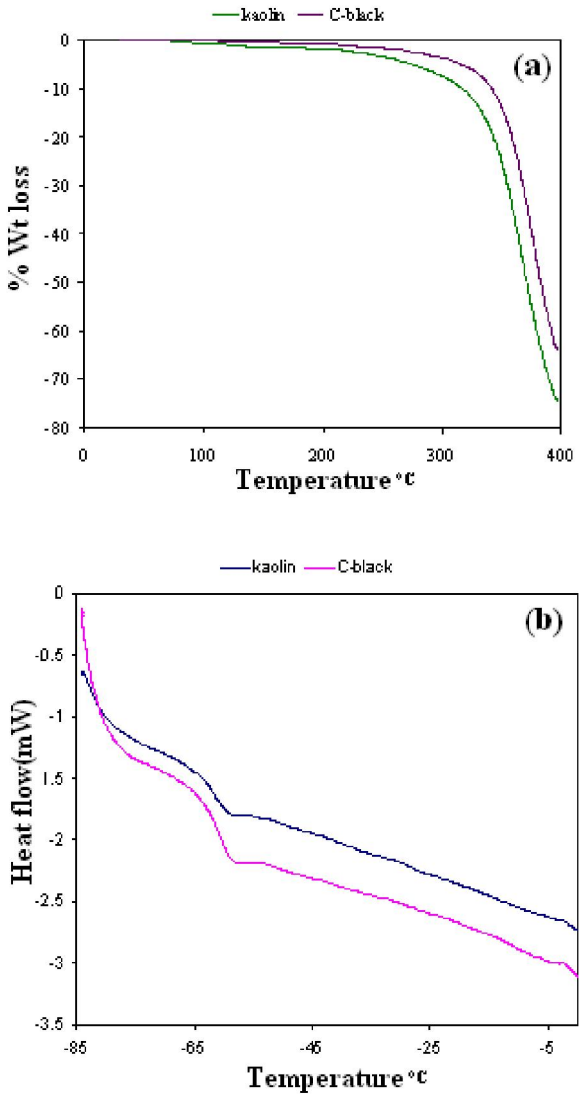

Figure. 2.1.3 (a) TGA and (b) DSC curves of NR composites

2.1.3 Conclusions

A comparison of the two commercial fillers proved the superiority of C-black especially above 20 phr. Hence for the rest of the work C-black was used as a reference to compare the performance of other reinforcing fillers.

2.2 Synthesis and characterization of biocomposites of natural rubber with polysaccharides

2.2.1 Introduction

Research efforts are currently being harnessed in developing a new class of fully biodegradable "green" composites. The major attraction about green composites is that they are environmentally friendly, fully degradable and sustainable, i.e., they are truly "green" in every way. At the end of their life, they can be easily disposed of or composted without harming the environment. During the last decade of the 20th century, agro fiber composites have gained much interest from both research and industrial communities. Environmental preservation, pollution control, and emphasis on the use of energy efficient materials and processing in the industrial sector have renewed interest in agro-based lignocellulosic (LC) fibers. In spite of the above advantages agro fiber based composites have some shortcomings in mechanical properties [28]. Nowadays, materials from renewable resources are being sought to replace not only the reinforcement element but also the matrix phase of composite materials. The influence of polysaccharides in elastomeric compounds has been studied in the past [29,30,31,32]. The reinforcing efficiency of polysaccharides in elastomer composites is related to its nature, its crystallinity, as well as its dispersion into the matrix [6-9].

As discussed earlier biopolymers such as starch, cellulose and chitin are important source of renewable polymer, and are among the most reliable reinforcing fillers due to their low density, low cost, biodegradability and abundance in nature. They have received an increased interest lately due to more environmentally aware consumers, increased price of crude oil and global warming. They are available freely and naturally [33,34].

Chitin constitutes the structure of the external skeleton in shellfish and insects and is one of the major components of the fibrous material of cellular walls in mushrooms and algae [35]. It is estimated that about 10^{10} to 10^{11} tons of this polymer are synthesized each year. Cellulose and its derivatives are an important class of natural macromolecules [36].

It is the most common component found in the cell walls of higher plants. Starch is one of the naturally occurring biomaterials that is abundantly available and has a low cost for commercial applications. Keeping all these factors in view we have prepared composites of natural rubber containing polysaccharides.

2.2.2 Experimental

2.2.2.1 Materials

Starch (soluble), microcrystalline cellulose and chitin from crab shells was supplied by Qualigens chemicals, Mumbai, India.

2.2.2.2 Preparation of Composites

As shown in scheme 2.2.1 the composites of NR are prepared on two roll mixing mill and the mastication has to be continued for a long time so as to obtain homogeneous composites. During this process the temperature was controlled at ~ 40 ^{o}C. Three sets of biocomposites were synthesized namely starch/NR, cellulose/NR and Chitin/NR. Upto 30 phr of fillers were added successfully along with the accelerators listed in table. 2.1.1.
This was followed by vulcanization carried out at 150 ºC for 7-8 min using a hot press. The pressure of the hot press was adjusted (~300 k Pa) to obtain rubber composite sheets with 2 mm thickness.

2.2.2.3 Characterization techniques

These biocomposites were characterized in a similar way as discussed in section 2.1.2.3. through hardness, mechanical properties such as tensile strength and % elongation, thermal properties and scanning electron microscopy. Their results were then compared with conventional composite i.e. C-black/NR.

Density

The density of biocomposites was determined by the method used for resins [37].

Water sorption studies

Water sorption was determined by a method reported elsewhere [38,39].The possibility of an error introduced due to evaporation of solvent while weighing was minimized by weighing as quickly as possible within 30 s. The sorption was carried out at (27±1) °C. Sorption experiments were continued until attainment of equilibrium.

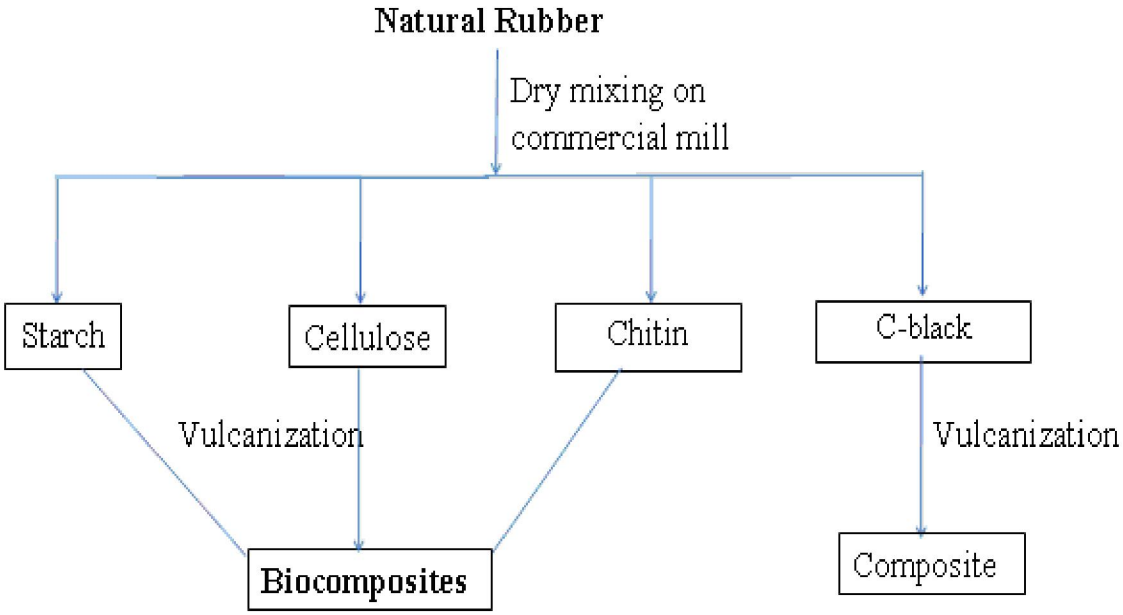

Scheme 2.2.1 Preparation of biocomposites

2.2.3 Results and Discussion

2.2.3.1 Mechanical properties

Hardness

The results of hardness of the various composites are expressed in Figure.2.2.1. It is observed that in all the composites the hardness increases with increase in concentration

of fillers as expected. Thus the biofillers did not have any negative effect on hardness at increased concentration although the increase was more rapid in case of carbon black. Up to 30 phr all the biofillers showed superior hardness than carbon black. Among the biofillers chitin imparted best hardness properties followed by, starch and cellulose. This is due to the hydrophobic nature of chitin as compared to starch and cellulose resulting in better interaction with NR. Increase in phr of carbon black leads to a steep increase in hardness of NR while the increase is not so pronounced in case of the biofillers.

Tensile strength (T. S.)

The value for tensile strength for unfilled rubber is 1.6 MPa. It can be seen from Figure.2.2.1 that the composites exhibit considerably high tensile strength even at 5 phr loading which increases further upto 20 phr. At this filler content all the composites have greater strength than C-black composite. Probably the polysaccharides form a polymer blend with NR with a certain degree of compatibility at these compositions. At higher ratios their hydrophilic nature leads to immiscibility and hence poorer mechanical strengths. Among biofillers the T. S. imparted by chitin is highest followed by starch, cellulose and C-black. Addition of 5 phr of chitin showed T.S. more than 20 phr of C-black. However, unlike hardness, further increase in amount of filler decreases the T. S. except in C-black. The increase in hardness and decrease in T.S. with amount of biofiller loading indicates that the composites become brittle as the amount of filler increases. This may be because of the poor compatibility of hydrophilic biopolymers with hydrophobic natural rubber at higher loading which results in loss of elasticity.

% Elongation at break

The % elongation for unfilled rubber is 93 % respectively which is much lower than that of composites with 5 phr of any of the fillers Figure. 2.2.1. A trend very similar to tensile strength was observed. Optimum % elongation was observed at 20 phr after which the elongation decreases along with T. S. as the concentration of biofiller increases. This is an interesting observation since generally elongation and T. S. show opposite trend. Thus we can say that upto 20 phr biopolymer preserves the elastic nature of NR. Once again

the hypothesis that at higher loadings the hydrophilic biofillers have poor interaction with natural rubber is supported.

Thus the results of T.S. and elongation show that the optimum loading of biofillers is 10 phr and chitin exhibited exceptional mechanical strength even at minimum loading.

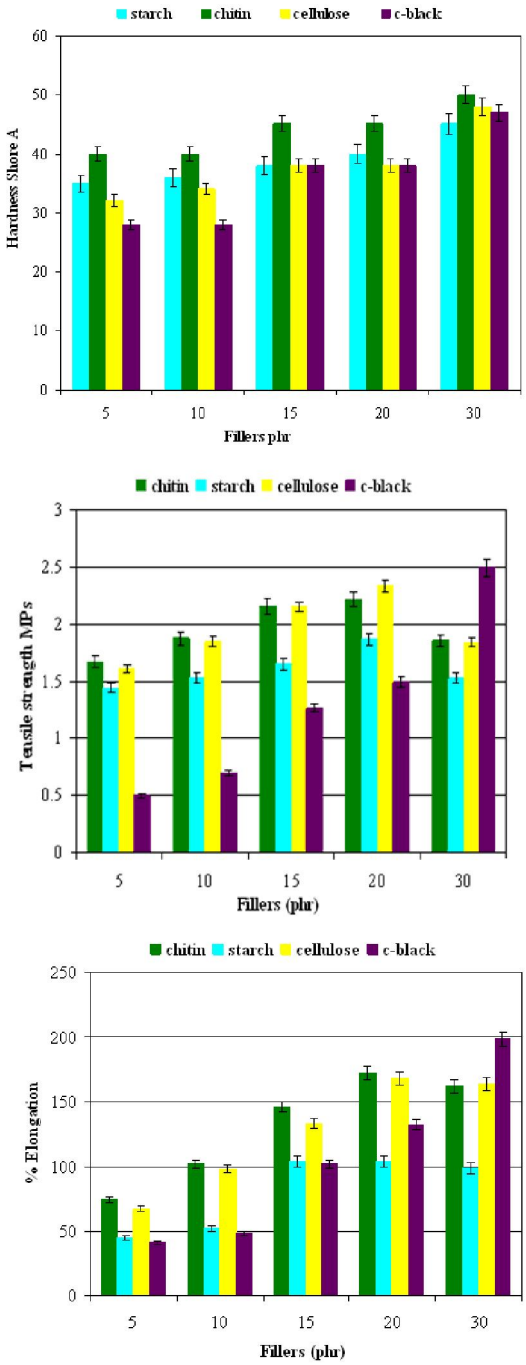

Figure. 2.2.1 Variation in mechanical properties of NR composites upon filler addition

2.2.3.2 Scanning electron microscopy (SEM)

The results of the mechanical properties can be interpreted on the basis of morphology. The fractured samples of tensile strength were tested for surface morphology. The SE micrographs of the composites at 20 phr loading are shown in Figure. 2.2.2. The micrographs of biocomposites show a very uniform morphology like a single phase with no distinction between the matrix and the dispersion phase. However the composites containing chitin and starch (Figure. 2.2.2 a&b) show better mixing of the two phases among all. The composite of C-black shows the presence of holes formed during fracture as evident from Figure. 2.2.2 c; while SEM of cellulose composite (Figure. 2.2.2 d) shows presence of particles on the surface, which may have leeched out during fracture. Overall the biocomposites exhibited strong filler-polymer interaction.

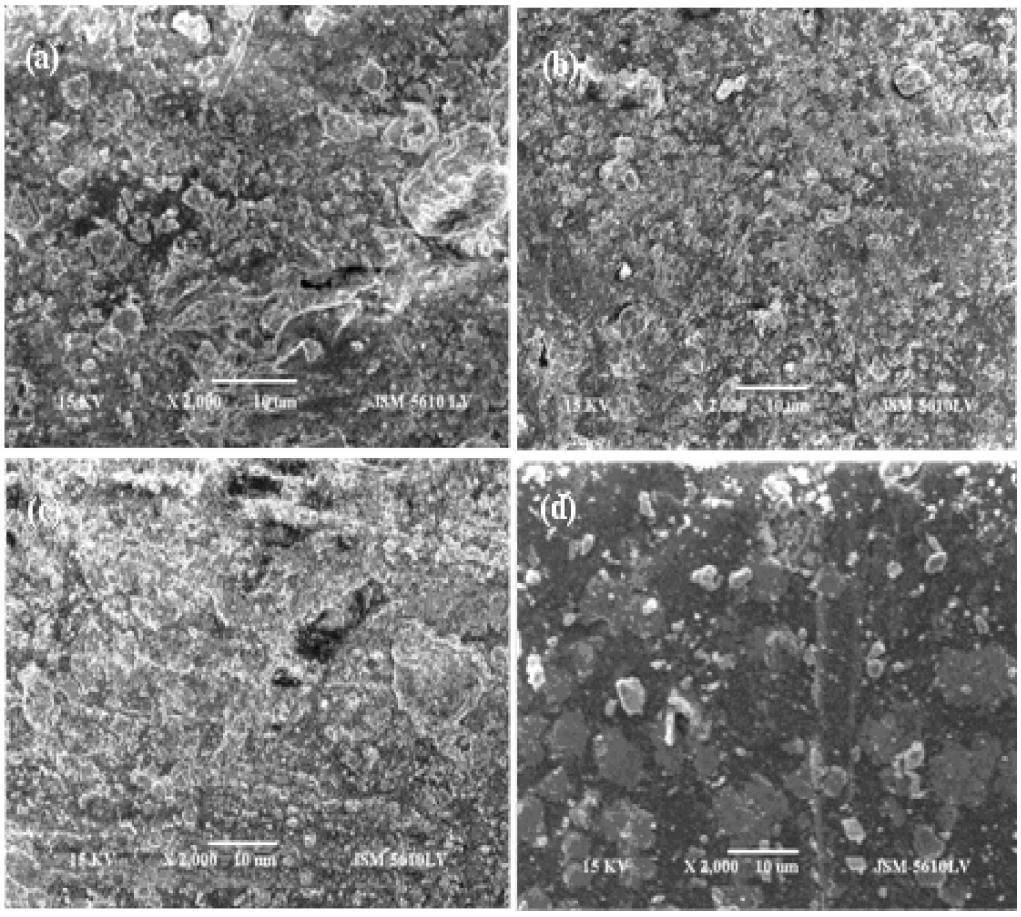

Figure. 2.2.2 SEM micrographs of NRs containing different biofillers at 20 phr: (a) chitin, (b) starch, (c) c-black, and (d) cellulose.

2.2.3.3 Thermal Properties

Thermo gravimetric analysis (TGA)

It is known that the thermal stability of polysaccharides is less and hence the thermal stability of biocomposites was studied. It was observed from Figure. 2.2.3(a) that the thermal stability of biocomposites was comparable with commercially used C-black composite (Table 2.2.1). This improvement in thermal stability of the biocomposites may result from the high vulcanization temperatures, which may have resulted in crosslinking within the polysaccharide network of the biocomposites. This crosslinking can be similar to that observed in the amylopectin units of starch.

Differential scanning calorimetry (DSC)

Figure 2.2.3(b) shows that Tg of NR biocomposites at 20 phr filler loading shows that all the biocomposites have Tg comparable with that of C-black/NR composites (Table-2.2.1). The Tg of unfilled NR is around -66 ºC [40]. The results suggested that biofiller imparts rigidity and strength to the network, which leads to increase in Tg.

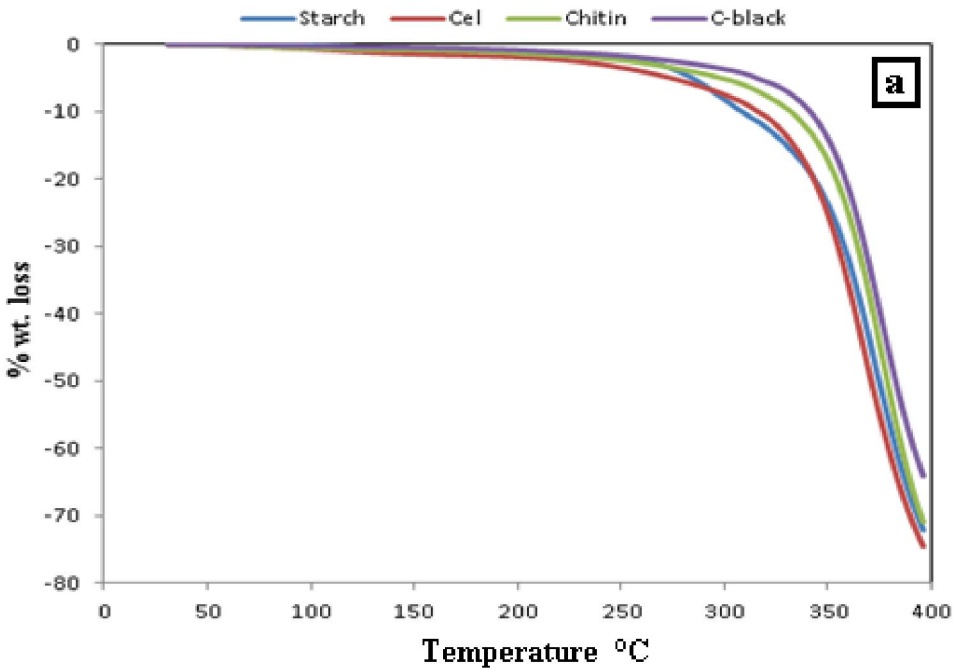

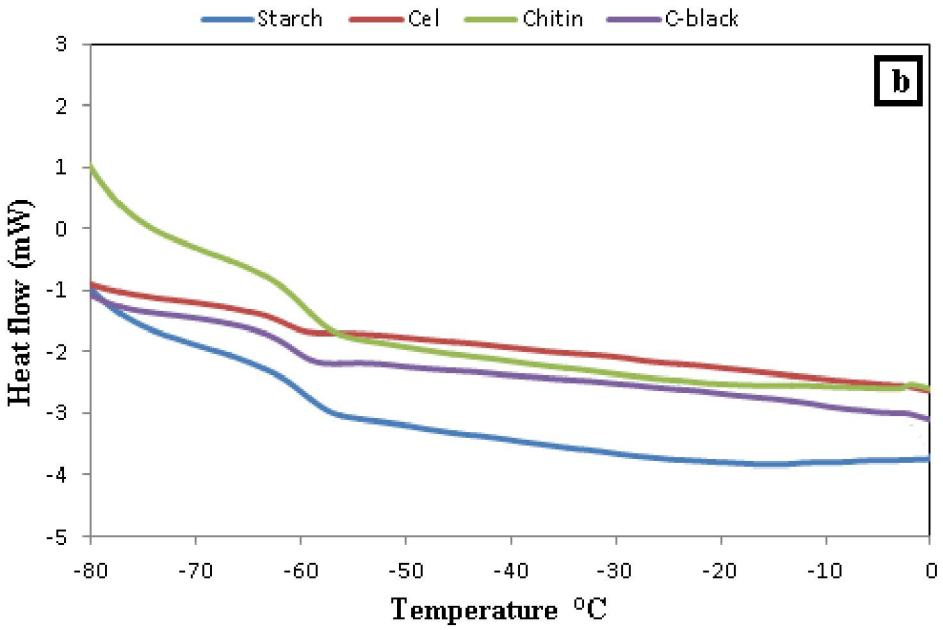

Figure. 2.2.3 (a) TGA and (b) DSC curves of NR composites.

Table. 2.2.1 Thermal Properties of composites at 20 phr loading

Fillers	Degradation temperature (°C) for % wt. Loss					Tg °C
	1	2	5	10	50	
Starch	128	179	250	303	351	-63.14
Cel	137	191	257	288	325	-62.96
Chitin	138	192	261	291	352	-62.44
C-black	114	192	264	304	364	-62.24

2.2.3.4 Density

The density data expressed in Figure.2.2.4 shows that as the percentage of filler increases the density goes on increasing as expected. Among the biofillers starch showed highest density followed by carbon black, chitin and cellulose. This is again because of the nature and texture of the biofillers.

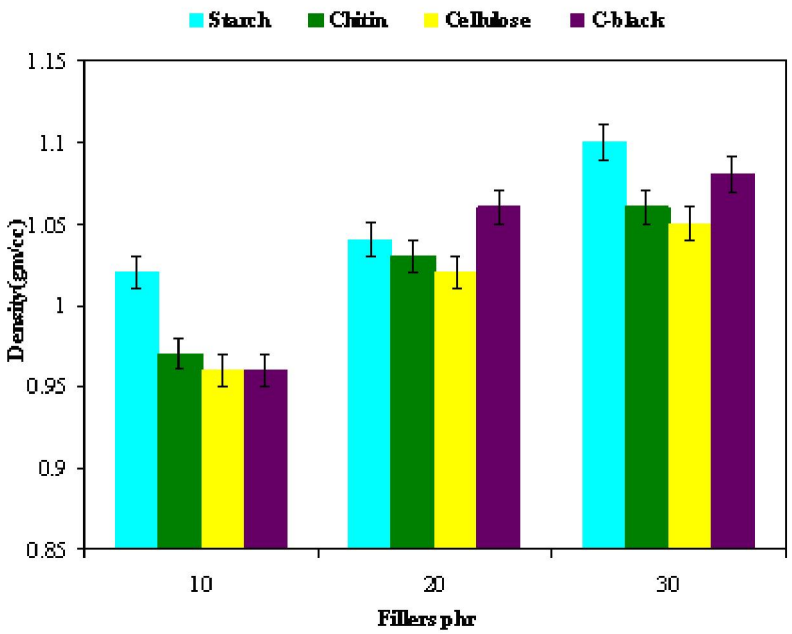

Figure. 2.2.4 Density of NR composites.

2.2.3.5 Sorption studies

The sorption studies were carried out by a reported procedure [18]. The possibility of an error introduced due to evaporation of solvent while weighing was minimized by weighing as quickly as possible within 30 sec. The sorption experiments were carried out at 27 ± 1 ^{O}C and continued until attainment of equilibrium.

The results of the sorption process are expressed as moles of solvent absorbed by 100gm of the composites (Q_t) at time t, because it is more convenient than the actual weight gain results and is the practice followed in literature. This was calculated by using equation 1 [18].

$$Q_t = \frac{M_s / M_{r(s)}}{M_p} \times 100 \qquad (1)$$

Where, M_s is the mass of the solvent absorbed at equilibrium, $M_{r(s)}$ is the relative molecular mass of the solvent and M_p is the initial mass of the composites sample. At equilibrium Q_t is taken as Q_∞, i.e. the mol% uptake at infinite time.

Sorption of solvents by the composites is expressed as mol % uptake (Q_t) versus square root of time. It is clear from the plots (Figure.2.2.5) that the extent of sorption goes on

increasing from chlorobenzene to toluene to dichlorobenzene in all cases. The solvent uptake is much higher in case of chlorobenzene compared to the other solvents (Figure.2.2.6), which can be attributed to its solubility parameter (discussed later in this section). Also the extent of sorption was observed to decrease with increasing filler concentration.

Diffusion Process

Diffusion of a liquid in a polymer matrix is described by Fick's laws [41]. In Fickian diffusion, the rate of diffusion is much less than that of relaxation due to mechanical and structural modes of the polymer-solvent interaction. Deviation from Fickian diffusion can occur for different reasons such as when sorption equilibrium is not achieved at a film surface due to an appreciable surface evaporation rate, or when diffusion and relaxation rates are comparable. As a result non-Fickian or anomalous sorption curves exhibit sigmoidal shapes.

The sorption curve in Figure 2.2.5 shows that the transport is very rapid in the beginning upto about 50% of equilibrium sorption and then levels off as equilibrium is approached. In order to study the diffusion mechanism the results were fitted into the equation 2

$$\log (Q_t/ Q_\infty) = \log \kappa + \eta \log t \qquad (2)$$

Where k is a constant, which indicates the extent of polymer-solvent interaction and is a property characteristic of the polymer. The value of n indicates the type of sorption phenomenon. For Fickian diffusion η is upto 0.5, whereas for values of n between 0.5 and 1, the diffusion is said to be anomalous. The values of η and κ are determined by linear regression analysis. Table 2.2.2 indicates that chitin and cellulose containing composites showed fickian diffusion almost entirely in all the solvents (cellulose only in dichloro benzene) with n values between 0.1 to 0.5. While, NR containing carbon black and starch exhibited non-fickian diffusion in chlorobenzene.

In the beginning, the curves seem to be showing a slight sigmoidal shape which indicates the non-Fickian trend. Thus the diffusion mechanism observed in the present study is mainly of non-Fickian type. All the solvents under the study causes a significant amount of swelling of the polymers which may result in greater surface vaporization and hence an anomalous type of diffusion. Hence the values of η in all the solvents are almost same

and are above Flory's critical value of 0.5 except in chitin filled composites where the solvent uptake is relatively low**.** The values of κ in all the solvents are almost same. In starch filled composites the sorption plot show a clear steep rise initially which account for the high values of η.

The observed order of sorption of the solvents under study can be explained on the basis of solubility parameter theory. Maximum swelling of a polymer composite can take place in the solvent whose solubility parameter is close to that of the polymer composite. The swelling coefficient α was calculated by using the equation 3.

$$\alpha = \{M_s/M_p\} \times \{1/\rho_s\} \qquad (3)$$

Where M_s is the mass of the solvent at equilibrium, ρ_s is density of the solvent and M_p is the initial mass of the polymer composite sample; α is indicative of the volume of solvent per unit mass of the polymer composite. The solubility parameters of toluene, dichlorobenzene and chlorobenzene are 8.8, 8.9 and 9.5 $(cal/cm^3)^{1/2}$ respectively. For the solvents under study it seems that chlorobenzene has the closest solubility parameter to the polymers and hence shows highest swelling coefficient (Table 2.2.3).

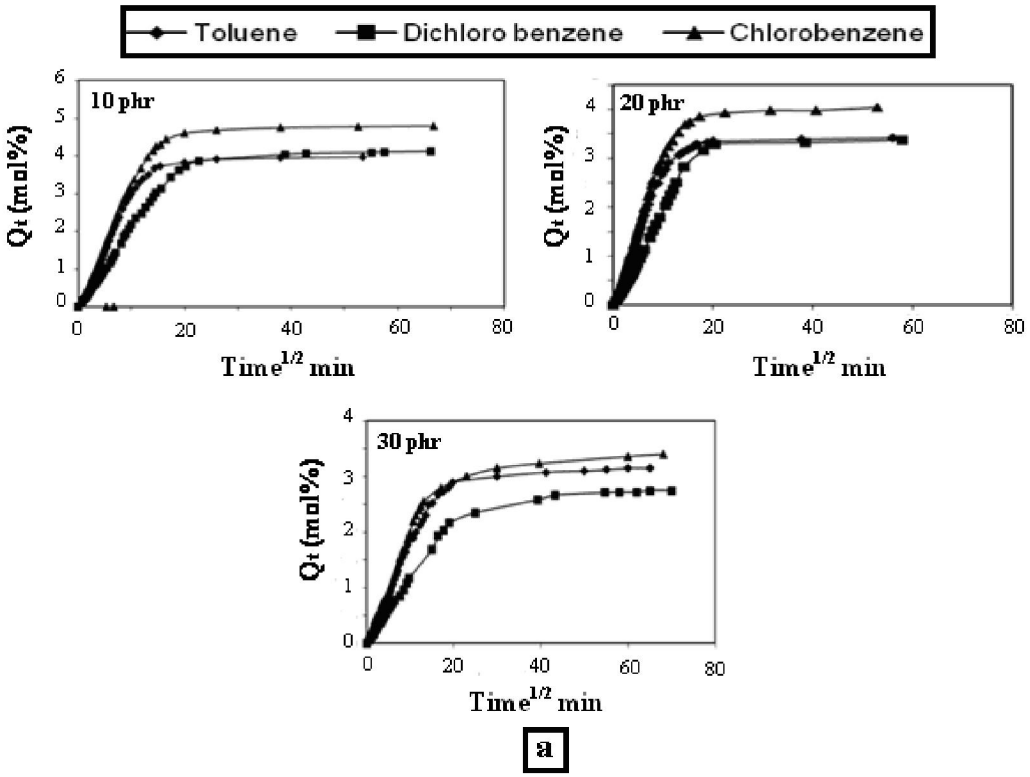

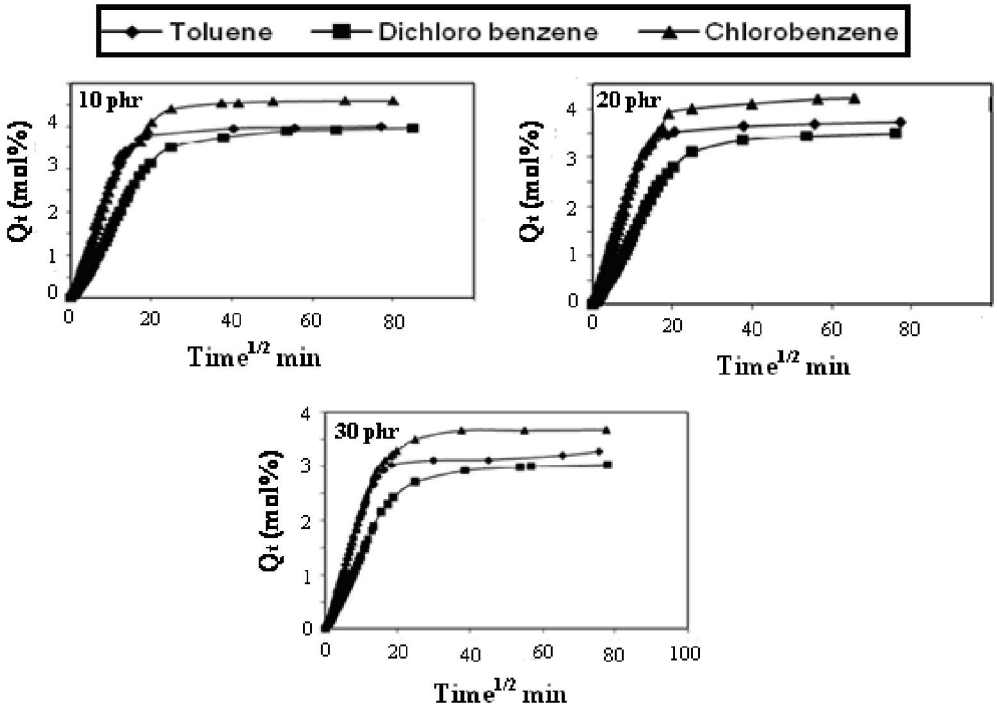
Toluene
Dichloro benzene
Chlorobenzene
10 phr
20 phr
30 phr
Qt (mol%)
Time1/2 min

b

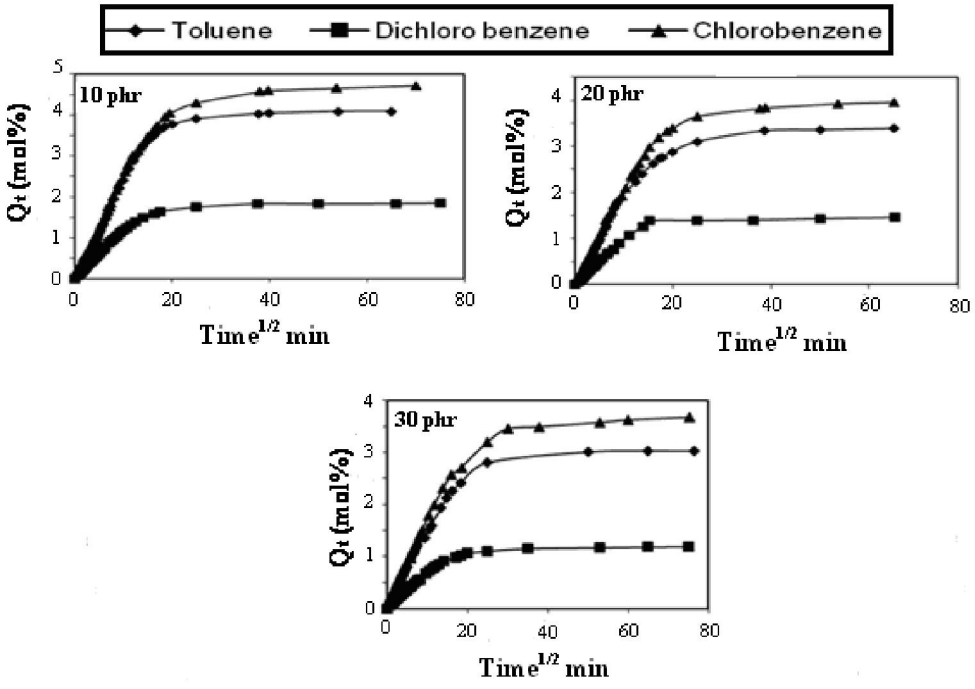
Toluene
Dichloro benzene
Chlorobenzene
10 phr
20 phr
30 phr
Qt (mol%)
Time1/2 min

c

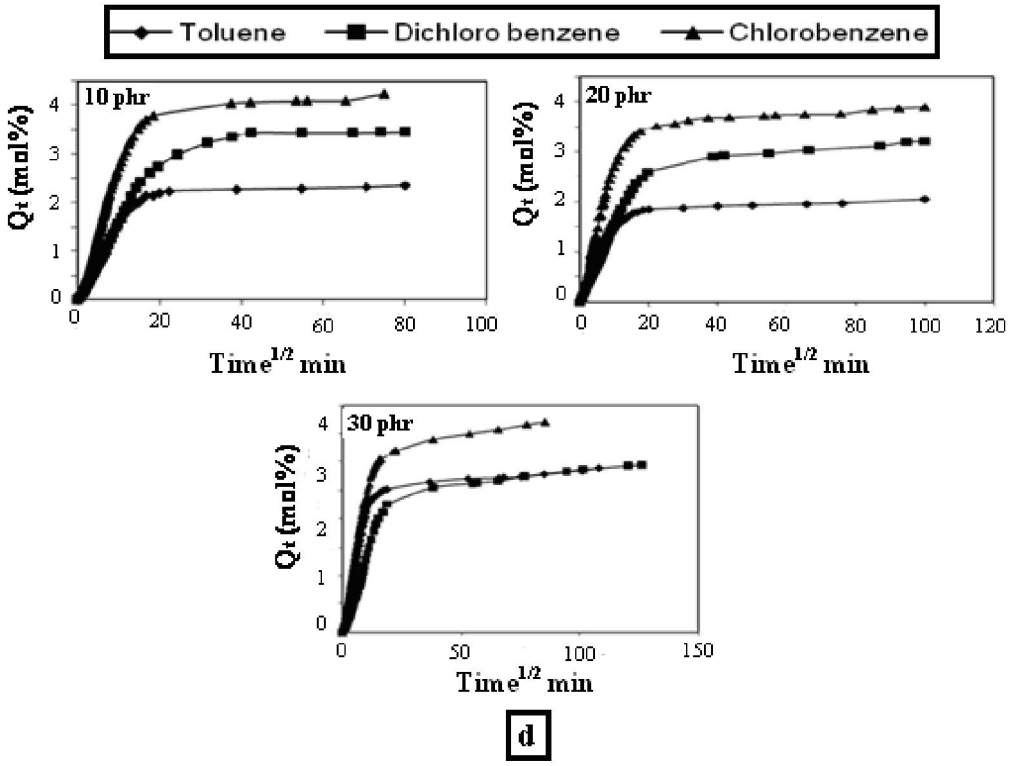

Figure. 2.2.5 Sorption plots of NR composites containing (a) C-black, (b) Cellulose, (c) Chitin and (d) Starch

The volume fraction of polymer ϕ in the solvent swollen sample was calculated by using the equation 4

$$\phi = \frac{M_p/\rho_p}{M_s/\rho_s + M_p/\rho_p} \qquad (4)$$

Where M_p is the initial weight of the polymer composite sample, ρ_p is its density, M_s the weight of the solvent in the fully swollen sample, and ρ_s is the density of the solvent. From the results in Table 2.2.4 it is observed that the volume fraction ϕ of the polymer is directly proportional to amount of the composites/filler and inversely proportional to the sorption extent of the solvents. Hence the volume equilibrium degree of swelling q was calculated as the reciprocal of the volume fraction of the polymer. The results are given in Table 2.1.5. The effect of variation of fillers on ϕ and q is seen in Figure. 2.2.7

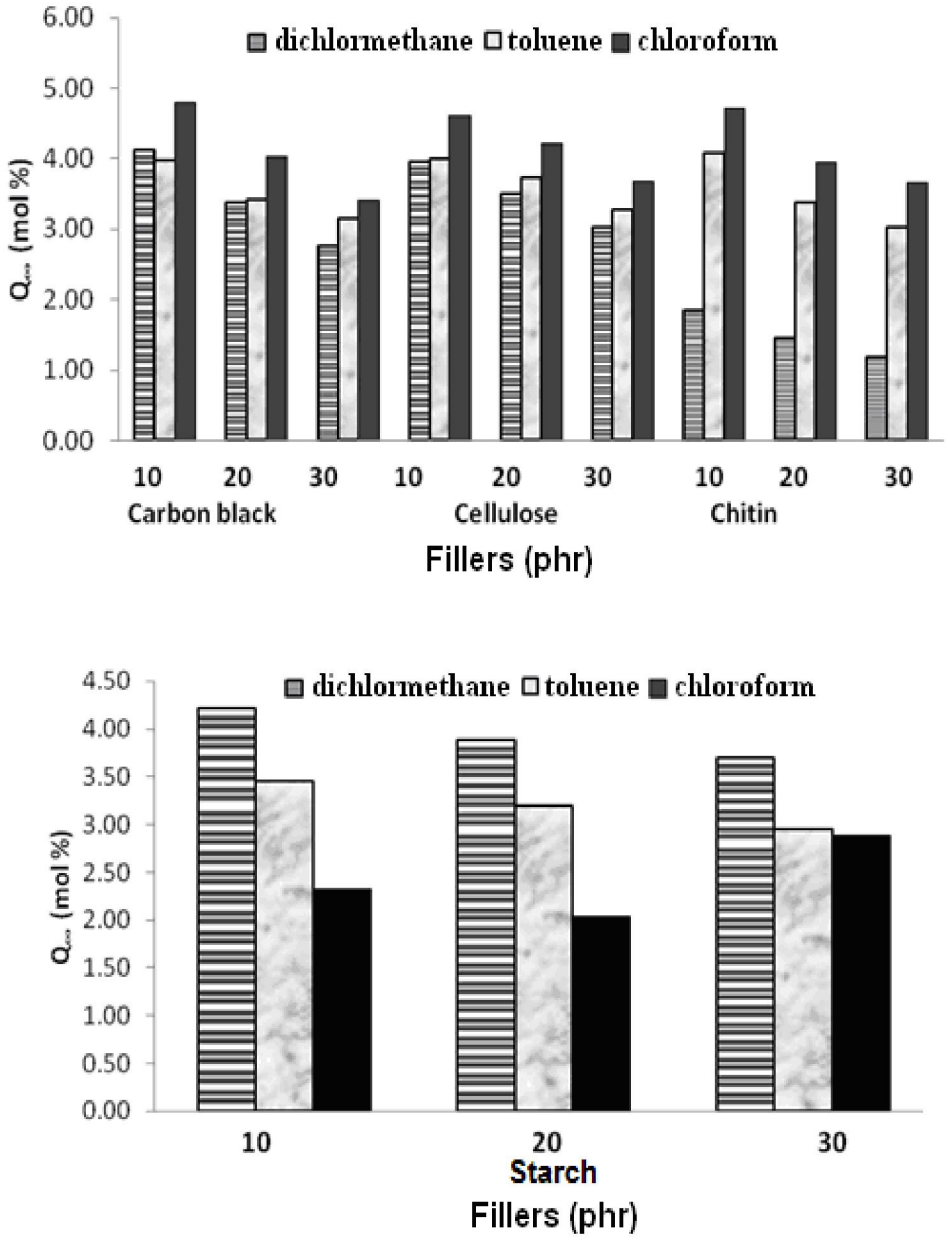

Figure. 2.2.6 Variation in solvent uptake of NR composites in different solvents

In order to calculate the degree of crosslinking and molecular weight between crosslinks the polymer solvent interaction parameter χ was calculated using the solubility parameter obtained and the equation 5

$$\chi = \beta + V_s \{(\delta_p - \delta_s)^2 / RT\} \qquad (5)$$

Where β is the lattice constant whose value is about 0.34 [42,43] V_s is the molar volume of the solvent and δ_p and δ_s are the solubility parameters of the polymer composite and the solvent, respectively. The polymer - solvent interaction parameter (χ) values for chlorobenzene, toluene and dichlorobenzene were found to be 0.34683, 0.36876 and 0.43268 respectively. Lower χ value indicates higher interaction of the polymer with chlorobenzene, resulting in greater sorption, as observed in the sorption studies

Table. 2.2.2 Values of η and κ (g / g min^2) for diffusional behavior of NR composites

Fillers	**Chlorobenzene**		**Toluene**		**Dichlorobenzene**	
C-black	η	K	η	K	H	κ
10 phr	0.58	0.04	0.62	0.05	0.54	0.04
20 phr	0.61	0.61	0.59	0.05	0.57	0.04
30 phr	0.58	0.58	0.50	0.05	0.51	0.04
Cellulose						
10 phr	0.59	0.03	0.60	0.04	0.47	0.06
20 phr	0.58	0.05	0.60	0.05	0.48	0.07
30 phr	0.63	0.05	0.64	0.04	0.03	0.08
Chitin						
10 phr	0.42	0.14	0.40	0.12	0.43	0.11
20 phr	0.47	0.13	0.36	0.07	0.37	0.12
30 phr	0.52	0.12	0.35	0.06	0.47	0.06
Starch						
10 phr	0.62	0.04	0.65	0.04	0.62	0.06
20 phr	0.62	0.04	0.67	0.04	0.73	0.04
30 phr	0.58	0.08	0.66	0.04	0.57	0.03

.

Table. 2.2.3 Values of the swelling coefficient (α) of NR composites

Fillers	Chlorobenzene	Toluene	Dichlorobenzene
C-black			
10 phr	4.71	4.22	4.58
20 phr	3.96	3.63	3.72
30 phr	3.29	3.30	2.99
Cellulose			
10 phr	4.51	4.24	4.40
20 phr	4.13	3.95	3.90
30 phr	3.61	3.46	3.53
Chitin			
10 phr	4.63	4.31	2.03
20 phr	3.94	3.52	1.60
30 phr	3.60	3.26	1.30
Starch			
10 phr	4.14	3.82	3.87
20 phr	3.81	3.54	3.56
30 phr	3.58	3.04	3.32

When the polymer composite sample is immersed in a solvent medium its molecules diffuse into the polymer until the elastic retraction of the network balances the osmotic pressure driving the solvent into the swollen polymer [44] Because the retraction of the network depends upon the molecular weight between crosslinks M_c was calculated from the Flory-Rehner equation [1]

$$M_c = \frac{\rho_p V_s \phi^{1/3}}{\ln(1-\phi) + \phi + \chi\phi^2} \qquad (6)$$

Where ρ_p is the density of the polymer composite.

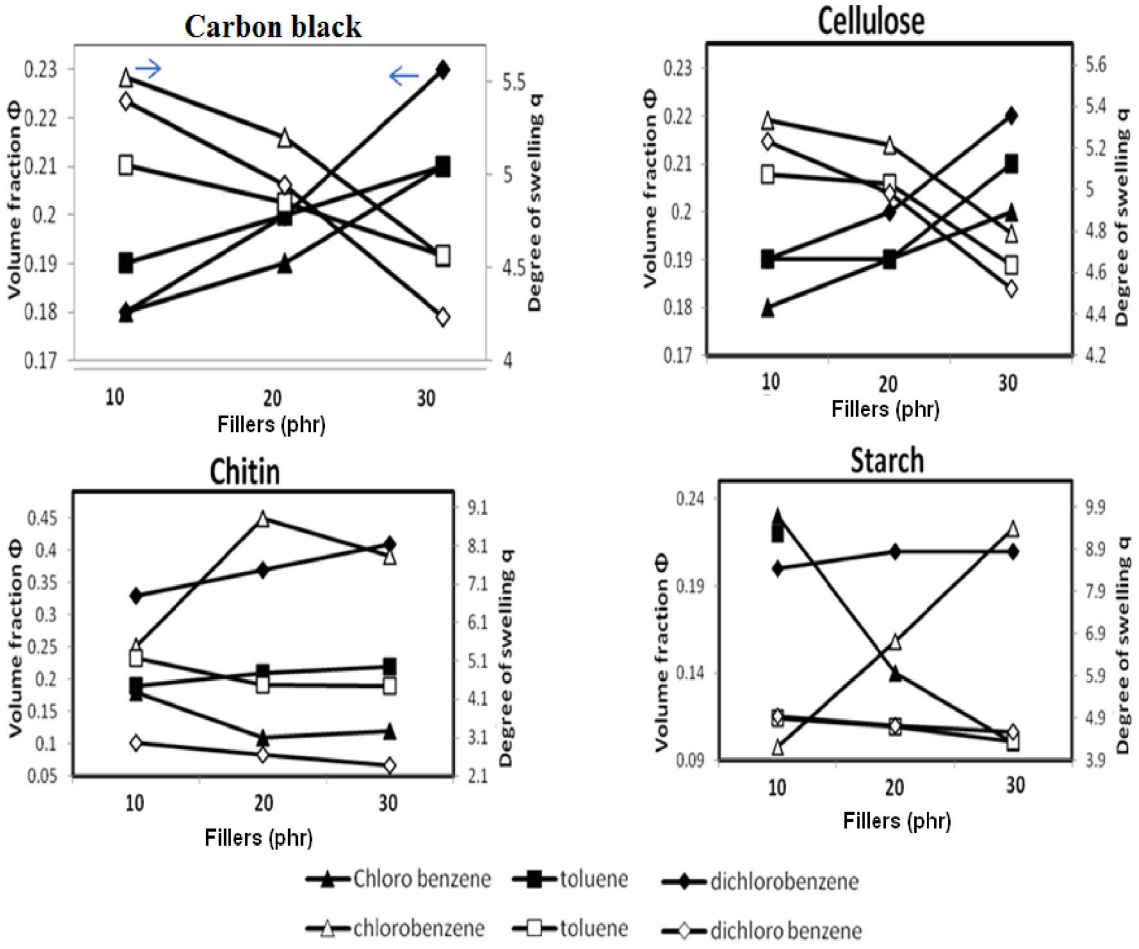

Figure. 2.2.7 Variation in Φ and q of NR composites with filler loading in different solvents

The degree of crosslinking is inversely proportional to the molecular weight between crosslinks and is given by the equation

$$\nu = 1/2M_c \qquad (7)$$

The values for M_c and ν are given in table's 2.2.7 and 2.2.8 respectively. The effect of variation of % of fillers on M_c and ν is seen in Figure.2.2.8. Since the composites under

study have the same extent of crosslinking the variations seen are due to diversity in the type of filler and filler loading which affects the solvent uptake capacity.

Table. 2.2.4 Volume fraction (Φ) of NR composites

Fillers	Chlorobenzene	Toluene	Dichlorobenzene
C-black			
10 phr	0.18	0.19	0.18
20 phr	0.19	0.20	0.20
30 phr	0.21	0.21	0.23
Cellulose			
10 phr	0.18	0.19	0.19
20 phr	0.19	0.19	0.20
30 phr	0.20	0.21	0.22
Chitin			
10 phr	0.18	0.19	0.33
20 phr	0.11	0.21	0.37
30 phr	0.12	0.22	0.41
Starch			
10 phr	0.23	0.20	0.20
20 phr	0.14	0.21	0.21
30 phr	0.10	0.22	0.21

The sorption coefficient which is related to the maximum sorption of the penetrant can be obtained from the ratio of weight of the solvent taken up at equilibrium to the initial weight of the polymer composites (equation 8).

$$S = M_s / M_p \quad (8)$$

Where M_s is the weight of sample at equilibrium and M_p is the initial weight of polymer

Table. 2.2.5 Volume equilibrium degree of swelling q of NR composites

Fillers	Chlorobenzene	Toluene	Dichlorobenzene
C-black			
10 phr	5.527	5.056	5.399
20 phr	5.205	4.849	4.943
30 phr	4.562	4.565	4.235
Cellulose			
10 phr	5.331	5.074	5.231
20 phr	5.214	5.030	4.982
30 phr	4.790	4.637	4.520
Chitin			
10 phr	5.494	5.187	2.971
20 phr	8.816	4.462	2.656
30 phr	7.833	4.457	2.385
Starch			
10 phr	4.227	4.904	4.951
20 phr	6.724	4.683	4.710
30 phr	9.387	4.353	4.578

As evident from Table.2.2.8 the sorption coefficient follows the same trend as that of swelling coefficient. As filler concentration decreases, the sorption coefficient increases. The diffusion coefficient characterizes the ability of the solvent molecules to move along the polymer segments. It can be calculated from the equation

$$D = \pi ((h\theta / 2Q_\infty)^2 \quad (9)$$

Where h is the initial thickness of the sample, θ is the slope of the linear portion of the sorption curves. The trend observed in the case of diffusion coefficient is quite opposite

to that observed in the case of sorption coefficient (Table 2.2.10). This implies that at higher filler loading sorption dominates diffusion. The permeability coefficient, product of diffusion coefficient and sorption coefficient, implies net effect of diffusion and sorption. Its values are given in Table.2.2.11.

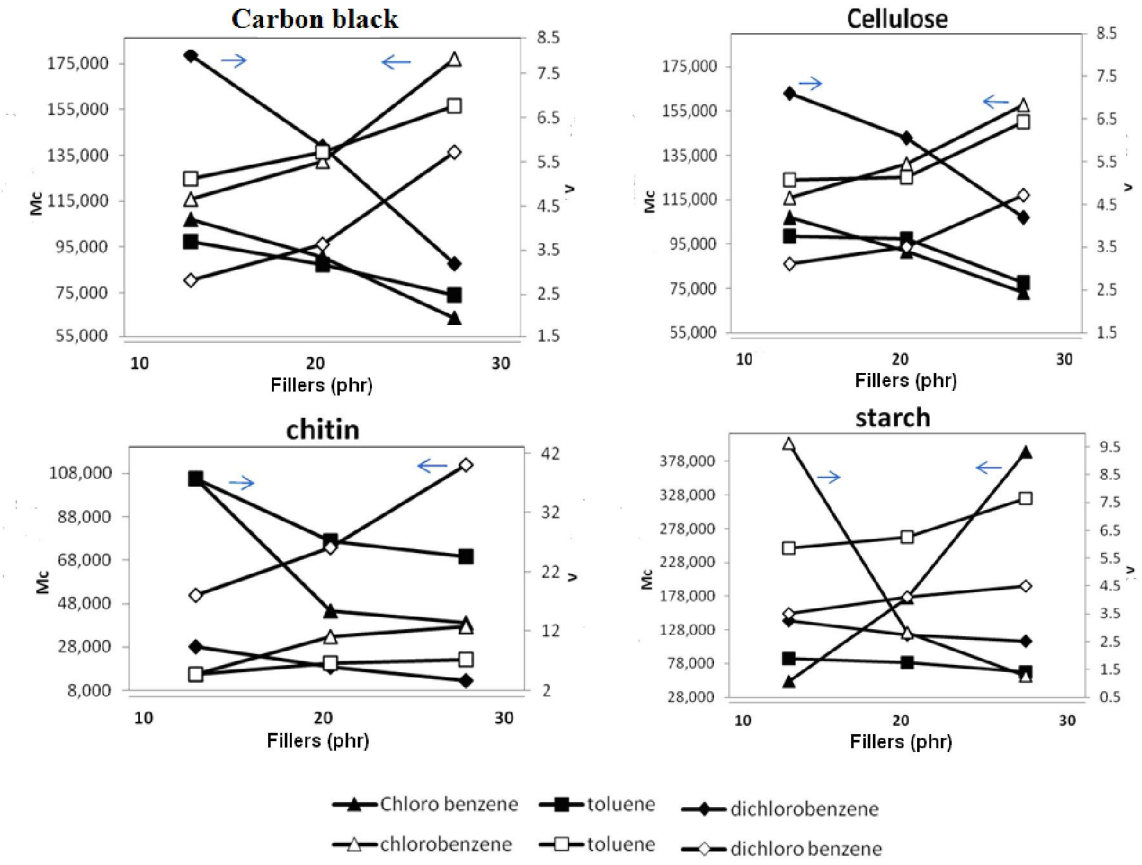

Figure. 2.2.8 Variation in Mc and ν of NR composites with filler loading in different solvents

A major drawback of these biopolymers is that they are hydrophilic in nature and therefore have affinity towards moisture, leading to low degrees of adhesion between fiber and matrix [45]. A reduction in water uptake was observed and was attributed to better compatibility between fiber and matrix.

Moisture absorption takes place by three types of mechanisms, namely, diffusion, capillarity, and transport via micro cracks [46]. Among the three, diffusion is considered

to be the major mechanism. Water absorption largely depends on the water-soluble or hygroscopic components embedded in the matrix, which acts as a semipermeable membrane.

Table 2.2.7 : Molecular Weight Between Crosslinks (M_c)

Fillers	Chlorobenzene	Toluene	Dichlorobenzene
C-black			
10 phr	73805.6	70813.1	124922
20 phr	64706.7	64846.1	102193
30 phr	49241.5	57028.8	70986.2
Cellulose			
10 phr	73805.6	71403.8	116185
20 phr	65402.9	70647.8	104561
30 phr	54846.2	59325.7	82911.3
Chitin			
10 phr	72980.9	75357.3	29505.5
20 phr	37455.3	58739.7	21913.7
30 phr	33814.3	54325.4	16288.7
Starch			
10 phr	42027.9	63661.1	103368
20 phr	109072	60521.9	91374.3
30 phr	207195	51794.1	85611.2

The fiber/matrix adhesion is an important factor in determining the sorption behavior of a composite. Moreover, fiber architecture has also been found to affect the moisture absorption.

As polysaccharides are highly hydrophilic in nature, the water sorption of composites was expected to be high. Also it was expected to increase with increase in filler loading. However the results of the experiment showed an interesting trend. From Figure.2.2.9 it is seen that as the amount of phr of filler increases the sorption co-efficient decreases. Thus we can say that as the amount of filler increases the adhesion between the polymer matrix and filler increases which lead to increase in hardness and decrease in water absorption. Also the water sorption of biocomposites was quite comparable to that of carbon black composites. This shows that the biopolymers do not possess the drawback of increased moisture absorption. This further supports the fact that the biofillers can be a potential substitute for C black.

Table 2.2.8: Degree of crosslinking (ν) of NR composites

Fillers	**Chlorobenzene**	**Toluene**	**Dichlorobenzene**
C-black			
10 phr	4.66	5.12	2.81
20 phr	5.51	5.73	3.63
30 phr	7.83	6.76	5.72
Cellulose			
10 phr	4.66	5.07	3.10
20 phr	5.44	5.14	3.51
30 phr	6.82	6.43	4.71
Chitin			
10 phr	4.73	4.73	18.00
20 phr	11.1	6.51	26.10
30 phr	12.7	7.20	40.00
Starch			
10 phr	9.62	5.87	3.50
20 phr	2.84	6.26	4.11
30 phr	1.27	7.66	4.50

Table 2.2.9 : Sorption coefficient (S) (g/g) of NR composites

Fillers	Chlorobenzene	Toluene	Dichlorobenzene
C-black			
10 phr	5.21	3.67	5.97
20 phr	4.38	3.15	4.85
30 phr	3.64	2.87	3.90
Cellulose			
10 phr	4.98	3.69	5.74
20 phr	4.56	3.43	5.09
30 phr	3.98	3.01	4.37
Chitin			
10 phr	3.75	3.75	2.64
20 phr	3.06	3.06	2.09
30 phr	3.97	2.83	1.70
Starch			
10 phr	4.57	3.33	5.05
20 phr	4.21	3.08	4..65
30 phr	3.96	2.65	4.33

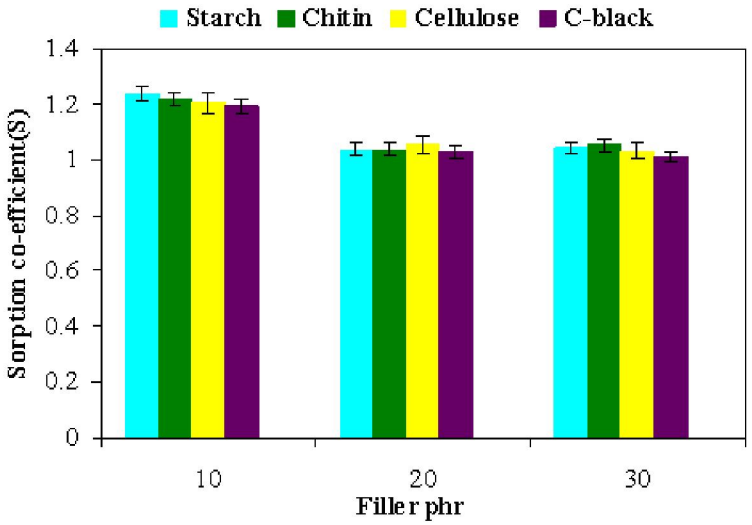

Figure.2.2.9 Effect of biofiller loading on the sorption coefficient of water in the composites.

Table. 2.2.10 Diffusion coefficient ($D \times 10^3 cm^2 sec^{-1}$) of NR composites

Fillers	Chlorobenzene	Toluene	Dichlorobenzene
C-black			
10 phr	4.05	6.86	4.81
20 phr	5.85	7.60	7.31
30 phr	13.51	11.84	16.52
Cellulose			
10 phr	4.84	8.19	366.24
20 phr	5.69	7.82	298.49
30 phr	8.57	11.14	286.37
Chitin			
10 phr	3.95	3.69	4.61
20 phr	5.06	4.96	7.91
30 phr	8.13	7.6	13.70
Starch			
10 phr	6.41	23.63	295.44
20 phr	6.60	28.51	257.17
30 phr	6.90	14.19	268.66

Table 2.2.11 : Permeability coefficient ($P \times 10^3$ cm^2s^{-1}) of NR composites

Fillers	Chlorobenzene	Toluene	Dichlorobenzene
C-black			
10 phr	21.92	25.22	28.79
20 phr	25.67	24.01	35.51
30 phr	49.28	34.02	64.52
Cellulose			
10 phr	24.15	30.27	210.52
20 phr	25.99	26.90	151.96
30 phr	34.20	33.58	125.21
Chitin			
10 phr	19.82	23.42	27.43
20 phr	23.45	25.12	34.64
30 phr	24.21	29.12	63.23
Starch			
10 phr	29.39	78.71	149.24
20 phr	27.86	87.87	119.63
30 phr	27.35	37.64	116.49

Table-2.2.12 The mol% uptake of water at equilibrium (Q_∞)

Fillers	10 phr	20 phr	30 phr
Starch	6.78	5.76	5.79
Chitin	6.73	5.76	5.85
Cellulose	6.63	5.86	5.73
C-black	6.59	5.71	5.61

Table-2.2.13 Volume fraction of polymer (ϕ) in the solvent swollen sample

Fillers	10 phr	20 phr	30 phr
Starch	0.4462	0.4814	0.4642
Chitin	0.4609	0.4843	0.4734
Cellulose	0.4654	0.4818	0.4806
C-black	0.4683	0.4777	0.4773

2.2.4 Conclusions

The results of the mechanical properties showed that upto 20 phr all the polysaccharides imparted superior strength and elongation behaviour than C-black. Composites of chitin showed best mechanical properties followed by those of cellulose and chitin. Addition of 5 phr of chitin resulted in better mechanical properties than 20 phr of C-black. After 20 phr the mechanical properties of biocomposites deteriorated with further addition of filler. This may be because of the poor compatibility of hydrophilic biopolymers with hydrophobic natural rubber. On the other hand, increasing quantity of C-black in composites led to a constant increase in the mechanical properties. SEM study revealed improved morphology, phase mixing and strong filler-polymer interaction in case of biocomposites. As the filler loading increases, the water absorption decreases which also indicates an increase in adhesion between polymer matrix and fillers. The study indicates that the biofillers under investigation are potential substitute for C-black.

The main hurdle for the use of these polysaccharides as a reinforcing phase is its hydrophillicity leading to incompatibility with polymer matrix and poor dispersion causing phase separation.

Some hydrophobic derivatives of starch synthesized previously were successfully used for blending with thermoplastic polymers like polyethylene, polystyrene and PMMA [46]. The blends exhibited enhanced biodegradability with little deterioration in

mechanical properties. Hence we decided to test the performance of these derivatives as reinforcing fillers in natural rubber.

2.3 Synthesis of biocomposites of natural rubber with starch derivatives

2.3.1 Introduction

A series of esters of starch viz starch acetate, starch phthalate and starch cinnamate were used [47]. Unlike native starch these esters are hydrophobic in nature so that they are expected to have better interaction with natural rubber.

2.3.2 Experimental

2.3.2.1 Materials

Phthalic anhydride, potassium acetate, acetyl chloride, cinnamoyl chloride and formamide were purchased from Qualigens chemicals, Mumbai, India.

2.3.2.2 Modification of starch

Modification of starch was carried out using the procedure reported elsewhere [56] (Scheme. 2.3.1). For the synthesis of starch acetate (StAc) and starch cinnamate (Stcin) the respective acid chlorides were used, while for starch phthalate (Stph) phthalic anhydride was used. Prior to synthesis, the starch was dried in an oven at 100 °C for 8 h.

2.3.2.3 Preparation of Composites

As shown in scheme 2.5 the composites of NR are prepared on two roll mixing mill and the mastication has to be continued for a long time so as to obtain homogenous composites. During this process the temperature was controlled at ~ 40 ^{o}C. These results were then compared with conventional composite i.e. C-black/NR. Upto 40 phr of fillers were added along with the accelerators listed in table. 2.1.1.

This was followed by vulcanization carried out at 150 ºC for 7-8 min using a hot press. The pressure of the hot press was adjusted (~300 k Pa) to obtain rubber composite sheets with 2 mm thickness.

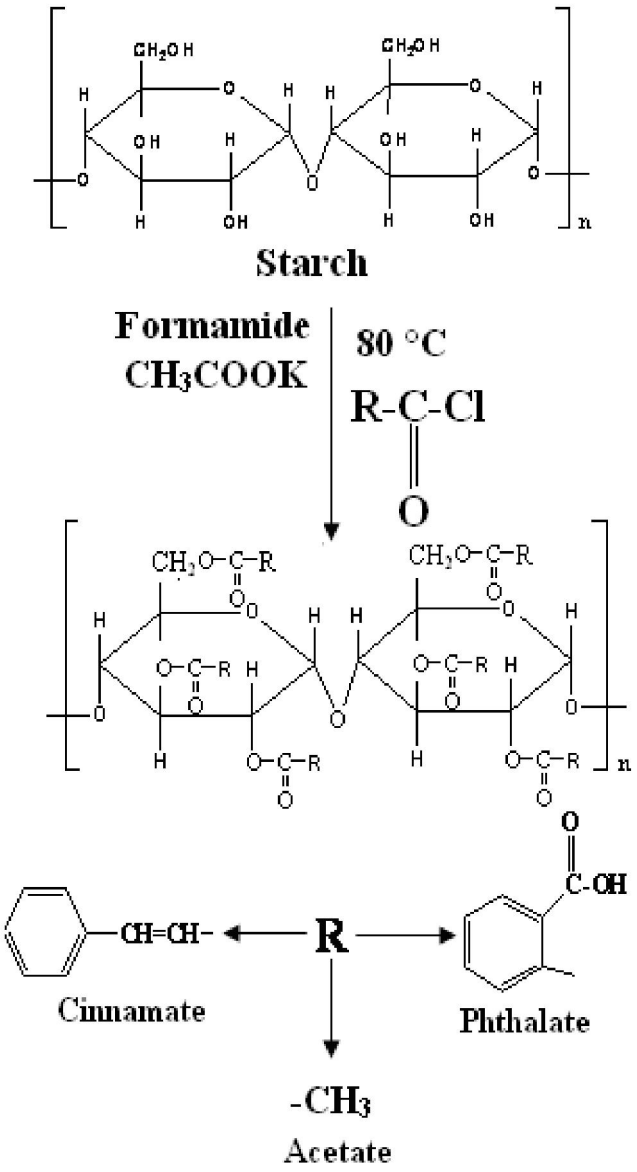

Scheme.2.3.1 Esterification of starch

2.3.2.4 Characterization

These biocomposites were characterized in a similar way as discussed in section 2.1.2.3. through hardness, mechanical properties such as tensile strength and % elongation, and morphology studies through scanning electron microscopy.

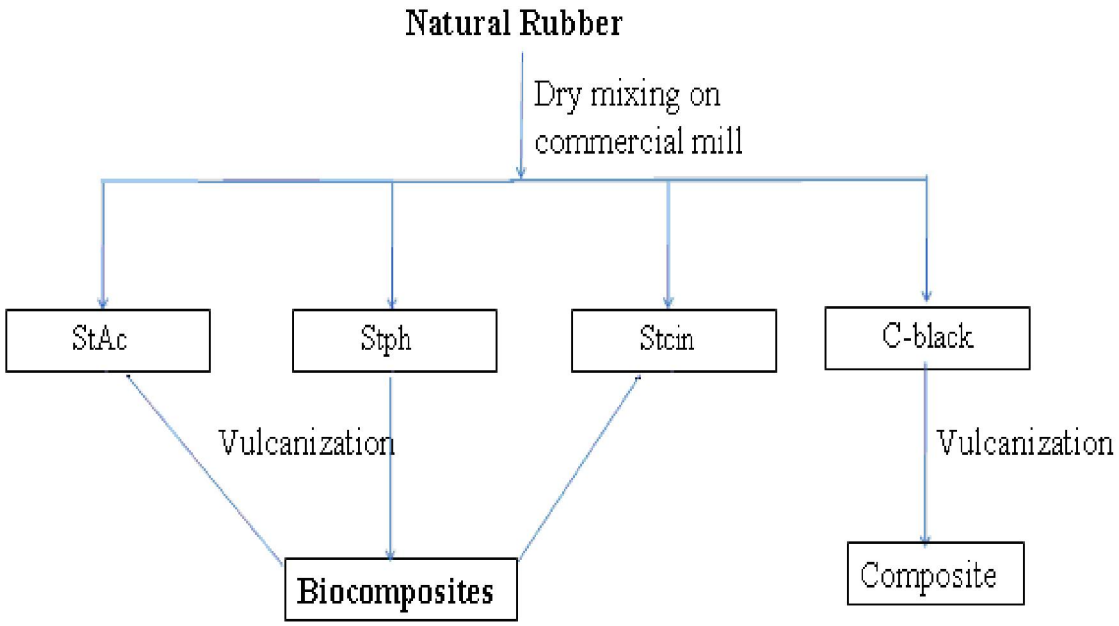

Scheme. 2.3.2 Preparation of biocomposites

2.3.3 Results and discussion

2.3.3.1 Mechanical properties

Hardness

Hardness of biocomposites increases with the amount of filler (Figure. 2.3.1). All biocomposites showed better hardness than C-black upto 40 phr.

Tensile Strength

Tensile strength of biocomposites increases with the amount of filler upto 30 phr. After this the tensile strength decreases although the hardness increases (Figure. 2.3.1). This shows that after 30 phr the biocomposites becomes brittle. Incase of C-black there was a steep increase in tensile increases upto 40 phr. Addition of starch phthalate led to best mechanical properties among all the fillers followed by cinnamate and acetate.

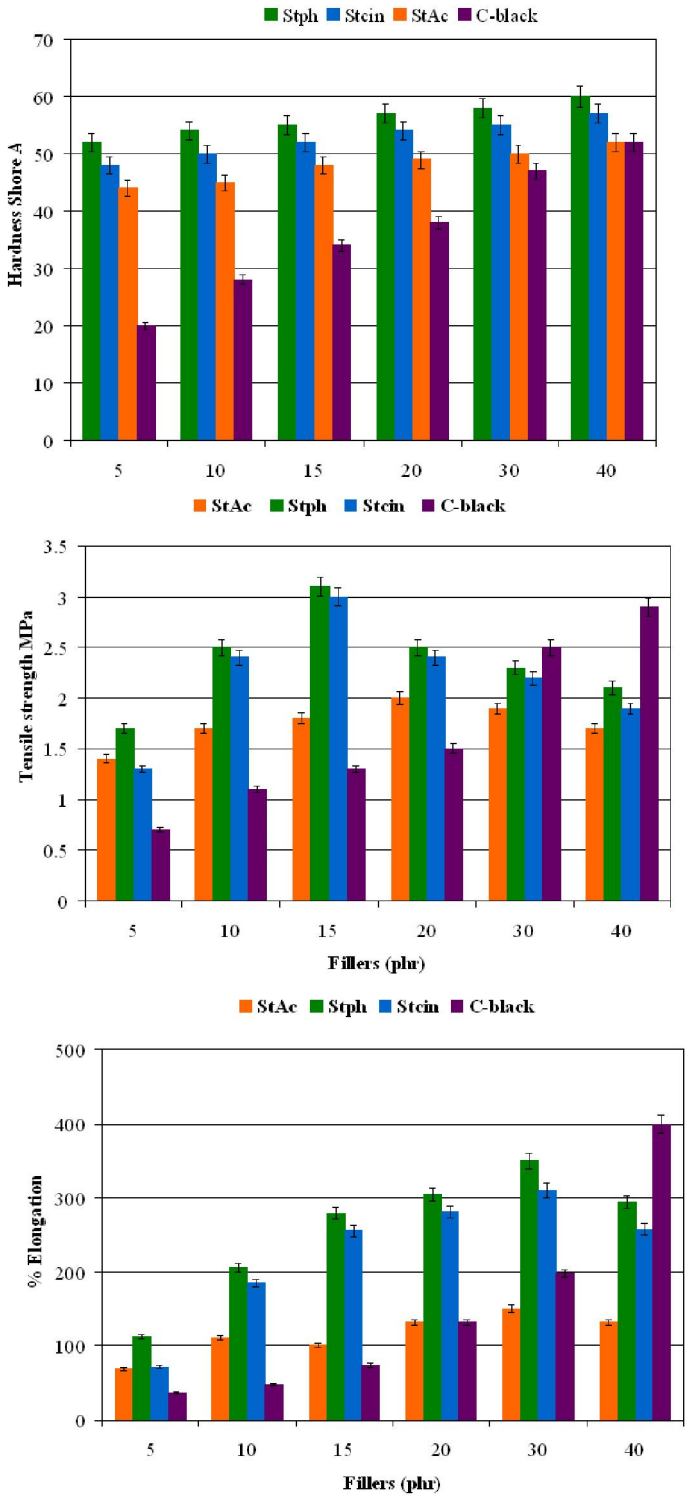

Figure. 2.3.1 Mechanical properties of biocomposites containing acetylated starch particles

% Elongation

A trend very similar to tensile strenght was observed. Optimum % elongation was observed at 30 phr after which the elongation decreases along with tensile as the amount of fillers increases (Figure. 2.3.1).

2.3.3.2 Scanning electron microscopy

The fractured samples of tensile strength were tested for surface morphology. The SE micrographs of the biocomposites at 30 phr loading are shown in Figure. 2.3.2. The micrographs of biocomposites show a very uniform morphology like a single phase with no distinction between the matrix and the dispersion phase.

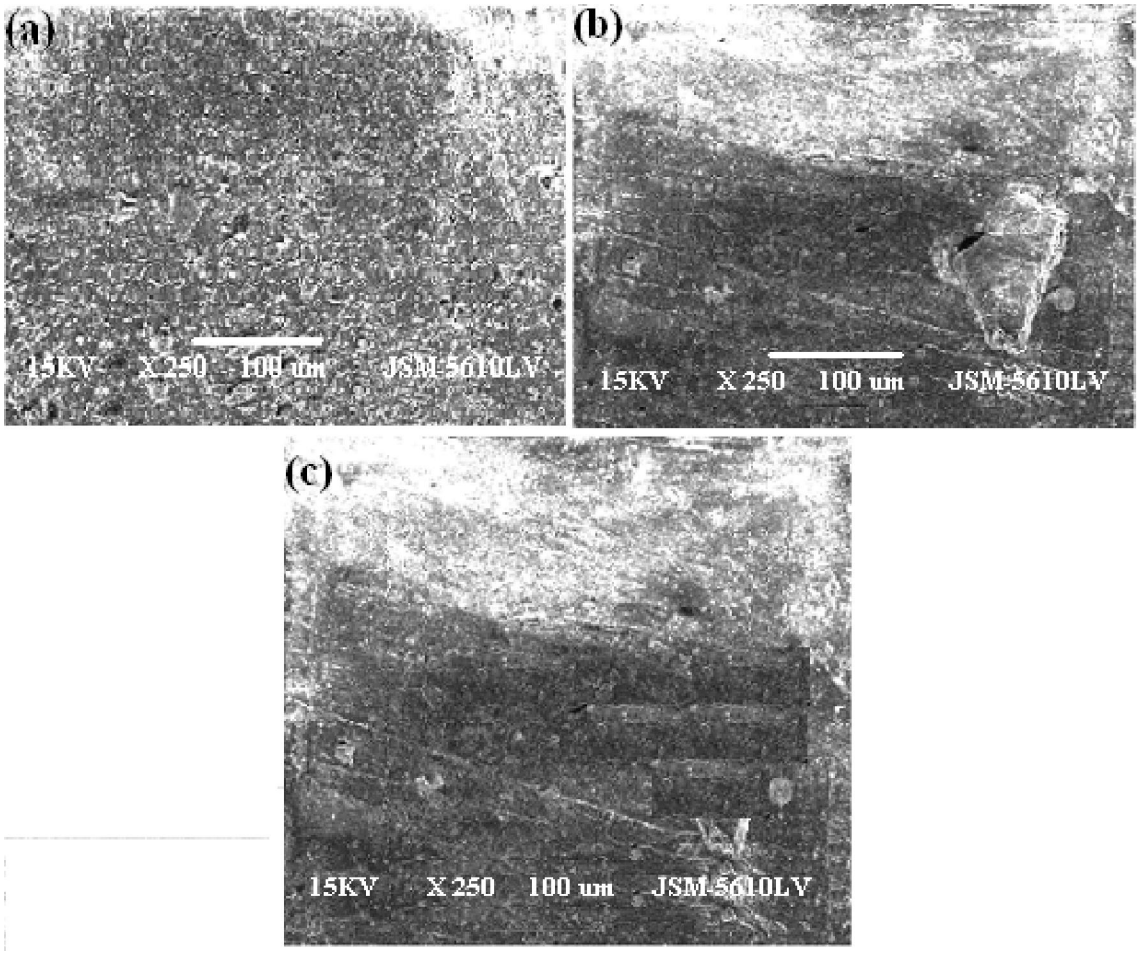

Figure. 2.3.2 Scanning electron microscopy of modified-starch biocomposite

2.3.3.3 Thermo gravimetric analysis

It is well known that the thermal stability of starch is poor but on its organic modification its thermal stability increases. This is due to the lower amount of remaining hydroxyl groups after modification (Figure. 2.3.3).

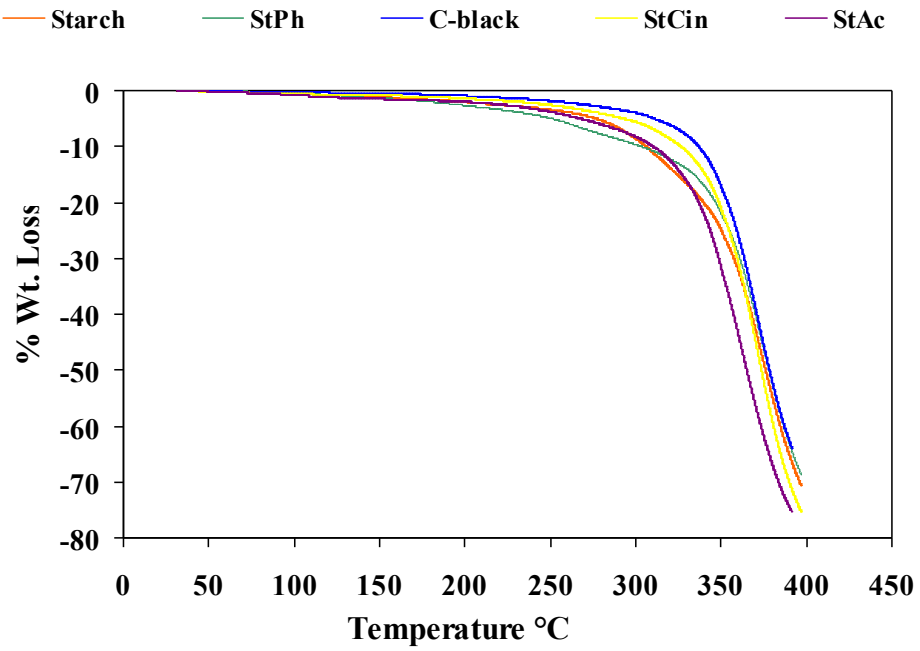

Figure. 2.3.3 TG curves of natural rubber containing acetylated starch particles

2.3.4 Conclusions

The present investigation leads to the conclusion that acetylated starch particles are potential fillers for natural rubber upto 30 phr loading. Scanning electron microscopy revealed single phase morphology. The thermal stability also improves after acetylation of starch. These results indicated a definite improvement in performance of fillers on organic modification. To enhance their performance further and to improve the dispersion the following strategy was adopted.

1. Reduction in particle size of the biopolymers to obtain nanofillers which can result in more uniform distribution within the polymer matrix.
2. Organic modification of the nanofillers to obtain hydrophobic derivatives having improved compatibility with the polymer.

2.3.5 References

1. B.B. Boonstra, Rubber Technology and Manufacture, C.M. BlowLondon, **1975**, 7.
2. M. Arroyo, M. A. López-Machado, B. Herrero, *Polymer*, **2003,** 44, 2447.
3. A.P. Meera, S. Said, *J. Phys. Chem. C*, **2009**, 113, 17997.
4. H. Angellier, S. Molina-Boisseau, A. Dufresne, *Macromolecules*, **2005**, 38, 9161.
5. K. Gopalan, A. Dufresne, *Biomacromolecules*, **2003,** 4, 657.
6. C. Sirisinha, S. Limcharoen, J. Thunyarittikorn, *J. Appl. Polym. Sci.,* **2003,** 87, 83.
7. P. Reichert, H. Nitz, S. Klinke, R. Brandsch, R. Thomann, R. Mulhaupt, *J. Macromol. Mater. Eng.,* **2000**, 275, 8.
8. A. Usuki, M. Kato, A. Okada, T. Kurauchi, *J. Appl. Polym. Sci.,* **1997**, 63, 137.
9. J.S. Shelley, P.T. Mather, K.L. DeVries, *Polymer*, **2001**, 42, 5849.
10. L. Liu, Z. Qi, X. Zhu, *J. Appl. Polym. Sci.,* **1999**, 71, 1133.
11. T.D. Fornes, P.J. Yoon, D.R. Paul, *Polymer*, **2003**, 44, 7545.
12. B. Hoffmann, C. Dietrich, R. Thomann, C. Friedrich, R. Mulhaupt, *Macromol. Rapid Commun.,* **2000**, 21, 57.
13. H.A. Stretz, J.H. Koo, V.M. Dimas, Y. Zhang, *Polym. Prepr.,* **2001**, 42, 50.
14. R.N. Hakim, H. Ismail, The comparison of organoclay with respect to silica on properties of natural rubber nanocomposites. *J. Reinforced Plast. Comp.* in press.
15 H. Ismail, R. Ramli, Organoclay filled natural rubber nanocomposites: The effects of filler loading and mixing method. *J. Reinforced Plast. Comp.,* **2008**, 27, 1909.
16. R. Alex, C. J. Nah, *Appl Polym Sci,* **2006**, 102, 3277.
17. A. Jacob, P. Kurien, A. S. Aprem, *Int J Polym Mater,* **2007**, 56, 593.
18. S. Sadhu, A. K. Bhowmick, *J Polym Sci Part B: Polym Phys,* **2004**, 42, 1573.
19. S. Sadhu, A. K. Bhowmick, *Rubber Chem Technol,* **2005**, 78, 321.
20. B. Liu, Q. Ding, Q. He, J. Cai, B. Hu, J. Shen, *J Appl Polym Sci*, **2006**, 99, 2578.
21. H. Zheng, Y. Zhang, Z. Peng, Y. Zhang, K. G. Gatos, Karger-Kocsis, *J. Polymer*, **2005**, 46, 3069.
22. Y.-P. Wu,; Q.-X. Jia, D.-S. Yu, L.-Q. Zhang, *J Appl Polym Sci,* **2003**, 89, 3855.
23. M. Maiti, A. K. Bhowmick, *J Polym Sci Part B: Polym Phys,* **2006**, 44, 162.

24. H.-C. Kuan, C.-C. M. Ma, W.-P. Chuang, H.-Y. Su, *J Polym Sci Part B: Polym Phys,* **2005**, 43, 1.

25. P. G. Rouxhet, N. Samudacheata, H. Jacobs, O. Anton, *Clay Miner,* **1977**, 12, 171.

26. V. J. Hurst, A. C. Kunkle, *Clays and Clay Minerals*, **1985,** 33, 1.

27. A. Dufresne, J. Y. Cavaille, W. Helbert, *Macromolecules*, **1996,** 29, 7624.

28. H. U. Zaman, M. A. Khan, R. A. Khan, Md. D. H. Beg, *Int. J. Polym. Mater.,* **2011,** 60, 303.

29. R. C. R. Nunes, E. S. Affonso, *Kautsch. Gummi Kunstst.,* **1999,** 52,12.

30 H. U. Zaman, M. A. Khan, R. A. Khan, D. H. Beg, Inter.J. Polym. Mater., 2011, 60, 303.

31 R. M. B. Fernandes, L. L. Y. Visconte, R. C. R. Nunes, Inter. J. Polym. Mater., **2011**, 60, 351.

32. V. L. C. Lapa, P. D. Oliveira, L. L. Y. Visconte, R. C. R. Nunes, *Polym. Bull.* **2008,** 60, 281.

33. S. Hribernik, M. S. Smole, K. S. Kleinscheck, M. Bele, J. Jamnikand, M. Gaberscek, *Polym. Degrad. Stab.* **2007,** 92, 1957.

34. J. Schrrz, Prog. Polym. Sci. 24, **1999,** 481.

35. D. K.Singh, A. R. Ray, *Macromol. Chem. Phys.,* **2000**, 40, 69.

36. Y. Guo, P. Wu, *Carbohyd. Polym.,* **2008,** 74, 509.

37. S. Desai, I. M. Thakore, S. Devi, *Polym. Int.,* **1998,** 47, 172.

38. X. Lu, M. Q. Zhang, M. Z. Rong, G. A. Shi, G. C. Yang, *Polym. Compos.,* **2003,** 24, 367.

39. A. K. Bledzki, F. Omar, *Appl. Compos. Mater,* **2003,** 10, 365.

40. A. Dufresne, J. Y. Cavaille, W. Helbert, *Macromolecules,* **1996,** 29, 7624.

41. B. S. Harogoppad, T. M. Aminabhavi, *J. Appl. Polym. Sci.,* **1992,** 46, 725.

42. S. Desai, I. M. Thakore, B. D. Sarawade, S. Devi, *Polym. Eng. Sci.,* **2000,** 40, 1200.

43. A. P. Mathew, S. Packirisamy, M. G. Kumaran, S. Thomas, *Polymer*, **1995,** 36, 4935.

44. S. Desai, I. M. Thakore, S. Devi, *Polym. Int.,* **1998,** 47, 172.

45. R. Lalwani, S. Desai, *J. Appl. Polym. Sci.,* **2010,** 115, 1296.

46. M. Jacob, K. T. Varughese, S. Thomas, *Biomacromolecules*, **2005,** 6, 2969.

Chapter-3 Synthesis, organic modification and characterization of polysaccharide nanoparticles

Outline

3.1 Introduction

The dispersion of filler into elastomeric matrix is an important factor. Improvement in dispersion can be achieved by reduction in size. Native starch is composed of two different types of polymers: a nearly linear amylose and branched amylopectin [1]. It occurs in the form of discrete and partially crystalline granules with more or less concentric growth rings. Aqueous acids can be employed to hydrolyze the amorphous sections of the polymer. As a result the crystalline sections of these polysaccharides are released, resulting in individual monocrystalline nanoparticles [2]. Acid treatment allows revealing the concentric lamellar structure of starch granules by dissolving region of low lateral order. The water insoluble and highly crystalline residue obtained from waxy corn starch granules have been found to be composed of nanoscale crystals [3,4].

Among the polysaccharides cellulose is the most abundant renewable organic material produced in the biosphere. It has been reported that colloidal suspensions of cellulose can be obtained by controlled sulfuric acid-catalyzed degradation of cellulose fibers [5]. Disordered or paracrystalline regions of cellulose are preferentially hydrolyzed, whereas crystalline regions remain intact [6]. Cellulose nanoparticles (CelNPs) obtained by acid hydrolysis have been used as filler in various polymers including important elastomer such as natural rubber [7]. Cellulose nanocrystals or whiskers are prepared by dissolving the amorphous or less ordered regions of the microfibrils by acid degradation. The resulting isolated crystalline regions are typically 200–400 nm in length. Some specific sources such as tunicin display nanocrystals as long as 1 μm.

The disadvantage of using polysaccharides as fillers is that they are hydrophilic in nature and due to this their compatibility with hydrophobic rubber is poor. To improve the compatibility reduction in size can be employed to have better dispersion of nanoparticles. Hence there is a growing interest in organically modified derivatives of polysaccharides for different applications. The amphiphillic nature imparted upon polysaccharides after hydrophobic modification gives them a wide and interesting applications spectrum, for instance as rheology modifier, emulsion stabilizer, surface modifier and as drug delivery vehicles. Therefore, chemical modifications of polysaccharides nanoparticles has been extensively studied [8,9,10]. In case of nanoparticles it is important that modification should be carried out at ambient

and fatty acids in organic and aqueous solvents [11,12]. Modification also has been done via graft polymerization of caprolactone, poly ethylene oxide etc. [13,14]. Similarly due to an abundance of hydroxyl groups at the surface of cellulose, chemical modifications like esterification, etherification, oxidation, silylation, polymer grafting, etc have been attempted [15,16,17]. However most of these modifications of polysaccharides nanoparticles require drastic or prolonged reaction conditions which may also lead to agglomeration of the polysaccharides nanocrystals and consequently decrease their effect. Hence we decided to carry out the modification at ambient temperatures in order to preserve the size of nanoparticles.

Diisocyanates being highly reactive compounds, reactions take place easily under mild ambient conditions. Among various isocyanates, hexamethylene diisocyanate (HMDI) has a flexible structure with an aliphatic chain of six methylene groups. Acetylation of polysaccharides nanoparticles can easily take place at ambient temperature and hence we have tried to carry out room temperature modification of polysaccharides nanoparticles.

3.2 Experimental

3.2.1 Materials

Waxy maize starch (containing mostly amylopectin and small traces of amylose), sulfuric acid, 1,4-hexamethylene diisocynate, dibutyl tin dilaureate (DBTDL), acetic anhydride, tetrahydrofuran (THF), toluenesulphonic acid (PTSA), acetic acid, microcrystalline cellulose, cellulose acetate were purchased from Sigma Aldrich, Bombay.

3.2.2 Synthesis of nanoparticles

Starch nanoparticles (StNPs)

The preparation of starch nanoparticles by sulfuric acid (H_2SO_4) hydrolysis of native waxy maize starch granules was carried out as per the procedure developed by Dufresne et al. [18] (Scheme 1). Briefly, 36 g of native waxy maize starch granules was mixed with 250 mL of 3.16 M H_2SO_4 and stirred for 5 days at 40 °C. The suspension was washed by successive centrifugations with distilled water until neutrality. The nanoparticles were dried under vacuum at 50 °C. The resulting nanoparticles had a weight of about 28.5 g.

Cellulose nanoparticles (CelNPs)

Similarly, for the synthesis of cellulose nanoparticles, 36 g of cellulose was mixed with 3.16 M H_2SO_4 and the suspension was continuously stirred for 5 days at 40 °C (scheme. 3.1). The nanoparticles were collected by centrifugation and washed repeatedly with distilled water until neutral. The nanoparticles were dried under vaccum at 50 °C. The resulting nanoparticles had a weight of about 28.2 g.

Isocyanate modification of StNPs (StINPs)

For isocyanate modification, dried StNPs (1 mole) and HMDI (0.9 mole) were allowed to react in dry tetrahydrofuran (THF) at room temperature in the presence of catalytic amount of DBTDL under nitrogen atmosphere to form a urethane linkage. Unlike 2, 4-toluene diisocyanate (TDI), the reactivity of the two hydroxyl groups of HMDI is identical. Hence the reaction proceeds instantly resulting in high degree of crosslinking (scheme 3.2). The mixture was immediately subjected to ultrasonication to obtain a homogeneous dispersion of isocyanate modified starch nanoparticles in THF. The suspension was then centrifuged and the product was dried at 50 °C under vacuum. The yield obtained was 84.54%.

Starch acetate nanoparticles (StAcNPs)

To prepare acetylated StNPs, 1 g of StNPs (1 mole) and 10 ml acetic acid were mixed and stirred for 10 minutes at room temperature. Acetic anhydride (0.6 mole) was added dropwise to the above mixture (scheme 3.2). After this 0.2 g of PTSA was added and the reaction mass was stirred for 6 h at 60 ºC. The product was poured in cold water and StAcNPs were collected by centrifuge and washed with water. The product was dried at 50 ºC under vacuum and weighed. The yield obtained was 85.54%.

Starch cinnamate (StcinNPs), benzoate (StbenNPs), palmitate (StpalNPs) and phthalate nanoparticles (StphNPs)

Modification of starch nanoparticles was carried out in two steps. In the first step, one gram of starch nanoparticles were dispersed in alkali medium (water) at room temperature. The mixture was stirred for 10 min at room temperature under nitrogen

atmosphere. In the second step, 0.6 mol equivalents of the required acid chlorides (Cinnamoyl chloride, benzoyl chloride and palmitoyl chloride) were added drop wise for 20 min (Scheme 3.2). The reaction was continued for 20 min at room temperature. The modified starch nanoparticles were isolated by precipitation in water. The product was centrifuged and washed with water to remove unreacted acid chlorides. It was then dried at 50 °C under vaccum. The modified starch nanoparticles were recrystallized by using 1,4-dioxane. For synthesis of starch phthalate nanoparticles, phthalic anhydride was used. The yield obtained in case of StCinNPs, StBenNPs, StPalNPs and StPhNPs was 88.75%, 85.32%, 79.23% and 91.12% respectively.

Cellulose acetate nanoparticles (CelAcNPs)

To a mixture of CelNPs (1 mole) and acetic acid, acetic anhydride (0.6 mole) was added dropwise at room temperature. After stirring for few minutes PTSA was added and the reaction mass was maintained with stirring for 1 h at 60 ºC. The product was centrifuged, washed with distilled water and dried at 50 ºC under vacuum.

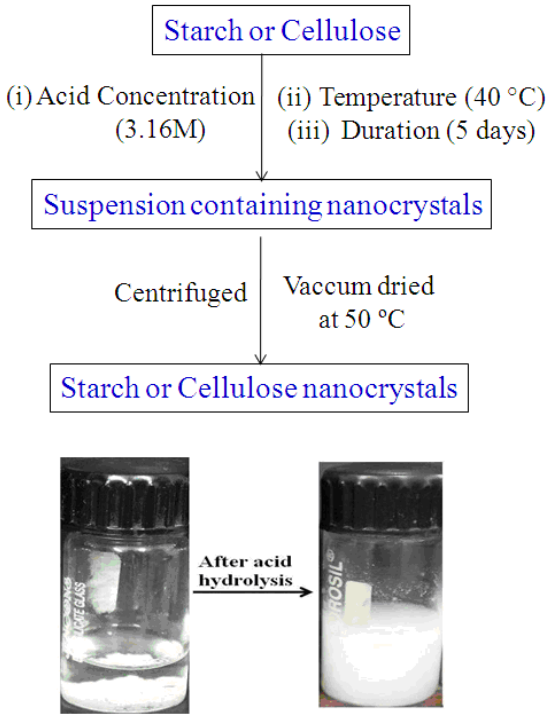

Scheme. 3.1 Synthesis of polysaccharides nanoparticles

3.2.3 Characterization of nanoparticles

Fourier transform infrared spectroscopy

FT-IR spectra of polysaccharides nanoparticles were recorded as KBr pellet on Perkin Elmer RX1 model in the range of 4000-400 cm^{-1}.

Nuclear magnetic resonance

^{1}HNMR spectra were recorded on Bruker Advance 400. It was used to determine the DS of the acetylated starch nanocrystals as it is used to evaluate starch. Based on the report [11] the substitution of the starch derivatives was calculated by the following eq. (1).

$$DS = 7A/3B \quad \ldots\ldots\ldots\ldots \quad (1)$$

Where, A is sum of areas of newer protons added to the anhydroglucose ring and B is the sum of areas of seven protons in anhydroglucose unit observed at higher than 3.95 ppm.

Morphology and size

Morphology was examined by means of Jeol Scanning Electron Microscope (model – JSM – 5610 LV). An accelerating potential of 15 kV was used for the analysis of the sample. Size and shape of the nanoparticles were determined by using TEM on a Philips, Holland Technai 20 model operating at 200 kV. The sample for TEM was prepared by putting one drop of the suspension onto standard carbon-coated copper grids and then drying under an IR lamp for 30 min.

X-ray diffraction

X-ray diffraction (XRD) was determined by using PANalytical 'X'PERT-PRO XRPD.

Thermal properties

TGA was recorded on TG-DTA 6300 INCARP EXSTAR 6000 in nitrogen atmosphere in temperature range of 30 º- 450 ºC at heating rate of 10 ºC/min.

Biodegradation studies

To prove the retention of biodegradation after modification, the growth of microbes on modified and unmodified polysaccharides nanoparticles was compared in a culture medium. Two sets of experiment (experimental and control) were conducted. The control sets were uninoculated, while for the experimental set the acclimatized microorganisms were inoculated into sterile medium. The flasks were incubated under shaking conditions (160–180 rpm) at 30 °C and growth of microorganisms (E. coli) was studied. The soluble protein was estimated by using method suggested by Lowry et al. [19] using Bovine Serum albumin as a standard.

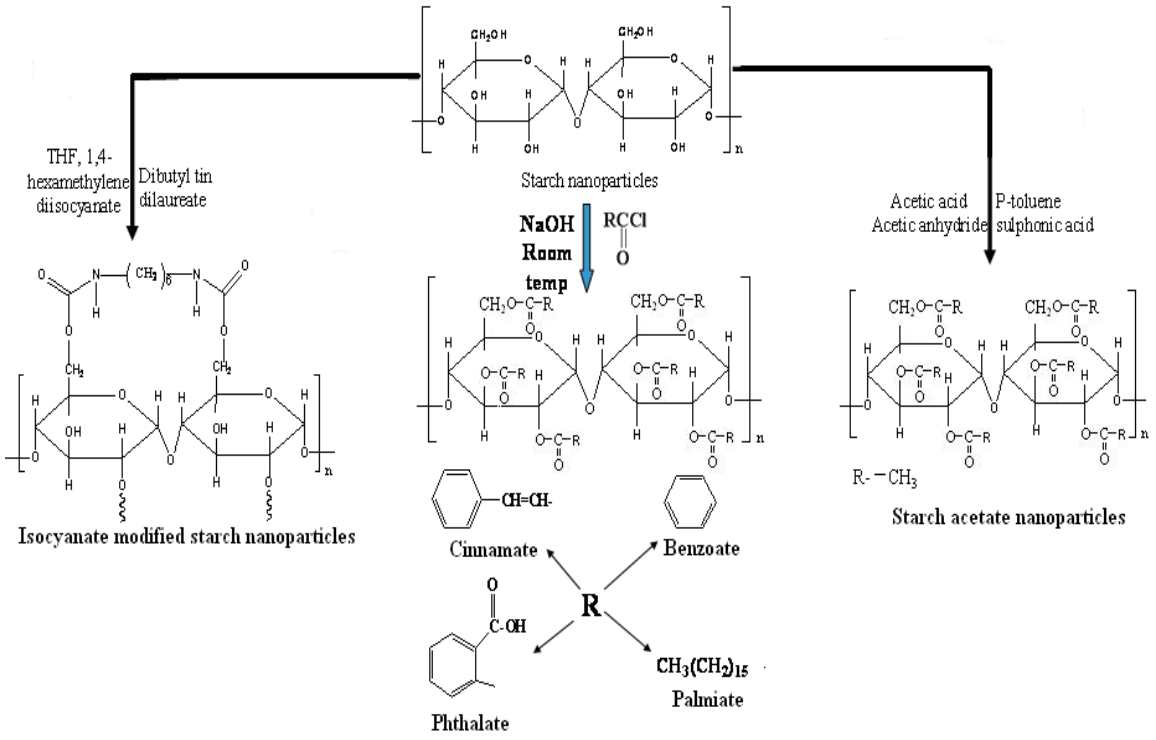

Scheme. 3.2 Organic modification of nanoparticles

3.3 Results and discussion

3.3.1 Fourier transform infrared spectroscopy (FT-IR)

Comparative FT-IR spectra of polysaccharides nanoparticles are shown in Figure.3.1. In the spectra of the starch nanocrystals, a broad band due to hydrogen bonded hydroxyl groups appeared at 3600-3200 cm^{-1}. The peak at 1650 cm^{-1} was due to tightly bound water present in the starch [20]. While absorption band between 1000 and 1200 cm^{-1} were characteristic of the –C-O stretching of polysaccharide skeleton. Similarly in case of cellulose nanoparticles the peak at 3400 cm^{-1} is due to -OH stretching and peak at 1640 cm^{-1} is due to tightly bound water [21] (Figure.3.1). While absorption band between 1000 and 1200 cm^{-1} are characteristic of the –C-O stretching of polysaccharide skeleton. The peak around 2930 cm^{-1} corresponds to the –C-H stretching in case of polysaccharides nanoparticles.

In case of isocyanate modified starch nanoparticles the characteristic carbonyl stretching of urethane linkage was observed at 1753 cm^{-1} while vibration of urethane N-H was seen at 1690–1650 cm^{-1}. The absorption resulting from –NH stretching vibration were observed as a broad peak at 3450-3250 cm^{-1}. Since HMDI consists of 6 consecutive $–CH_2$ group the bending vibration at 758 cm^{-1} was observed. The IR spectrum also indicates the completion of the reaction between diisocyanate and starch by the absence of the NCO absorption band at 2250 cm^{-1}. In acetylated starch nanoparticle a strong absorption peak at 1751 cm^{-1} was attributed to stretching of ester carbonyl –C=O [22]. The peak at 3400 almost disappeared indicating that modification of StNPs has taken place. The other peak at 1237 cm^{-1} was attributed to C-O-C- bond stretching of ether linkage.

In acetylated cellulose nanoparticles a strong absorption peak at 1736 cm^{-1} can be attributed to stretching of ester carbonyl >C=O (Figure.3.1). The intensity of peak corresponding to 3400 cm^{-1}decreases indicating that acetylation process has taken place. The other peak around 1200 cm^{-1} can be attributed to -C-O-C- bond stretching of ether linkage [23].

Also the FT-IR spectra after acylation, showed the existence of a carbonyl absorption band at 1736, 1740, 1742 and 1750 cm^{-1} for palmiate, benzoate, cinnamate and phthalate starch nanoparticles respectively. The peak due to stretching and bending of aromatic -C-H appears around 3000 and 800 cm^{-1} respectively in case of aromatic derivatives.

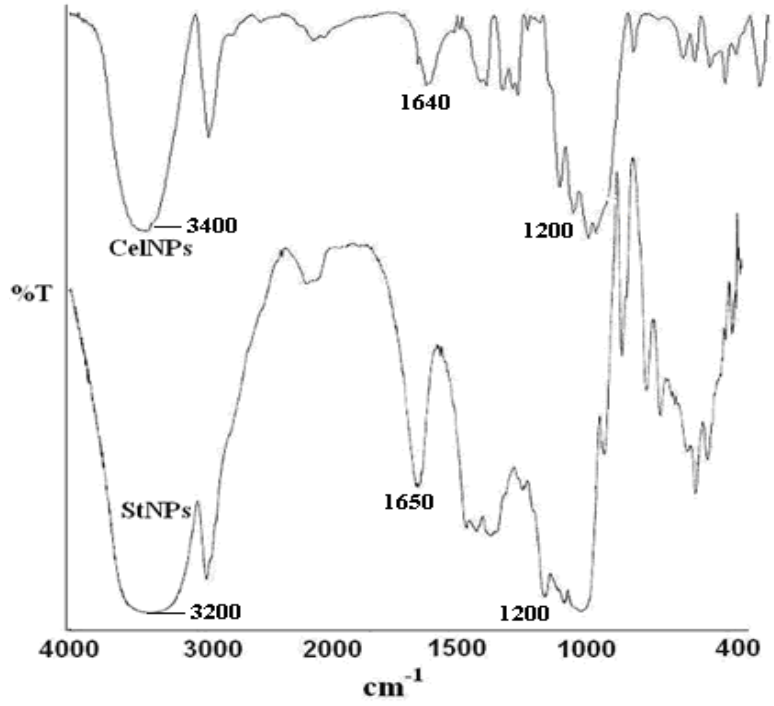
1640
3400
CelNPs
1200
%T
StNPs
1650
3200
1200
4000
3000
2000
1500
1000
400
cm-1

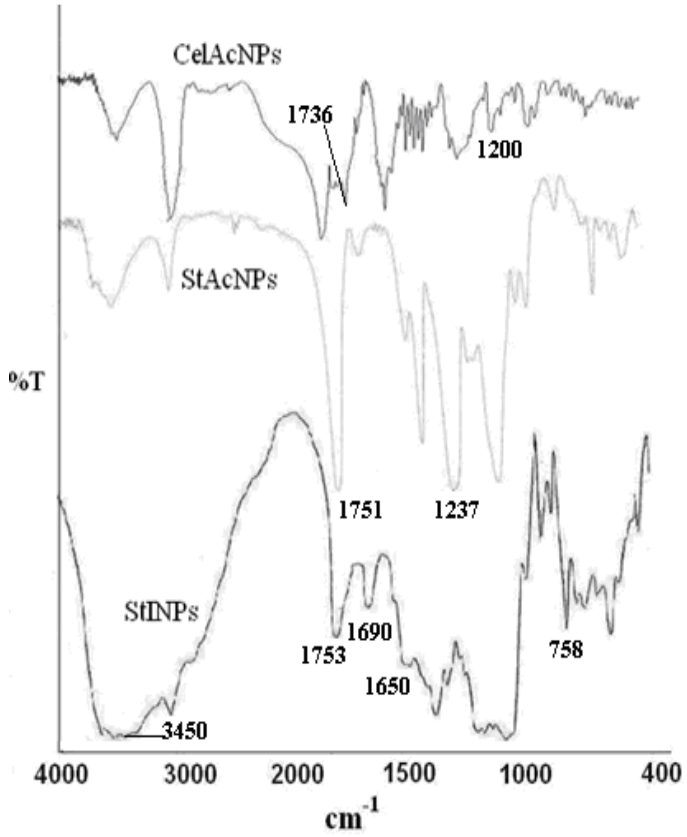
CelAcNPs
1736
1200
StAcNPs
%T
1751
1237
StlNPs
1690
1753
758
1650
3450
4000
3000
2000
1500
1000
400
cm-1

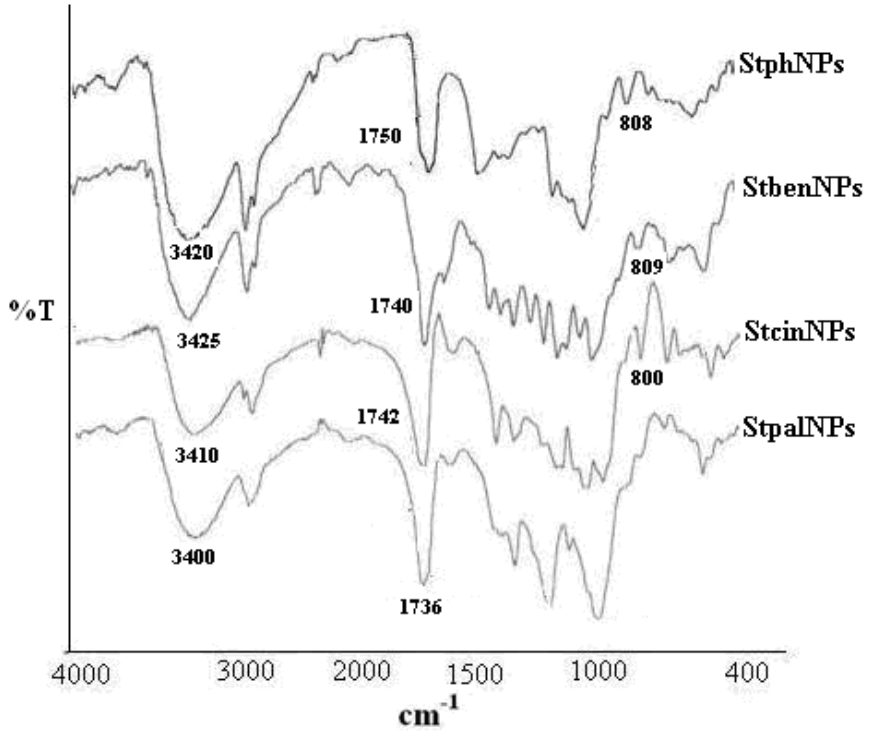

Figure 3.1 FT-IR spectra of nanoparticles

3.3.2 Nuclear magnetic resonance spectroscopy (NMR)

The ^{1}H NMR data of the polysaccharides nanoparticles is given below. The degree of substitution (DS) calculated by using equation 1 is given in table. 3.1

Cellulose acetate (DS=2.42)

^{1}H NMR (400 MHz, $CDCl_3$) δ 5.35 (s, 1H), 5.25 (s, 1H), 4.85 (s, 1H) 4.22–4.32 (s, 1H) (Figure. 2.3.2(a)).

Starch acetate (DS=2.37)

^{1}H NMR (400 MHz, $CDCl_3$) δ 5.25 (s, 1H), 5.17 (s, 1H), 4.75 (s, 1H) 4.22–4.32 (s, 1H) (Figure. 2.3.2(b)).

Starch phthalate NPs (DS=2.63)

^{1}H NMR (400 MHz, $CDCl_3$) δ 11.0 (s, 1H), 7.89 (d, 2H), 7.81 (d, 2H), 4.95 (s, 1H), 4.01 (s, 1H), 3.57 (s, 1H), 3.23 (s, 1H) (Figure. 3.2(c)).

Starch cinnamate NPs (DS=2.59)

^{1}H NMR (400 MHz, $CDCl_3$) δ 7.91 (d, 2H), 7.67 (d, 2H), 6.45 (d, 2H), 4.97 (s, 1H), 4.45 (s, 1H), 4.11 (s, 1H), 3.44 (s, 1H) (Figure. 3.2(d)).

Starch benzoate NPs (DS=1.98)

^{1}H NMR (400 MHz, $CDCl_3$) δ 8.12 (s, 2H), 7.52 (s, 2H), 5.5 (s, 1H), 5.01 (s, 1H), 4.45 (d, 1H), 3.52 (s, 1H) (Figure. 3.2(e)).

Starch palmiate NPs (DS=2.49)

^{1}H NMR (400 MHz, $CDCl_3$) δ 4.98 (s, 1H), 4.04 (s, 1H), 3.47 (s, 1H), 2.97 (s, 1H), 2.34 (s, 2H), 1.67 (s, 2H), 1.21 (s, 2H), 0.85 (t, 3H) (Figure. 3.2(f)).

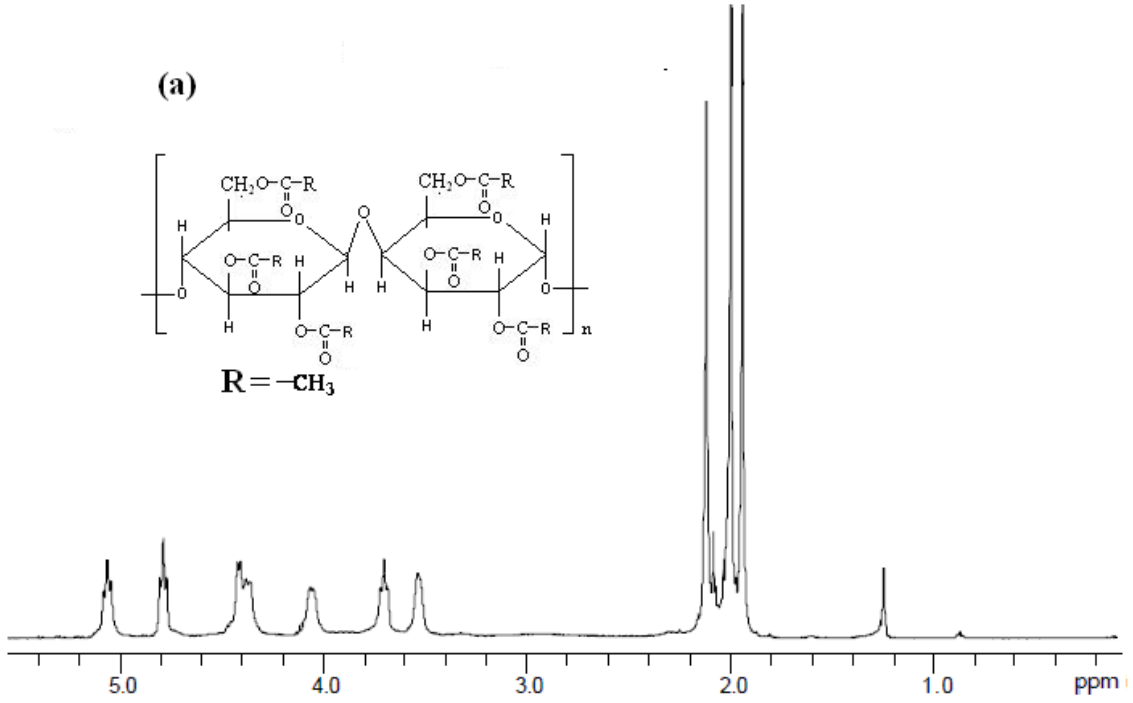

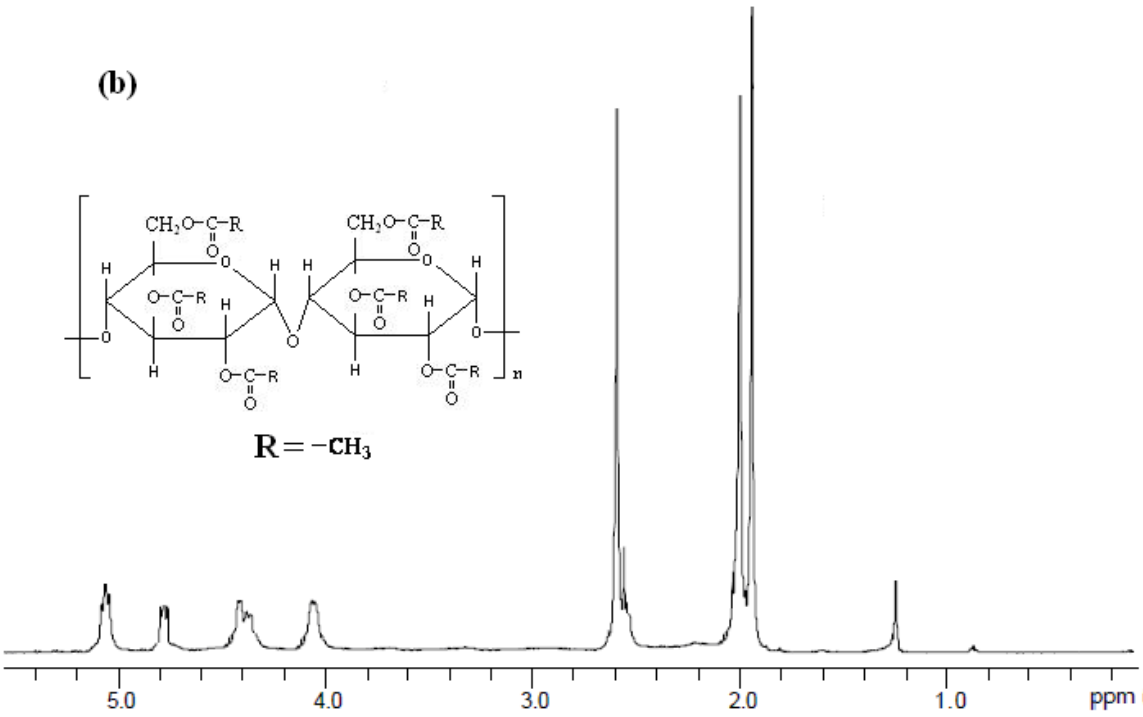
(b)
R = −CH3
5.0
4.0
3.0
2.0
1.0
ppm

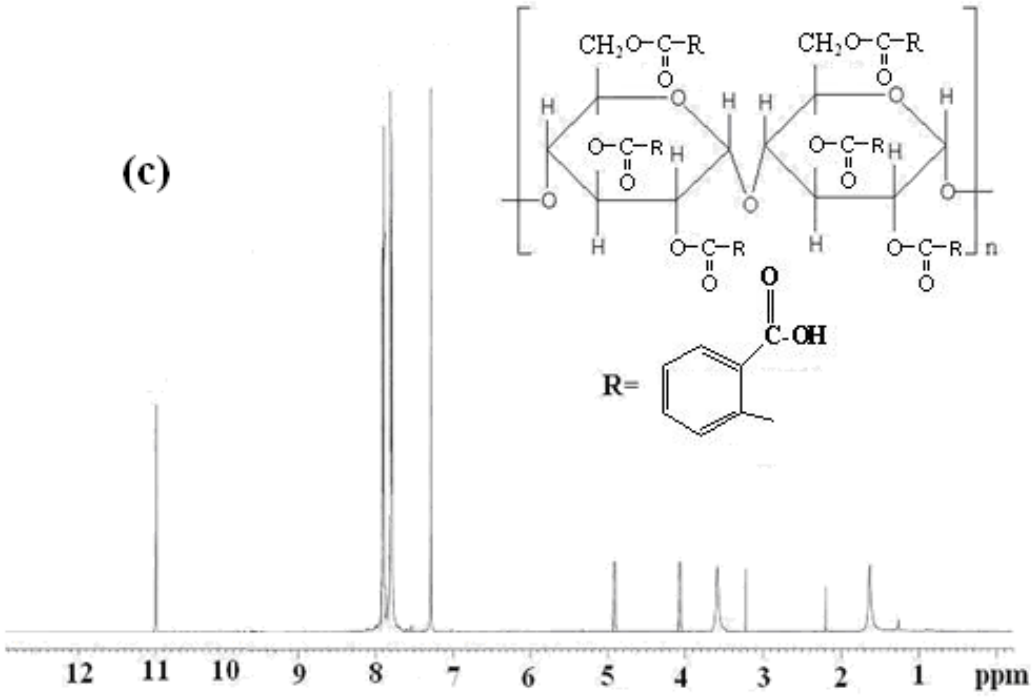
(c)
R=
12
11
10
9
8
7
6
5
4
3
2
1
ppm

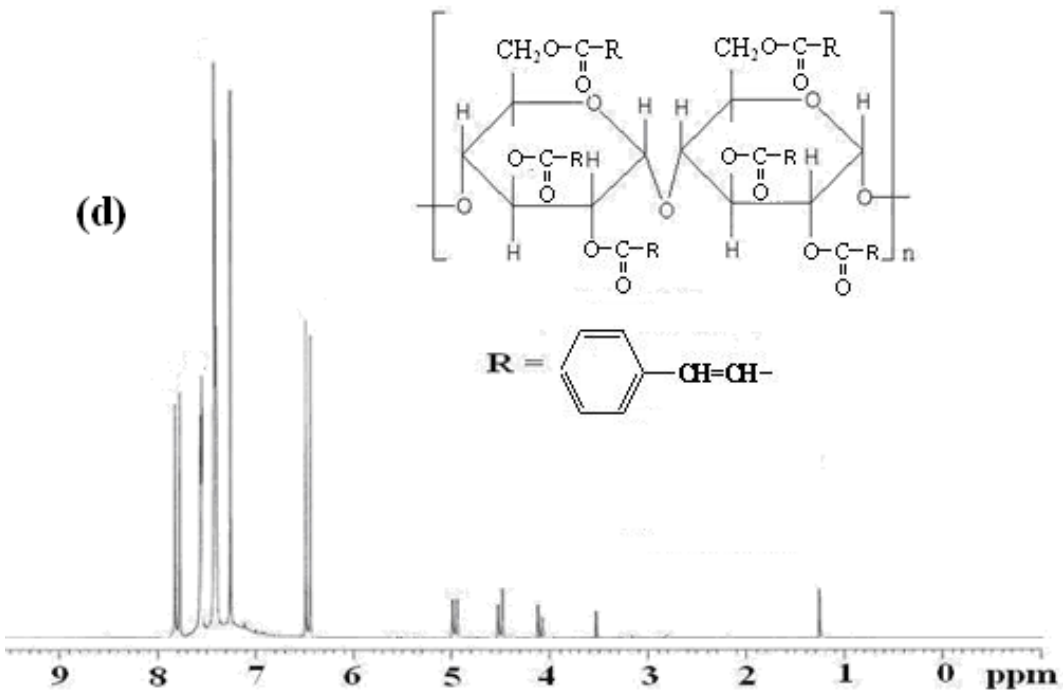
(d)
R = CH=CH
9 8 7 6 5 4 3 2 1 0 ppm

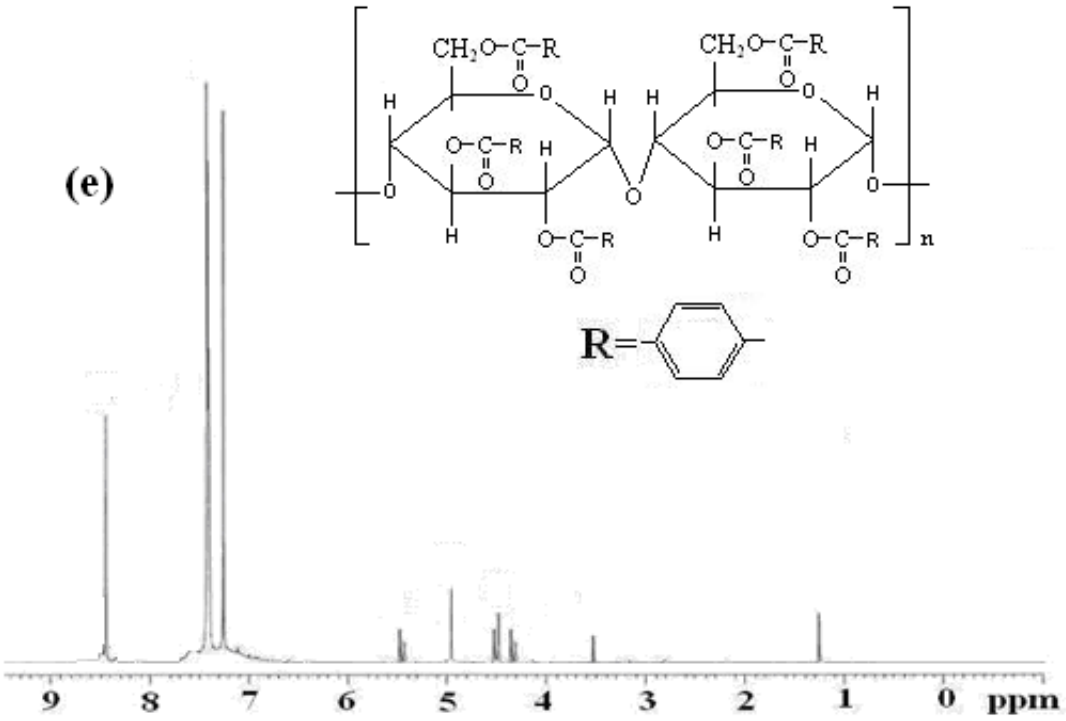
(e)
R=
9 8 7 6 5 4 3 2 1 0 ppm

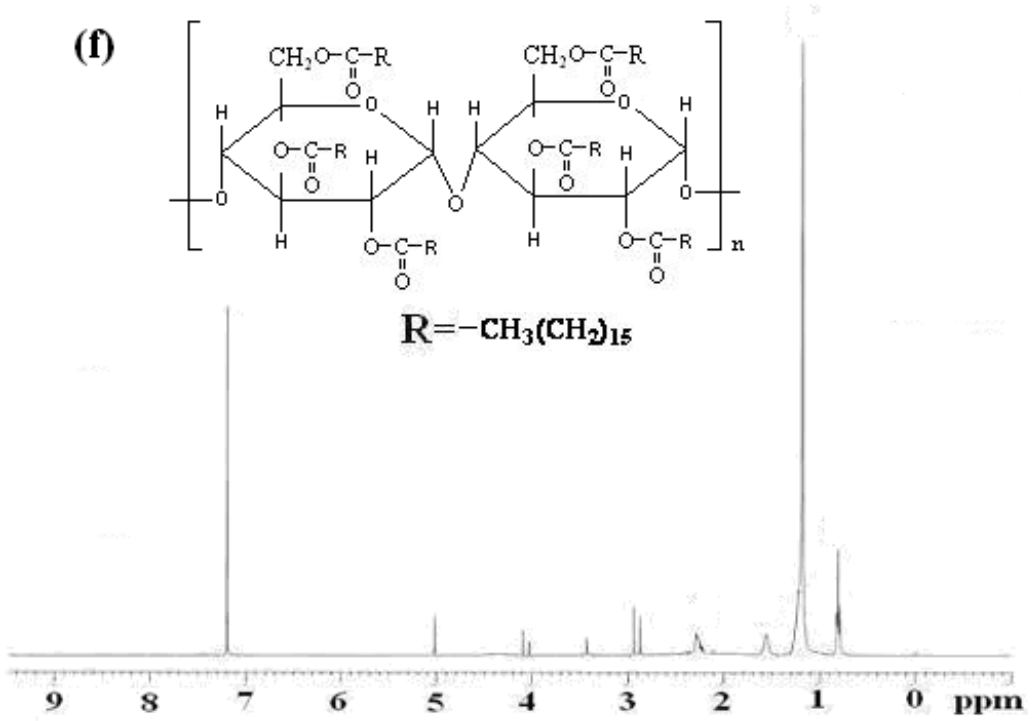

Figure. 3.2 1H NMR spectra of nanoparticles (a) CelAcNPs, (b) StAcNPs, (c) StphNPs, (d) StcinNPs, (e) StbenNPs and (f) StpalNPs

3.3.3 X-ray diffraction pattern (XRD)

Starch is a biosynthesized polymer containing semi-crystalline granules with varying polymorphic types and degree of crystallinity. Polymorphism of the α-glucans is one of the main characteristics of the crystalline parts in starch granules. Native starch granules contain crystalline regions as shown by their unique X-ray diffraction patterns (XRD). Therefore, granular crystallinity also can be studied with X-ray diffraction technique. Figure.3.3 shows the XRD pattern of starch & modified starch nanoparticles. The diffraction pattern displays typical peaks of A-type amylose allomorph [24]. It was characterized by peaks at 2 theta value at 11.23° and a strong peak at 15.03°, a double strong peak at 17.2° and 17.97° and a strong peak at 22.99° [25]. The acid hydrolysis does not change or transform the native crystalline state of starch nanocrystals. Isocyanate modification does not appear to have any pronounced effect on diffraction

other than the appearance of broad peak at 11° and 19° [26]. In case of starch acetate nanoparticles (StAcNPs) peak at 21° was observed [27]. This indicates that all the hydroxyl group of StNPs are replaced by isocyanate and acetyl group and no intermolecular hydrogen bonding was formed which destroy the ordered crystallinity. The A- style crystallinity of StNPs was destroyed after modification and V-type crystallinity was observed as confirmed by wide peaks at 11° and 19° in case of StINPs and peak 21° in case of StAcNPs [10]. The average particle size calculated from the width of the reflection according to the Debye–Scherrer equation (eq^{n} 2) of StNPs, StINPs and StAcNPs was about 65, 42 and 34 nm respectively.

$$\mathbf{D(nm) = K\lambda/\beta Cos\theta \ldots\ldots\ldots\ldots\ldots\ldots (2)}$$

where K is a constant equal to 0.89, λ is the X-ray wavelength (1.54 Å), β is the full-width at half-maximum (fwhm) of the major peak expressed in radians, and θ is the Bragg angle (deg) corresponding to that peak.

The XRD pattern of cellulose and cellulose acetate nanoparticles are shown in Figure.3.3. The peak at 22.6 º is characteristic for cellulose [28]. While in case of acetylated cellulose nanoparticles the peaks at 10.4 º and 13.2 º were observed. This indicates that the hydroxyl groups of CelNPs are replaced by acetyl group. The average particle size calculated from the width of the reflection according to the Debye–Scherrer equation (eq^{n} 1) of CelNPs and CelAcNPs was 57 and 31 nm respectively.

3.3.4 Microscopic studies

Transmission electron microscopy (TEM)

TEM was used to investigate the morphological changes of the polysaccharides fragments associated with modification. Figure.3.4 shows TEM images of nanocrystals before and after modification. After acid treatment process of native waxy corn starch granules, the granules have been destructured and degraded to be nanocrystals with a size range of 70–100 nm (Figure.3.4 (a)). We did not recognize anymore the platelet shape of unmodified starch particles, although the crystallinity type was preserved as revealed in XRD analysis.

TEM image of fatty acid modified starch nanocrystals showed a slight increase in size [29]. But in this case hydrophobicity increases and induced a partial solubilization of starch molecules located at the surface of the nanocrystal leading to a decrease in size. Moreover, the particles are more individualized and monodispersed than their unmodified counterparts (Figure.3.4 (c and d)). Similar results were obtained in case of CelNPs and CelAcNPs. TEM images of nanocrystals before and after modification are shown in Figure.3.4. Thicker bundles of fibrils around 70-80 nm corresponding to bigger cellulose aggregates were observed along with some individual fibrils (Figure.3.4 (b)). The polysaccharides nanoplatelets are believed to aggregate as a result of hydrogen bond interactions due to the surface hydroxyl groups [30]. After modification process the crystallinity of CelNPs is lost and spherical particles of 25-30 nm were observed (Fig. 3.4(e)). Blocking the hydroxyl groups by relatively large molecular weight molecules obviously improves the individualization of the nanoparticles. The decrease in the polar contribution reduces the strength of the interparticle interactions and results in the individualization of the nanoparticles. Other esters viz. StphNPs, StcinNPs, StbenNPs and StpalNPs also showed spherical morphology after modification with the diameter ranged from 40-50 nm (Figure.3.5).

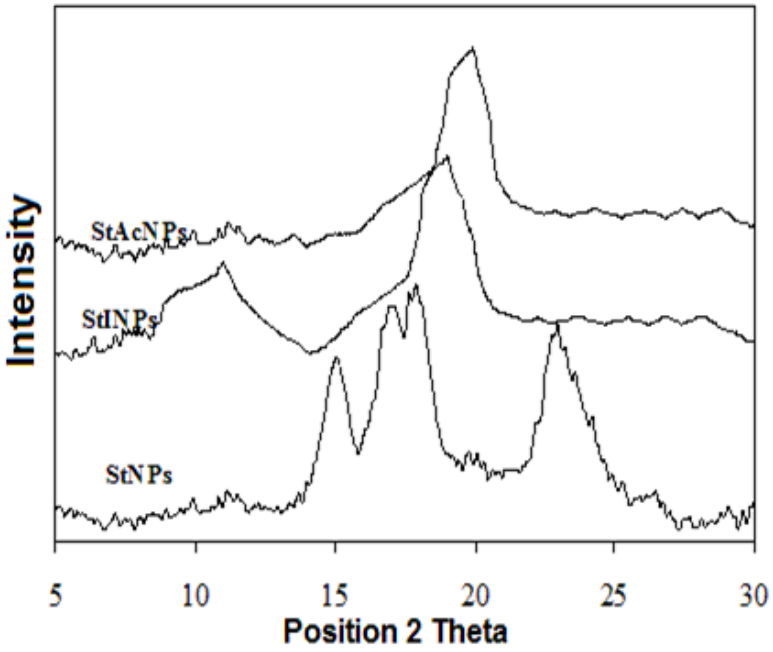

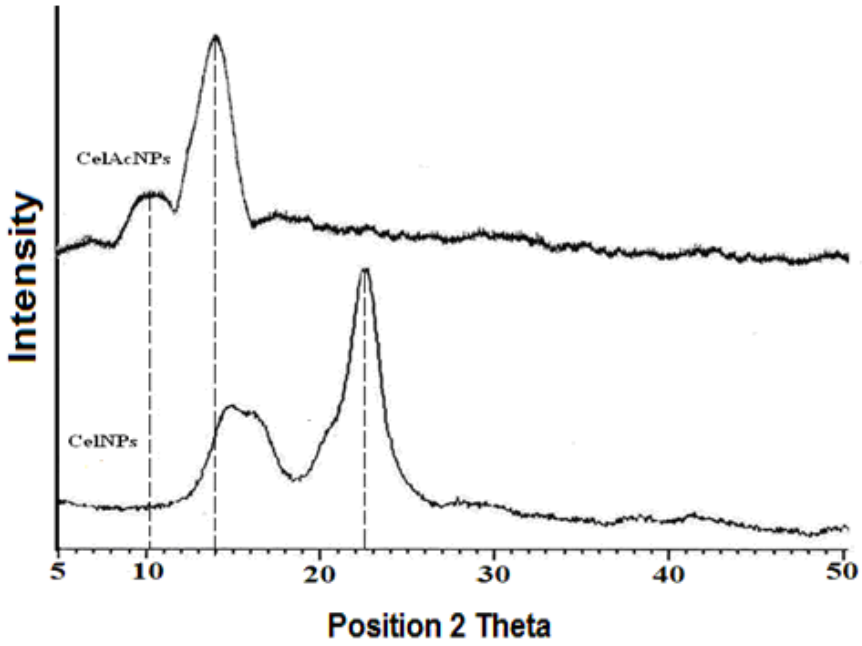

Figure. 3.3 XRD pattern of nanoparticles

Scanning electron microscopy (SEM)

Scanning electron micrographs (SEM) (Figure.3.6) of the polysaccharides nanocrystals shows the existence of aggregates. Modified polysaccharides nanoparticles increase the hydrophobicity and thus limit chain mobility. However, a porous structure as reported in the phenyl isocyanate modification was not observed [31]. The clusters obtained after modification show the presence of more spherical particles.

3.3.5 Thermal Analysis

Thermo gravimetric analysis (TGA)

Thermo gravimetric curves are shown in Figure.3.7. It can be seen that the degradation process of polysaccharides occurred in two steps. The first range (50–150 °C) is associated with the loss of water, whereas the second range (150–350 °C) corresponds to the degradation of polysaccharides. The collected data showed that the thermal stability of modified polysaccharides nanoparticles was higher probably due to the lower amount

of remaining hydroxyl groups after modification. Higher substitution resulted in only one degradation peak and higher thermal stability. The gelatinization temperature was lower while thermal stability was higher for modified polysaccharides nanoparticles [32] (Table.1). This suggests improved processibility which is necessary for various applications of polysaccharides nanoparticles.

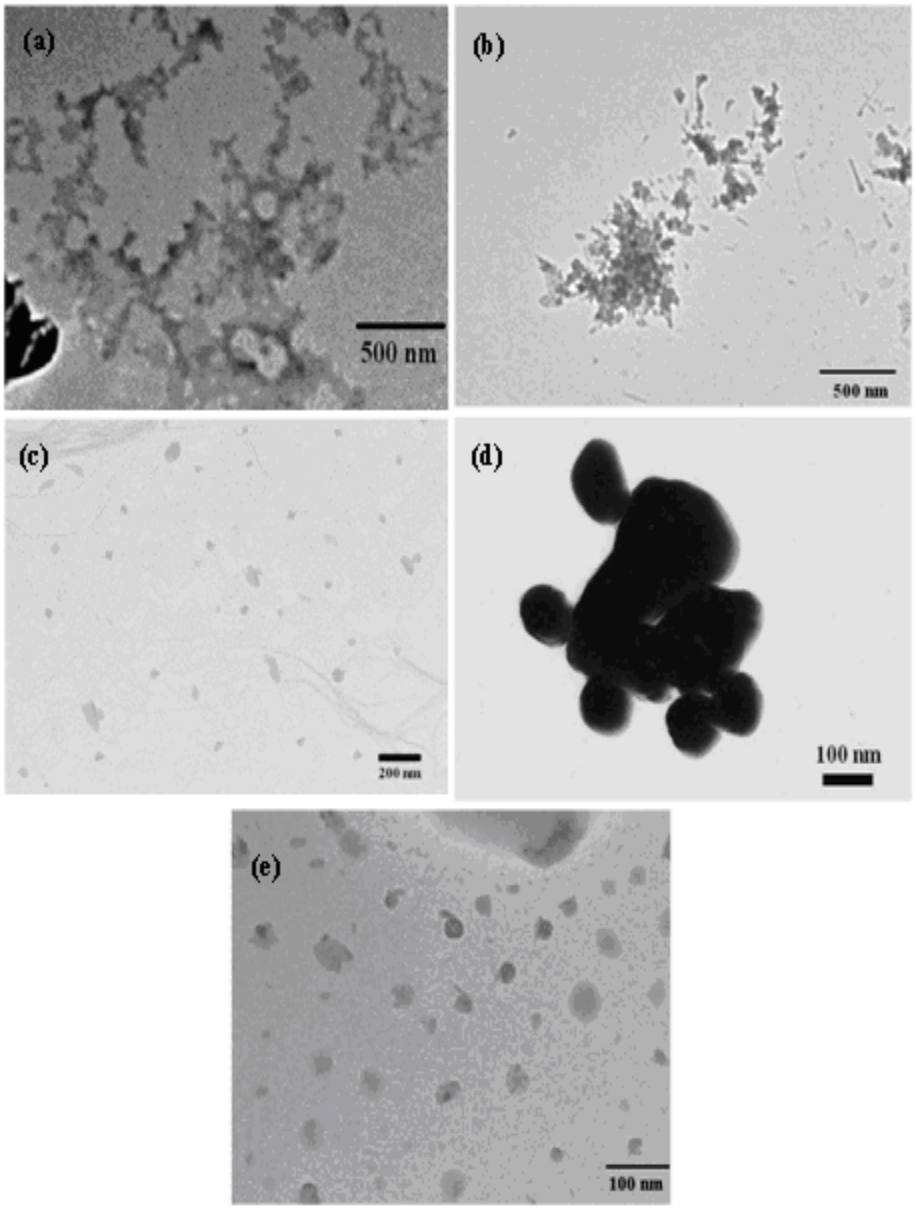

Figure. 3.4 TEM images of nanoparticles (a) StNPs, (b) CelNPs, (c) StAcNPs, (d) StINPs and (e) CelAcNPs

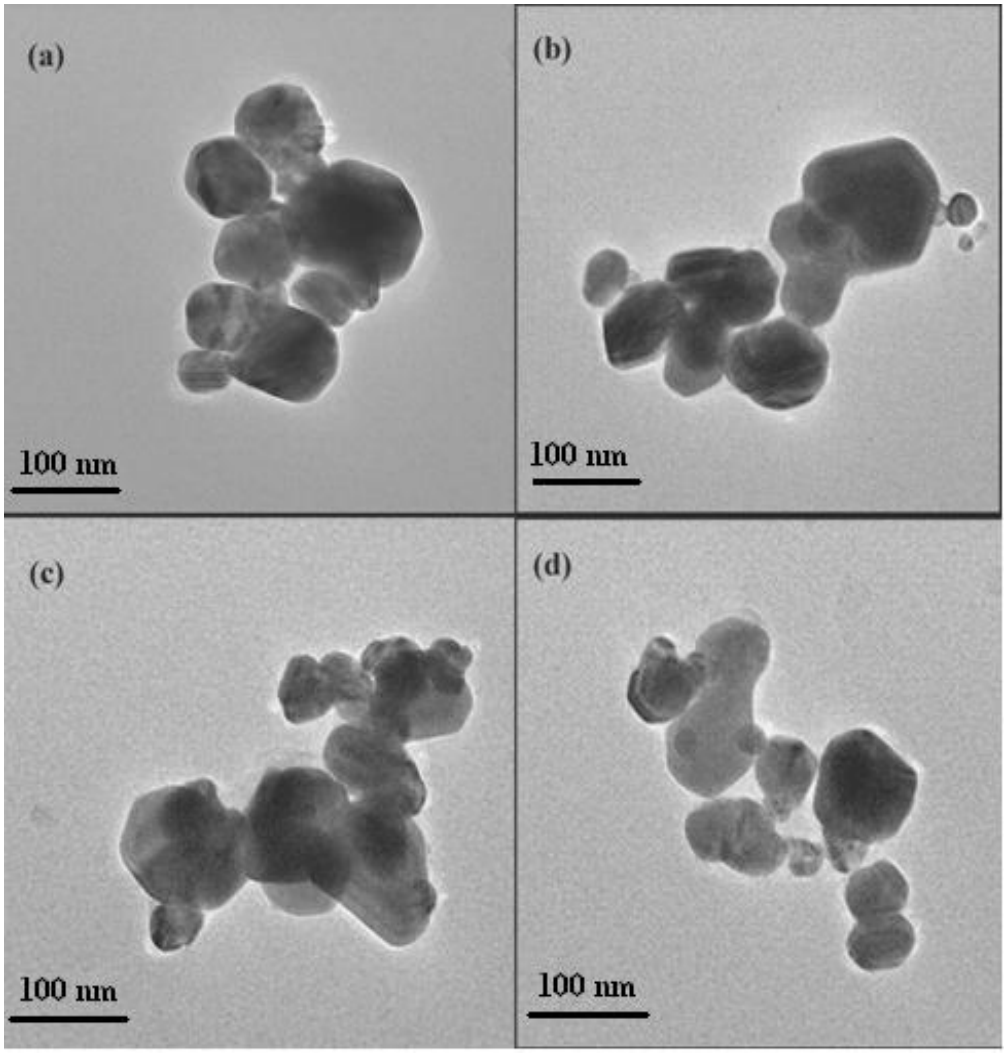

Figure. 3.5 TEM images of nanoparticles (a) StphNPs, (b) StcinNPs, (c) StbenNPs and (d) StpalNPs.

3.3.6 Swelling studies of nanoparticles

The polysaccharides nanoparticles were dispersed in water, ethanol, N,N-dimethylformamide, acetone and toluene at a concentration of 10 mg/ml at room temperature. Digital photographs of both appeared to show a stable uniform dispersion as illustrated in Figure.3.8. But on prolonged standing, the isocyanate modified nanoparticles tend to swell to a different extent in each of the solvent. As a result the

isocyanate modified StNPs gets aggregated and settle down (Figure.3.9). The highest swelling was observed in toluene while lowest was observed in water. Thus solvent uptake clearly follows the order of decreasing polarity. This indicates that the isocyanate modified StNPs are highly hydrophobic in nature. On the other hand CelAcNPs and StAcNPs were soluble in acetone, THF, DMF and DMSO.

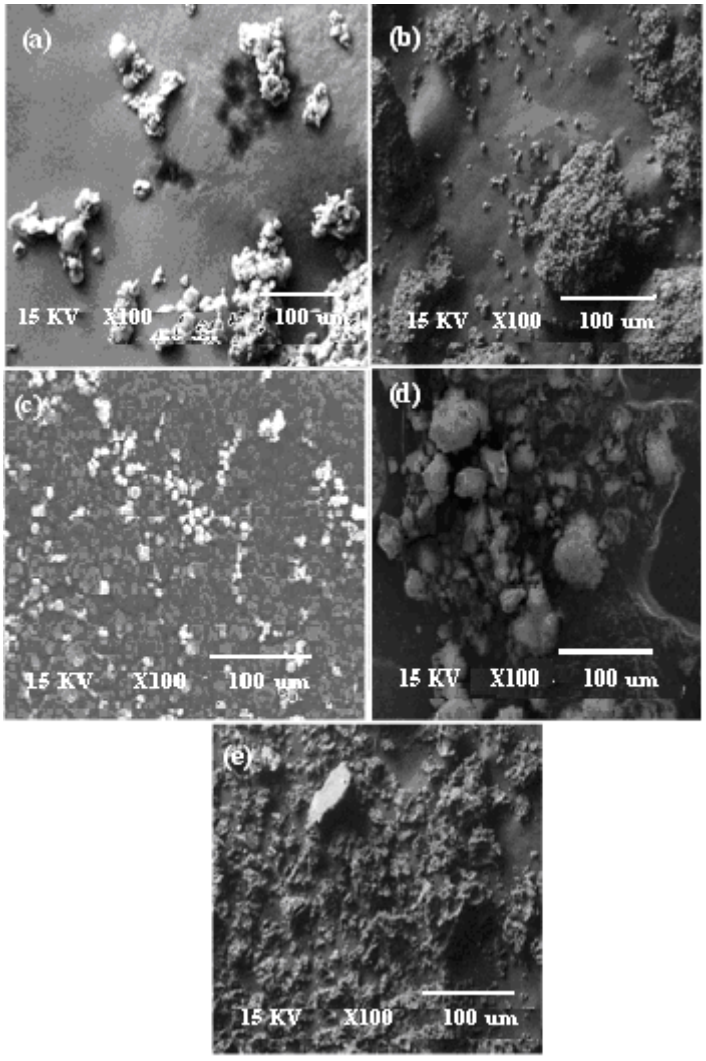

Figure. 3.6 SEM images of (a) StNPs, (b) CelNPs, (c) StAcNPs, (d) StINPs and (e) CelAcNPs

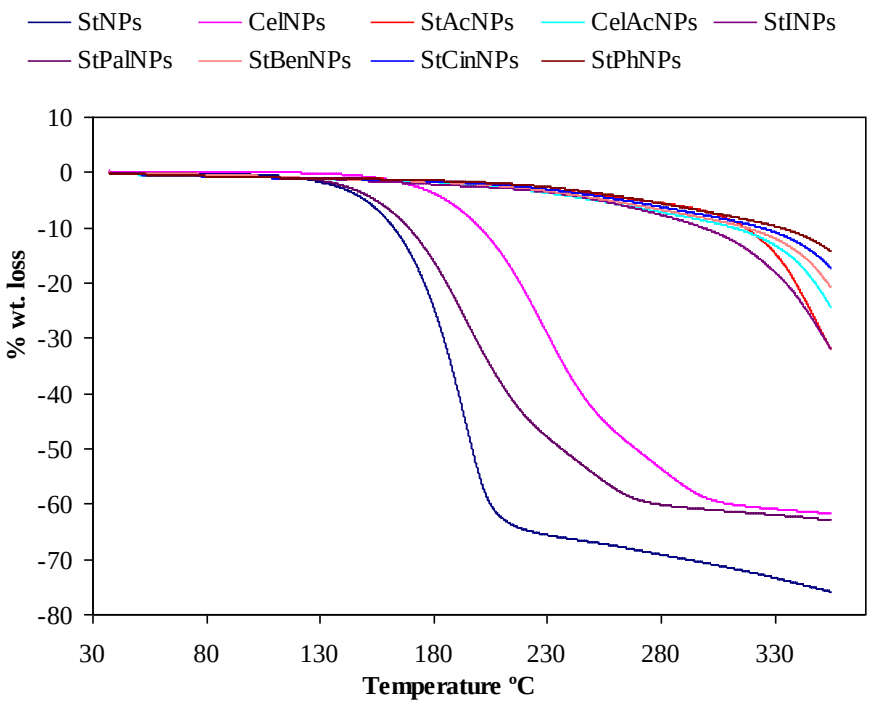

Figure. 3.7 TGA curves of nanoparticles

Table. 3.1 TG values of nanoparticles

Polysaccharides nanoparticles	**Degree of substitution**	**Gelatinization temperature (°C)**	**Degradation temperature (°C) at 10 % wt. loss**
StNPs	-	94.0	162.3
CelNPs	-	88.0	176.8
CelAcNPs	2.39	79.4	253.2
StAcNPs	2.34	78.2	248.6
StINPs	-	91.6	323.8
StphNPs	2.63	87.4	317.9
StcinNPs	2.51	81.2	298.2
StbenNPs	1.98	72.2	200.4
StpalNPs	2.49	65.3	311.4

Figure. 3.8 Digital photographs of nanoparticles showing uniform dispersion (a) StNPs, (b) CelNPs, (c) StAcNPs, (d) StINPs and (e) CelAcNPs

Figure. 3.9 Digital photographs of HMDI-modified StNPs showing swelling in (a) water, (b) ethanol, (c) toluene, (d) N,N-dimethylformamide and (e) acetone

3.3.7 Biodegradability test

Figure.3.10 represents biodegradation tests in both modified and unmodified polysaccharide nanoparticles carried out in E. coli culture. The results showed that the modified polysaccharide nanoparticles can act as a source of nutrient as much as unmodified polysaccharide. Thus reaction with toxic isocyanate and acetic anhydride does not destroy the basic virtue of biodegradability of polysaccharide. However the extent of degradation is lower in modified polysaccharide compared to that of unmodified polysaccharides in the culture medium. This may be attributed to the increased hydrophobicity which leads to poor swelling in the culture medium.

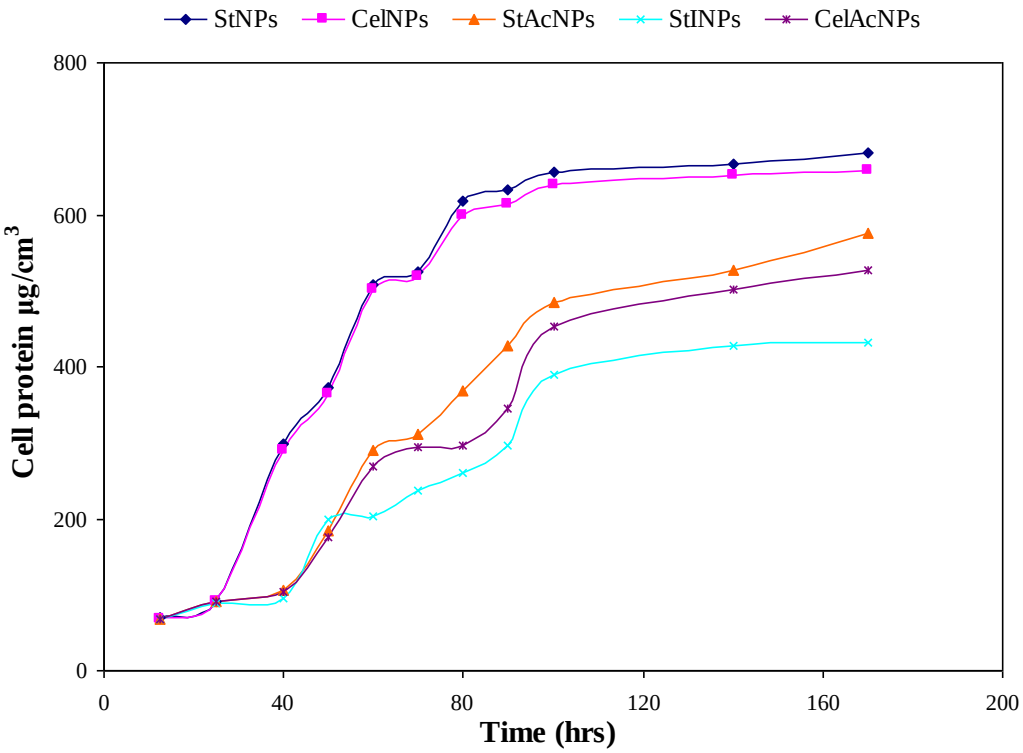

Figure. 3.10 Plot of estimated cell protein of polysaccharides nanoparticles with time

3.4 Conclusions

Polysaccharide nanoparticles synthesized by acid hydrolysis were modified using acetyl chloride and hexamethylene diisocyanate. The size and morphology of the resulting nanosized derivatives was examined by electron microscopy. The evidence for the chemical modification was provided by FT-IR spectroscopy and X-ray diffraction. The X-ray diffraction results indicated that, after modification, crystallinity of polysaccharides nanoparticles is lost. The hydrophobic polysaccharide nanoparticles exhibited enhanced solubility in organic solvents and greater thermal stability. These characteristics offer additional advantages for potential reinforcing applications.

3.5 References

1. H. Namazi, M. Mosadegh, A. Dadkhah, *Carbohydr. Polym.*, **2009,** 75, 665.
2. S. Ahmed Said Azizi, F. Alloin, A. Dufresne, *Biomacromolecules*, **2005**, 6, 612.
3. H. Angellier, J. L. Putaux, S. Molina-Boisseau, D. Dupeyre, A. Dufresne, *Macromolecules*, **2005,** 221, 95.
4. H. Angellier, S. Molina-Boisseau, P. Dole, A. Dufresne, *Macromolecules*, **2006,** 7, 531.
5. Y. Habibi, A. L. Lucia, O. J. Rojas, *Chem. Rev., 2010,* 110, 3479.
6. M. N. Angles, A. Dufresne, *Macromolecules*, **2001**, 34, 2921.
7. A. Bendahou, H. Kaddami, A. Dufresne, *Eur. Polym. J.*, **2010**, 46, 609.
8. W. Thielemans, M. N. Belgacem, A. Dufresne, *Langmuir*, **2006,** 22, 4804.
9. S. Tsuji, H. Kawaguchi, *Langmuir*, **2005,** 21, 2434.
10. Y. Xu, W. Ding, J. Liu, Y. Li, J. F. Kennedy, Q. Gu, S. Shao, *Carbohydr. Polym.*, **2010**, 80, 1078.
11. H. Namazi, A. Dadkhah, *Carbohydr. Polym.*, **2010**, 79, 731.
12. H. Namazi, M. Mosadegh, A. Dadkhah, *Carbohydr. Polym.*, **2009,** 75, 665.
13. W. Thielemans, M. N. Belgacem, A. Dufresne, *Langmuir*, **2006**, 22, 4804.
14. J. M. Fang, P. A. Fowler, J. Tomkinson, *Carbohydr. Polym.*, **2002**, 47, 245.
15. X. Fan, Z. T. Liu, Z. W. Liu, *J. Hazard. Mater.*, **2010**, 177, 452.
16. K. Y. Lee, F. Quero, J. J. Blacker, C. A. S. Hill, S. J. Eichhorn, A. Bismarck, *Cellulose*, **2011**, 18 595.
17. S. Berlioz, S. Molina-Boisseau, Y. Nishiyama, L. Heux, *Biomacromolecules*, **2009**, 10, 2144.
18. H. Angellier, S. Molina-Boisseau, L. Lebrun, A. Dufresne *Macromolecules*, **2005,** 38, 3783.
19. O. H. Lowry, N. J. Rosenbrough, A.L. Farr, R. G. J. Randall, *Biol. Chem.* **1951,** 193, 265.
20. A. Buleon, C. Gerard, C. Riekel, R. Vuong, H. Chanzy, *Macromolecules*, **1998,** 31, 6605.

21. M. Valodkar, S. Thakore, *Carbohydr. Polym.*, **2011**, 86, 1244.
22. M. Valodkar, S. Thakore, *Carbohydrate Research*, **2010**, 345, 2354.
23. M. J. Sobkowicz, B. Braun, J. R. Dorgan, *Green. Chem.*, **2009**, 11, 680.
24. Y. Habibi, A. Dufresne, *Biomacromolecules*, **2008,** 9, 1974.
25. T. Graziella, A. S. Edgar, C. N. Salvador, P. M. Ivonne, O. C. Gilberto, *J. Appl. Polym. Sci.*, **2010,** 115, 263.
26. H. L. Angellier, L. Choisnard, S. Molina-Boisseau, P. Ozil, A. Dufresne, *Biomacromolecules*, **2004,** 5, 1545.
27. Y. Xu, V. Miladinov, M. A. Hanna, *Cereal Chemistry*, **2004**, 81, 735.
28. Q. Wu, M. Henriksson, X. Liu, L. A. Berglund, *Biomacromolecules*, **2007**, 8, 3687.
29. H. Namazi, A. Dadkhah, *Carbohydr. Polym.*, **2010**, 79, 731.
30. N. Vigneshwaran, R. P. Nachane, R. H. Balasubramanya, P. V. Varadarajan, *Carbohydr. Res.*, **2006,** 341, 2012.
31. W. Thielemans, M. N. Belgacem, A. Dufresne, *Langmuir*. **2006,** 22, 4804.
32. C. K. Simi, T. Emilia Abraham, *Bioprocess Biosyst Eng*, 30, **2007,** 173.

Chapter-4 Synthesis and characterization of bionanocomposites of natural rubber

Outline

4.1 Introduction

The term “nanocomposite” refers to every type of composite material having fillers in the nanometer size range, at least in one dimension. For such nanocomposites the total interfacial phase becomes the critical parameter, rather than the volume fraction of the filler [1,2,3]. In recent years, hybrid organic–inorganic nanocomposites consisting of a polymeric matrix and a layered silicate has inspired scientists to a range of potential applications [4,5,6]. Due to their nanometer phase dimensions, nanocomposites exhibit significant improvements in physical and mechanical properties in relation to the polymer host [7,8,9]. The addition of just a low percentage of nanolayered inorganic fillers can increase the stiffness and strength with a minimal loss in ductility and impact resistance, decreases the permeability and swelling in solvents, improves the abrasion, flame resistance and thermal endurance, with an enhancement in electrical conductivity and optical properties [10]. Rubber nanocomposites with an exfoliated morphology have been successfully prepared by several methods, in situ polymerization, solution blending, latex compounding and direct melt intercalation. Consequently, the main advantage of nanocomposites is that the enhanced properties can be obtained with a smaller filler amount [11,12,13].

The inclusion of nanosized particles, in particular layered silicates (nanoclays) [14], enables the enhancement of properties in polymers with even small amounts of fillers, a feature not possessed by conventional composites. It was found that the inclusion of 10 phr (parts per hundred of rubber) of nanoclay greatly improves the mechanical properties of NR compounds over the conventionally filled systems [15]. Nevertheless, the mechanism of the reinforcement is still poorly understood. For example, why does it make NR-nanoclay materials stronger than conventionally filled rubbers without sacrificing properties like elongation at break, resilience, or compression set? According to the molecular models of conventional rubber compounds, for filled and crystallizable vulcanized rubbers, the main reason for the rise in the tensile strength at low deformations (below crystallization) has been considered as the formation of additional cross-links resulting from the filler-elastomer interactions due to the presence of fillers. Regarding the effect of nanoclay, we note that for the same weight/volume fraction of filler the nanosized platelets would lead to 4-6 orders of magnitude more particles per

volume than conventional fillers [16]. A large amount of surface area will be exposed to the rubber molecules, leading to a huge interfacial volume around the nanofillers. Another important issue, mentioned above, is the assumption of the strength increase in NR-nanocomposite has often been attributed to rubber-filler interactions [16].

The concept of reinforced polymer materials with polysaccharide nanofillers has known rapid advances and considerable interest in the last decade owing to their renewable character, high mechanical properties, low density and diversity of the sources [17]. Starch nanocrystals have been used as filler in a synthetic polymeric matrix and proved to be an interesting reinforcing agent [18,19,20,21,22]. In this context, waxy maize starch nanocrystals have been considered as potential filler for natural rubber, which is one of the most important elastomers widely used in industrial and technological areas [23]. However most of the composites have been prepared by solution blending.

Since the first publication related to the use of cellulose nanocrystals (CNs) as reinforcing fillers in poly(styrene-*co*-butyl acrylate) (poly(S*co*- BuA))-based nanocomposites by Favier et al. [24] CNs have attracted a great deal of interest in the nanocomposites. This is due to their appealing intrinsic properties such as nanoscale dimensions, high surface area, unique morphology, low density and mechanical strength. Cellulose nanocrystals have been incorporated into a wide range of polymer matrices, including polysiloxanes [25], polysulfonates [26], poly(caprolactone) [27], styrenebutyl acrylate latex [28], poly(oxyethylene) cellulose acetate butyrate [29], carboxymethyl cellulose [30], poly(vinyl alcohol) [31], poly(vinyl acetate) [32], poly(ethylene-vinyl acetate) (EVA) [33], polypropylene [34], poly-(vinyl chloride) [35], polyurethane [36], and water-borne polyurethane [37]. Their incorporation into biopolymers, such as starch-based polymers [38, 39,40], soy protein [41], chitosan [42], or regenerated cellulose [43], and biopolymer-like poly(lactic acid) [44], poly(hydroxyoctanoate) [45], and polyhydroxybutyrates [46] have also been reported. Recently, cellulose nanocrystals have also been used to form nanocomposites with natural rubber [47].

We have mainly concentrated on studying the reinforcement ability of starch by employing commercial mixing methods. Both native starch as well as starch nanoparticles are found to induce excellent reinforcement in natural rubber [21,48]. Moreover, there is a growing interest in organically modified derivatives of

polysaccharides for different applications [49]. The hydrophobic derivatives (described in chapter 3) were used for the development of bionanocomposite of natural rubber by commercial mastication process. A comparison was made with mechanical and thermal properties of conventional composite counterparts.

Starch-natural rubber bionanocomposites

4.2 Experimental

4.2.1 Materials

Waxy corn starch was purchased from Sigma Aldrich, Mumbai.

4.2.2 Preparation of bionanocomposites

The bionanocomposites of NR were prepared on two roll mixing mill (as shown in scheme-1). Four sets of bionanocomposites were synthesized using each of waxy corn starch (Waxy starch), starch nanocrystals (StNPs), HMDI modified starch nanoparticles (StINPs) & acetylated starch nanoparticles (StAcNPs) as reinforcing fillers in NR by dry process on two roll mixing mill [50]. Upto 40 phr of fillers were added along with the along with other additives viz., sulphur (1.8 phr), tetramethylene thiuram disulphide (0.5 phr), mercaptobenzo thiazyl disulphide (1 phr), zinc oxide (5 phr), and stearic acid (1 phr). The mastication was continued until homogenous composites were obtained. This was followed by vulcanization at 150 ºC and ~300 k Pa pressure for 7-8 min to obtain composite sheets with 1 mm thickness. Composites with carbon black (C-black/NR) were also prepared for comparison.

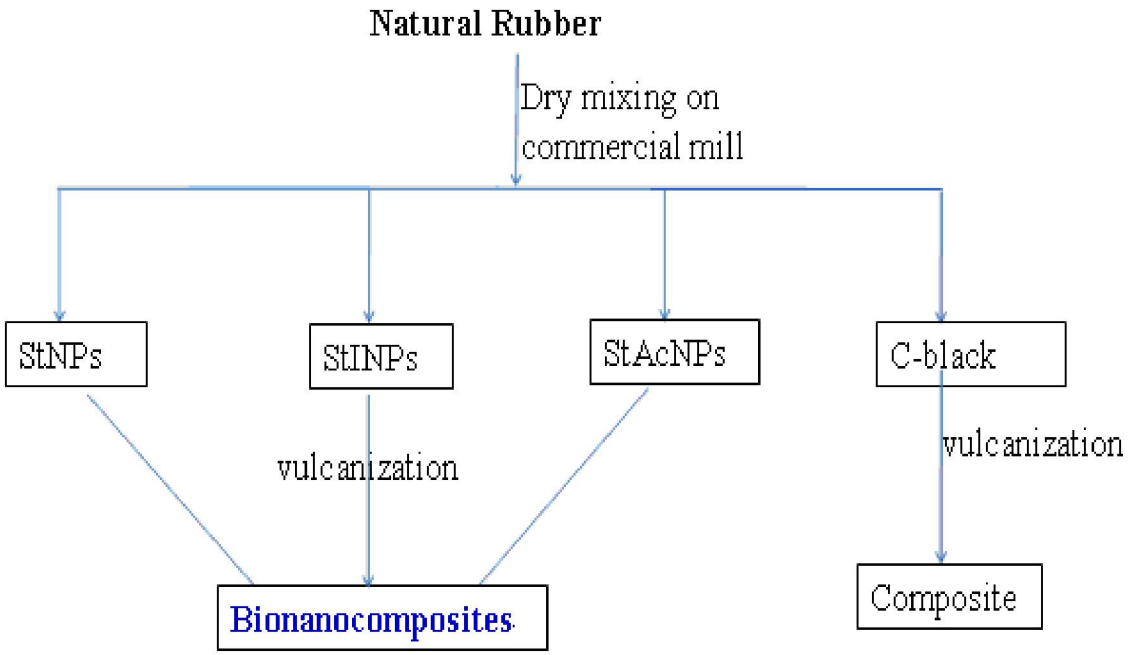

Scheme 4.1 Preparation of bionanocomposites

4.2.3 Characterization of bionanocomposites

Hardness

See section 2.2.3

Mechanical properties

See section 2.2.3

Scanning Electron Microscopy (SEM)

See section 2.2.3

Thermal analysis

Thermal Gravimetric Analysis (TGA)

See section 2.2.3

Differential Scanning Calorimetry (DSC)

See section 2.2.3

Water sorption studies :

Water sorption was determined by a method reported elsewhere [51].

Dynamic Mechanical Analysis

Dynamic mechanical tests were carried out using NETZSCH DMA 242. The specimen was a thin rectangular strip (15 x 5.1 x 0.959). The range of temperature in which the analysis was carried out between -80 º to 0 ºC at the frequencies of 1, 5 and 10 Hz in nitrogen atmosphere. The setup measured the complex tensile modulus E*, i.e., the storage component E' and the loss component E''. The ratio between the two components, tan δ was also determined.

X-ray diffraction :

X-ray diffraction (XRD) was determined by using PANalytical 'X'PERT-PRO XRPD.

4.3 Results and discussion

4.3.1 Mechanical properties

Hardness

The results of hardness of the various nanocomposites are expressed in Figure.4.1. It is observed that in all the nanocomposites the hardness increases with increase in concentration of fillers. Up to 30 phr all the four fillers showed superior hardness than C-black. After this the hardness imparted by waxy starch and StNPs is less than that of C-black whereas, that imparted by StINPs and StAcNPs is more than that of C-black. This is due to hydrophobic nature of modified StNPs the interaction with hydrophobic rubber is better which results in increase hardness. Among the biofillers StINPs imparted best hardness properties followed by, StAcNPs, StNPs and Waxy starch.

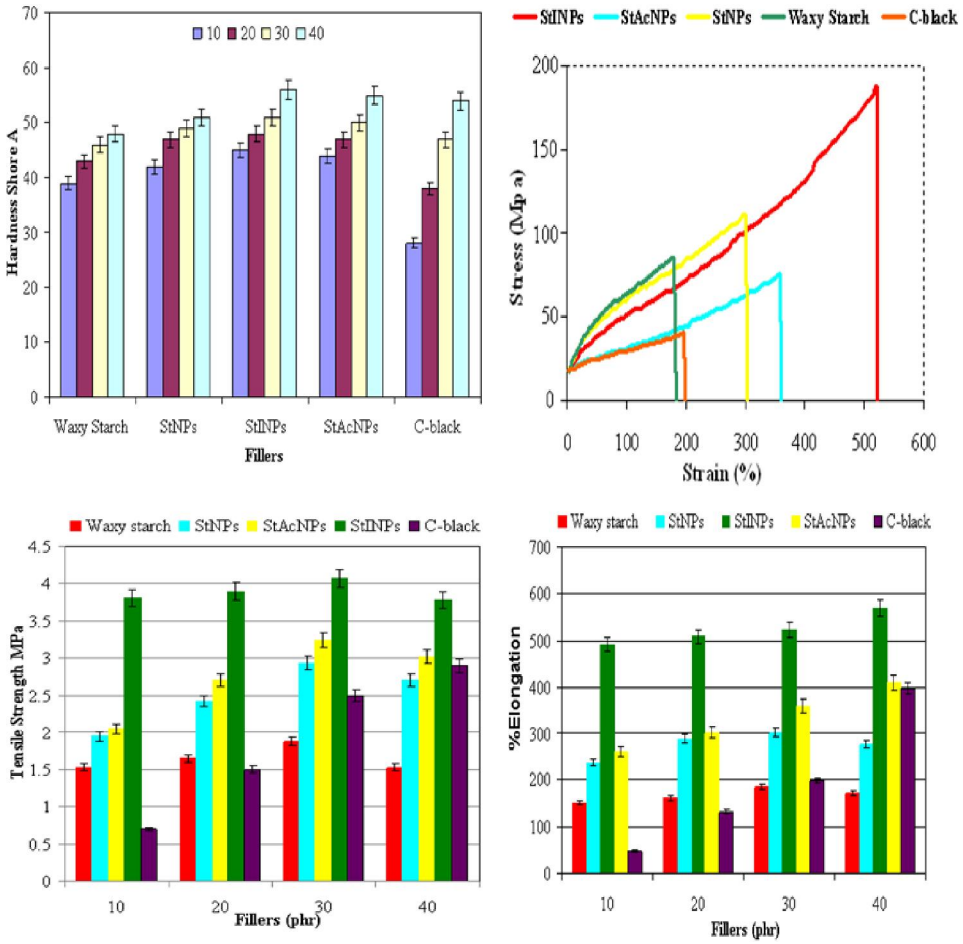

Figure 4.1 Mechanical properties of NR composites

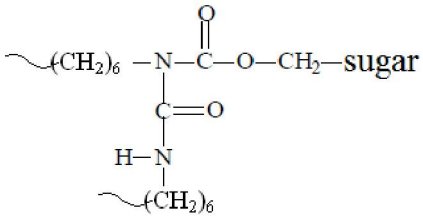

Scheme 4.2 Structure of allophanate formation

Stress-Strain Curve

Typical stress vs. strain curves for the NR nanocomposites at 40 phr are shown in Figure.4.1. For each measurement, it was observed that the strain was macroscopically homogenous and uniform along the sample until it breaks. The lack of any necking phenomenon confirms the homogenous nature of these nanocomposites. The samples

exhibit an elastic behavior at $T > T_g$. The stress continuously increases with strain and the amount of fillers as shown in Figure.4.1. Incorporation of nanofillers leads to an increase in strength as well as elongation at break. These results are contradictory to the observations of Angellier et al. [20] who recorded a decrease in elongation as the amount of filler increases. The behavior is consistent with respect to all the nanofillers. Thus we can say that the nanofillers used retain the elastic property of natural rubber which is also concluded by dynamic mechanical analysis (described later). The initial high stress is due to the reinforcement of the rubber with nanofillers [52]. As the strain increases, stress induced crystallization comes into role, which increases proportionally along with strain [30]. The dispersion of nanofillers leads to an efficient reinforcement, which leads to improved stiffness. The unmodified starch nanoparticles (StNPs) showed lower strength as compared to modified starch nanoparticles. Due to hydrophilic nature of StNPs and hydrophobic nature of NR the adhesion between the two is poor. As a result the stress transfer from the matrix to the filler is poor and the mechanical properties of nanoparticles are not fully utilized.

Tensile Strength

It can be seen from Figure.4.1 that as the amount of nanofillers increases the tensile strength (T.S.) goes on increasing as expected. It follows the order StINPs/NR > StAcNPs/NR > StNPs/NR > Waxy starch/NR. In case of C-black composites the initial lower T. S. value rapidly increases from 10 to 40 phr loading but remains lower than nanocomposites at all levels. Nanocomposites of modified StNPs showed greater strength and elongation due to their improved dispersion and better compatibility with NR due to its hydrophobic nature and small particle size. Among the modified StNPs, StINPs showed higher mechanical properties which can be explained on the basis of chemical reactions that are likely to occur during the process of vulcanization. At this high temperature the free NCO groups of isocyanate terminated StINPs may react further to form three-dimensional allophanate structure (Scheme 4.2) thus leading to increased chemical crosslinking [53] which imparts higher mechanical strength to the nanocomposite.

% Elongation

Figure.4.1 shows that as the amount of nanofillers in NR goes on increasing the elongation increases along with T.S. which is also seen in C-black composites. This is an interesting observation as generally elongation and T.S. show opposite trend. Also the increase in % elongation in case of modified StNPs is more progressive than C-black composites. High nanofiller content seems to preserve the elastic behavior of NR-based nanocomposites. In case of Waxy starch/NR the increase is obtained because it has high amylopectin content and hence higher molecular weight. Waxy starch imparts lower mechanical strength than other nanofillers due to poor compatibility with hydrophobic NR.

4.3.2 X-ray diffraction pattern

The XRD of nanocomposites at 40 phr loading (Figure.4.2) showed no diffraction peak corresponding to pure NR unlike other reports [54,55]. This is because the filler loadings in the present case are much higher than those reported by Huang et al., and Pojanavaraphan et al. for nanoclays (10 phr or less). On the other hand, for high filler loadings Dufresne et al. have observed that the processing by casting and evaporation at 40 °C did not affect the crystallinity of starch in nanocomposite [20]. While the vulcanization process in the present case may have led to change in the structure of the nanocrystals from crystalline to amorphous. This accounts for the absence of peaks coreesponding to modified and unmodified starch in XRD of present nanocomposites.

4.3.3 Morphology studies

The results of the mechanical properties can be explained on the basis of morphology. The SE micrographs of fractured samples of biocomposites at 40 phr loading are shown in Figure.4.3(a-e). It can be seen that all the bionanofillers are well dispersed into polymer matrix without much agglomeration. Uniform distribution of modified and unmodified StNPs into NR matrix is observed. This is due to the compatibility between the modified StNPs and the NR matrix (Figure.4.3a and b). While in case of unmodified StNP the reduction in size compensates for the hydrophilic nature (Figure.4.3c), in case

of waxy maize starch it seems to be lack of interfacial adhesion (Figure.4.3d). The lack of any evidence of agglomeration combined with the significant increase in mechanical properties indicates even distribution of nanofillers in NR. In case of CB composites (Figure.4.3e) relatively coarse, two-phase morphology is seen.

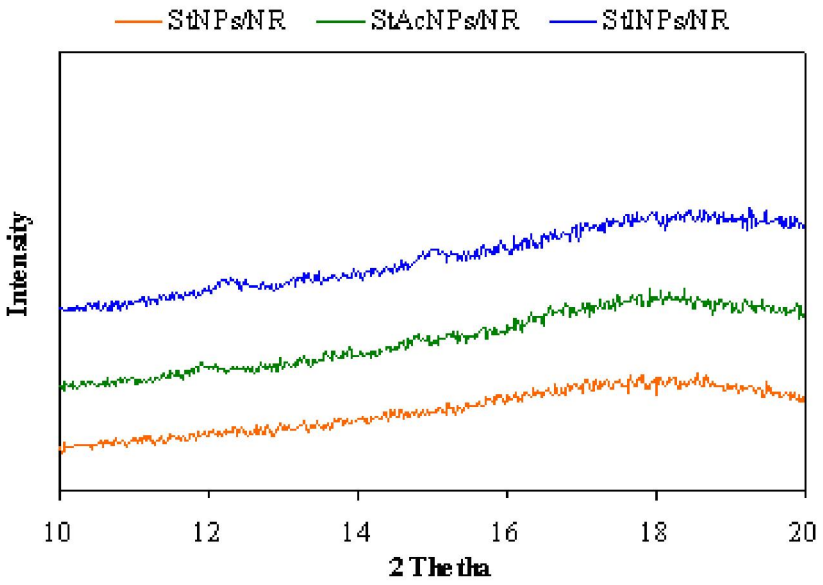

Figure. 4.2 XRD spectra of nanocomposites at 40 phr loading.

4.3.4 Thermal analysis

Thermo gravimetric analysis

Typical TG curves (Figure.4.4(a)) of the nanocomposites at 40 phr loading showed an initial mass loss from temperature 150-250 ºC attributed to elimination of volatile components such as water [18]. At 350 ºC the percentage of weight retained is higher for nanocomposite (Table-1). This increase in thermal stability of the hybrid may result from the dispersion of the nanoparticles and strong interaction between the nanoparticles and rubber molecules. High vulcanization temperatures may have resulted in crosslinking within the polysaccharide network which led to unusual thermal stability of the nanocomposites.

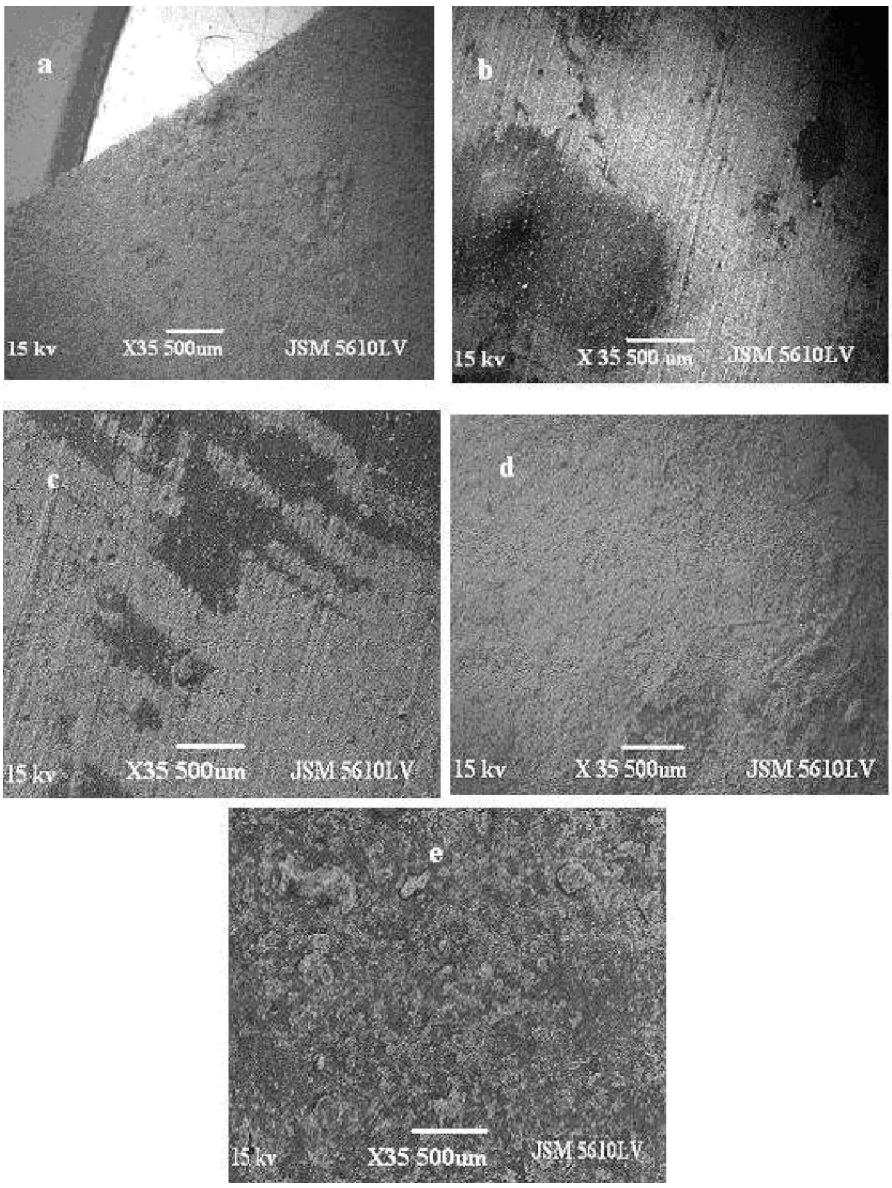

Figure. 4.3 SE Micrographs of NR composites at 40 phr loading of (a) StINPs, (b) StAcNPs, (c) StNPs, (d) Waxy starch and (e) C-black.

Differential scanning calorimetry

DSC curves of NR composites at 40 phr filler loading (Fig. 4.8) shows that all the nanocomposites have Tg comparable with that of C-black/NR composites, while that of unfilled NR is around -66ºC [18]. The Tg also goes on increasing with the nanofillers loading as expected (Fig. 4.9). The Tg of StINPs/NR is highest followed by StAcNPs/NR, StNPs/NR, Waxy starch/NR and C-black/NR composites. The results of

thermal properties support the observation that increased hydrophobicity and reduced particle size of filler imparts rigidity and strength to the network. Also isocynate modification leads to a greater increase in Tg due to increased crosslinking as already explained for enhanced mechanical strength.

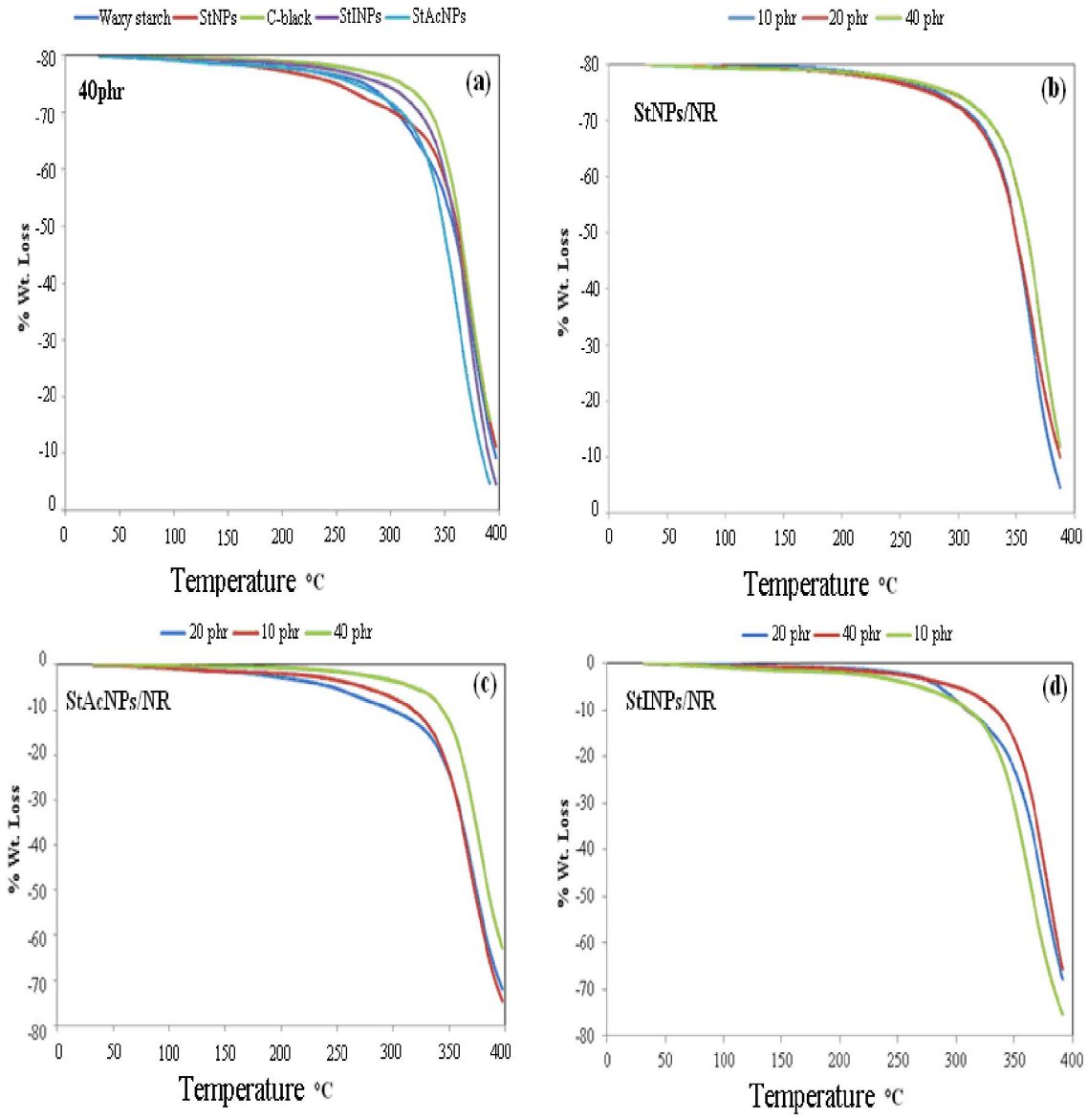

Figure. 4.4 TG curves of (a) NR composites and NR nanocomposites containing (b)StNPs, (c) StAcNPs and (d) StINPs at various filler loadings

Dynamic mechanical analysis

Figure.4.6 depicts the dynamic mechanical spectra (logarithm of dynamic storage modulus log(E') and E" and loss factor (tan δ)) as a function of temperature for the nanocomposites at 1, 5 and 10 Hz. A sharp decrease over 3 decades is observed around -60 °C, corresponding to the primary relaxation process associated with the glass-rubber transition determined by differential scanning calorimetry (DSC) measurements. This modulus drop corresponds to an energy dissipation phenomenon displayed in the concomitant relaxation process where tan δ passes through a maximum. Dynamic mechanical analysis involves weak stresses, the adhesion between the filler and the matrix is not damaged. Under higher stress, as used for tensile tests, the adhesion is involved. Nanocomposites obtained similar tan δ curve as that of Teh et al. [56]. The tan δ curve of nanocomposites showed a broad relaxation process from -80 ºC to -10 ºC (Figure.4.6). This may be due to the relaxation of rubber fraction confined inside the layers. The reduction in the tan δ maxima suggests a strong adhesion between NR and modified starch nanoparticles. Sliding along the exfoliated interlayer is suppressed. In addition, chain slipping at the outer surfaces of the aggregates is likely also hampered. Therefore the loss maximum is smallest in case of the nanocomposites system with the strongest filler matrix coupling [30]. Mondragon et al. [57] observed that E' increases with clay content above Tg which shows that the clay content affects the elastic properties associated to the rubber phase (Figure.4.6). Whereas in the present study the values of E' and E" does not increase with the filler loading above Tg. This indicates that the nanofillers does not affect the elastic properties associated to the rubber phase. The Tg values of DSC somewhat differ from DMA. This may be attributed to the frequency dependence of transition phenomenon. The activation energy (Table-2) for glass transition was calculated from following equation (eq^n 1) [58].

$$\ln \omega_1/\omega_2 = E_A/R\ (1/T_2-1/T_1)\ldots\ldots\ldots\ldots\ldots \quad (1).$$

where ω_1 and ω_2, are the frequencies and T_1 and T_2 are the Tg's obtained at ω_1 and ω_2, respectively.

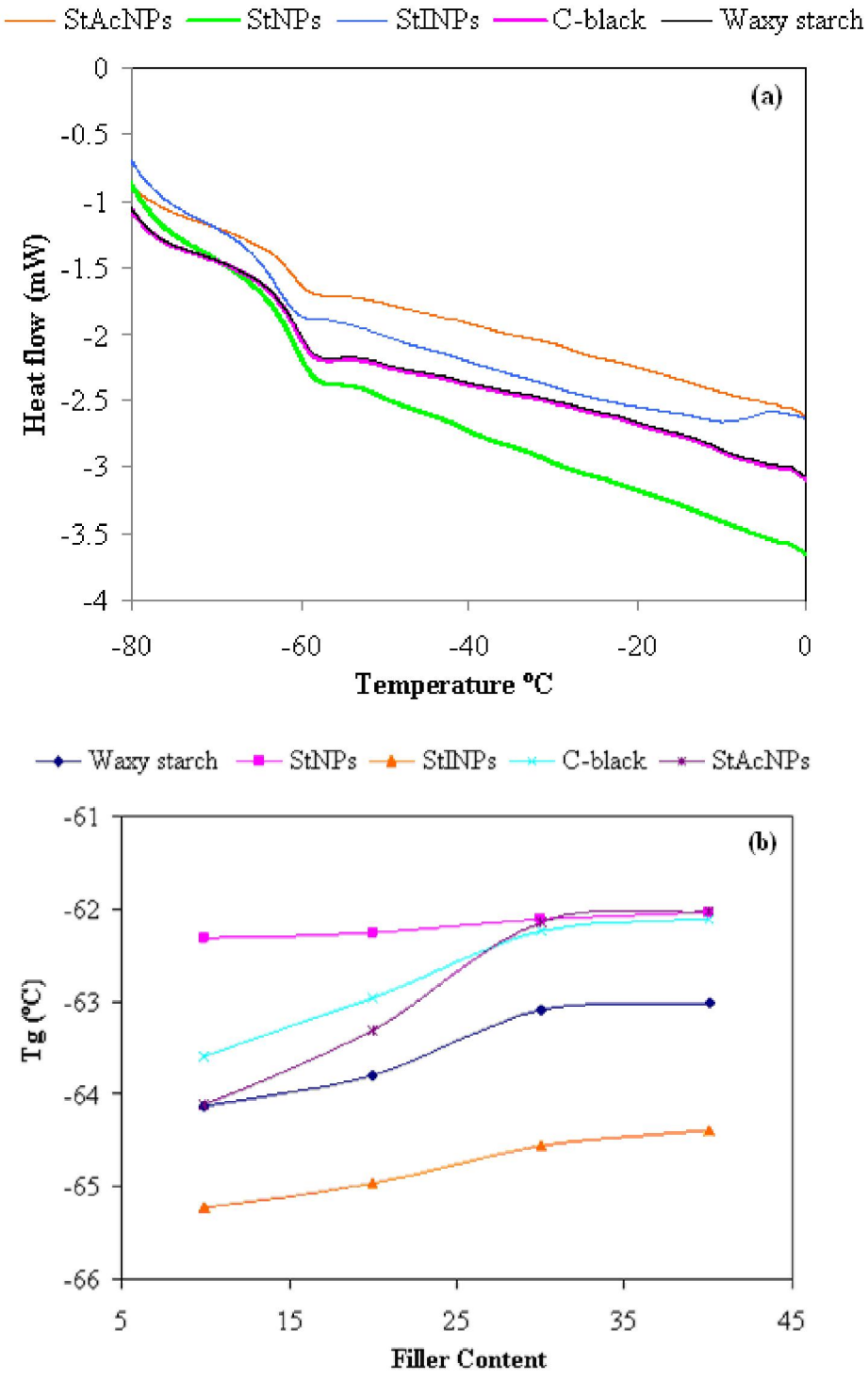

Figure. 4.5 (a) DSC curves of NR composites at 40 phr and (b) Effect of filler on Tg of NRcomposites

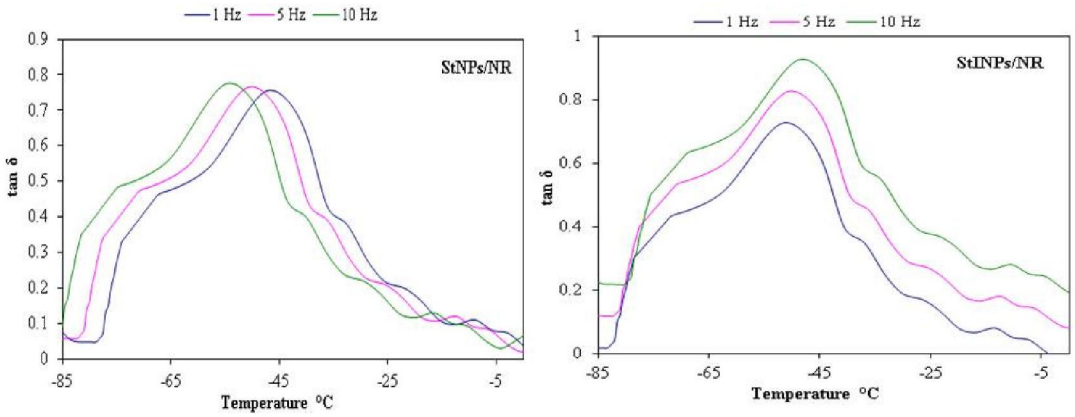
1 Hz
5 Hz
10 Hz
StNPs/NR
tan δ
Temperature °C
StINPs/NR
StAcNPs/NR

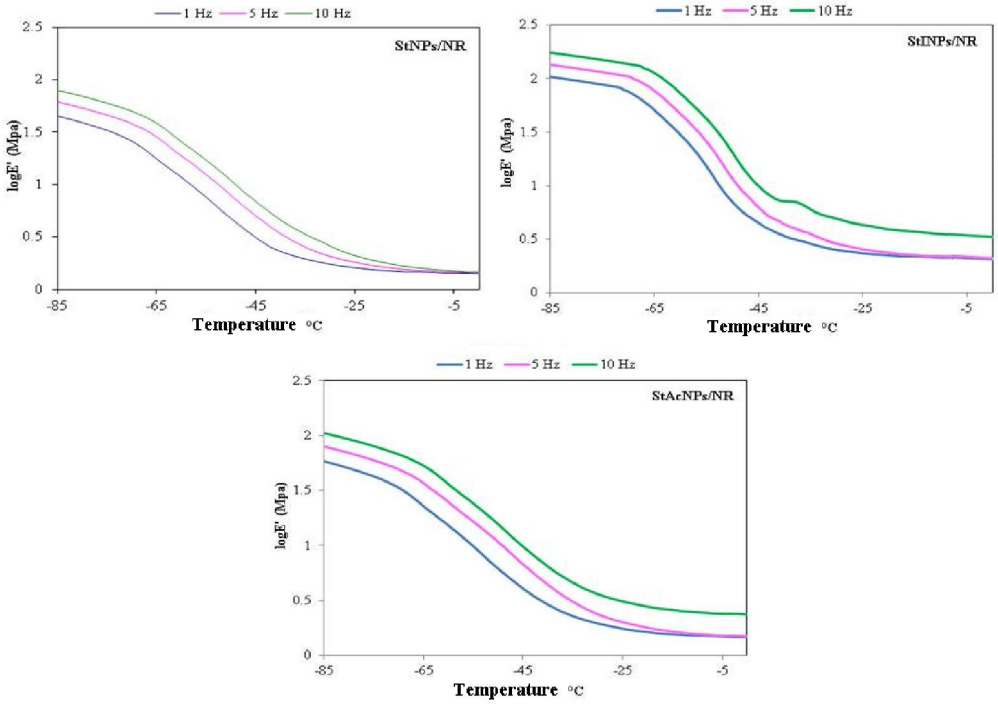
1 Hz
5 Hz
10 Hz
StNPs/NR
logE' (Mpa)
Temperature °C
StINPs/NR
StAcNPs/NR

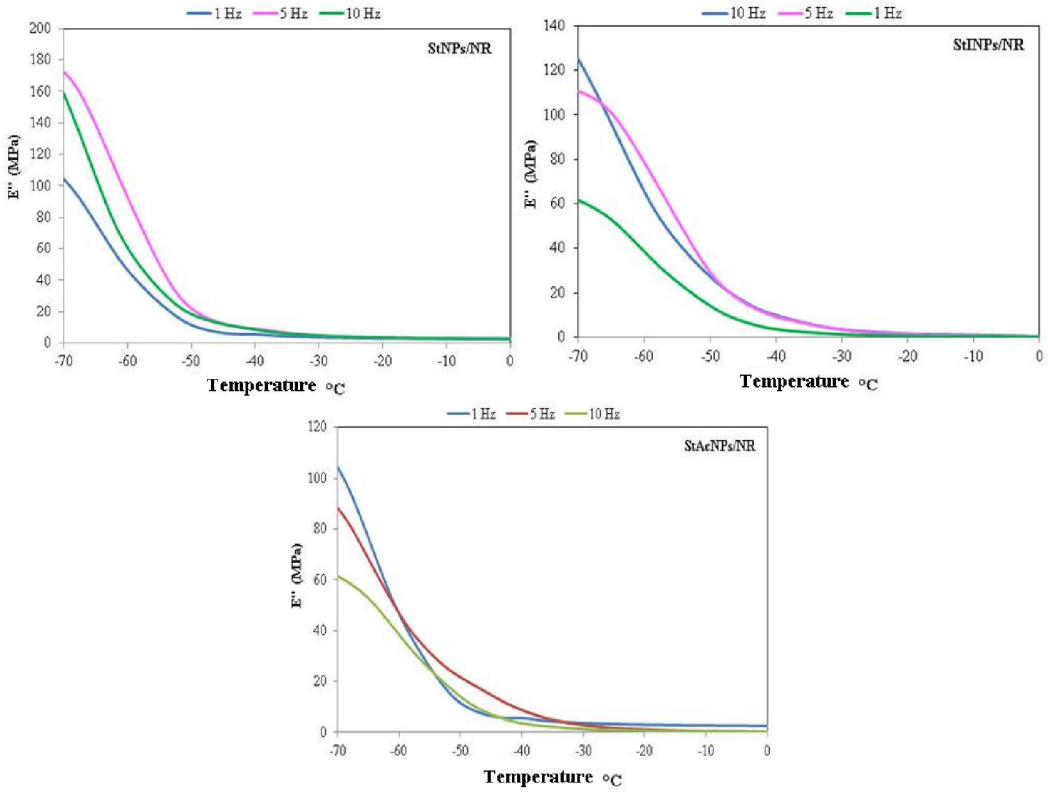

Figure. 4.6 Effect of starch based nanoparticles on mechanical loss factor tan δ, logarithm of storage modulus E' and loss modulus E" at various frequencies

4.3.5 Water sorption of composites

Absorption largely depends on the hydrophobic or hydrophilic components embedded in the matrix, which acts as a semipermeable membrane. The fiber/matrix adhesion is an important factor in determining the sorption behavior of a composite [59]. Moreover, fiber architecture has also been found to affect the absorption. Sorption studies were performed in water and nonpolar solvent toluene in order to understand the degree of hydrophobicity. As the bionanofillers used here are polysaccharides the water sorption was expected to be high and proportional to filler loading. However the results of the experiment (Table-3) showed an interesting trend. The maximum water uptake even at 30 % filler loading is 3.46 % which is not significant. Further, the sorption values decreases with filler loading. The low sorption indicates increasing adhesion between the polymer matrix and filler. The interaction leads to the formation of a bound polymer in close proximity to the reinforcing filler, which restricts the solvent uptake. As the amount of

filler loading increases, the amount of the bound polymer is lower and, consequently, the solvent uptake is lower. Also, the high curing temperatures may have introduced certain degree of crosslinking which also decreases the uptake. However the modified fillers led to decreased water sorption and increased toluene sorption of the nanocomposites which is well in agreement with their hydrophobic nature. The lower toluene sorption values of StINPs/NR also favour the greater crosslink density of StINPs/NR filled nanocomposites compared to StAcNPs / NR nanocomposites.

Table.1 TG data of bionanocomposites of NR / starch

Fillers	**Degradation temperature for % wt. loss**					**Activation energy Ea(KJ/mol)**
	1	2	5	10	50	
Waxy starch	128	179	250	303	371	33.23
StNPs	135	198	276	305	375	54.17
StINPs	203	255	310	336	378	57.61
StAcNPs	170	231	292	326	376	56.32
C-black	114	192	264	304	364	29.10

Table. 2 DMA data for bionanocomposites of NR / starch

Fillers	**Tg ºC**	**Activation Energy Ea (KJ/mol)**
StNPs	-55	312.61
StINPs	-50	369.81
StAcNPs	-48	324.75

Table.3 Water and toluene sorption of bionanocomposites of NR / starch

Fillers	% mole Uptake							
	Water				Toluene			
	10 phr	20 phr	30 phr	40 phr	10 phr	20 phr	30 phr	40 phr
StINPs	0.98	0.37	0.21	0.18	2.73	2.39	2.06	1.97
StAcNPs	1.13	0.51	0.26	0.24	2.76	2.44	2.12	2.04
StNPs	3.10	2.87	2.44	2.41	1.22	0.65	0.34	0.22
Starch	3.46	2.81	2.51	2.47	1.30	0.82	0.60	0.52
C-black	1.15	0.71	0.56	0.32	2.77	2.38	1.97	1.74

4.4 Conclusions

Unmodified as well as modified starch nanoparticles were incorporated upto 40phr in natural rubber matrix successfully. All the bionanocomposites showed superior strength and elongation than conventional Carbon Black/NR composites at all loadings. The modified starch nanoparticles showed better compatibility with NR matrix as per the morphology and XRD studies of bionanocomposites which revealed the uniform morphology and nearly exfoliated structure. Isocyanate modified starch nanoparticles imparted highest strength, increased the Tg and decreased solvent sorption probably due to formation of additional crosslinks during vulcanization process. Despite the polysaccharide origin the starchy fillers did not deteriorate the thermal stability of the nanocomposites. The broad tan δ peak suggested high degree of compatibility of reinforcing fillers with NR matrix with potential application over a wide temperature range. The study opens up a new and green alternative for reinforcement of rubbers.

In the past, cellulose nanocrystals were used upto 30 phr to form nanocomposites with polymers. Starch derivatives are found to induce excellent reinforcement in natural rubber upto 40 phr filler loading (chapter 4A). Hence here the development of nanocomposites highly filled (> 50 phr) with cellulosic fillers has been attempted.

4.5 Experimental

4.5.1 Materials

Cellulose and cellulose acetate were purchased from Sigma Aldrich, Bombay.

4.5.2 Preparation of bionanocomposites

The bionanocomposites of NR were prepared on two roll mixing mill (as shown in scheme 4.2). Four sets of biocomposites were prepared using upto 60 phr each of cellulose (Cel), cellulose nanoparticles (CelNPs), cellulose acetate (CelAc), cellulose acetate nanoparticles (CelAcNPs) as reinforcing fillers in NR. The procedure and ratio of other ingredients were as mentioned in Chapter 2 (table.2.1.1).

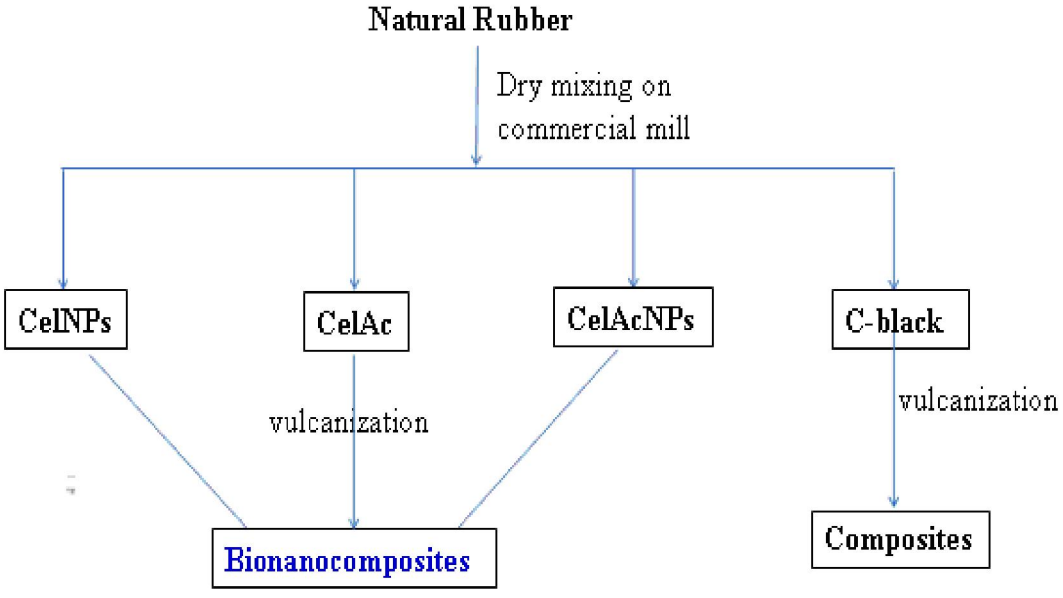

Scheme 4.1 Preparation of bionanocomposites of NR / cellulose

4.6 Results and Discussions

4.6.1 Mechanical Properties

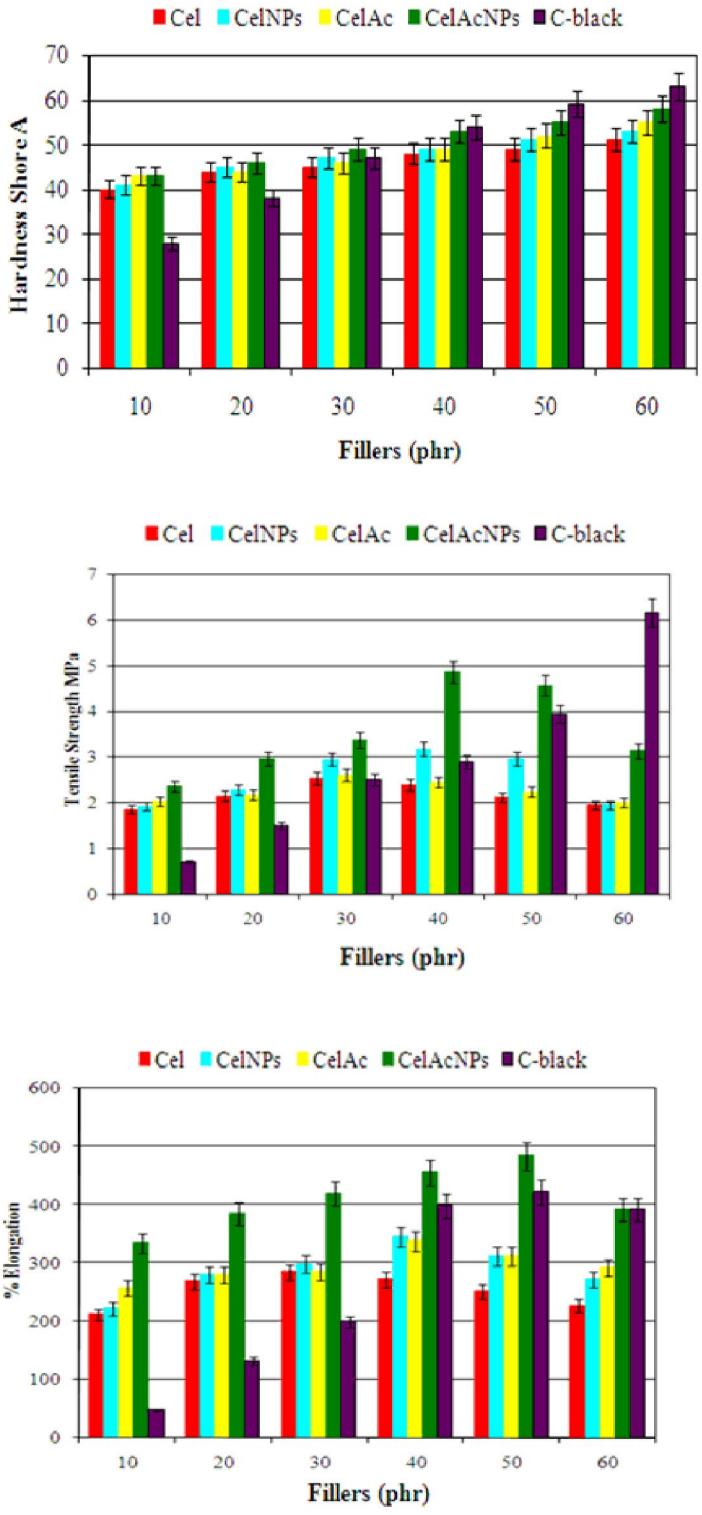

Figure. 4.7 Mechanical properties of NR composites

Hardness

The results of hardness of the various nanocomposites are expressed in Figure.4.7. It is observed that in all the nanocomposites the hardness increases with increase in concentration of fillers. The results showed that up to 30 phr all the four fillers showed superior hardness than C-black. After this the hardness increases but is less than that of C-black CelAcNPs imparted best hardness properties followed by, CelAc, CelNPs and Cel.

Tensile strength and % elongation

The mechanical properties of the composites were evaluated in terms of tensile strength and % elongation as seen in Figure.4.7. The values for ultimate tensile strength and % elongation for unfilled rubber are 0.58 MPa and 41 % respectively. At 10 phr cellulosic fillers impart very high tensile strength and elongation properties compared to C-black. As the filler loading increases there is a steep rise in mechanical properties of C-black composites. This increase is gradual in case of cellulose composites except for those containing CelAcNPs. Among all the fillers CelAcNPs exhibit best reinforcing ability upto 50 phr preserving the elastic behavior of nanocomposites. At still higher loading the performance of C-black was observed to be much superior to the cellulosic fillers. The results of mechanical properties also indicate that the combined effect of size reduction and organic modification drastically improves the filler matrix adhesion and hence the performance of cellulosic fillers.

4.6.2 X-ray diffraction pattern

The XRD of nanocomposites at 60 phr loading (Figure.4.8) showed no diffraction peak corresponding to pure NR unlike other reports [60,61]. This is due to higher filler loading. On the other hand, for high filler loadings Dufresne et al. have observed that the processing by casting and evaporation at 40 °C did not affect the crystallinity of starch in nanocomposite [62]. While the vulcanization process in the present case may have led to change in the structure of the nanocrystals from crystalline to amorphous. This accounts

for the absence of peaks coreesponding to modified and unmodified cellulose in XRD of present nanocomposites.

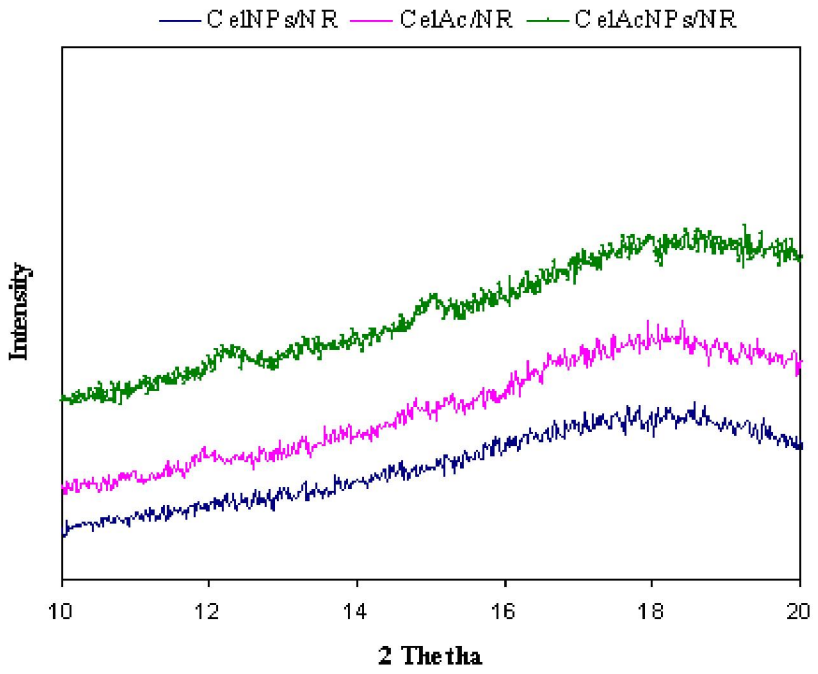

Figure. 4.8 XRD spectra of cellulose based composites at 60 phr loading.

4.6.3 Morphology studies

The results of the mechanical properties can be explained on the basis of morphology. The SE micrographs of fractured samples of composites at 40 phr loading are shown in Figure.4.9. SEM image of Cel/NR composite showed the presence of particles on the surface which may have leached out during fracture (Figure.4.9(a)). The CelAc/NR composite revealed somewhat homogeneous surface characteristics indicating filler-matrix compatibility (Figure.4.9(b)). CB/NR composite shows two-phase morphology and the presence of holes formed during fracture as evident from Figure.4.9(c). Against this, the nanofillers are more evenly distributed in the polymer matrix (Figure.4.9d) and (e)). In case of unmodified CelNPs/NR nanocomposite the reduction in size compensates for the hydrophilic nature (Figure.4.9(d)). Among all CelAcNPs/NR nanocomposite appears to show almost single phase morphology which does not reveal any particles on the surface (Figure. 4.9(e)). This probably means the filler particles are deeply embedded

in the matrix. The decrease in mechanical properties of CelAcNPs/NR nanocomposite at 60 phr may be due to formation of aggregates of excessive filler resulting in improper distribution. This is evident from the micrograph in Figure.4.9(f) which shows the occurrence of holes similar to those seen in CB/NR composite at 40 phr.

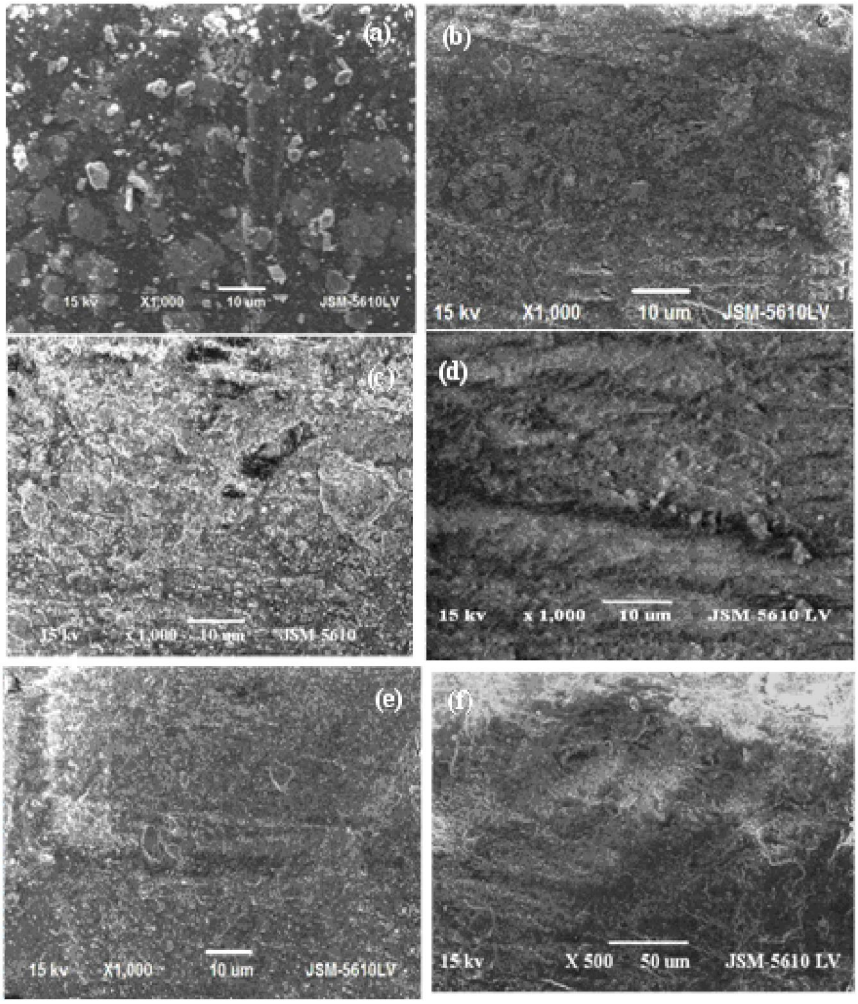

Fig. 4.9 SE Micrographs of NR composites at 40 phr loading of (a) Cel (b) CelAc (c) C-black (d) CelAcNPs (e) CelNPs and (f) CelAcNPs at 60 phr

4.6.4 Thermal analysis

Thermal gravimetric analyzer

The TG data of all the composites at 60 phr loading showed an initial mass loss from temperature 150-250 ºC attributed to elimination of volatile components such as water [63] (Figure.4.10(a)). The degradation temperatures of biocomposites are in close

proximity with those of C-black composites. This may be because high vulcanization temperatures may have resulted in some extent of crosslinking within the polysaccharide network. The results also show that modified cellulose imparts better thermal stability to the composites compared to native cellulose. As already seen in the mechanical properties due to combined effect of size reduction and organic modification, the decomposition temperatures of CelAcNPs/NR nanocomposite are even higher than those of C-black/NR composite (Table-4). This is due to increase in onset temperature as compared to other composites which leads to increase in thermal stability. Also the thermal stability of increases as the amount of CelAcNPs increases (Figure.4.10(b)). This is due to the improved reinforcement imparted by CelAcNPs to hydrophobic NR matrix.

Differential scanning calorimetry

DSC analysis of NR composites at 60 phr filler loading show that the biocomposites have Tg comparable with that of C-black/NR composite (Table-4). This means that cellulosic fillers does not have affect the Tg of NR (Figure.4.11(a)) The Tg also goes on increasing with the filler loading as expected (Figure.4.11(b)). The Tg of CelAcNPs/NR nanocomposite is highest due to its hydrophobic nature and small size which imparts rigidity and strength to the network.

Table.4 Thermogravimetry data and Tg values of NR composites containing various fillers

Fillers	**Degradation temperature for % wt. loss**					**Tg ^{o}C at 40 phr**
	1	**2**	**5**	**10**	**50**	
Cel	137	191	257	288	325	-62.96
CelNPs	161	202	271	309	359	-62.06
CelAc	145	198	266	297	357	-62.81
CelAcNPs	187	222	286	312	369	-61.88
C-black	114	192	264	304	364	-62.24

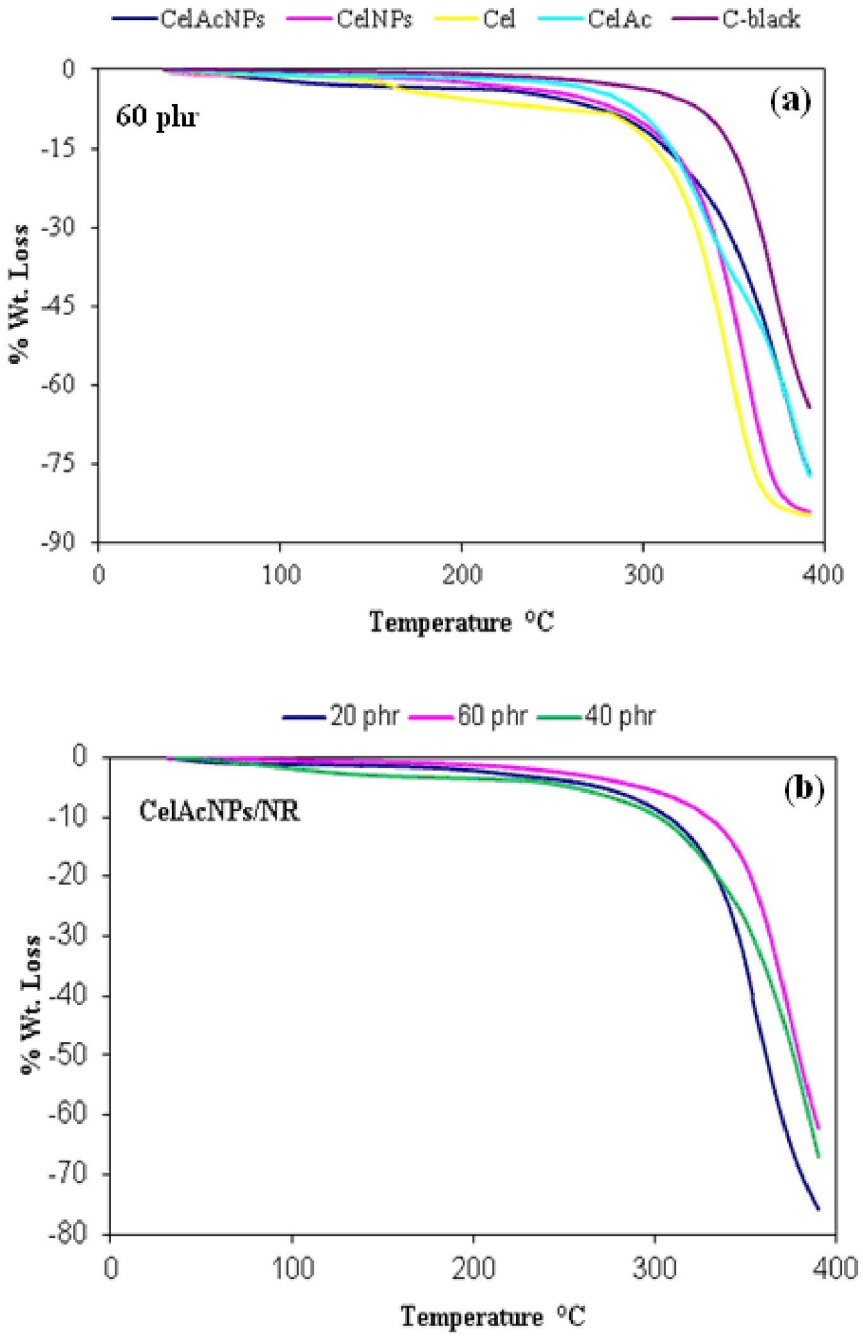

Figure. 4.10 TG curves of (a) NR composites and (b) NR nanocomposites containing CelAcNPs at various filler loadings

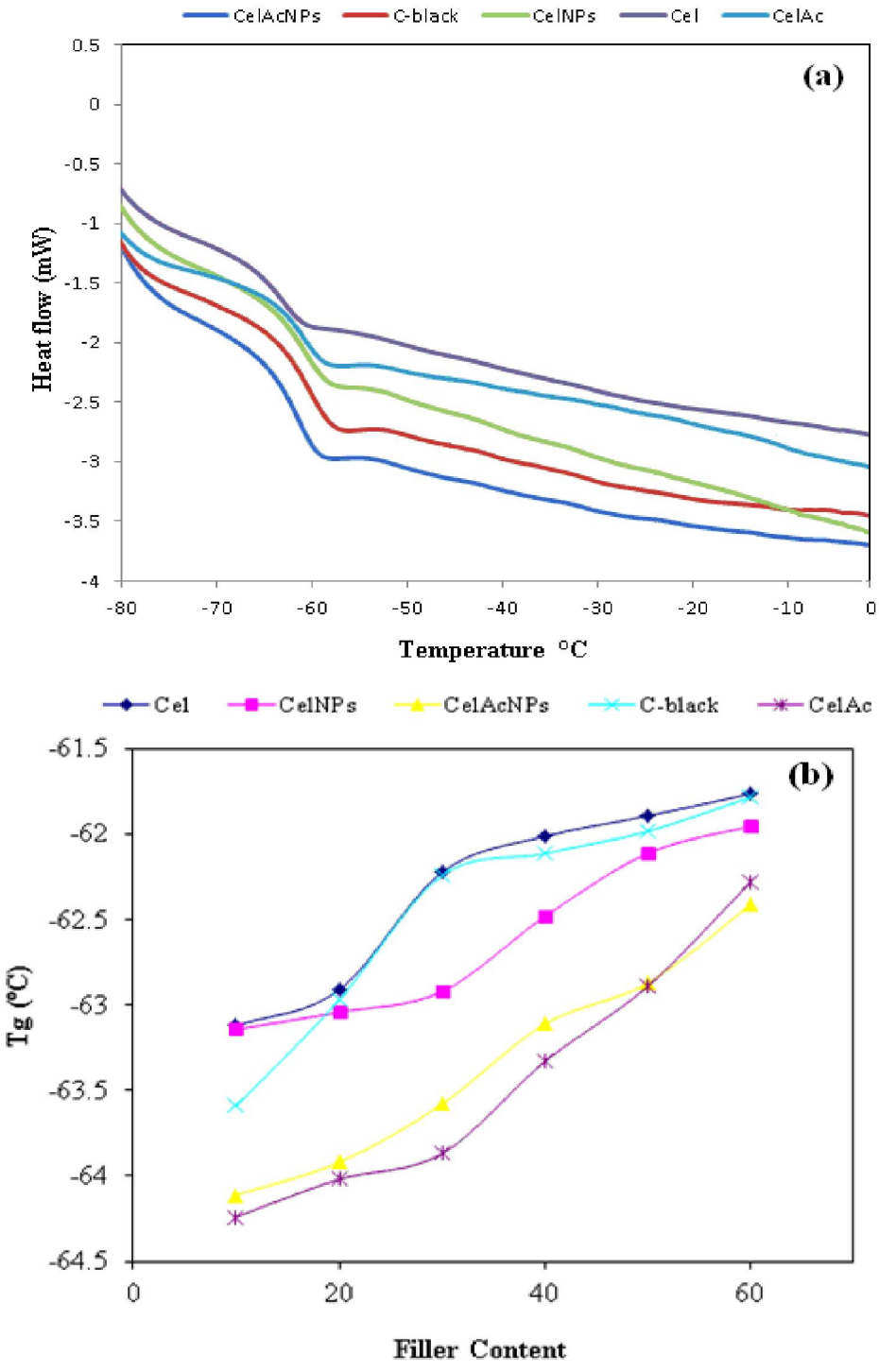

Figure. 4.11 (a) DSC curves and (b) effect of filler on Tg of NR composites

Dynamic mechanical analyzer

Figure.4.12 shows the dynamic mechanical spectra (logarithm of dynamic storage modulus log(E'), E" and loss factor (tan δ)) of CelAcNPs/NR nanocomposite at 60 phr loading, as a function of temperature at 1 Hz. A sharp decrease is observed around -62 °C, corresponding to the primary relaxation process associated with the glass-rubber transition determined by differential scanning calorimetry (DSC) measurements. In this temperature range the loss angle passes through a maximum (Figure.4.12). A low temperature, i.e., below Tg, the reinforcing effect of cellulosic nanoparticles was low justifying the normalization of the modulus. Above Tg, a much more significant reinforcing effect of nanoparticles was observed. Dynamic mechanical analysis involves weak stresses, the adhesion between the filler and the matrix is not damaged. Under higher stress, as used for tensile tests, the adhesion is involved. The values of E' and E" does not increase with the filler loading above Tg (Figure.4.12). This indicates that cellulose acetate nanoparticles do not affect the elastic properties associated to the rubber phase. The tan δ curve of CelAcNPs/NR nanocomposite shows a broad relaxation process from -90 ºC to 25 ºC. This may be due to the relaxation of rubber fraction confined inside the layers [6].

4.6.5 Water sorption

The filler/matrix adhesion along with the components embedded in the matrix is important factor in determining the sorption behavior of composite. In cellulosic composites, the water sorption was expected to increase with the amount of filler. However, the results demonstrated in Table-5 showed that water uptake decreases with the amount of filler. Adsorption of macromolecular chains at the filler/matrix interface through interactions between cellulose nanoparticles and NR could reduce swelling. Indeed, the formation of a three-dimensional network has already been reported for polysaccharide nanoparticles [6]. It may result from hydrogen bonding forces between unreacted hydroxyl groups of nanoparticles during the vulcanisation. At higher loadings, nanoparticles connect to form an infinite percolating network, which could be a barrier limiting the diffusion of toluene within the material. A fraction of the matrix material

thus becomes inaccessible for swelling (entrapped NR fraction). This indicates that the interaction between polymer matrix and filler leads to the formation of a bound polymer in close proximity to the reinforcing filler, which restricts the solvent uptake. However, this hypothesis needs deeper analysis.

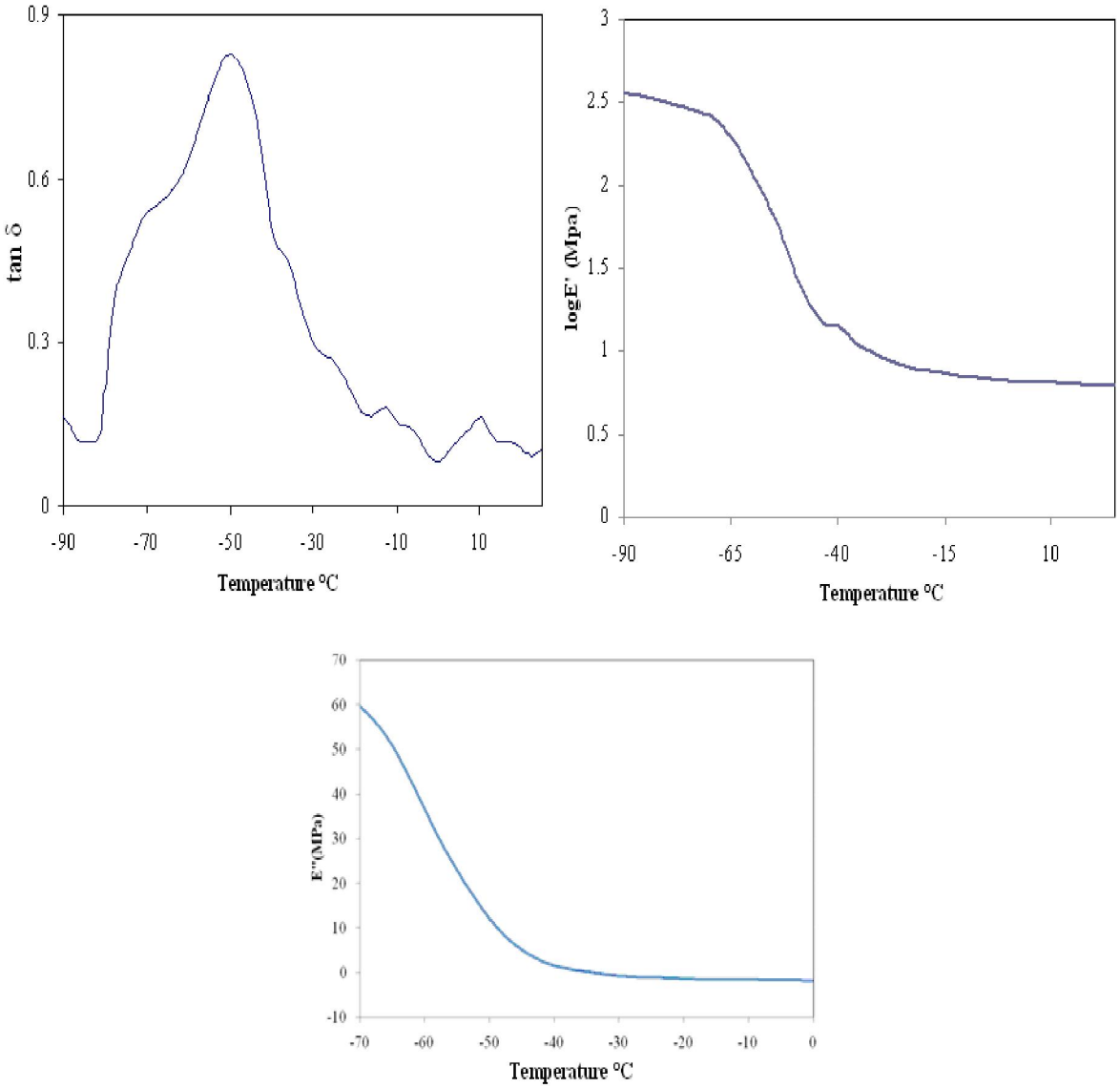

Figure. 4.12 Effect of CelAcNPs on (a) mechanical loss factor tan δ, (b) logarithm of storage modulus E' and (c) loss modulus E"

Table.5 Water and toluene sorption of NR composites containing various fillers

Fillers	% mole uptake					
	water			Toluene		
	20 phr	40 phr	60 phr	20 phr	40 phr	60 phr
Cel	2.81	1.94	1.07	2.77	2.19	1.76
CelNPs	1.05	0.56	0.25	2.56	2.11	1.67
CelAc	1.37	0.88	0.31	2.86	2.33	1.87
CelAcNPs	0.87	0.31	0.17	2.85	2.22	1.81
C-black	0.71	0.42	0.22	2.38	1.61	1.12

4.7 Conclusions

The study led to the conclusion that filler–matrix adhesion dominates the performance of fillers. Cellulose acetate nanoparticles with the special advantage of nanosize as well as hydrophobicity exhibited the best mechanical strength, optimum being at 40 phr. Similar to carbon black composites the water sorption of the biocomposites was found to decrease linearly independent of the nature of the filler. Further, the polysaccharides did not lead to significant thermal degradation of the composite while acetylation improved the thermal stability. It can be concluded that the cellulose acetate nanoparticles can be potential green reinforcing agents even at higher loadings.

4.8 References

1. R. A. Vaia, H. D. Wagner, *Mater. Today,* **2004**, 6, 32.
2. S. Ray, A. J. Easteal, In Advances in Polymer-Filler Composites: Macro to Nano; International Composites Conference, Sydney, Australia, July 11-14, 2006; Taylor & Francis Inc.: Sydney, Australia, **2006**, 741.
3. D. Schmidt, D. Shah, E. P. Giannelis, *Curr. Opin. Solid State Mater. Sci.,* **2002**, 6, 205.
4. A. Usuki, M. Kawasumi, Y. Kojima, S. Okada, T. Kurauchi, O. A. Kamigaito, *J Mater Res*, **1993,** 8, 1174.
5. A. Usuki, Y. Kojima, M. Kawasumi, A. Okada, Y. Fukushima, T. Kurauchi, *J Mater Res*, **1993,** 8, 1179.
6. Z. Wang, T.J. Pinnavaia, *Chem Mater*, **1998,** 10, 1820.
7.M. Alexandre, P. Dubois, *Mater Sci Eng R-Reports*, **2000,** 28, 1.
8. E.P. Giannelis, R. Krishnamoorti, E. Manias, *Adv Polym Sci*, **1999,** 138, 107.
9. H. Shi, T. Lan, T.J. Pinnavaia, *Chem Mater*, **1996,** 8, 1584.
10. M. Arroyo, M.A. Lo´pez-Manchado, J.L. Valentı´n, *J. Carretero, Composites Science and Technology*, **2007**, 67, 1330.
11. Y.P. Wu, Q.X. Jia, D.S. Yu, L.Q. Zhang, *J Appl Polym Sci*, **2003,** 89, 3855.
12. S. Su, D.D. Jiang, C.A. Wilkie, *Polym Dgrad Stabil*, **2004**, 83, 321.
13. H.D. Lu, Y. Hu, J.F. Xiao, Q.H. Kong, Z.Y. Chen, W.C. Fan, *Mater Lett*, **2005,** 59, 648.
14. K. I. Winey, R. A. Vaia, *MRS Bull.* **2007**, *32*, 314.
15. M. A. Lo´pez-Manchado, J. L. Valentı´n, J. Carretero, F. Barroso, M. Arroyo, *Eur. Polym. J.,* **2007**, 43, 4143
16. R. A. Vaia, *Mater. Today* **2004**, *7*, 32 .
17. A. Bendahou, H. Kaddami, A. Dufresne, *European Polymer Journal*, **2010**, 46, 609.
18. A. Dufresne, J. Y. Cavaille, W. Helbert, *Macromolecules*, **1996**, 29, 7624.
19. A. Dufresne, J. Y. Cavaille, *Journal of Polymer Science Part B Polymer Physics*, **1998**, 36, 2211.

20. H. Angellier, S. Molina-Boisseau, A. Dufresne, *Macromolecules*, **2005**, 38, 9161.
21. E. Bouthegourd, K. R. Rajisha, N. Kalarical, J. M. Saiter, S. Thomas, *Mater. Lett.*, **2011,** 65, 3615.
22. D. Lecorre, J. Brass, A. Dufresne, *Carbohydr. Polym.* **2012,** 87, 658.
23. M. Valodkar, S. Thakore, *Int. J. Polym. Anal. Charact.* **2010**, 15, 1.
24. V. Favier, H. Chanzy, J. Y. Cavaille, *Macromolecules,* **1995**, 28, 6365.
25. M.Grunnert, W. T. Winter, *Polym. Mater. Sci. Eng.***, 2000**, 82, 232.
26. S. Noorani, J. Simonsen, S. Atre, Oksman, K., Sain, M., Eds.; In Cellulose Nanocomposites: Processing, Characterization and Properties; ACS Symposium Series 938; American Chemical Society: Washington, D.C., **2006**.
27. A. Morin, A. Dufresne, *Macromolecules,* **2002**, 35, 2190.
28. M.Paillet, A. Dufresne, *Macromolecules,* **2001**, 34, 6527.
29. L.Petersson, A. P. Mathew, K. J. Oksman, *Appl. Polym. Sci.,* **2009**, 112, 2001.
30. Y. Choi, J. J. Simonsen, *Nanosci. Nanotechnol.,* **2006**, 6, 633.
31. S. A. Paralikar, J. Simonsen, J. J. Lombardi, *Membr. Sci.***, 2008**, 320, 248.
32. N. L. Garcia de Rodriguez, W. Thielemans, A. Dufresne, *Cellulose,* **2006**, 13, 261.
33. G. Chauve, L. Heux, R. Arouini, K.Mazeau, *Biomacromolecules***, 2005**, 6, 2025.
34. C. Bonini, Ph.D. Thesis, Joseph Fourier University, Grenoble, France, **2000**.
35. L.Chazeau, J. Y. Cavaille, J. Perez, *J. Polym. Sci., Part B: Polym. Phys.* **2000**, *38*, 383.
36. N. E. Marcovich, M. L. Auad, N. E. Bellesi, S. R. Nutt, M. I. Aranguren, *J. Mater. Res.,* **2006**, 21, 870.
37. X. Cao, Y. Habibi, L. A. Lucia, *J. Mater. Chem.***, 2009**, 19, 7137.
38. M. N. Angles, A. Dufresne, *Macromolecules,* **2001**, 34, 2921.
39. X. Cao, Y. Chen, P. R. Chang, M. Stumborg, M. A. Huneault, *J. Appl. Polym. Sci.,* **2008**, 109, 3804.
40. Y. Lu, L. Weng, X. Cao, *Carbohydr. Polym.,* **2006**, 63, 198.
41. Y. Wang, X. Cao, L. Zhang, *Macromol. Biosci.***, 2006**, 6, 524.
42. Q. Li, J. Zhou, L. J. Zhang, *Polym. Sci., Part B: Polym. Phys.,* **2009**, 47, 1069.
43. H. Qi, J. Cai, L. Zhang, S. Kuga, *Biomacromolecules,* **2009**, 10, 1597.

44. K. Oksman, A. P. Mathew, D. Bondeson, I. Kvien, *Compos. Sci. Technol.,* **2006**, 66, 2776.

45. A. Dufresne, *Compos. Interfaces,* **2000**, 7, 53.

46. L. Jiang, E. Morelius, J. Zhang, M. Wolcott, J. Holbery, *J. Compos. Mater.,* **2008**, 42, 2629.

47. A. B. Abdelkader Bendahou, A. Hamid Kaddami, A. Dufresne, *European Polymer Journal*, 2010, 46, 609.

48. M. Valodkar, S. Thakore, *J. Appl. Polym. Sci.,* (in press).

49. W. Thielemans, M. N. Belgacem, A. Dufresne, *Langmuir,* **2006**, 22, 4804.

[50]. M. Valodkar, S. Thakore, *Carbohydr. Polym.* 2011, 86, 1244.

51. R. Lalwani, S. Desai, *J. Appl. Polym. Sci.*, **2010**, 115, 1296.

52. S. Varghese, J. Karger-Kocsis, *Polymer*, **2003**, 44, 4921.

53. S. Desai, I. M. Thakore, B. D. Sarawade, S. Devi, *European Polymer Journal*, **2000**, 36, 711.

54. L.Qu, Huang, G. Z. Liu, P. Zhang, G. Weng, Y. Nie, *Acta Materialia,* **2009**, 57, 5053.

55. T. Pojanavaraphan, R. Magaraphan, *European Polymer Journal*, 2008, 44, 1968.

56. P. L. Teh, Z. A. Mohd Ishak, A. S. Hashim, J. Karger-Koesis, U. S. Ishiaku, *European Polymer Journal*, **2004**, 40, 2513.

57. M. Mondragon, E. M. Hernandez, J. L. Rivera-Armenta, F. J. Rodriguez-Gonzalez, *Carbohydrate Polymer*, **2009,** 77, 80.

58. S. Desai, I. M. Thakore, A. Brennan, S. Devi, *Journal of Macromolecule Science Pure and Applied Chemistry A*. **2001**, 38, 711.

59. M. Jacob, K. T. Varughese, S. Thomas, *Biomacromolecules*, **2005**, 6, 2969.

60. L. Qu, G. Huang, Z. Liu, P. Zhang, G. Weng, Y. Nie, *Acta Materialia*, **2009**, 57, 5053.

61. T. Pojanavaraphan, R. Magaraphan, *European Polymer Journal*, **2008**, 44, 1968.

62. H. Angellier, S. Molina-Boisseau, A. Dufresne, *Macromolecules*, **2005**, 38, 9161.

63. A. Dufresne, J. Y. Cavaille, W. Helbert, *Macromolecules*, **1996**, 29, 7624.

Chapter-5 Other applications of starch nanoparticles

Outline

5.1 Biological applications of starch nanoparticles

5.1.1 Introduction

Starch-based polymers have recently been proposed as having great potential for several applications in the biomedical field such as bone replacement implants [1], bone cements [2], drug delivery systems [3] and tissue engineering scaffolds [4]. The development of new processing technique [5] and the reinforcement with various fillers results in materials with mechanical properties matching those of bone [6]. However, other conditions should be met for a material to be considered suitable for any biomedical use. The evaluation of the in vitro cytotoxicity of a biomaterial is the initial step on a biocompatibility study, and is usually performed using immortalised cell lines [7,8].

Chitin and chitosan are biocompatible, biodegradable and nontoxic polymers. Because of these properties, they have many applications such as biomaterials for tissue engineering, in wound healing, as excipients for drug delivery [9] and also in gene delivery [10]. Chitosan nanoparticles used for the delivery of polypeptides such as insulin, tetanus toxoid, and diphtheria toxoids are widely explored [11,12,13]. Chitosan is soluble only under acidic conditions, which limits some of its applications. The limited solubility of chitosan in water can be overcome by chemical modification. Thus chemical modifications of chitin/chitosan are generally preferred to improve the polymer processability as well as to modify some of its properties such as solubility, antimicrobial activity and the ability to interact with other substances.

Cytotoxic drugs continue to play a major role in cancer therapy but often produce side effects, especially through the destruction of lymphoid and bone marrow cells [2]. Therefore, strategic improvements in cancer therapy are needed to improve efficacy while decreasing side effects. Over the past decades, nanoparticles (NPs) have been of great interest in applications for biological fields such as drug delivery systems and anticancer applications. The antitumor activities of natural biopolymer chitosan and its NPs are well reported. Another abundant polysaccharide starch, is relatively, more competent than chitosan due to its low cost, easy availability and better solubility but suffers from drawback of hydrophilic nature.

In recent years, many researches [14,15] have been focused on interaction of small molecules with DNA. DNA is generally the primary intracellular target of anticancer drugs, so the interaction between small molecules and DNA can cause DNA damage in cancer cells, blocking the division of cancer cells, and resulting in cell death [16]. Small molecule can interact with DNA through the following three non-covalent modes: intercalation, groove binding and external static electronic effects. Among these interactions, intercalation is one of the most important DNA-binding modes, which is related to the antitumor activity of the compound. Recently, there is a great interest on the binding of nanoparticles with DNA, owing to their possible applications as new cancer therapeutic agents and their photochemical properties that make them potential probes of DNA structure and conformation [17,18,19].

As seen in earlier chapters nanosized derivatives of starch showed excellent reinforcing abilities. In order to assess their potentiality as nanocarriers for drugs and also their anticancer properties we investigated the cytotoxic potential of nanosized acyl derivatives of starch with A549 human lung carcinoma cells as well as mouse embryonic fibroblast (3T3L1) cells. DNA binding studies were also carried out.

5.1.2 Experimental

5.1.2.1 Measurement of cell viability by MTT assay

A549 cells (5.0×10^3 cells/well) were maintained in 96 well cell culture plates (Tarson India Pvt Ltd.) for 24 hour in absence or presence of acetylated StNPs (1000- 10,000 µg/ml). At the end of incubation period 10 µl of 3-(4, 5-dimethylthiazol-2-yl)-2, 5-diphenyl tetrazolium bromide (MTT; 5 mg/ml) was added to the wells and plates were incubate at 37 ºC for 4 hours. Later, culture media was discarded and wells were washed with Phosphate Buffer Saline (HiMedia, India Pvt. Ltd.), followed by addition of 150 µl DMSO and subsequent incubation for 30 min and absorbance was read at 540 nm in ELX800 Universal Microplate Reader [20].

5.1.2.2 Statistical analysis

Data was analyzed for statistical significance using one way analysis of variance (ANOVA) followed by Bonferroni's multiple comparison test and results were expressed as mean±S.E.M. using Graph Pad Prism version 3.0 for Windows, Graph Pad Software, San Diego, CA, USA.

5.1.2.3 DNA solution preparation

CT-DNA was dissolved in Tris buffer (50 mM Tris-HCL pH 7.2) overnight at 4°C. DNA concentration was adjusted with the buffer to 3 mg/mL. This stock solution was stored at 4°C and was stable for several days. A solution of CT-DNA in water gave a ratio of UV absorbance at 260 and 280 nm, A260/A280 of 1.89–2.01, indicating that DNA was sufficiently free of protein. The concentration of DNA was determined from the UV absorbance at 260 nm using the extinction coefficient ε260=6600 M^{-1} cm^{-1}.[5]

5.1.2.4 UV titration

The absorbance titrations were performed at a fixed concentration of the compounds (0.1mg/mL) and varying the concentration of double stranded CT-DNA within the range 200–400 nm. For an individual experiment, 2 mL of a stock solution of compound in DMSO was added to DNA solution of varying concentrations.

5.1.2.5 Fluorescence titration

Fluorescence experiments were conducted by adding different concentrations of the solution of compound to a mixture containing 40 μM EB and 50 μL DNA. All the samples were excited at 340 nm and emission was recorded at 650-700 nm.

5.1.3 Results and discussion

5.1.3.1 Cytotoxicity study

The MTT assay and the MTS assay are colorimetric assays for measuring the activity of enzymes that reduce MTT or close dyes (XTT, MTS, WSTs) to formazan dyes, giving a purple color. A main application allows to access the viability (cell counting) and the

proliferation of cells (cell culture assays). It can also be used to determine cytotoxicity of potential medicinal agents and toxic materials, since those agents would stimulate or inhibit cell viability and growth.

MTT (3-(4,5-Dimethylthiazol-2-yl)-2,5-diphenyltetrazolium bromide, a yellow tetrazole), is reduced to purple formazan in living cells [21]. A solubilization solution (usually either dimethyl sulfoxide, an acidified ethanol solution, or a solution of the detergent sodium dodecyl sulfate in diluted hydrochloric acid) is added to dissolve the insoluble purple formazan product into a colored solution. The absorbance of this colored solution can be quantified by measuring at a certain wavelength (usually between 500 and 600 nm) by a spectrophotometer. The absorption maximum is dependent on the solvent employ.

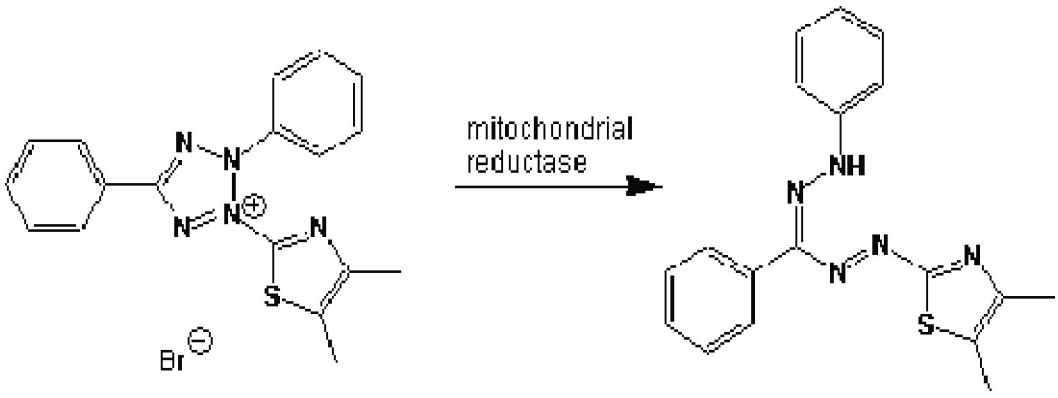

Figure. 5.1.1 Reduction of MTT dye

These reductions take place only when reductase enzymes are active, and therefore conversion is often used as a measure of viable (living) cells. However, it is important to keep in mind that other viability tests (such as the CASY cell counting technology) sometimes give completely different results, as many different conditions can increase or decrease metabolic activity. Changes in metabolic activity can give large changes in MTT results while the number of viable cells is constant. When the amount of purple formazan produced by cells treated with an agent is compared with the amount of formazan produced by untreated control cells, the effectiveness of the agent in causing death, or changing metabolism of cells, can be deduced through the production of a dose-response curve.

The in vitro cytotoxicity was evaluated at various doses by exposure of A549 cells as well as 3T3L1 cells to acetylated StNPs. A dose range of 1000-10,000 μg/mL recorded moderate cytotoxicity in 3T3L1 cells (Figure. 5.1.2) while StNPs induced practically no cell death. At this dose, in tumor cells interesting dose dependent cytotoxicity was observed within 24 h (Figure. 5.1.2). Among all the NPs tested herein, StcinNPs showed highest cytotoxicity (table-1) and its highest dose (10,000μg/mL) recorded nearly 80% cytotoxicity (Figure. 5.1.2). On the other hand, StpalNPs recorded lowest cytotoxic potential.

In biological activities, cell must interact with the extracellular environment which is generally through chemical, electrical or mechanical signaling. In the present studies, DS of acetylated starch NPs are ≥ 2 which indicates the hydrophobic nature of acetylated starch NPs. Cytotoxicity is reported to increase with increasing hydrophobicity [22]. Based on this it can be concluded that there is hydrophobic interaction between tumor cells and starch derivatives which is responsible for cytotoxicity. The order of anticancer activity was StcinNPs > StbenNPs > StphNPs > StpalNPs respectively (table 5.1.1) shows that the cytotoxicity of derivatives of StNPs containing aromatic groups was found to be more compared to that containing aliphatic group. There may be a structure activity relationship which requires further investigation.

The cytotoxicity of chitosan NPs and derivatives has been attributed to positive surface charge. However zeta potential measurements of acetylated StNPs (table 5.1.1) showed that they have negative surface charge. This is because, neither size nor zeta potential alone determine the optimal cellular response induced by NPs [23]. It has also been proposed that, in regions where the columbic repulsion of similar charges is not too pronounced, the presence of a high electric field may cause local electroporation. So, high electrical fields of the NPs of about 50 nm, which may succeed even with negative zeta potential, may eventually lead to cytotoxicity. This phenomenon is known to facilitate permeation of various nanoscale objects through biological membranes. It is reported in literature, that the proteins from the growth media adsorb to the surfaces of both cationic and anionic NPs, increase their hydrodynamic radius, and flips their charge immediately to similar negative value of the serum proteins in the original media [24].

Thus size, aggregation state, surface charge and surface chemistry would be significantly acetylated via electrostatic screening which in turn could influence their ability to interact with or enter cells [25,26] Therefore, NPs that had a positive effective surface charge upon preparation are no longer cationic in the cellular media. This is important when considering the molecular effect of charge on toxicity and cellular uptake, and argues against the simple picture, still propagated in the literature, that cationic nanoparticles disrupt the negatively charged cellular membrane by electrostatic interactions. Protein adsorption to the NPs surface can mediate the uptake of the nanomaterial via receptormediated endocytosis [27,28,29]. This is believed to be the reason for the interaction of the nanosized derivatives with biological systems.

Table.5.1.1 Degrees of substitution, thermal analysis, IC_{50} values, thermal degradation and zeta potentials of acetylated starch nanoparticles.

Sample	**IC_{50} value (µg/mL)**	**Zeta potential (mV)**
StPhNPs	2010±120	-24.52
StCinNPs	1110±110	-45.14
StBenNPs	1410±140	-23.41
StPaNPs	4450±200	-15.01
StNPs	-	-26.70

Previous studies have reported polysaccharide NP induced cytotoxicity against various tumor cell resulting due to oxidative damage to the cell membrane and mitochondrial dysfunction [30,31]. Similar alterations observed in our study are in accordance with these reports and thus establish the doses and the resultant cellular damage caused by acetylated StNPs.

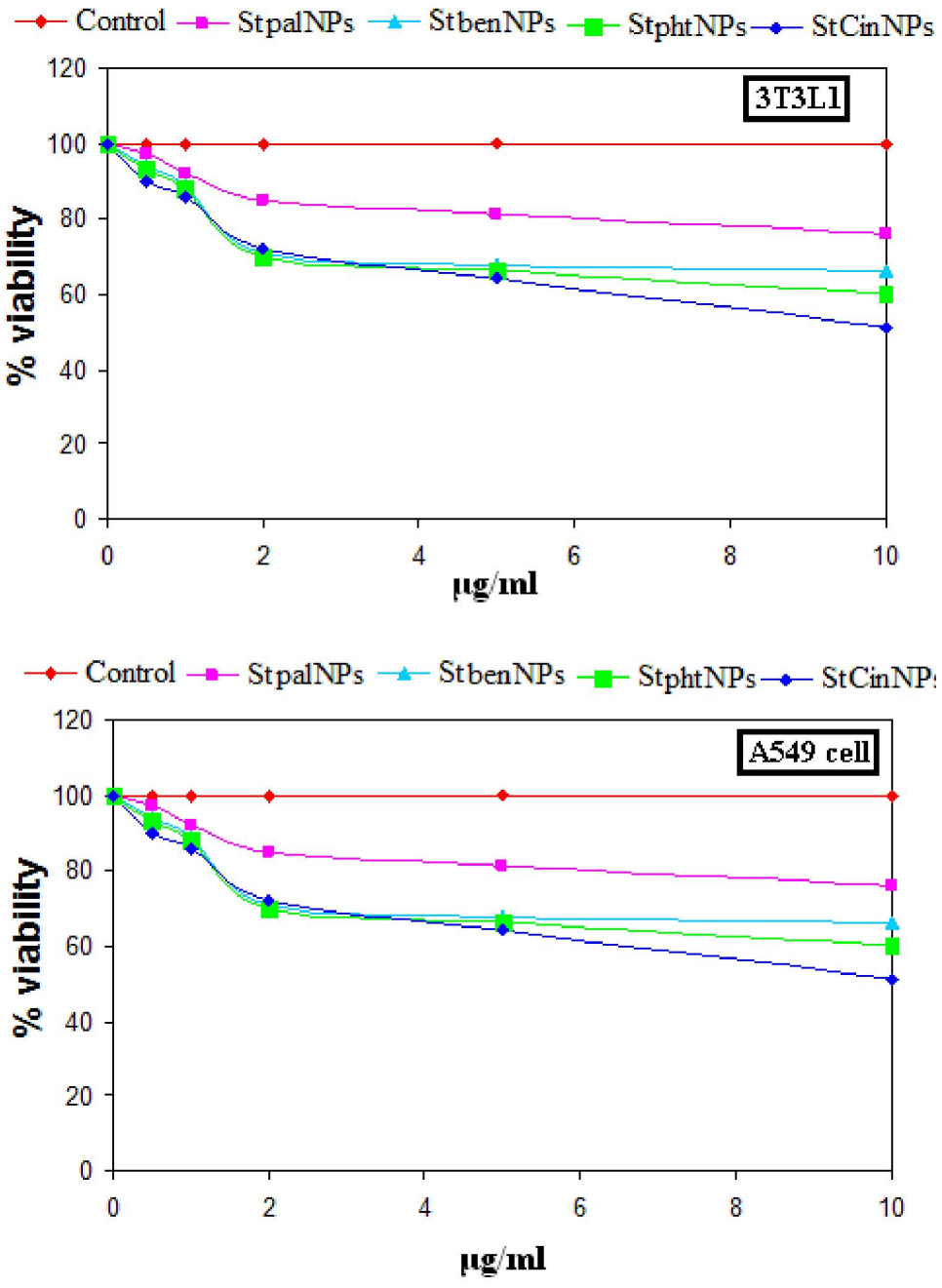

Figure. 5.1.2 Effect of acetylated starch nanoparticles exposure on cell viability in 3T3L1 and A549 cells. Results are expressed as mean±S.E.M. for n = 3 (replicates). Where NS = non-significant, *p < 0.05, **p < 0.01 and ***p < 0.001 compared to untreated cells.

5.1.3.2 DNA binding studies

UV-visible spectroscopy

The binding interaction of many organic carcinogens such as polycyclic aromatic hydrocarbons with DNA is the key step in their genotoxic effect. Titration with UV absorption spectroscopy is an effective method to examine the binding mode of DNA with the molecules [32]. In general, the spectra of the compounds show UV absorption bands that are usually symmetrical with no obvious splitting. In the UV region, compounds exhibited bands between 240-320 nm, which are assigned to the $\pi \rightarrow \pi^*$ transitions, due to long living triplet excited state. Hypochromism results from the contraction of DNA helix axes as well as the conformational changes on molecule of DNA, while hyperchromism results from the secondary damage of DNA double helix structure [33,34.]. Upon increasing concentration of CT DNA, the UV region exhibited an increase in absorption intensity 'hyperchromic' effect with a blue shift of 2-10 nm in $\pi \rightarrow \pi^*$ region (Figure.5.1.3). The strong hyperchromic effect with a blue shift is suggestive of higher binding propensity to CT DNA due to stabilization of the nanoparticle-DNA adduct. These changes are typical of compounds bound to double stranded DNA through non-covalent interaction [35]. In the present case, the complete intercalation of the compounds between a set of adjacent base pairs seems sterically impossible, but some partial intercalation can be envisioned [36].

Photoluminescence spectroscopy

Enhancement of the fluorescence emission when binding with the biomacromolecules (such as DNA and proteins), is a very useful fluorescent probe in genomics and proteomics [37]. In present study we found that luminescence was not observed for compounds either in DMSO or in presence of DNA. Hence, competitive binding studies using ethidium bromide (EB) bound DNA was carried out. EB is a conjugate planar molecule. Its fluorescence intensity is very weak but it is greatly enhanced when EB is specifically intercalated into the adjacent base pairs of double stranded DNA. The enhanced fluorescence can be quenched by the addition of a second molecule [38]. The

addition of compounds to DNA-EB system displayed an increase in emission intensity of the DNA-EB system (Figure. 5.1.4).

Increase in fluorescent intensity indicates that the StNPs derivatives have not completely intercalated into the DNA helix, as complete intercalation would decrease the emission intensity due to the replacement of the intercalated EB from DNA. The observed results suggest that the nanoparticles can make a contraction in the helix axis of DNA [39]. The binding affinity seems to follow the order StpalNPs ≥ StphNPs > StcinNPs > StbenNPs.

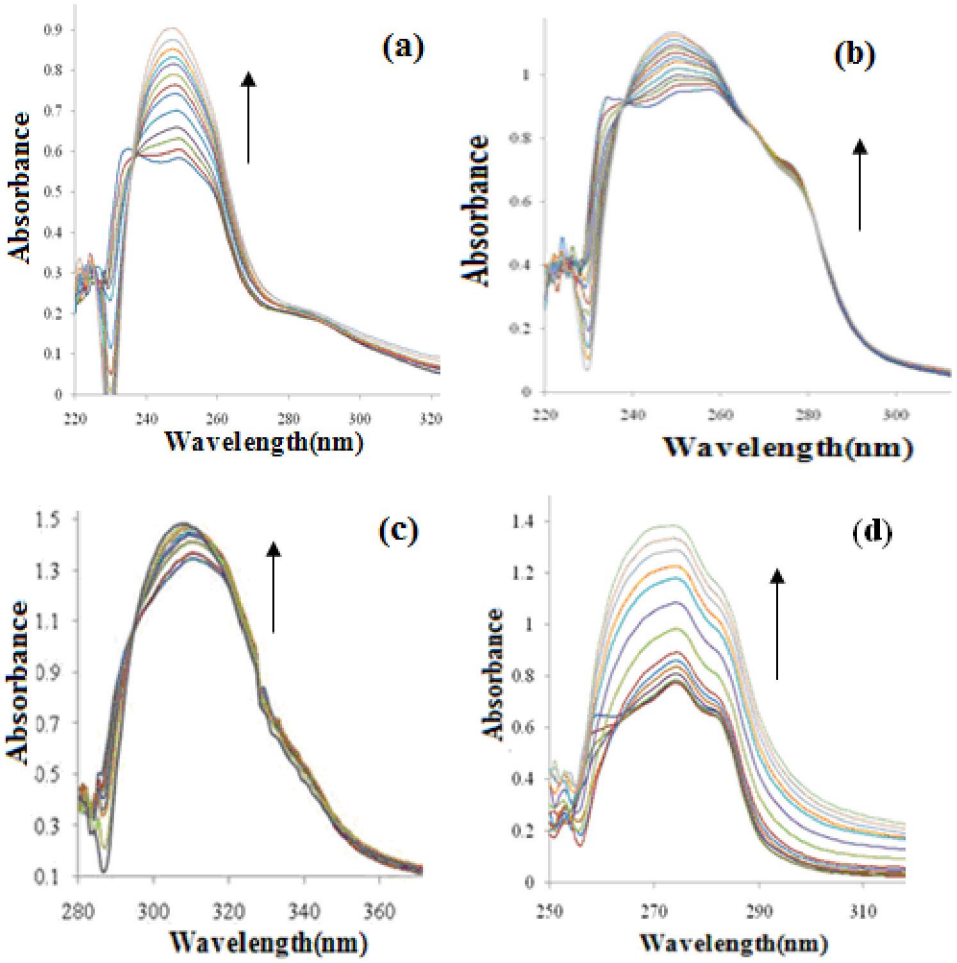

Figure. 5.1.3 Absorption spectra of (a) StpalNPs, (b)StphNPs, (c) StcinNPs and (d) StbenNPs (0.1 mg/mL) without and with CT-DNA at different concentrations (0.05, 0.10, 0.15, 0.20, 0.25, 0.30, 0.35, 0.40, 0.45, 0.50, 0.55 and 0.60 mL of stock solution). The arrow shows the intensity changes on increasing the acylated StNPs concentration

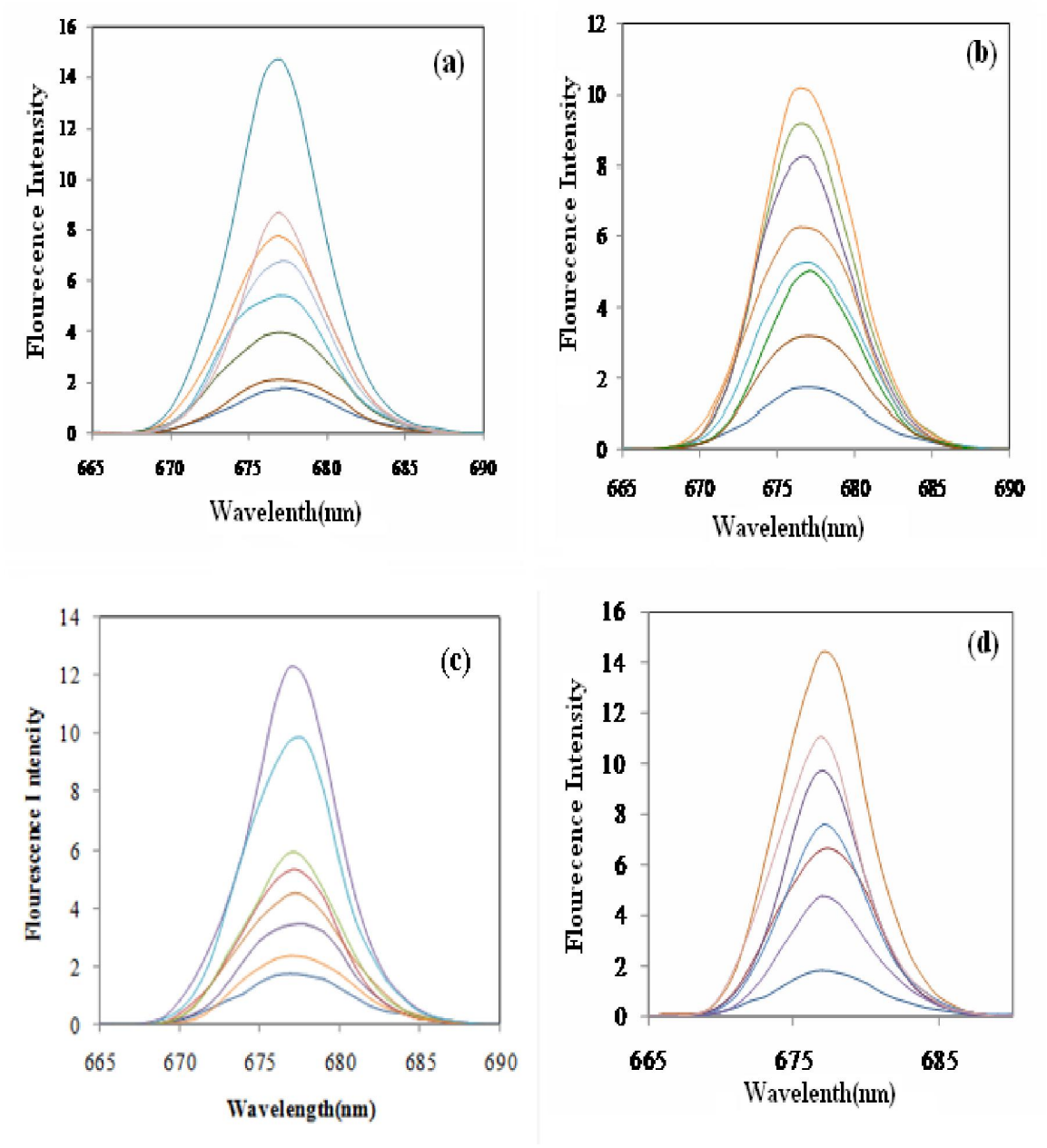

Figure. 5.1.4 Emission spectra of EB bound to DNA in the absence and presence of (a) StpalNPs, (b) StbenNPs, (c) StcinNPs and (d) StphNPs [EB] = 40 µM, [DNA] = 50 mL, [St- benzoate NPs] = 2, 4, 6, 8, 10, 12 and 14 µL, respectively; λ_{mex} = 340 nm. The arrow shows the intensity changes on increasing the acylated StNPs concentration.

5.1.4 Conclusions

The present study reports cytotoxic potential of the acetylated starch nanoparticles along with its biocompatible nature and warrants further evaluation at preclinical and clinical levels. The non-cytotoxicity to noncancerous cells suggest promising drug delivery applications of these materials at lower concentrations while higher doses would be useful as anticancer agents. The cytotoxicity of derivatives with aromatic groups and high degree of substitution was higher relative to those containing aliphatic group. The details of the mechanism of action, especially to clarify the mode of interaction with tumor cells, effect of degree of substitution and particle size are still to be investigated. Despite negative zeta potential the nanoparticles exhibited reasonable biding propensity with CT-DNA, although complete intercalation was not observed.

5.2 Starch nanoparticles as crosslinkers for polyurethane

5.2.1 Introduction

Polyurethanes (PUs) are unique polymer materials with a wide range of physical and chemical properties [40]. With well-designed combinations of monomeric materials, PUs can be tailored to meet diversified demands of various applications such as coatings, adhesives, fibers, thermoplastic elastomers, and foams. Extensive work has been focused to develop chemical and physical methods for their surface modification and treatments. PU materials and especially PU membranes and coatings need to bear functionalities to improve their intrinsic properties such as wettability, adhesion, biocompatibility, conductivity, cross-linking density and many others [41]. There are some interesting areas such as agricultural and medicinal applications, wherein it is desirable to introduce biodegradability by using natural materials for the synthesis of PUs [42,43]. Their non-biodegradability is restricting their utility in commodity applications. Hence, the possibility of converting them into partially biodegradable products is investigated. Carbohydrates are multihydroxyl compounds and hence can be employed as crosslinkers for PU Among carbohydrates, the use of starch in the synthesis of PUs has been reported in only a few publications [44,45,46,47,48]. Dosmann and Steel [34] added starch to urethane systems to yield shock-absorbing foams. Lu et al. [35] have studied the miscibility and physical properties of plasticized starch acetylated with PUs. They observed that the occurrence of hydrogen bonding interaction between starch and PUs plays a key role in the improvement of the performance of the material. A study of rheological properties of PU incorporated with starch granules was carried out by Ha and Broecker [49]. Biodegradable PUs containing starch have been synthesized and characterized in our laboratory [50]. Further, synthesis of biodegradable PUs using a series of carbohydrate like glucose (monosaccharide), sucrose (disaccharide), and starch (polysaccharide) as crosslinkers by varying the NCO : OH and diol : triol ratios were also carried out [51].

5.2.2 Experimental

5.2.2.1 Materials

The polypropylene glycol, molecular weight 2000 g / mole 1,4- hexamethylene diisocyanate (HMDI) Dibutyl tin dilaureate (DBTDL) and Tetrahydrofuran (THF) were purchased from Fluka AG, Switzerland.

5.2.2.2 PPG-HMDI modified StNPs PU nanocomposite film

PPG and 1, 4-hexamethylene diisocyanate were reacted at room temperature in the presence of nitrogen to form a urethane linkage followed by crosslinking with StNPs.

PPG modification involves a two-step process. The first step requires the reaction of PPG with one isocyanate functionality of HMDI. During the second step, the unreacted isocyanate of HMDI is then reacted with the surface hydroxyl groups of the starch nanoparticles.

PPG (1 mole) was vacuum dried at 80 ^{O}C. Dry THF was added followed by dropwise addition of 1.9 moles of HMDI with stirring in nitrogen atmosphere. The prepolymer formation was continued for 1 hour. Previously dried starch nanoparticles (1 mole) were added as dispersion in THF. Stirring was continued till homogeneous mixture was achieved and then catalytic amount of DBTDL was added. When the solution attained certain viscosity, degassing was carried out and polyurethane film was obtained by solution casting.

Previous studies showed that the properties of waterborne PU could be significantly improved when a small amount of nanoparticles were well mixed in the polymer matrix [52]. Introduction of nano Ag could not only improve the physical properties and biocompatibility of PU, but also inhibit the growth of bacteria even when nano Ag were embedded in the PU matrix in low concentrations. Metal nanoparticles have been doped in polymer matrix by a variety of chemical and physical methods in which the formation of metal nanoparticles was performed first. However, it is extremely difficult to disperse metal nanoparticles homogeneously into polymer matrix by these methods because of easy agglomeration of metal nanoparticles and high viscosity of polymer solution [46].

Hence, for practical applications it is important to get nanoparticles uniformly dispersed into polymer matrices.

The swelling and electrical properties of polyurethanes containing starch as crosslinker have been previously investigated [53,54]. With a view to enhance the conducting properties we attempted the incorporation of metal nanoparticles into the crosslinked PU membranes by novel sorption method in a manner similar to hydrogels [55]. The sorption ability of polyurethane could be very well exploited to facilitate transport of metal ions into the membranes. Subsequent reduction of the ions within the membrane resulted into the formation of stable nanoparticles.

5.2.2.3 Synthesis of polyurethanes immobilization with metal nanoparticles for electrical applications

From the kinetic study of sorption of alcohol in the PU membrane the optimum time was observed to be about 5 h. Circular shaped sample was immersed in 10 ml of 0.1 M alcoholic solution of metal salt for 5 h. During this equilibrium stage the metal ions were exchanged from solution to PU network through their free space between the cross-links or anchored to the –NHCOO- groups of PU chains (Scheme 5.2.1). The metal salt loaded membranes were wiped with tissue paper and immersed in 10 ml of 50 % alcoholic hydrazine hydrate solution. The swelling was continued till the color of the membrane changed to the characteristic wine reddish in case of copper and yellowish brown in case of and silver respectively. This indicated the formation of metallic nanoparticles within the PU network. The membranes were dried under vacuum at 40 ºC. At the end of the process there was no change in shape and size of PU membrane.

Alternatively PU membrane was immersed in alcoholic solution containing mixture of cupric acetate and 20 % ascorbic acid for 5 h. The solution containing the membrane was subjected to microwave irradiation for 2 min whereby formation of copper nanoparticles (CuNPs) occurred.

5.2.2.4 Characterization

Characteristic optical properties of the nanoparticle solutions were recorded using PerkinElmer Lambda 35 UV–vis spectrophotometer. Emission spectrum was recorded by

photoluminescence (PL) spectroscopy using spectrofluorometer from JASCO. Size and shape of the metal immobilized nanoparticles was determined by using TEM on a Philips, Holland Technai 20 model operating at 200 kV. AFM measurements were performed using an AFM Explorer microscope (ThermoMicroscopes, USA) in air and at room temperature, in a non-contact mode with Si cantilevers of a 1650-00 type (ThermoMicroscopes) with a nominal tip radius of 10 nm and resonant frequencies of about 220 kHz. XRD was determined by using PANalytical 'X'PERT-PRO XRPD of Cu Kα radiation (λ=0.15406 nm) with scanning rate of 2º/min and 2θ ranging from 10º to 80º. Thermal Gravimetric Analysis (TGA) was recorded on TG-DTA 6300 INCARP EXSTAR 6000. The glass transition temperature (Tg) was measured using DSC200 F3MAIA, NETZSCH. Both TGA and diffential scanning calorimetry (DSC) were carried out under nitrogen atmosphere at heating and cooling rate of 10 ºC/min respectively. Conductivity spectra of PU membranes have been recorded by Solartron Impedance analyzer in the frequency range 100Hz-1MHz at temperature from 298 to 383K.

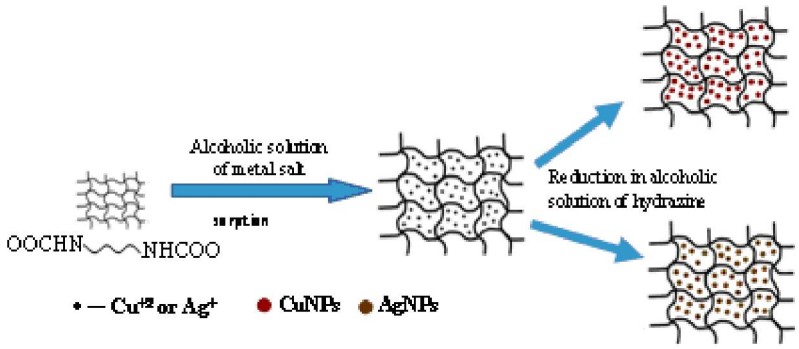

Figure. 5.2.1 Schematic representation of formation of PU-Cu and PU-Ag.

5.2.3 Results and discussion

The white translucent PU membrane gained a blue color upon sorption of the copper acetate solution, (Figure. 5.2.1 (a)) changing to reddish brown after reduction (Figure. 5.2.1 (b)), whereas in case of silver the white membrane changed to yellowish brown (Fig. 5.2.1 (c)). The process of immobilization has been represented in scheme 5.2.1. The metal nanoparticle immobilized membrane was removed from the reducing agent and wiped. It was dried at room temperature for an hour followed by vacuum drying.

Subsequently it was immersed in fresh alcohol for 72 h. There was no leaching out of the nanoparticles which was confirmed by UV-vis spectrophotometer. The color of the membrane remained unchanged which ensured immobilization of the nanoparticles in the membrane. Similar results were obtained with dichloromethane and acetone.

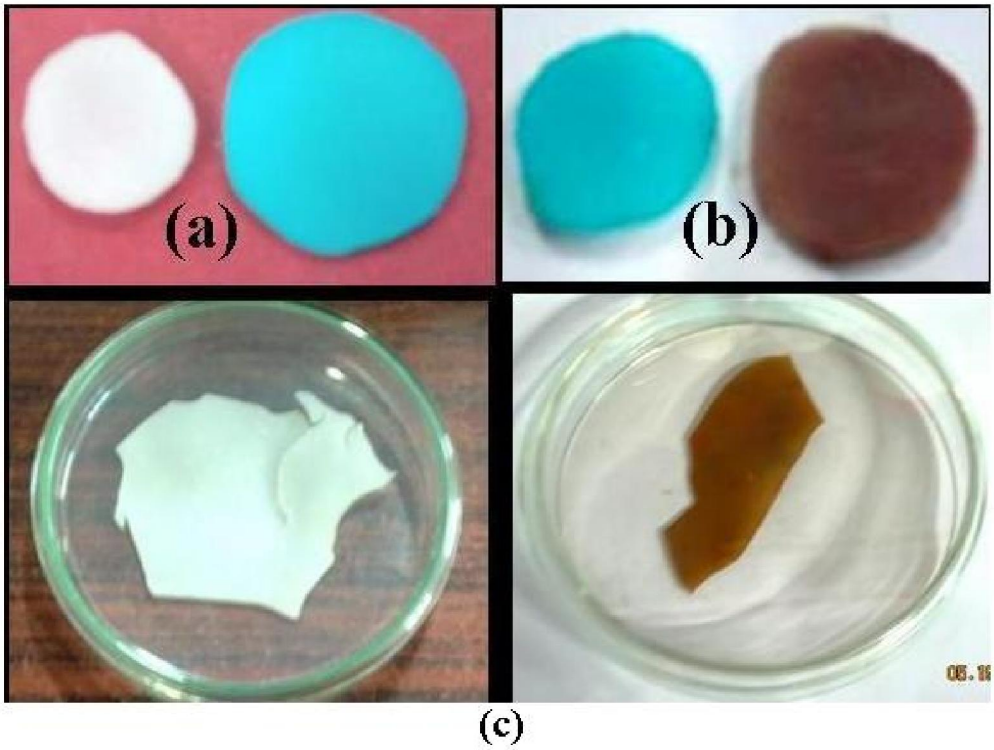

Figure. 5.2.1 Digital photographs of PU membranes to demonstrate (a) swelling in alcoholic solution of 0.1 M cupric acetate reduction of (b) Cu ions and (c) Ag ions to obtain immobilized Cu and Ag nanoparticles PU membranes respectively.

5.2.3.1 Optical properties

Formation and stability of metal nanoparticles in aqueous solution was confirmed using UV-vis spectral analysis of the CuNPs solution. The extinction spectra of CuNPs at different time intervals are shown in Figure. 5.2.2 (a). The characteristic absorption peak at 569 nm is due to the surface plasmon resonance (SPR) of CuNPs, which can be predicted by the well-known Mie resonance condition [56]. The surface plasmons are collective electronic excitations at the interface between metal and dielectrics. The optical properties of Ag and Cu nanoparticles change with size, shape, and dielectrics of the medium. The intensity of the peak increases with time. Figure. 5.2.2 (b) represents

photoluminescence spectrum of the CuNPs which shows emission at 660 nm on excitation at 569 nm due to the electronic transitions from excited states to d orbitals [57].

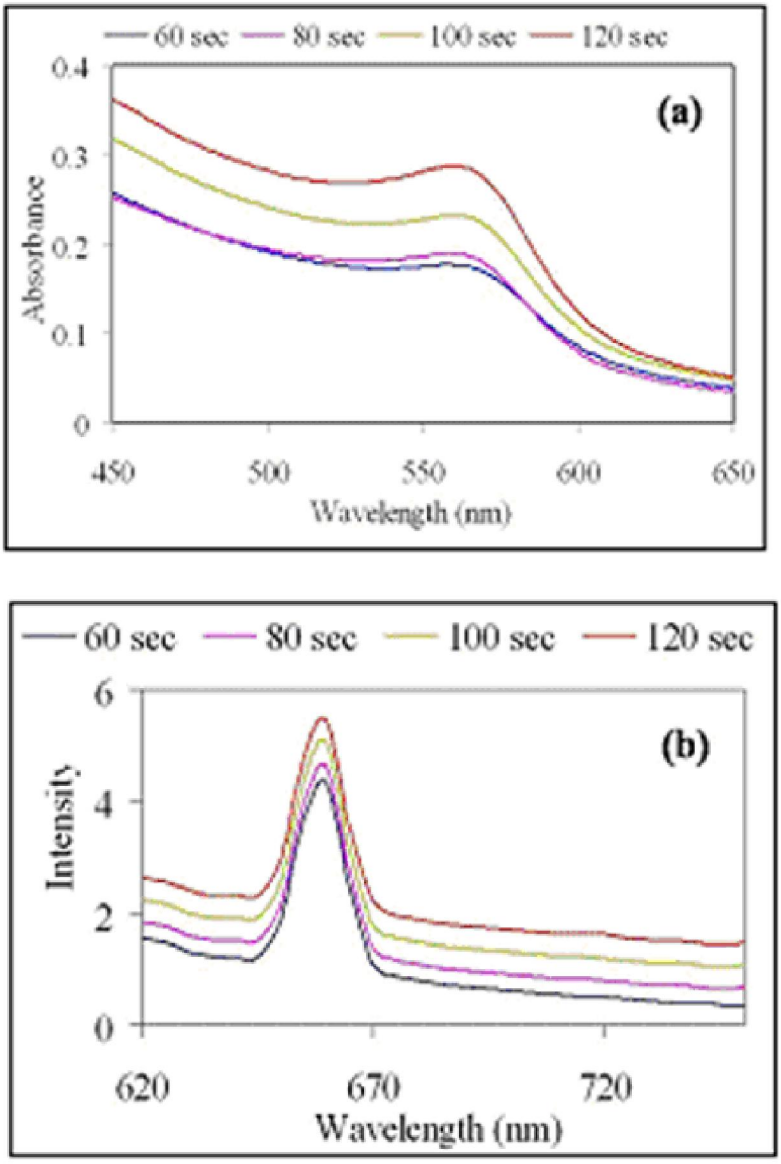

Figure. 5.2.2 (a) UV–vis absorption spectra (b) photoluminescence spectra of CuNPs

5.2.3.2 Transmission electron microscopy

As per our earlier observations the solubility parameter of the starch crosslinked PUs matched with that of acetic acid [53]. Hence when the silver nanoparticles immobilized

PUs membrane (PU-Ag) was immersed in acetic acid extensive swelling of the membrane took place. As equilibrium approached the membrane disintegrated. The TEM image of this membrane clearly reveals that the particles are somewhat spherical with a diameter ranging from 10 - 20 nm dispersed in the PU matrix (Figure. 5.2.3 (a)). However the particles are not very monodisperse. The surface morphology of PU-Ag was recorded using AFM. The two- and three-dimensional topography of the nanoparticles is shown in Figure. 5.2.3 b and c. Direct observation of the image revealed that the size of Ag nanoparticles was of the order 20–30 nm. The particles appeared to be almost spherical in shape. The size distribution of the nanoparticles along with the line profiles drawn at 9.87 μm horizontally and vertically indicates that the majority of the Ag nanoparticles were falling in the range of 20–30 nm. The data obtained from the AFM matched well with the TEM results.

5.2.3.3 X-ray diffraction

The XRD pattern of metal immobilized membranes showed the crystalline phases of the metals embedded in the amorphous matrix of crosslinked PU. In case of both PU-Cu and PU-Ag, the pattern matches well with the cubic phase of Cu and Ag (JCPDS 04-0836). In case of PU-Ag all Bragg's reflections representing b111N, b200N b220N and b311N planes of fcc crystal structures due to metallic silver are observed at 38.3 º, 44.7 º, 65.1 º and 77.7 º respectively [58]. While in case of PU-Cu all Bragg's reflections due to metallic copper are observed at 43.29, 50.42 and 74.11 representing b111N, b200N and b220N planes of fcc crystal structures of bulk copper [58] (Figure. 5.2.4). The average sizes of the NPs within the PU matrix were determined from the width of the reflection according to the Debye–Scherrer equation (eq^{n} 1). It was 27$\pm$2 for Cu and 33$\pm$2 nm for Ag respectively [58].

$$D(nm) = K\lambda/\beta Cos\theta \quad \ldots\ldots\ldots\ldots\ldots\ldots \quad (1)$$

where K is a constant equal to 0.89, λ is the X-ray wavelength (1.54 Å), β is the full-width at half-maximum (fwhm) of the major peak expressed in radians, and θ is the Bragg angle (deg) corresponding to that peak.

5.2.3.4 Thermal properties

TGA curves of PU membranes are shown in Figure. 5.2.5 (a). From the decomposition temperatures in the Table 2 it can be seen that the metal nanoparticles considerably improve the thermal stability of PU. This indicates effective entrapment and a high degree of adhesion between the NPs and the PU matrix. The DSC curves shows that the Tg of PU containing immobilized NPs is higher as compared to PU (Figure. 5.2.5 (b)). The increase is nominal and is greater in case of PU-Cu, compared to PU-Ag. Inorganic nanoparticles can usually hinder the motion of polymer chains, leading to an increase in α-transition peak temperature of the PUs [59]. The variation in Tg was also observed due to effect of hydrogen bonding between the polymer matrix and metal nanoparticles and improved dispersion as also seen in TGA. Thus incorporation of CuNPs improves the thermal stability as well as increases the glass transition temperature even more than nanosilver. This indicates a greater compatibility between copper and the PU matrix which can be explained as follows. Due to greater valency, initially the cuprous ions bind more strongly with the urethane groups through the nitrogen atom compared to silver. This facilitates the anchoring and alignment of the nanoparticles onto the PU network on subsequent reduction so that continuity of metal nanoparticles is better.

Table.2 Representing the thermal analysis data of PU membranes.

Materials	Ea KJ/mol	Glass Transition Temperature (Tg) º C	Degradation temperature (ºC) for % Wt. loss				
			1	5	10	30	50
PU	227	-55.2	101	285	307	339	354
PU-Ag	107	-54.0	72	249	298	350	363
PU-Cu	81	-53.0	82	230	256	340	-

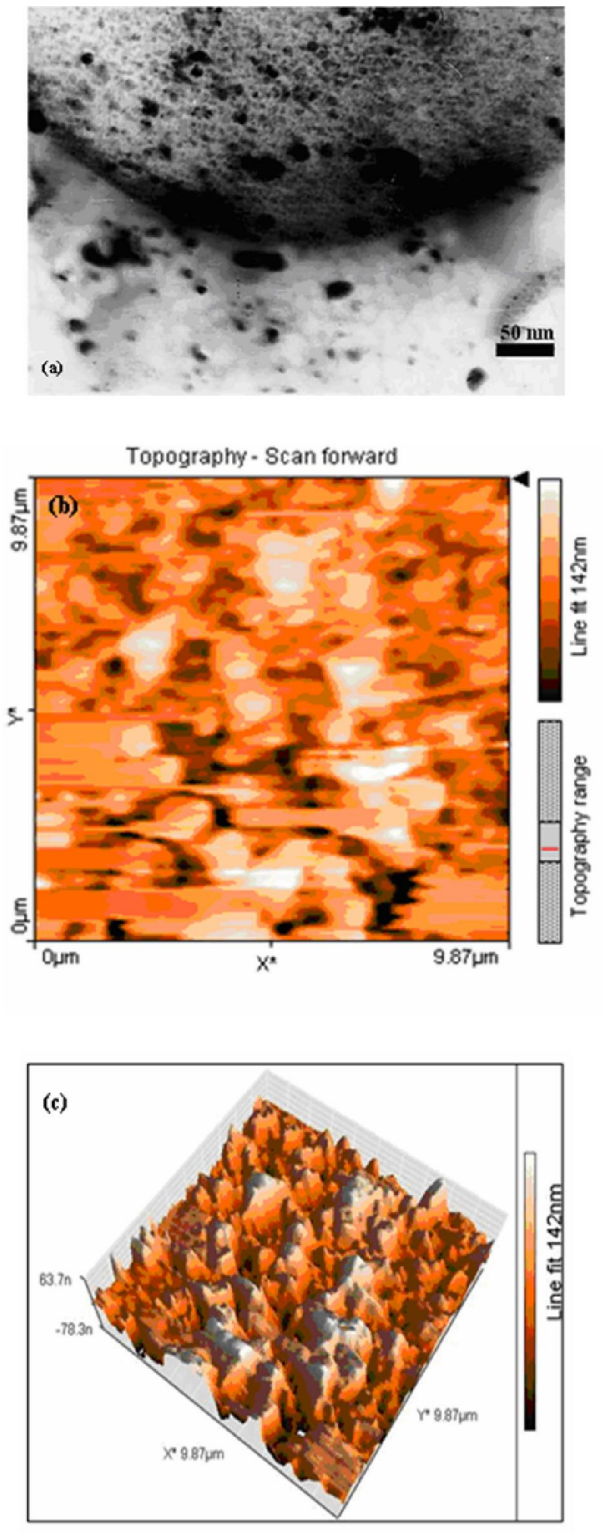

Figure. 5.2.3 (a) TEM and (b) 2 and 3-D AFM images of PU-Ag membranes

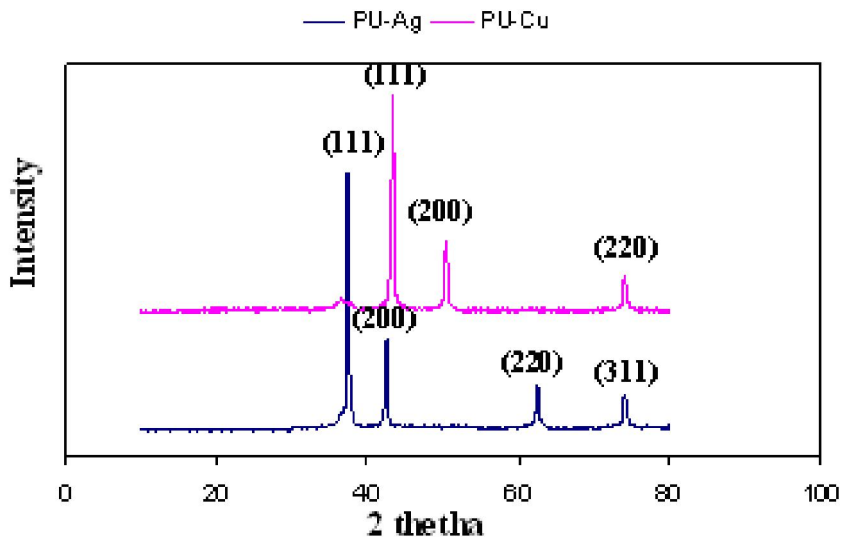

Figure. 5.2.4 X-ray diffraction patterns of metal immobilized PU membranes

5.2.3.5 Electrical properties

The PU membranes were examined for the electrical properties to see how the metallic nanoparticles improve the ionic conductivity of the polymer chain. The electrical properties of metal immobilized nanoparticles are strongly influenced by the metal filling factor and nanoparticle sizes [60,61]. The important mechanisms of electric conductivity in polymer metal nanoparticles dispersed in polymer matrix are

1. Ion conductivity, due to the ions remaining dispersed in the polymer matrix;
2. Electron conductivity in the metal nanoparticles network,
3. Tunnelling conductivity.

Generally, at high volume fractions of metal nanoparticles a 3D conducting network can develop in the matrix, leading to a sudden increase in the electric conductivity known as percolation. Our sample is well below the percolation threshold.

The results showed that ionic conductivity increases with temperature, with activation energy of 0.15 eV which indicates a thermally activated conduction mechanism in metal immobilized polymer membrane (Figure. 5.2.6 (B)). This behavior is attributed to increase of charge carrier energy with increase in temperature. The frequency dependent conductivity of the metal immobilized nanoparticles at different temperatures exhibits a typical frequency independent plateau at lower frequencies and a crossover or a

dispersive region at higher frequencies (Figure. 5.2.6 (A)). At higher frequencies, the mobility of charge carriers is high due to which the conductivity increases with frequency. As frequency decreases, more and more charge accumulation occurs at the electrodes, which leads to a decrease in the number of mobile ions and eventually to a drop in conductivity at low frequency. The conductivity increases in the order PU-Cu > PU-Ag > PU which again may be due to better compatibility of Cu nanoparticles with polymer matrix. This assumption is well supported by thermal analysis. Thus, the electrical conductivity along with better thermal stability of these materials can lead to the development of novel sensors for biomedical applications.

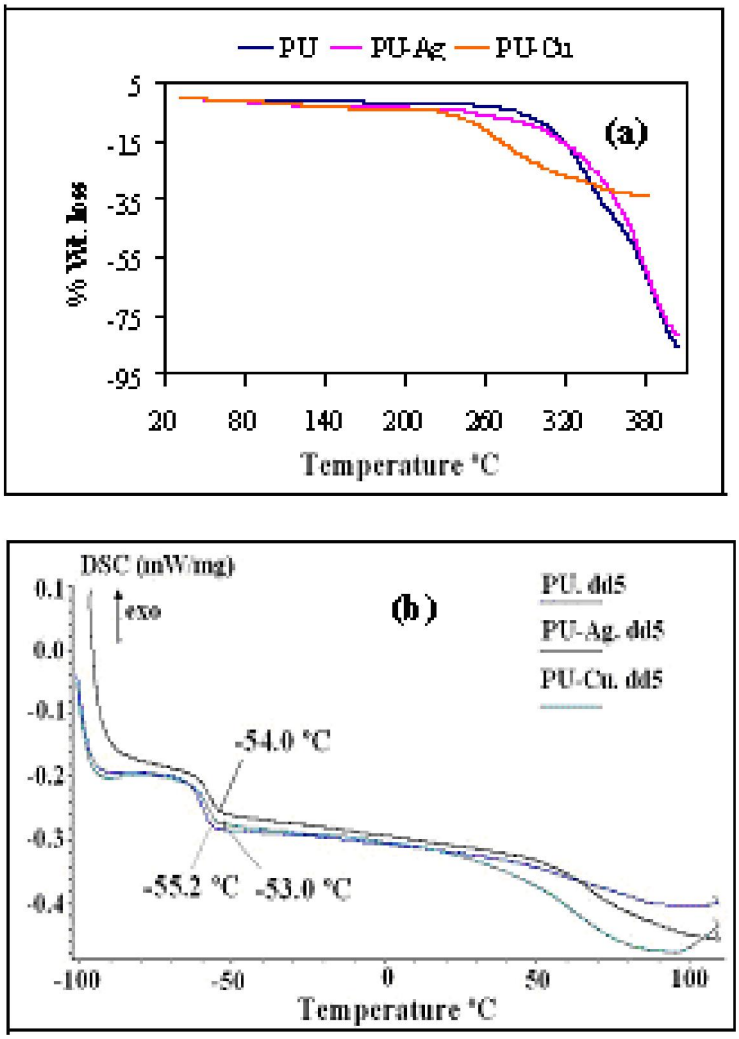

Figure. 5.2.5 (a) Thermogravimetric and (b) Differential Scanning Calorimetry curves of PU membranes.

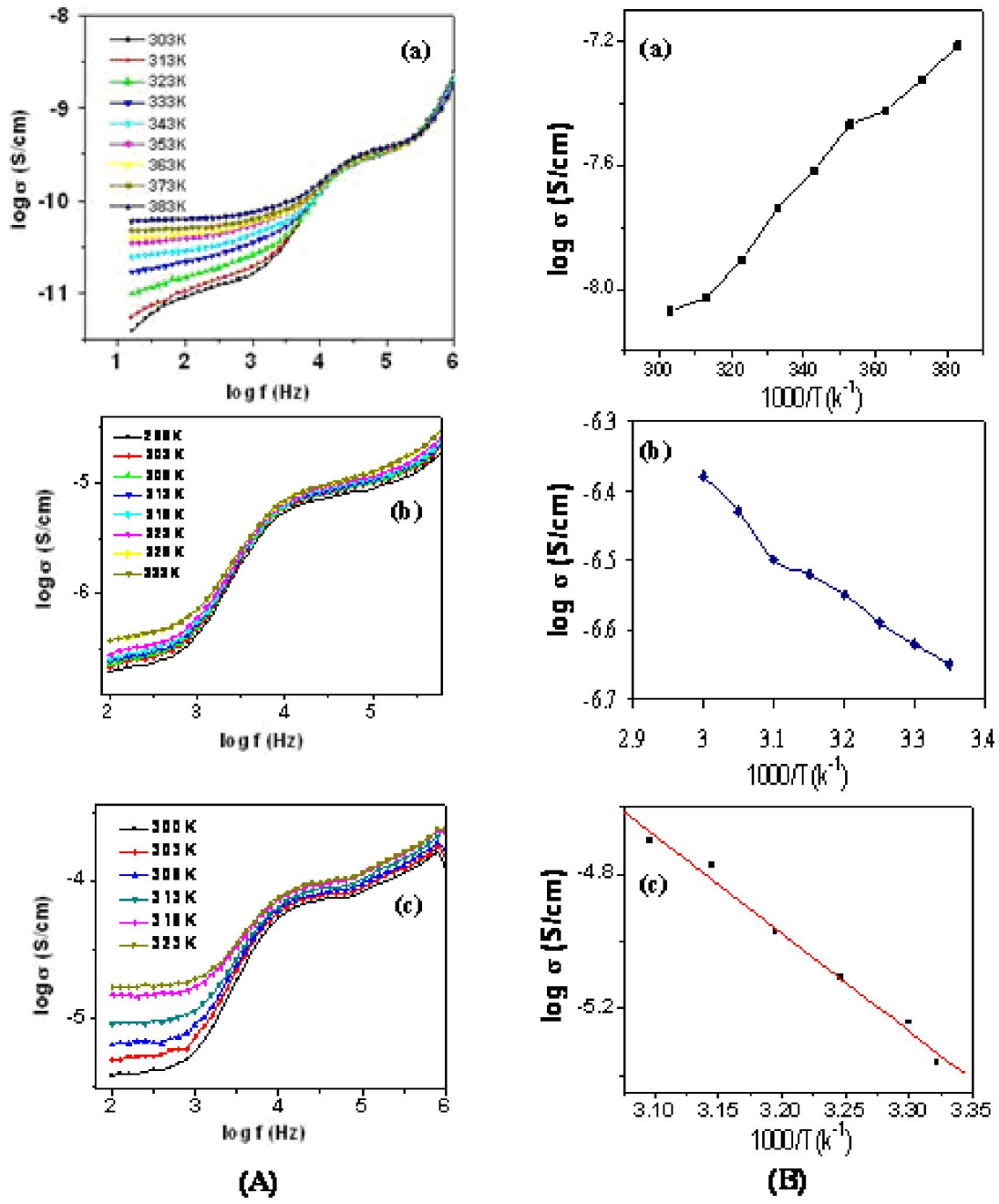

Figure. 5.2.6 (A) shows frequency dependent conductivity at different temperatures of PU membranes and (B) shows variation of ionic conductivity with temperature (a) PU (b) PU-Ag (c) PU-Cu

5.2.4 Conclusions

A novel sorption method of immobilizing metallic nanoparticles on starch crosslinked PU membranes was developed. The immobilization of the metal NPs was ensured by microscopy. The resulting membranes exhibited high thermal stability and higher Tg. The metallic nanoparticles improved the ionic conductivity of PU which exhibited Arrhenius relation. AC conductivity is found to increase with frequency as well as temperature. Copper nanoparticles exhibited a pronounced effect compared to silver. The temperature sensing ability, thermal stability and permeability of these novel membranes can lead to development of sensors for biomedical applications or conducting wires for connection of minitype devices.

5.3 References

1. S. K. Sahoo, J. Panyam, S. Prabha, V. Labhasetwar, *Adv Drug Deliv Rev*, **2003**, 55, 329.
2. R. L. Reis, A. M. Cunha, *J. Mater. Sci. Mater. Med.,* **1995**, 6, 786.
3. R. L. Reis, S. C. Mendes, A. M. Cunha, M. Bevis, *Polym. Int.,* **1997**, 43, 347.
4. A. P. Marques, R. L. Reis, J. A. Hunt, *Biomaterials,* **2002**, 23, 1471.
5. R. L. Reis, A. M. Cunha, M. J. Bevis, Shear controlled orientation injection moulding of polymeric composites with enhanced properties. Antec'98-Plastics on my Mind, Soc Plastics Eng., Atlanta, USA, **1998**, 487.
6. C. K. Simi, T. E. Abraham, Bioprocess *Biosyst. Eng.,* **2007**, 30, 173.
7. R. Peter, F. A. Y. C. A. D. J. H. Chang, *Journal of Applied Polymer Science*, **2009**, 111, 619.
8. M.Labet, W. Thielemans, & A. Dufresne, *Biomacromolecules*, **2007**, 8, 2916.
9. G. J. Tsai, W.-H. Su, *J. Food. Protect.*, **1999**, 62, 239.
10. T. H. Kim, I. K. Park, J. W. Nah, Y. J. Choi, Cho, S. Chong. *Biomaterials*, **2004**, 25, 3783.
11. K. A. Janes, M. P. Fresneau, A. Marazuela, A. Fabra, M. J. Alonso, *J. Control. Release*, **2001**, 73, 255.
12. A. M. De Campos, A. Sanchez, M. J. Alonso, Appl. Cyclosorin A, *Int. J. Pharm.* **2001**, 224, 159.
13. Y. Xu, Y. Du, *Int. J. Pharm.,* **2003**, 250, 215.
14. M. Kozurkova, D. Sabolova, L. Janovec, J. Mikes, J. Koval, J. Ungvarsky, M. Stefanisinova, P. Fedorocko, P. Kristian, J. Imrich, *Bioorg. Med. Chem.* **2008,** 16, 3976.
15. C. P. Tan, J. Liu, L. M. Chen, S. Shi, L. N. Ji, *J. Inorg. Biochem.* **2008,** 102, 1644.
16. S. M. Hecht, J. Nat. Prod. **2000,** 63, 158
17. A. Silvestri, G. Barone, G. Ruisi, M. T. Lo Giudice, S. Tumminello, *J. Inorg. Biochem.* **2004,** 98, 589.
18. M. Navarro, E. J. Cisneros-Fajardo, A. Sierralta, M. Fernandez-Mestre, P. Silva, D. Arrieche, E. Marchan, *J. Biol. Inorg. Chem.* **2003,** 8, 401.

19. C. Metcalfe, J. A. Thomas, *Chem. Soc. Rev.* **2003,** 32, 215.
20. M.S. Moron, J.W. Kepierre, B. Mannervick, *Biochim. Biophys. Acta,* **1979**, 582, 67.
21. T. Mosmann, *J. Immunological Methods,* **1983**, 65, 55..
22. J-Y. Je, Y-S. Cho, S-K Kim, *Bioorg. Med. Chem. Lett.,* **2006**, 16, 2122.
23. H. K. Patra, A. Dasgupta, Nanomed. Nanotechnology, **2011,** (in press)
24. A. M. Alkilany, P. K. Nagaria, C. R. Hexel, T .J. Shaw, C. J. Murphy, M. D. Wyatt, Small, **2009**, 5, 701.
25. T. Cedervall, I. Lynch, Foy, M. Angew. *Chem., Int. Ed.*, **2007**, 46, 5754.
26. A. M. Alkilany, C. J. Murphy, *J Nanopart Res,* **2010**, 12, 2313.
27. S. D. Conner, S. L. Schmid, *Nature* **2003**, 422, 37.
28. J. Boonstra, J. A. Post, Gene. **2004**, 337, 1.
29. J.F. Turrens, *J. Physiol.,* **2003**, 552, 335.
30. P. V. AshaRani, G. L. K. Mun, M. P.Hande, S. Valiyaveettil, *ACS Nano.,* **2009**, 3, 279.
31. S.M. Hussain, K. L. Hess, J. M. Gearhart, K. T. Geiss, J. Schlager, *J. Toxicol. in Vitro.*, **2005**, 19, 975.
32. T.M. Kelly, A. B. Tossi, D. J. McConnell, T. C. Strekas, *Nucleic Acids Res.,* **1985**, 13, 6017.
33. J. K. Barton, A. T. Danishefsky, J. M. Goldberg, *J. Am. Chem. Soc.,* **1984**, 106, 2172.
34. C. S. Chow, J. K. Barton, *Methods Enzymol.,* **1992**, 212, 219.
35. T. Hirohama, Y. Kuranuki, E. Ebina, T. Sugizaki, H. Arii, M. Chikira, P. T. Selvi, M. J. Palaniandavar, *Inorg. Biochem.,* **2005**, 99, 1205.
36. R .S. Kumar, S. Arunachalam, V. S. Periasamy, C. P. Preethy, A. Riyasdeen, M. A. Akbarsha, *Polyhedron,* **2008**, 27, 1111.
37. J. Kang, H. Wu, X. Lu, Y. Wang, L. Zhou, *Spectrochim. Acta A,* **2005**, 61, 2041.
38. J. B. Lepecq, C. J. Paoletti, *Mol. Biol.,* **1967**, 27, 87.
39. Z. C. Yong, X. X. Li, Y. Pin, *Biochemistry (Moscow),* **2007**, 72, 37
40. Y. Chen, Y. Liu, H. Fan, H. Li, B. Shi, H. Zhou, *J Membr Sci,* **2007**, 287; 192.
41. X. Cao, L.J. Lee, T. Widya, C. Macosko, *Polymer,* **2005**, 46, 775.

42. D. K. Bozanic, L. V. Trandafilovic, A. S. Luyt, V. Kjokovic, *React Funct Polym,* **2010**, 70, 869.
43. J.L. Rivera-Armenta, T.H. Heinze, A.M. Mendoza-Martinez, *Eur Polym J,* **2004**, 40, 2803.
44. P. Dosmann, R. N. Steel, U.S. Pat. 3, 004, 934, 1961.
45. Y. Lu, L. Tighzert, F. Berzin, S. Rondot, *Carbohydr Polym*, **2005**, 61, 174.
46. H. R. Lin, C. J. Kuo, Y. J. Lin, *J Cell Past,* **2003**, 39, 101.
47. R. Alfani, S. Iannace, L. Nicolais, *J Appl Polym Sci,* **1998**, 68, 739.
48. X. Cao, L. Zhang, *J Polym Sci Part B, Polym Phys,* **2005**, 43, 603.
49. S. K. Ha, H. C. Broecker, *Macromol Mat Eng,* **2003**, 28, 569.
50. S. Desai, I. M. Thakore, B. D. Sarawade, S. Devi, *Polym Eng Sci,* **2000**, 40, 1200.
51. R. Lalwani, S. Desai, *Journal of Applied Polymer Science,* **2010**, 115, 1296.
52. H. Shan-Hui, T. Hsiang-Jung, L. Yu-Chun, *Biomaterial,* **2010**, 31, 6796.
53. R. Lalwani, S. Desai, *J Appl Polym Sci,* **2010**, 115, 1296.
54. M. Valodkar, S. Thakore, *Carbohydr Res,* **2010**, 345, 2354.
55. P. Saravanan, R.M. Padmanabha, S. Alam, *Mater Chem Phys***, 2007,** 103, 278.
56. M. Valodkar, S. Modi, A. Pal, S. Thakore, *Mater Res Bull,* **2011**, 46, 384.
57. T. Klaus, R. Jorger, E. Olsson, C.G. Granqvist, *Trend Biotechnol,* **2001**, 19, 15.
58. M. Valodkar, S. Modi, A. Pal, S. Thakore, Mater. Res. Bull. **2011,** 46, 384.
59. C. Chih-Wei, H. Shan-Hui, C. Han, T. Sheng-Mao, L. Hong-Ru, *Polym Degradation Stability,* **2006**, 91, 1017.
60. H. Du, H. Chenb, J. Gong, T.G. Wang, C. Sun, S.W. Lee, *Appl Surf Sci,* **2004**, 233, 99.
61. U. Schurmann, H. Takele, V. Zaporojechenko, F. Faupel, *Thin Solid Film,* **2006**, 515, 801.

Chapter 6

Conclusions

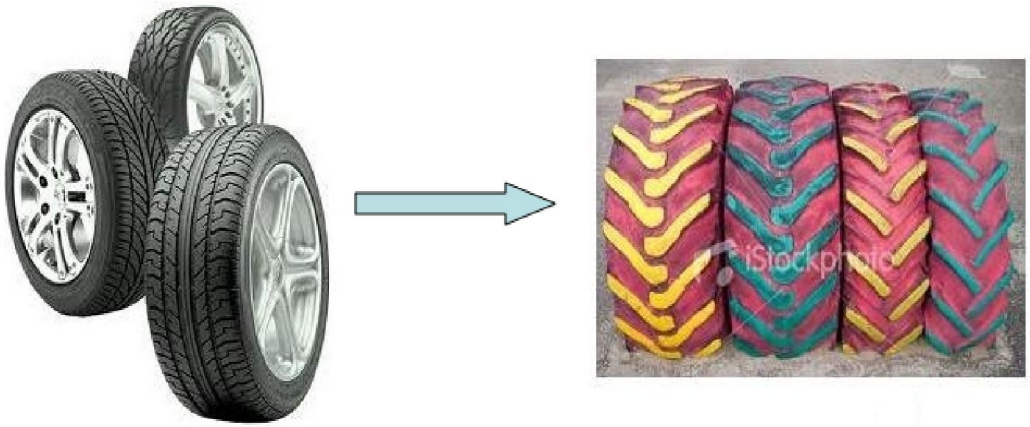

The conclusions of the work carried out on the synthesis and characterization of bionanocomposites of natural rubber are outlined in this chapter.

The basic motivation of the present work was to develop a green, eco-friendly alternative for carbon black which is the most important reinforcing agent used in the rubber industry. Due to easy availability and economical viability, materials from renewable resources are being sought to replace the reinforcement of composite materials. Hence, we decided to used polysaccharides such as starch, chitin and cellulose as reinforcing agents in natural rubber. Biocomposites containing up to 30 phr of the above mentioned fillers were prepared on a two roll mixing mill.

The composites were characterized by following techniques:

- Mechanical properties (Tensile strength, % Elongation)
- Thermal Gravimetric Analysis (TGA) : for thermal stability and degradation
- Scanning Electron Microscopy (SEM): to study the morphology of fractured samples
- Differential Scanning Calorimetry (DSC): for determination of glass transition temperature (Tg) and
- Sorption studies

The results showed that

- Upto 20 phr all the biofillers imparted superior strength and elongation behavior than C-black. Morphology revealed strong polymer-filler interaction in case of biocomposites.
- Among the biofillers chitin and cellulose imparted best mechanical properties followed by starch. Chitin imparted better mechanical properties because one of its hydroxyl groups is substituted by acetyl amine group. Thus it is hydrophobic in nature as compared to starch and cellulose and therefore has better compatibility with natural rubber.
- After 20 phr the mechanical properties of biocomposites deteriorated with further addition of filler. This may be because of the poor compatibility of hydrophilic biopolymers with hydrophobic natural rubber. While increasing quantity of C-black in composites lead to constant increase in the mechanical properties.

Thus the above mentioned polysaccharides can be potential substitutes for C-black only at low filler loadings.

To improve the compatibility of hydrophilic polysaccharide with natural rubber matrix hydrophobic starch particles were synthesized and their composites with natural rubber were prepared upto 30 phr.

- These hydrophobic starch particles imparted better strength than C-black upto 30 phr loading.
- Scanning electron microscopy revealed single phase morphology with uniform distribution of particles within the natural rubber matrix.
- The thermal stability of composites was also comparable with that of commercially used composite.

Thus they can be potential eco-friendly substitute for environmental pollutant carbon black as filler in natural rubber upto 30 phr. Further, to enhance their performance and to improve dispersion the following strategy was adopted.

1. Reduction in particle size of the biopolymers to obtain nanofillers which can result in more uniform distribution within the polymer matrix.
2. Organic modification of the nanofillers to obtain hydrophobic derivatives having improved compatibility with the polymer.

Synthesis of nanoparticles of starch and cellulose was carried out using acid hydrolysis. Further, acetylation of starch nanoparticles was carried out at room temperature. Similarly, acetyl derivative of cellulose nanoparticles were synthesized and these nanoparticles were characterized by ^{1}H NMR, TEM, XRD and IR.

Development of bionanocomposites of natural rubber was carried out using these fillers.

- Results of mechanical properties and morphology of starch based nanoparticles reveled that the modified starch nanoparticles showed better compatibility than C-black even at 40 phr with NR matrix.
- Starch isocyanate nanoparticles imparted highest strength due to formation of additional crosslinks during vulcanization process.
- Highly filled bionanocomposites were successfully developed upto 60 phr using cellulosic fillers.
- Bionanocomposites of cellulose acetate nanoparticles exhibited superior properties that carbon black even at 50phr.
- Despite the polysaccharide origin the fillers did not deteriorate the thermal stability of the nanocomposites.

- The broad tan δ peaks suggested high degree of compatibility of reinforcing fillers with NR matrix with potential application over a wide temperature range.
- Filler–matrix adhesion dominates the performance of composites.
- The combined effect of size reduction and organic modification improves the performance of polysaccharides.

Thus the derivatives of starch and cellulose proved to be promising substitutes for carbon black for reinforcement even at higher loadings using a commercially viable process.

Apart from using these nanoparticles as fillers we tried to find out some other applications of these nanoparticles.

Biological applications of acetylated starch nanoparticles

The results showed that

- The non-cytotoxicity of acetylated starch nanoparticles to noncancerous cells suggest promising drug delivery applications of these materials at lower concentrations while higher doses would be useful as anticancer agents.
- The cytotoxicity of acetylated starch nanoparticles with aromatic groups and high degree of substitution was higher relative to those containing aliphatic group.
- Despite negative zeta potential the nanoparticles exhibited reasonable biding propensity with CT-DNA, although complete intercalation was not observed.
- The details of the mechanism of action, especially to clarify the mode of interaction with tumor cells, effect of degree of substitution and particle size need further investigation.

Starch nanoparticles as crosslinkers for polyurethane

- Simple reaction of HMDI with starch nanoparticles resulted in crosslinked hydrophobic nanoparticles with almost spherical shape.
- A novel sorption method of immobilizing metallic nanoparticles on starch crosslinked PU membranes was developed.
- The immobilization of the metal NPs was ensured by microscopy. The resulting membranes exhibited high thermal stability and higher Tg.

- The metallic nanoparticles improved the ionic conductivity of PU which exhibited Arrhenius relation. AC conductivity is found to increase with frequency as well as temperature. Copper nanoparticles exhibited a pronounced effect compared to silver.
- The temperature sensing ability, thermal stability and permeability of these novel membranes can lead to development of sensors for biomedical applications or conducting wires for connection of minitype devices.

Future work

The results obtained in the current study by using bionanofillers should be applied to other synthetic rubber also. Various interesting phenomena taking place at the interface of the polymer and filler, polymer-polymer and filler-filler interfaces need to be understood properly. Though it has been found that bionanofillers impart good reinforcing property in NR matrix and shows synergism with carbon black, much light could not be shed on the synergistic effect of these bionanofillers with other reinforcing fillers like silica and carbon black. The effect of ageing on these composites should be studied over a period of time. Application of other hydrophobic polysaccharides as fillers in rubbers and their cost effectiveness is to be studied. The composites developed in the study are of natural origin and hence are biodegradable. Use of these composites in medical application such as in drug delivery system is to be studied.

List of publications

1. Isocyanate crosslinked reactive starch nanoparticles for thermo-responsive conducting applications

   Mayur Valodkar, Sonal Thakore

   Carbohydrate Research 345, 2354, 2010.

2. Biopolymers as effective natural fillers in natural rubber: Composites versus Biocomposites

   Mayur Valodkar and Sonal Thakore

   Journal of Applied Polymer Science 124, 3815, 2010.

3. Thermal and mechanical properties of nanobiocomposites of Natural rubber and Starch

   Mayur Valodkar and Sonal Ishit Thakore

   International Journal of Polymer Analysis and Characterisation 15, 1, 2010.

4. Organically modified nanosized starch derivatives as excellent reinforcing agents for bionanocomposites

   Mayur Valodkar, Sonal Thakore

   Carbohydrate Polymers 86, 1244, 2011.

5. Nanosized cellulose derivatives as green reinforcing agents at higher loading in natural rubber

   Mayur Valodkar, Puran Singh Rathore, Arun Vadgama, Sonal Thakore

   Journal of applied polymer science (Communicated).

6. Immobilization of metal nanoparticles on polyurethane membranes: synthesis and electrical properties

   Mayur Valodkar, Puran Singh Rathore, Poonam Sharma, Dinesh Kanchan, Mehul Patel and Sonal Thakore

   Polymer international 2012 (in press DOI: 10.1002/pi.4265)

Other publications

7. Synthesis and cytotoxicity evaluation of novel acylated starch nanoparticles

   Sonal Thakore, **Mayur Valodkar,** Jigar Y. Soni, Komal Vyas, Rajendrasinh N. Jadeja,

   Ranjitsinh V. Devkar, Puran Singh Rathore.

   Biomacromolecules (Communicated)

8. Morphology and anti-bacterial activity of carbohydrate stabilized silver nanoparticles
   Mayur Valodkar, Arti Bhadoria, Jayshree Pohnerkar, Mukta Mohan Sonal Thakore

   Carbohydrate Research 345, 1767, 2010

9. Conducting and antimicrobial properties of silver nanowire - waxy starch nanocomposites
   Mayur Valodkar, Poonam Sharma, D. K. Kanchan, Sonal Thakore

   International Journal of Green Nanotechnology 2, 10, 2010

10. Synthesis and anti-bacterial activity of Cu, Ag and Cu–Ag alloy nanoparticles : A green approach
    Mayur Valodkar, Shefaly Modi, Angshuman Pal and Sonal Thakore

    Materials Research Bulletin 46, 384, 2011.

11. Synthesis and characterization of cuprous oxide dendrites : New simplified green hydrothermal route
    Mayur Valodkar, Amit Thakore, Angshuman Pal and Sonal Thakore

    Journal of Alloys and Compounds 509, 523, 2011.

12. Euphorbiaceae latex induced green synthesis of non-cytotoxic metallic nanoparticle solutions: a rational approach to antimicrobial applications
    Mayur Valodkar, Padamanabh S. Nagar, Ravirajsinh N. Jadeja, Menaka Thounaojam, Ranjitsinh V. Devkar, Sonal Thakore

Colloids and Surfaces A: Physichemical and Engineering Aspects 384, 337, 2011.

13. Biocompatible synthesis of peptide capped copper nanoparticles and their biological effect of tumor cells

    Mayur Valodkar, Ravirajsinh N. Jadeja, Menaka Thounaojam, Ranjitsinh V. Devkar, Sonal Thakore

    Materials Chemistry and Physics 128, 83, 2011.

14. Oxidative stress induced apoptosis of human lung carcinoma cells by almond skin extract stabilized copper nanorods

    Menaka C Thounaojam, Ravirajsinh N Jadeja, **Mayur Valodkar**, Padamanabh S. Nagar, Ranjitsinh V Devkar, Sonal Thakore

    Food and Chemical Toxicology 49, 2990, 2011.

15. Cytotoxicity evaluation and antimicrobial mechanism of starch capped water soluble copper nanoparticles

    Mayur Valodkar, Puran Singh Rathore, Ravirajsinh N. Jadeja, Menaka Thounaojam, Ranjitsinh V. Devkar, Sonal Thakore

    Journal of Hazardous Materials 201-202, 244, 2012

16. Invitro toxicity study of plant latex capped silver nanoparticles in human lung carcinoma cells

    Mayur Valodkar, Ravirajsinh N. Jadeja, Menaka Thounaojam, Ranjitsinh V. Devkar, Sonal Thakore

    Materials Science and Engineering C 31, 1723, 2011.

Oral/Poster presentations

- **Biocomposites of Natural Rubber: Effect of various biopolymers as fillers**
  Mayur Valodkar & Sonal Ishit Thakore*

  Poster presented at MACRO 2009 held at IIT Madras in March 2009.

- **Synthesis of hydrophobic biopolymer derivatives for potential application in nanobiocomposites.**
  Mayur Valodkar & Sonal Ishit Thakore*

  Oral presentation PSE-2010, held at Panjab University, Chandigarh on 26-27th November 2010.

- **Nanosized polysaccharides as potential fillers in the development of bionanocomposites.**
  Mayur Valodkar, Arun Vadgama, Puran Rathore, and Sonal Thakore*

  Poster presented at MACRO 2010 held at IIT Delhi on 15-17th December 2010.

- **The magical role of polysaccharides in nanocomposites**
  Mayur Valodkar and Sonal Thakore*

  Oral presentation at AGRSM, held at M. S. University of Baroda, Vadodara on 30th January 2010.

- **Synthesis and toxicity studies of novel starch derivatives**
  Mayur Valodkar and Sonal Thakore*

  Oral presentation at WIRSM, held at M. S. University of Baroda, Vadodara on 17th September 2011.

- **Cellular uptake and biological studies of metal nanoparticles : generation of reactive oxygen species (ROS) and superoxide;**
  Mayur Valodkar, Puran Rathore, Ravirajsinh Jadeja, Menaka Thounaojam,

  Ranjitsinh Devkar, Sonal Thakore*

Poster presented during 2nd international conference on nanomedicine, Kottayam Kerala, march 2011.

Patents

- A process for synthesis of nanosized hydrophobic polysaccharide derivatives
  Sonal Thakore and **Mayur Valodkar**

  Application No. 2330/MUM/2010

- Bionanocomposites of natural rubber and hydrophobic polysaccharide derivatives
  Sonal Thakore and **Mayur Valodkar**

  Application No. 2360/MUM/2010